Characterisation of Novel Methodologies for In-Vitro Prediction of Human Drug-Induced Cardiotoxicity

Carol De Santis

BSc (Hons), MRes.

Thesis submitted for the degree of Doctor of Philosophy

Newcastle University

Faculty of Medical Sciences

Translational and Clinical Research Institute

December 2020

Declaration

I hereby declare that this thesis has been composed by myself and has not been accepted in application of a degree. All work was performed by myself unless otherwise stated. All sources of information have been acknowledged appropriately by means of a reference.

Carol De Santis

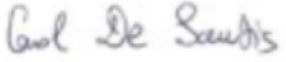

Abstract

Detrimental effects upon the cardiac system are a major cause of drug attrition. Current *in-vitro* methodologies for identification of drug-induced structural and functional cardiotoxicity and their underlying mechanism are sub-optimal and have limited utility for longer-term analyses and clinical translation. The emergence of innovative technologies combined with human stem-cell-derived cardiomyocytes has revolutionised preclinical identification of drug-induced cardiotoxicity. However, major limitations to these approaches include their complexity, specialised culture conditions, high cost and incomplete ability to fully detect drug-induced cardiotoxicity. A supplementary option is the use of immortalised cardiac cell lines, with capability for continuous growth and screening approaches. However, the limitations of these models for detecting both structural and functional cardiotoxicity are unknown. In this study, pathophysiological responsiveness of current cardiac cell lines to both structural and functional cardiotoxicants were evaluated using two-dimensional real-time impedance-based methodologies (xCELLigence) and three-dimensional spheroid systems. Specifically, using these cardiac cell models, the study evaluated effects of the histone deacetylase inhibitor (HDACi) sub-classes of drugs. The AC10 cell-line, although non-contractile, was able to detect HDACi-induced structural changes. The HL-1 cell-line exhibited a contractile phenotype *in vitro*, albeit non-uniformly and time-limited, and also detected drug-induced structural cardiotoxicity. In terms of HDACi, the occurrence of structural changes in both AC10 cells and HL-1 cells in response to sub-pharmacologically active concentrations of the drugs was observed, implicating their potential for clinical cardiotoxicity. In summary, this study supports the inclusion of cardiac cell-lines alongside primary cells and stem-cell-derived cardiomyocytes in preclinical evaluation of drug-induced cardiotoxicity.

Acknowledgements

First and foremost, I would like to thank the Medical Research Council for funding this Integrative Toxicology Training Partnership: without their sponsorship this project would not have been possible. In particular, I would like to thank Dr Andy Smith and the whole team at the MRC Toxicology Unit at the University of Cambridge.

Equally, I would like to express my gratitude to my supervisory panel. Especially Dr Jason Gill, Dr Parveen Sharma and Dr Jean-Pierre Valentin for their invaluable guidance and support throughout this project.

Jason, thank you for supporting me over the past four years. I cannot thank you enough for never doubting me! Through your mentorship, you taught me to be an independent scientist. But most importantly, through your endless patience you have helped me grow as a person and as a professional: for this I am forever grateful.

Parveen, I would not have completed this thesis without you. Thank you for always being there for me, and for your constant encouragement. I know I could always count on you. Through your support and friendship, you have inspired and empowered me to become a confident scientist.

Dr Valentin, thank you for your guidance and for enabling my internship at UCB Pharma. This has been an incredibly inspiring experience that undoubtedly defined my career aspirations. Merci beaucoup!

Thank you to my colleagues and friends from the Gill Lab at Durham University/Newcastle University: Kim Rockley, Simon Findlay, Asma Mohamed, thanks for the banter, you have made this PhD adventure much more enjoyable.

Kim, you will always be a dear friend. I am glad that we got through the longest days in labs (and numerous conferences) together. Thank you for the parties and for all the shared sandwiches! For all the times you've reminded me that "*this is not real*" – I know you always understood.

Thank you to my colleagues and friends from the Sharma Lab and Pharmacology and Therapeutics team at the University of Liverpool: Chris Cox, Robert Bentley, Sophie Penman, Chrysa Koukorava, Robyn Kiy and Rebecca Jensen. My Liverpool stays would not have been the same without you, from the long days spent in the Sherrington Labs, to the numerous bar crawls, you always made me feel welcome. I could not have asked for a better placement experience.

Thank you to my colleagues and friends from UCB Pharma in Belgium: Dr Vitalina Gryshkova, thank you for your guidance and extensive research advice. Izzy Lushbough, Benoit Cox, and the whole team at the Investigative Toxicology Department, thank you for proving that science in industry is much more fun than academia!!!

A special thanks must go to my friend and colleague (and fellow coffee addict) Wil Reynolds: thank you for supporting me, for listening to my rants, and for the daily coffee sessions that fuelled me through this PhD. I could not have done it without you.

A shout out to my friends and colleagues from the glorious Team Wright for the countless drinks and terrible karaoke nights! On a serious note, Prof Matt Wright, thank you for being a mentor for all these years.

A special thank you goes to Mr Bergin, for the truly extraordinary help.

I am grateful to my closest friends and family for always supporting me. Frankie, George, JP, Kate, Ben, Audrey and Marco, Alessandra, Emma, Ezio, thank you all.

A massive thank you must go to my husband William. Will, thank you for being my rock. Your love and support got me through the darkest times.

Last, but not least, I would like to thank my parents Jarmila and Arnaldo. Even though we live far apart, you always showed me the greatest support. Grazie di tutto, vi voglio bene.

Personal awards

- MRC Discovery Medicine North Flexible Fund bursary award 2020
- British Toxicology Society Travel Award 2019
- British Toxicology Society Annual Congress Bursary Award 2019
- *In Vitro* Toxicology Society (IVTS) Early Career Scientist Prize 2017
- *In Vitro* Toxicology Society (IVTS) Meeting bursary Award 2017

Publications and presented abstracts

- Findlay, S., Gill, JH., Plummer, R., **De Santis, C.**, Plummer, C. (2019). Chronic cardiovascular toxicity in the older oncology patient population. *Journal of Geriatric Oncology*. 10:685-689
- **De Santis C**., Findlay S., Gill JH., (2019). Poster Presentation Qualification of in-vitro Cardiac Cell Models for Preclinical Assessment of Oncology Drug-induced Cardiotoxicity. *European Cardio-Oncology Symposium*, Barcelona, Spain.
- **De Santis, C**. Sharma, P. and Gill, JH. (2019). Poster Presentation. Qualification of in vitro cardiomyocyte cell models for prediction of drug-induced toxicity studies. *IUTOX 2019 Meeting*, Honolulu, Hawaii
- Gill, JH., Rockley, KL., **De Santis, C.**, Mohamed, A. (2019). Vascular Disrupting Agents in cancer treatment: Cardiovascular toxicity and implications for co-administration with other cancer chemotherapeutics. *Pharmacology & Therapeutics*, 202:18-31
- **De Santis, C**. and Gill, JH. (2019). Oral Presentation Evaluation of in-vitro cellular models for use in functional and structural studies of drug-induced cardiotoxicity. *British Toxicology Society annual congress*. Cambridge, UK
- Fairhall, E., Leitch, A., Lakey, A., Probert, P., Richardson, G., **De Santis, C.** and Wright, M. (2018). Glucocorticoid-induced pancreatic-hepatic trans-differentiation in a human cell line *in vitro*. *Differentiation*, 102:10-18
- **De Santis, C**. and Gill, JH. (2018). Invited speaker Evaluation of *in vitro* cellular models for use in functional and structural studies of drug-induced cardiotoxicity. *4th Conference on Impedance-based Cellular Assays*, Edinburgh, UK.
- **De Santis, C**. and Gill, JH. (2018). Poster Presentation Characterisation of *in vitro* cardiac models for preclinical assessment of oncology drug-induced cardiotoxicity. *British Toxicology Society annual congress*, Newcastle upon Tyne, UK.
- **De Santis, C**. and Gill, JH. (2017). Invited Keynote speaker. Preclinical *in vitro* identification of drug-induced cardiotoxicity. *In vitro Toxicology Society annual meeting*, London, UK.
- **De Santis, C**. and Gill, JH. (2017). Poster Presentation. Evaluation of *in vitro* cellular models for use in functional and structural studies of drug-induced cardiotoxicity. *In vitro Toxicology Society annual meeting*, London, UK.

Table of Contents

List of Figures

List of tables

List of abbreviations

AA	Ascorbic acid
AC10	AC10 human ventricular cell line
ADME	Absorption, distribution, metabolism, excretion
ADP	Adenosine diphosphate
ANOVA	Analysis of variance
AOP	Adverse outcome pathway
AP	Action potential
ATP	Adenosine triphosphate
AV	Atrioventricular
BA	Beat amplitude
BPM	Beats per minute
BR	Beat rate
BRI	Beat rate irregularity
BS	Brugada syndrome
BSA	Bovine serum albumin
Ca	Calcium
CAD	Coronary artery disease
CD31	Cluster of differentiation 31
CF	Cardiac fibroblast
CI	Cell index
CICR	Calcium induced calcium release
CIPA	Comprehensive in-vitro Proarrhythmia assay
CM	Cardiomyocyte
Cmax	Maximum serum concentration
CO_2	Carbon dioxide
CPTV	Catecholaminergic polymorphic ventricular tachycardia

CTnI	Cardiac troponin I
DC	Drug candidate
DMEM	Dulbecco's modified eagle medium
DMSO	Dimethylsulfoxide
DNA	Deoxyribonucleic acid
DTT	Dithiothreitol
EAD	Early afterdepolarisation
EC	Endothelial cell
ECAR	Extracellular acidification rate
ECG	Electrocardiogram
ECL	Enhanced chemiluminescence solution
ECM	Extracellular matrix
ECR	xCELLigence Cardio ECR system
EDTA	Ethylenediaminetetraacetic acid
EF	Ejection fraction
EFPIA	European Federation of Pharmaceutical Industries and Associations
EGF	Epidermal growth factor
EGTA	Ethylene glycol-bis(β-aminoethyl ether)-N,N,N',N'-tetraacetic acid
ELISA	Enzyme linked immunosorbent assay
E-Pacing	Electrical pacing
ESC	European society of cardiology
ETC	Electron transport chain
FB	Fibroblast
FBS	Foetal bovine serum
FCCP	Carbonyl cyanide-4-phenylhydrazone
FCS	Foetal calf serum (also see FBS)
FDA	Food and drug administration
FP	Field potential
FPD	Field potential duration

FPDc	Corrected field potential duration
h	Hour
HBSS	Hank's balanced salt solution
HCL	Hydrochloric acid
HDAC	Histone deacetylase
HDACi	Histone deacetylase inhibitor
HERG	Human Ether-à-go-go-Related Gene
HF	Heart failure
HFpEF	Heart failure with preserved ejection fraction
hiPSC-CM	Human induced pluripotent stem cell derived cardiomyocytes
HL-1	HL-1 murine atrial cell line
HRP	Horseradish peroxidase
hSC-CM	Human stem cell derived cardiomyocyte
$I_{Ca\text{-}L}$	Calcium channel current L-type
$I_{Ca\text{-}T}$	Calcium channel current T-type
IC_{50}	Half maximal inhibitory concentration
ICH	International Council for Harmonisation of Technical Requirements for Pharmaceuticals for Human Use
I_F	Pacemaker 'funny' current
IGF	Insulin-like growth factor
I_{Kr}	Delayed rectifier, fast current
I_{KAch}	G-protein gated potassium channel
I_{KATP}	ATP-sensitive potassium current
I_{KP}	Background current
I_{Ks}	Delayed rectifier, slow current
I_{Kur}	Delayed rectifier, ultra rapid current
I_{Na}	Sodium current
I_{to}	Transient outward current
iPSC	Induced pluripotent stem cell

ITS	Insulin transferrin selenium
IVIVE	In-vitro-in-vivo extrapolation
K	Potassium
kDa	kilodalton
KDAC	Lysine deacetylase (also HDAC)
LONG R3 IGF	Recombinant analogue of human insulin-like growth factor-I
LQTS	Long QT syndrome
M	Molar
MEA	Multi electrode array
MI	Myocardial infarction
MID-3	Model informed drug discovery and development
ms	Millisecond
MS-275	N-(2-aminophenyl)-4-[N-(pyridine-3yl-methoxy-carbonyl) aminomethyl] Benzamide (also Entinostat)
MTT	3-(4,5-dimethylthiazol-2-yl)-2,5-diphenyltetrazolium bromide
mV	Millivolt
Na	Sodium
NAD	Nicotinamide adenine dinucleotide
NCE	Novel chemical entity
NC3R	The National Centre for the Replacement, Refinement, and Reduction of Animals in Research
NCX	Sodium calcium exchanger
NE	Norepinephrine
OCR	Oxygen consumption rate
PBS	Phosphate buffered saline
PCR	Polymerase chain reaction
PFA	Paraformaldehyde
PVDF	Polyvinylidene difluoride
QRS	Electrocardiogram QRS wave complex

QT	Electrocardiogram QT segment
QTc	Corrected electrocardiogram QT interval
RA	Retinoic acid
RCF	Relative centrifugal force
RTCA	Real time cell analyser
Ryr	Ryanodine receptor
SA	Spike amplitude
SAHA	Suberanilohydroxamic acid (also Vorinostat)
SAN	Sinoatrial node
SCD	Sudden cardiac death
SD	Standard deviation
SDS	Sodium dodecyl sulphate
SDS-PAGE	Sodium dodecyl sulphate–polyacrylamide gel electrophoresis
SEM	Standard error of the mean
SIRT	Sirtuin
SR	Sarcoplasmic reticulum
ST	Electrocardiogram ST segment
SV40	Simian vacuolating virus 40
TBS-T	Tris-buffered saline and Tween-20
TdP	Torsade de pointes
TEMED	Tetramethylethylenediamine
TSA	Trichostatin A
T-tubule	Transverse tubule
ULA	Ultra low adhesion
WP	Whole peak
2D	Two-dimensional
3D	Three-dimensional

1 Introduction

Over the past 30 years, increasing evidence has proven that a wide number of compounds and drugs are responsible for critical and potentially life-threatening cardiac damage. Cardiac toxicity remains one of the primary causes of drug attrition and withdrawal from the market (Gintant, Sager, and Stockbridge 2016b; Vicente, Stockbridge, and Strauss 2016). An increasing number of reports since the early 1980s have led to the conclusion that even non-cardiovascular agents could contribute to serious risk to the normal functioning of the heart, thus leading to potentially dangerous outcomes. The urgent need for the development of standardised paradigms for the prediction and assessment of cardiotoxicity was thus recognised.

The cardiotoxic effects of a compound relate to its ability to induce either disruption of cardiac function or structural alterations of the heart. To date most efforts, in terms of identifying the potential for drug-induced cardiac liabilities, have focused on preclinical evaluation of acute effects and drug-induced functional disturbances. In particular, the *in-vitro* characterisation of disturbances in the electrophysiological regulation of cardiomyocyte contraction, primarily related to the interference and disruption of cardiac ion channels (Pointon et al. 2013). However, in contrast to preclinical evaluation of potential drug-induced functional disturbances, much less has been developed towards robust *in-vitro* methodologies for detection of drug-induced morphological and structural effects upon the heart. Currently, drug-induced structural cardiotoxicity and morphological cardiac disturbances are detected during *in-vivo* studies, with no *in-vitro* methodologies reliably available to either identify or imply such a potential risk (Fermini et al. 2016). Major limitations in this context are the low number of cardiac cell models for such purposes, a lack of optimisation of culture methodologies for cardiomyocyte models, poor understanding of the interplay between cardiomyocytes themselves and the other cell types present in cardiac tissue, and until recently, lack of technologies to non-invasively assess such changes. Additionally, unlike the mechanisms of drug-induced functional disturbances in cardiac tissue, a lot remains yet to be elucidated in relation to the molecular and mechanistic understanding of structural cardiac toxicity.

1.1 Mammalian cardiac system

The human heart is an organ situated in the middle mediastinum within the thoracic cavity, positioned posteriorly to the sternum and the costal cartilages and surrounded by the pericardium. The main function of this vital organ is to achieve efficient perfusion in all organs and tissues via the circulatory system, which is essential in order to maintain optimal organ oxygenation and homeostasis, and provide nutrients to the organism (Netter 2014). Anatomically, the heart is divided into four main chambers, the upper part consisting of the left and right atria and the lower part consisting of the left and right ventricles. The left heart and the right heart are separated by the interatrial septum and the interventricular septum, whereas each atrioventricular portion is separated by an atrioventricular valve, the bicuspid valve in the left heart portion and the tricuspid valve in the right heart portion (Netter 2014).

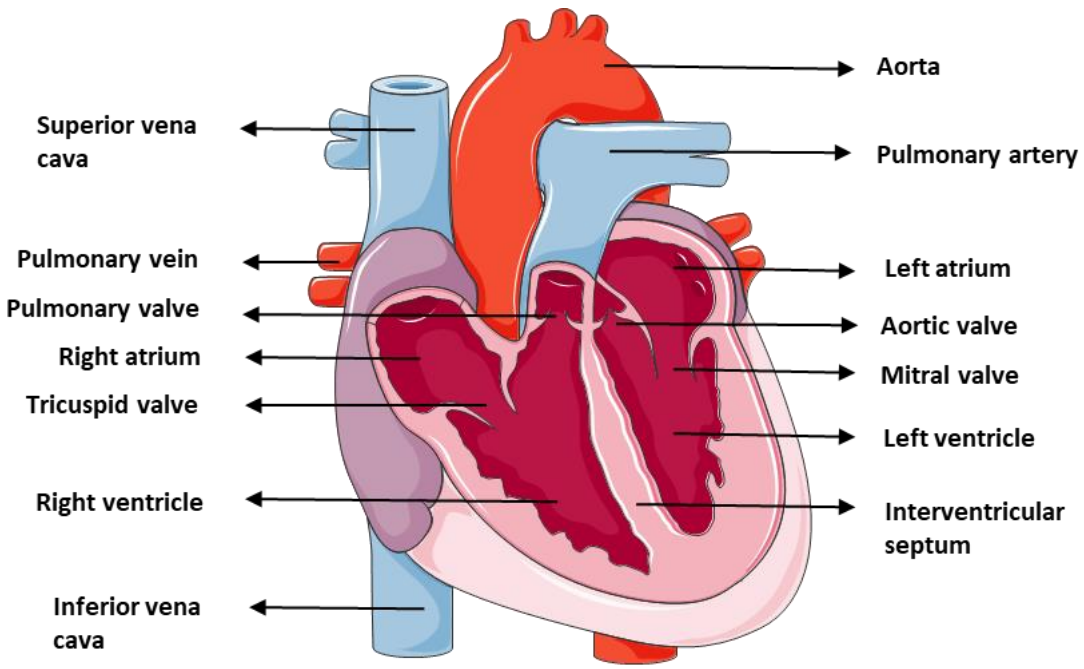

Figure 1.1. **Basic gross anatomy of the human heart:** diagram shows the frontal cross section revealing the cardiac lumen. The four cardiac chambers, valves and major vessels are labelled. (Image adatpted from Servier Medical Art).

In the right heart, deoxygenated blood is collected and drained to undergo pulmonary circulation and re-oxygenation; oxygenated blood enters the left heart where it is pumped back into systemic circulation via the aorta (Silverthorn 2016).

1.1.1 Cellular structure of the cardiac system

The human heart is composed of a variety of cell types, broadly classified into myocytes and non-myocytes, which vary in proportion depending on their location and function within the organ, as well as depending on the age of the subject (Bergmann et al. 2015). The different layers of the mammalian adult heart contribute to distinct roles, providing both functional and structural features, with the myocardium being the muscular contractile layer, the endocardium being the innermost layer that lines the heart chambers, and the epicardium constituting the outermost layer of the cardiac wall. Myocyte-type cells occupy a large proportion of the adult human heart, accounting for approximately 70 to 85% of its volume (Zhou and Pu 2016). Non myocyte-type cells include endothelial cells (ECs) and cardiac fibroblasts (FBs), with ECs accounting for the largest proportion of non-myocyte-type cells in the adult human myocardium (Pinto et al. 2016). In minor proportion, macrophages are found in healthy myocardium where they are thought to be involved in the maintenance of tissue homeostasis as well as having a role in pathological diastolic dysfunctions (Nahrendorf 2019).

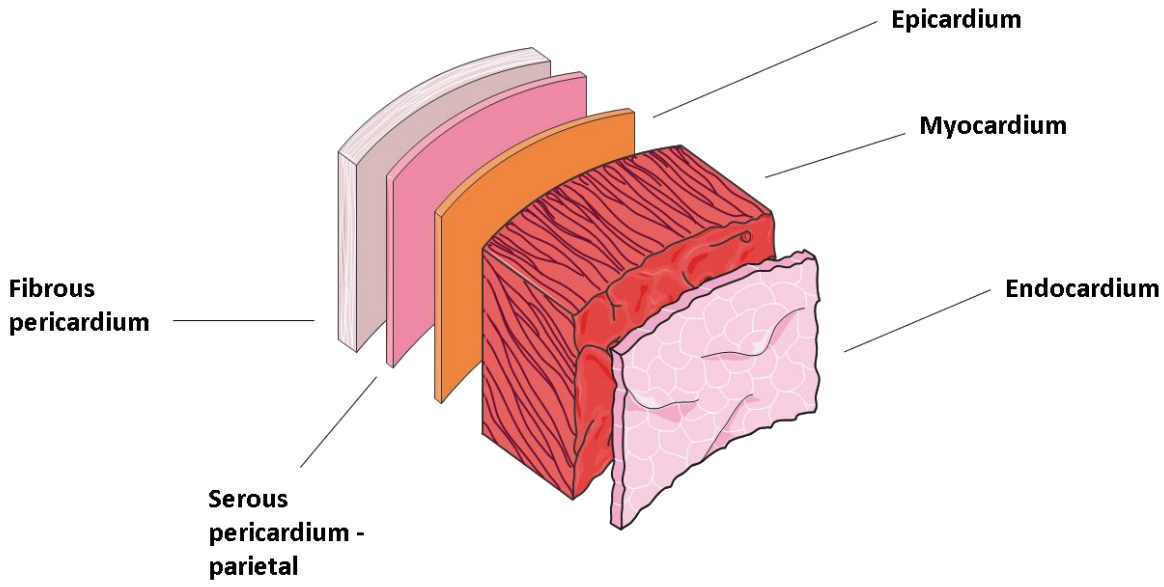

Figure 1.2 Illustration of the cardiac wall structure, from the innermost endocardial layer to the outermost pericardial layer. (Adapted from Servier Medical Art).

1.1.1.1 Cardiomyocytes

Cardiomyocytes are among the first cells to develop in the embryo, with cardiac progenitor cells forming shortly after gastrulation. Neonatal cardiomyocytes retain a limited ability to divide after differentiation, with cell division terminating approximately three days postnatally (Litviňuková et al. 2020). Despite recent attempts at identification of cell division and regeneration mechanisms in adult cardiomyocytes and cardiomyocyte progenitor cells, the current consensus is that human cardiomyocytes are not generated ex-novo in adult life, and any limited occurrence of generation of new cardiomyocytes is to be attributed to cell cycle re-entry mechanisms of pre-existing adult cells (Gray et al. 2018). Cardiomyocytes constitute roughly 32% of the total number of heart cells in humans and rodents (Bergmann et al. 2015), and are key resident cells of the myocardium: given that they form the contractile core of the heart, and considering their limited regenerative capacity, it is perhaps not surprising that any myocardial injury (and subsequent cardiomyocyte damage or loss) would severely undermine the physiological functionality of the heart.

Cardiomyocytes are typically mononucleated and organised into myofilaments, with individual myocytes being surrounded by the sarcolemmal cell membrane. Effective contractility of the heart is ensured by the coordinated contraction of cardiomyocytes as discussed in section 1.1.2 and 1.1.3. The direct electrical contact between individual myocytes and other cardiac cells is achieved through a distinct pattern of cell-cell interactions, gap junctions and ion channels expressed in the cardiomyocytes (Netter 2014). The integrity of the cardiomyocytes as well as the efficiency of these cellular communication mechanisms are at the basis of the excitation-contraction coupling mechanism of the cardiac muscle as described in section 1.1.3.

1.1.1.2 Cardiac fibroblasts

Cardiac fibroblast (CF) cells are of mesenchymal origin and are the second largest cardiac cell lineage by number in the adult human heart (Pinto et al. 2016). CFs have a key role in maintaining cardiac tissue homeostasis, and are essential in providing structural features in the heart by synthesising the cardiac extracellular matrix (ECM) components, including collagens and fibronectin (Tocchetti et al. 2020). The ECM has the critical role of providing

structural support to the cardiac cells, but recent evidence has demonstrated its involvement as the main signalling mediator between fibroblasts and cardiomyocytes (Tocchetti et al. 2020; Pellman, Zhang, and Sheikh 2016), where it is involved in the modulation and conduction of electrical signals. Interestingly, fibroblasts themselves are incapable of initiating an action potential, but were shown to exhibit distinct conductive features (Pellman, Zhang, and Sheikh 2016).

A major function of CFs includes the ability to provide tissue reparative mechanisms following disease states such as myocardial infarction (MI), by undergoing a phenotype transition into proliferative myofibroblasts capable of increasing matrix formation, and thus favouring scar tissue generation (Humeres and Frangogiannis 2019). Disruption of cardiac fibroblast homeostasis following cardiac injury is directly linked to fibrosis and cardiac remodelling that could result in severe pathological outcomes (Humeres and Frangogiannis 2019). In terms of drug-induced effects upon the cardiac system, cardiac fibroblasts are now believed to be centrally involved rather than just spectators in these effects. The importance of cardiac fibroblasts for cardiotoxicity of cancer therapeutics was recently highlighted at the joint meeting of the European Society of Cardiology (ESC) myocardial function and cellular biology of the heart working groups, wherein several interactions between fibroblasts and cardiomyocytes were defined in pathogenesis of cancer drug-induced heart failure (Tocchetti et al. 2020). Drug-induced toxicity against cardiac fibroblasts thereby has an indirect secondary effect upon cardiomyocyte survival and stability, alongside contributing to cardiac remodelling and subsequent cardiac failure.

1.1.1.3 Cardiac endothelial cells and pericytes

Excluding myocyte-type cells, endothelial cells (ECs) make up the largest proportion of cardiac cells (Pinto et al. 2016). Cardiac ECs provide vital functions which underpin the maintenance of vascular homeostasis, as well as contributing to healing and vascular regeneration following myocardial injury (Lother et al. 2018). ECs are located on the innermost vascular layer of cardiac vessels, where they are critical in the successful perfusion of the heart, and in the endocardium lining cardiac chambers: here they are involved in a range of EC-to-cardiomyocyte paracrine communication pathways (Pinto et al. 2016). Cardiac ECs have been

shown to have a crucial role in the communication with immune cells, and subsequently have a role in cardiac inflammatory responses (Lother et al. 2018). Cardiac pericyte cells are perivascular cells, meaning they are found adjacent to ECs, where they provide synergetic structural support and EC stabilisation during angiogenesis, vascular maturation and vascular remodelling (Chen et al. 2015).

With regards drug-induced cardiotoxicity, ECs are now known to also play a significant contribution and underpin the development of heart failure. In cancer treatment, several therapeutics have now been shown to affect the ECs, resulting in a loss of barrier function, causing increased tissue permeability and myocardial injury (Tocchetti et al. 2020). Furthermore, ECs are believed to be the main contributor to heart failure caused by radiation therapy since cardiomyocytes and predominantly non-proliferative and considered resistant to this insult (Tocchetti et al. 2020). However, the mechanisms and interplay of ECs with cardiomyocytes in the development of drug-induced cardiotoxicity has yet to be fully addressed.

1.1.2 Cardiac contraction: Excitation-contraction coupling

Cardiac muscle contraction is dependent on the integrity of the anatomical structure of the heart. Normal physiological cardiac contraction is initiated at the sinoatrial node (SAN), with a synchronised electrical signal travelling across the atria, through the atrioventricular (AV) node located in the interatrial septum, down the bundle of His and bilateral Purkinje fibres, and across the ventricles towards the apex of the heart, culminating in contraction of the cardiac muscle. This coordinated process allows the atrial chambers to transfer blood into the corresponding right and left ventricular chambers, and then subsequently eject blood into the pulmonary artery and aorta, respectively (Silverthorn 2016).

In order for the cardiac muscle to contract, the excitation process needs to be translated into a mechanical force. Cardiac muscle is arranged into myofibrils containing contractile proteins, namely actin (thin) filaments and myosin (thick) filaments, together with regulatory proteins troponin and tropomyosin (Silverthorn 2016). Contraction involves the controlled movement of these filaments and fibres over one another, causing their shortening and a contraction (cardiac systole), followed by their relaxation (cardiac diastole) (Bers 2002). Cardiac excitation-contraction coupling describes the series of events required to translate the electrical impulse into this mechanical contraction. At the level of the cardiomyocyte, the received electrical impulse triggers the initiation of an action potential (AP) and depolarisation of the sarcolemma through the concerted action of a sequential series of ion-selective channels (Bers 2002).

The different regions of the heart exhibit a different expression and activity profile of ion channels and cell gap junction interactions to facilitate their respective roles (Bers 2002; Silverthorn 2016). The action potential triggered in atrial and ventricular cardiomyocytes, following initiation of a signal from the SAN and propagation of the contraction, has five specific phases (Figure 1.3 and table 1-1), each associated with movement of defined ions and activation of specific ion channels (Table 1-3), controlling initiation of contraction and relaxation. Upon receipt of an electrical signal from adjacent cardiomyocytes and attainment of the required threshold potential of -70mV, phase 0 of the action potential is triggered and depolarisation is initiated through activation and opening of fast Na^+ voltage-gated time-dependent channels, allowing Na^+ entry into the cell. When the membrane potential reaches approximately -40mV Ca^{2+} channels are triggered to open, allowing Ca^{2+} to flow into the cardiomyocyte. Upon reaching approximately +30mV, wherein the membrane is depolarised,

the Na^+ channels are closed and K^+ channels are activated to open, initiating a partial repolarisation of the cardiomyocyte sarcolemma and phase 1 of the action potential. As the membrane potential approaches 0mV, the rate of Ca^{2+} entry is counterbalanced by K^+ efflux from the cardiomyocyte for a short period of time, resulting in phase 2 of the action potential, termed the plateau phase. It is during phase 2 of the action potential that cardiomyocyte contraction occurs. Phase 3 of the action potential occurs when the Ca^{2+} channels that opened during phase 1 begin to close and the permeability of the cardiomyocyte to K^+ increases, triggering further K^+ channels to open and rectify the membrane potential and cause subsequent repolarisation of the cardiomyocyte. This allows the membrane potential to return to baseline and phase 4 of the action potential. In phase 4, also known as resting phase, K^+ currents are the main determinant of the sarcolemma membrane potential as specific K^+ ion channels remain open whilst Na^+ and Ca^{2+} channels remain closed. Therefore, at rest, the membrane potential is close to the equilibrium potential for K^+ at -90mV (Grant 2009; Bartos, Grandi, and Ripplinger 2015; Bers 2002).

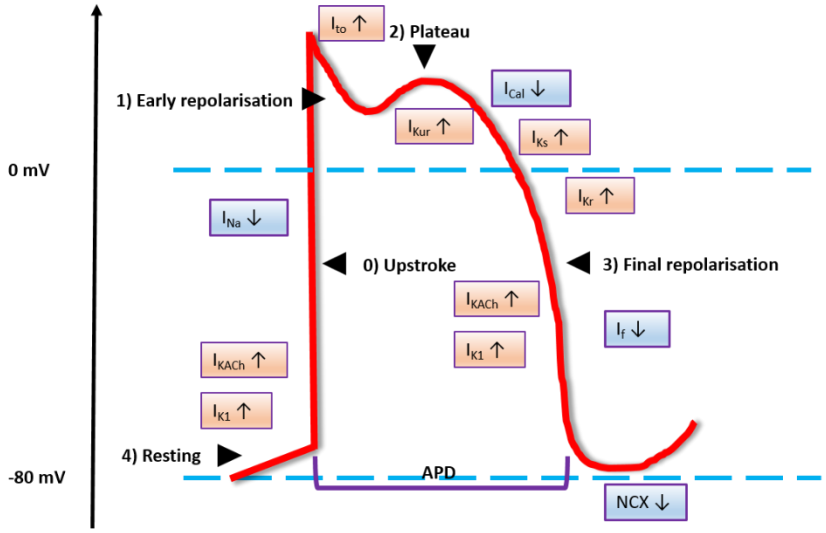

Figure 1.3 Ventricular cardiomyocyte action potential. Depolarisation and repolarisation of the sarcolemmal membrane depend on ionic current mechanisms and are modulated by the activation and inactivation of ion channels Arrows indicate movement of ions.

Phase	Comments
0	Rapid membrane depolarisation, increase of Na+ and decrease of K+ conductance
1	Membrane repolarisation
2	Plateau
3	Membrane repolarisation
4	Resting potential

Table 1-1 Phases of the ventricular cardiomyocyte action potential.

In contrast to the atrial and ventricular cardiomyocytes, an action potential of cardiomyocytes within the SAN occurs in response to spontaneous membrane depolarisation and is termed the pacemaker potential. Compared to non-pacemaker (atrial and ventricular) cardiomyocytes, those in the SAN lack phases 1 and 2 of the action potential, with the baseline of phase 4 being unstable and an action potential been triggered spontaneously by Ca^{2+} flowing into the cell primarily via T-type calcium channels. In these cells there are two principal mechanisms contributing to the initiation of the action potential, one being dominated by the I_f ionic current (known as the "funny current"), and one being dominated by the Ca^{2+} intracellular handling, which is spontaneously released from the sarcoplasmic reticulum (SR) to initiate diastolic depolarisation (Lakatta and DiFrancesco 2009).

Phase	Comments
0	Rapid membrane depolarisation, increase of Na+ and decrease of K+ conductance
3	Membrane repolarisation
4	Resting potential

Table 1-2 Phases of the SAN action potential.

Current	*Description*	*AP Phase*	*Activation Mechanism*
	Action potential: inward current channels		
I_{Na}	Sodium current	Phase 0	Voltage, depolarisation
$I_{Ca,L}$	Calcium current, L type	Phase 2	Voltage, depolarisation
$I_{Ca,T}$	Calcium current, T type	Phase 2	Voltage, depolarisation
	Action potential: Outward K^+ current channels		
$I$to,f	Transient outward current, fast	Phase 1	Voltage, depolarisation
$I$to,s	Transient outward current, slow	Phase 1	Voltage, depolarisation
I_{Kur}	Delayed rectifier, ultra-rapid	Phase 1	Voltage, depolarisation
I_{Kr}	Delayed rectifier, fast	Phase 3	Voltage, depolarisation
I_{Ks}	Delayed rectifier, slow	Phase 3	Voltage, depolarisation
I_{K1}	Inward rectifier	Phase 3 and 4	Voltage, depolarisation
I_{KATP}	ADP activated potassium current	Phase 1 and 2	[ADP]/[ATP]↑
I_{KAch}	Muscarinic-gated potassium current	Phase 4	Acetylcholine
I_{KP}	Background current	All phases	Metabolic, mechanical
I_F	Pacemaker “funny” current	Phase 4	Voltage, depolarisation

Table 1-3 Membrane currents involved in the generation of cardiac AP. *Adapted from* (Grant 2009)

As defined above, cardiomyocyte contraction occurs during phase 2 of the action potential and is driven by Ca^{2+} movement into the cardiomyocyte. The deep invaginations of the sarcolemma, known as transverse tubules (t-tubules), facilitate the entry of Ca^{2+} through L-type Ca^{2+} channels in response to membrane depolarisation driven by voltage-gated Na^{+} channels in phase 0 and 1 of the action potential, as described above. The Ca^{2+} influx into the intracellular fluid through L-type Ca^{2+} channels triggers the activation of ryanodine receptors located on the sarcoplasmic reticulum, releasing further Ca^{2+} and further increasing the intracellular Ca^{2+} concentration: a positive-feedback process known as calcium-induced calcium release (CICR) (Bers 2002) (illustrated in Figure 1.4). The free Ca^{2+} in the cytosol interacts with the myofibrils by binding to the troponin, causing troponin to undergo a configuration change. This ultimately allows actin to interact with myosin, shifting the actin filament towards the centre of the sarcomere, resulting in the contraction of the cardiomyocyte (Figure 1.4). The subsequent depolarisation of the cardiomyocyte, closure of the L-type Ca^{2+} channels, and disassociation of Ca^{2+} from the troponin complex, coupled to return of Ca^{2+} to stores in the sarcoplasmic reticulum and exportation of Ca^{2+} from the cytosol via several mechanisms including Ca^{2+} ATPase enzymes, resulting in cessation of cardiomyocyte contraction and its subsequent relaxation.

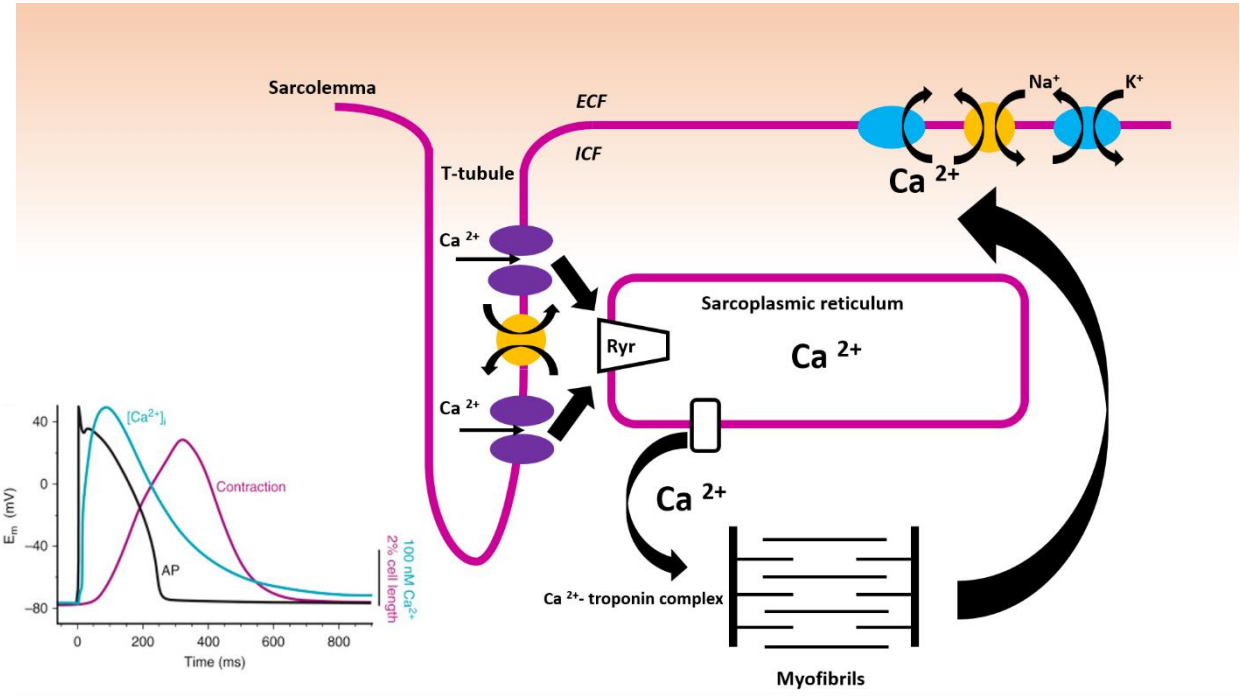

Figure 1.4. Excitation-contraction coupling mechanisms in the adult cardiac muscle. Depolarisation of the cardiomyocyte membrane, allowing calcium influx into cytosolic space via L-type Ca^{2+} channels. This triggers the release of additional Ca^{2+} stored in the sarcoplasmic reticulum, increasing levels of free Ca^{2+} in the cytosol. The release of Ca^{2+} modulates the activity of contractile proteins troponin and tropomyosin in the cardiac myofibrils, triggering muscle contraction and relaxation.

1.2 Drug-induced cardiotoxicity

Cardiotoxicity is a term first coined in the 1940's in relation to the effects on the heart observed with the use of local anaesthetics, and plant preparations derived from digitalis purpurea such as digoxin (Banerjee, Chung, and Kumar Ghosh 2018). In the 1970's, the term cardiotoxicity was increasingly used to describe the more complex cardiomyopathy-inducing effects caused by the anthracycline class of cancer chemotherapeutics (Banerjee, Chung, and Kumar Ghosh 2018). Increasing evidence and understanding of xenobiotic-induced adverse effects on the cardiovascular system have led to the evolution of the concept of cardiotoxicity as it is currently defined, inducing both cardiac dysfunction, such as dysrhythmias, ischaemia and cardiac conduction defects, and injury to cells of the myocardium (Ferdinandy et al. 2019). Several different pathophysiological mechanisms underpin the development of drug-induced cardiac dysfunction: disruption of excitation/contraction coupling mechanisms and intracellular calcium homeostasis, perturbations in mitochondrial respiration and activity, changes in cardiac rate and the force-frequency relationship, mismatch of cardiac preload and afterload, unbalancing of the dynamic relationship between cardiomyocytes and cardiac support cells, and alterations of the composition of the myocardial extracellular matrix composition (Ferdinandy et al. 2019; Melendez et al. 2020; Poluzzi et al. 2017). Adverse effects that occur at the structural level can manifest as either reversible or irreversible, involving sub-toxic effects such as increases in cellular permeability and restructuring of cellular membranes, alongside lethal irreversible damage as a result of drug-induced induction of cell death (Cardinale et al. 2020). Functional and structural drug-induced cardiotoxicities are often 'hidden', presenting only in the presence of an additional pre-existing cardiac condition, providing an explanation for the disparity in drug-induced cardiac effects between preclinical evaluation in healthy subjects and clinical use in patients with comorbidities (Ferdinandy et al. 2019; Cardinale et al. 2020).

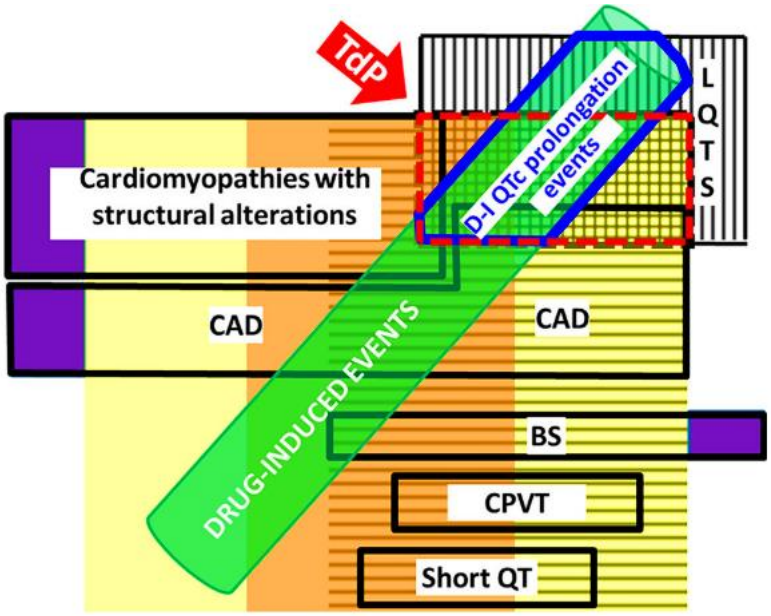

Figure 1.5 Spectrum of cardiac abnormalities associated with drug-induced events. The yellow area indicates ventricular arrhythmias overall. The orange area indicates sudden cardiac death secondary to ventricular tachyarrhythmias. Horizontal lines indicate polymorphic tachycardia and vertical lines represent QTc prolongation. Torsade de Pointes is represented by the intersection of horizontal and vertical lines. The purple area indicates atrial fibrillation, and the green area indicates events with a concurrent/causative effect of drugs used by the patient. BS Brugada syndrome, CAD coronary artery disease, CPTV catecholaminergic polymorphic ventricular tachycardia, D-I drug-induced, LQTS long QT syndrome (either genetic or acquired), TdP Torsades de Pointes" (adapted from Poluzzi et al. 2017)

1.2.1 Functional drug-induced cardiotoxicity

Disruption of cardiac ion channel mechanisms by xenobiotics can lead to the development of life-threatening arrhythmias, or to the occurrence of proarrhythmic events which can exacerbate pre-existing cardiac dysfunctions (Saxena et al. 2016). In this context, one of the most studied and well-defined ion channel disruptions involves the human ether-à-go-go (hERG) gene-related K^+ channel. Numerous studies have identified a direct relationship between drug-induced hERG potassium channel blockade and the development of asymptomatic long QT interval (Vicente, Stockbridge, and Strauss 2016), which has been directly correlated with the incidence of the dangerous ventricular arrhythmia Torsade de Pointes (TdP) (figure 1.6)(Grilo, Carrupt, and Abriel 2010). Specifically, the hERG gene encodes for the α-subunit of the I_{kr} channel, which is critical for cardiomyocyte repolarisation during phase 3 of the ventricular action potential: as a consequence of its blockade, a slower membrane repolarisation occurs thus prolonging the QT wave interval detected via surface electrocardiography (Figure 1.6). This slowed repolarisation determines the reactivation of Ca^{2+} and Na^+ channels, which in turn trigger the initiation of early afterdepolarisations (EADs). These EADs can result in a series of uncoordinated and erratic ventricular contractions, ultimately leading to TdP. A range of structurally diverse drugs, including antiarrhythmics, antipsychotics, antimicrobials and antihistamines, have demonstrated the "off target" ability to bind to the I_{kr} (hERG) channel subunit causing significant functional disturbances in cardiac rhythm (Saxena et al. 2016). Despite estimations that "as many as 60% of novel molecular entities developed as potential therapeutic agents, when assessed for hERG blocking liability, test positive and are thus abandoned early in development" (Poluzzi et al. 2017; Gintant, Sager, and Stockbridge 2016a; Sager et al. 2014) recent evidence clearly suggests that hERG blockade alone is not specific for the prediction of early afterdepolarisation or other forms of proarrhythmia (Gintant, Sager, and Stockbridge 2016b). For example, the antiarrhythmic drug verapamil is a potent I_{kr} blocker but does not cause significant QT prolongation due to its ability to simultaneously block the inward I_{CaL} channel Cav1.2 subunit which buffers the effects of the I_{kr} outward current blockade (Gintant, Sager, and Stockbridge 2016a).

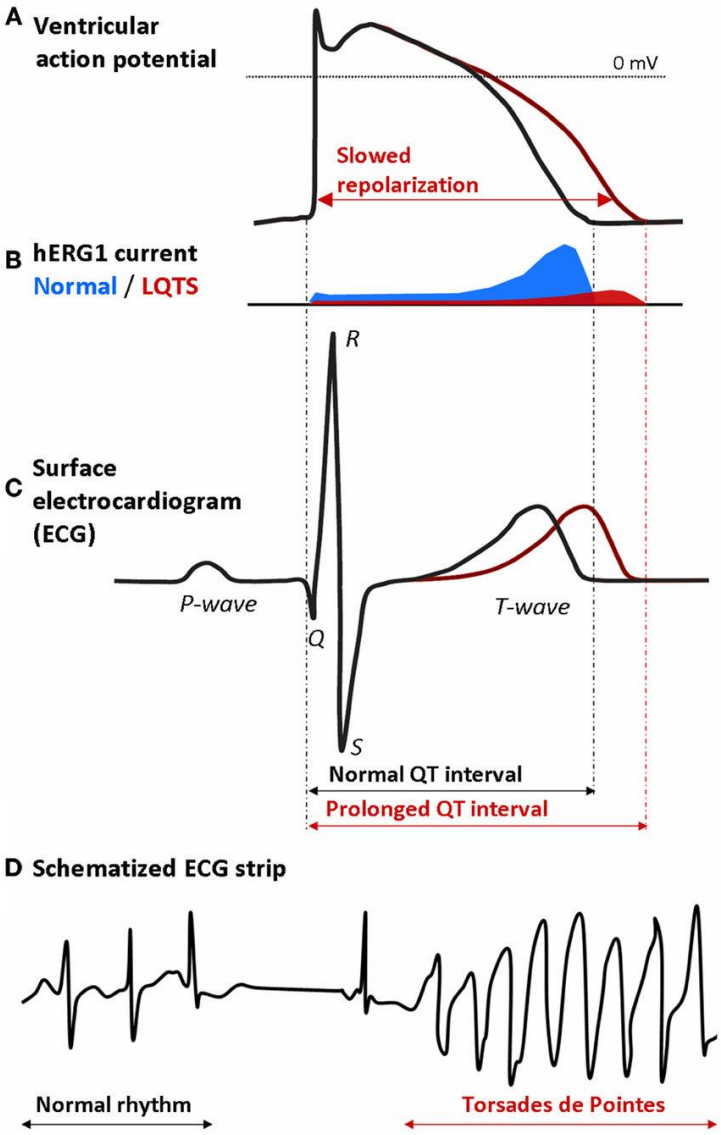

Figure 1.6: Correlation between hERG channel blockade and development of TdP. Prolongation of cardiac AP, observed on ECG as a prolongation in QT interval, is directly correlated to the development of the ventricular arrhythmia Torsade de Pointes (TdP) (adapted from Grilo et al, 2010)

Despite evidence suggesting that hERG channel blockade underlies the majority of drug-induced cases of QT prolongation, functional cardiotoxicity is not exclusively mediated by the disruption of hERG. A series of leading studies by Hondeghem and Katzung, and subsequently expanded by Campbell and Vaughn-Williams, demonstrated that drug-mediated Na^+ channel interactions are time and voltage dependent (Hondeghem and Katzung 1977; Vaughan Williams 1989).

The lack of tight association between hERG inhibition and clinical development of TdP led to concerns by several pharmaceutical and drug development companies as to the predictability and specificity of hERG inhibition as an indicator of clinical TdP risk, as dictated by the ICH S7B guidelines (E14/S7B 2020). Additionally, the value of non-human species for determination of functional and structural cardiotoxicity, in light of clear species-related differences, has also been questioned as a factor in drug attrition in preclinical development because of perceived cardiac liabilities (Fermini et al. 2016). Such issues have now led to the development of a new paradigm for preclinical evaluation of drug-induced cardiac liabilities, the Comprehensive *in vitro* Proarrhythmia Assay (CiPA) ("Https://Cipaproject.Org/" n.d.). The CiPA defines proarrhythmic risk based on an integrated assessment of drug effects on multiple ion channels, in silico reconstructions of human ventricular electrical activity, confirmation of effects in human stem-cell derived cardiomyocytes (hSC-CMs) and finally clinical ECG of the drugs in early phase clinical trial. This assay paradigm ultimately provides an assessment of drug-induced cardiac liabilities based on multi-parametric integrated signatures of human cardiomyocyte responses, as opposed to the single ion channel and non-human evaluation outlined in the ICH S7 guidelines. The potential greater predictability of the CiPA will only become apparent over the next few years, but outcomes so far have supported the value of this approach (Vicente, Stockbridge, and Strauss 2016).

1.2.2 Drug-induced structural cardiotoxicity

Structural cardiotoxicity comprises two associated but distinct definitions: i) the alteration in overall cardiac cellular balance as a consequence of drug-induced loss of cardiac cells, resulting in cardiac restructuring, ii) the modification of sub-cellular components of cardiac cells, such as the cytoskeleton or mitochondria, resulting in a change in cellular morphology or a change in cellular contractility (Pointon et al. 2013; Doherty et al. 2015). Structural cardiotoxicity can manifest in the clinic as a cardiomyopathy, caused by the imbalance of cardiomyocytes versus cardiac support cells, or changes in cellular morphology and overall 'shape'/size of the heart (Higgins, O'Halloran, and Chang 2015; Zamorano et al. 2016; Michel and Rassaf 2019). Unlike functional (electrophysiological) cardiotoxicity, structural cardiotoxicity is commonly irreversible. Several classes of drugs have demonstrated direct structural cardiac or more widespread vascular alterations, including antiretroviral compounds, antidiabetics and several substances of abuse (Ferdinandy et al. 2019). The most notable direct structural cardiotoxicants, however, belong to the oncological chemotherapeutic class of drugs, which notoriously include anthracyclines, kinase inhibitors, immunotherapeutic agents and other novel targeted therapies (Zamorano et al. 2016).

1.3 Drug-induced cardiotoxicity of oncology therapeutics

Recent progress in the development of oncological therapeutics over the past decade has significantly increased therapeutic outcomes and patient survival. The downside to this success is that this is unfortunately often associated with adverse toxic effects, with a tangible increase of chemotherapy-induced cardiac damage (Alameddine et al. 2014; Dy and Adjei 2013; Raschi et al. 2010; Tocchetti et al. 2020). Furthermore, improvements in patient survival raise an issue with cardiotoxicity as the long-term detrimental effects of the specific therapeutics are now becoming apparent, significantly impacting upon a patient's quality of life (Mann and Krone 2010). The prognosis of a patient presenting with drug-induced cardiotoxicity worsens dramatically, often overtaking the underlying primary condition, thus outweighing the therapeutic risk-to-benefit ratio (Higgins, O'Halloran, and Chang 2015).

Cancer chemotherapy over the past decade has undergone significant advancements, moving from approaches based on 'conventional' chemotherapies, inhibiting cellular division and inducing cell death, to one which now incorporates 'molecular targeted' therapies focused on targeting the molecular characteristics and exploiting the hallmarks of cancer (Hanahan and Weinberg 2011). An underlying theory behind this effort is that by making cancer therapeutics more targeted, some of the toxicities seen with conventional cytotoxic chemotherapeutics could be eliminated or at least ameliorated. This unfortunately has not been the case for many chemotherapy-related toxicities, cardiovascular toxicity included. One hypothesis was that the cardiovascular toxicity associated with cancer chemotherapy was due to the activity of the 'conventional' cytotoxic chemotherapeutic agent administered alongside the 'molecular-targeted' therapeutic within the regimen (Swain, Whaley, and Ewer 2003), and that the toxic effects would be removed with increased targeting of cancer therapies (Ky, et al., 2013). However, this simplistic hypothesis has now been invalidated due to our greater understanding of molecular pharmacology and improved understanding of drug-induced cardiovascular toxicity in cancer patients (Dy and Adjei 2013; Eschenhagen et al. 2011; Poluzzi et al. 2017). Many of these molecular-targeted agents have demonstrated adverse effects upon the heart, from mild electrophysiological changes, to myocarditis and fatal heart failure (Bellinger et al. 2015; Varricchi et al. 2017). Consequently, we now know that drug-induced detrimental effects upon the heart are not limited to the 'conventional' cytotoxins or a single

type of therapeutic but are an inherent problem with many oncology agents, including molecular-targeted agents (Bellinger et al. 2015; Tocchetti et al. 2020).

Cardiotoxicity induced by oncology therapeutics, both 'conventional' and 'molecular-targeted', can elicit both functional and structural effects, and can be classified into three types: symptomatic acute toxicity occurring soon after administration, and early- and late-onset toxicity, occurring before or after one year of treatment, respectively (Bagnes, Panchuk, and Recondo 2009; Curigliano et al. 2010). In order to address the clinical issue and current high level of attrition during cancer drug development, efforts are needed to better understand the mechanistic basis of drug-induced cardiotoxicity in oncology, both in the acute and longer term, and in preclinical studies to predict cardiotoxicity of putative chemotherapeutics. In order to fulfil this objective better predictive and translatable models for assessment of drug-induced cardiotoxicity, amenable to molecular characterisation and manipulation, and models with scope for integrated evaluation of both functional and structural cardiotoxicity are urgently required.

The cytotoxic and antineoplastic functions of chemotherapeutics determine the development of adverse effects, resulting in a range of cardiovascular problems including functional abnormalities, dysrhythmias and cardiac conduction defects, alongside structural effects, such as cardiomyocyte death and cardiac remodelling, cellular hypertrophy, and drug-induced cardiomyopathies (Varricchi et al. 2017; Gill et al. 2019). Although several cancer chemotherapeutics are reported to cause acute effects, such as drug-induced proarrhythmias observed with kinase inhibitors and conduction disturbances associated with the newly identified immune-checkpoint inhibitor drugs, a more prevalent problem is development of delayed cardiotoxicity as a consequence of the required cellular-lethal nature of many of these drugs (Gintant, Sager, and Stockbridge 2016a). Consequently, improved understanding and better preclinical models for prediction and evaluation of sub-acute drug-induced cardiotoxicity of cancer chemotherapeutics are required.

1.3.1 Histone/Lysine deacetylases (HDACs/KDACs) and their Inhibitors as therapeutic agents

Histone deacetylases (HDACs) are known to be essential players in the posttranslational regulation of several processes and pathways, dysregulated in many diseases such as inflammatory conditions, and notably, cancer (R. R. Shah 2019; Gryder, Sodji, and Oyelere 2012a). The action of these enzymes was primarily characterised by their central role in nucleosomal histone deacetylation, as main drivers of epigenetic regulation of genetic expression (Falkenberg and Johnstone 2014). However, although initially believed to act purely as epigenetic regulators, this family of proteins is now known to play a role in acetylation of several proteins involved in regulation of both nuclear and cytoplasmic cellular functions (Toro and Watt 2020; Delcuve, Khan, and Davie 2012). These activities include DNA damage repair, RNA splicing, cell cycle control, metabolism, and cytoskeletal remodelling (Delcuve, Khan, and Davie 2012). Members of this enzyme family also display tissue and organ-specific roles: for instance, recent discoveries evidenced their involvement in cardiac-related events including fibrotic processes, hypertrophy protection, metabolic functions and contractility (Schiattarella et al. 2016; Weeks 2019). Consequently, recent studies have reclassified this enzyme family as lysine deacetylases (KDACs), rather than HDACs, to better represent their diverse activities (Toro and Watt 2020).

Mammalian HDACs/KDACs are currently categorised into four different classes, based on similarities in their genetic and protein sequence and function (West and Johnstone 2014). Three of the classes, I, II and IV, are zinc-mediated modulatory enzymes, whereas the class III sub-family comprises the Sirtuins (SIRT1–7), which although share features with both class I and class II HDAC enzymes, are NAD+ dependent and functionally and structurally distinct (McKinsey 2012; De Ruijter et al. 2003). The sirtuin family is therefore omitted when considering the functions and roles of HDACs/KDACs, with the focus being upon those enzymes reliant on zinc for their catalytic activities (McKinsey 2012). In terms of members for each of the HDAC/KDAC sub-families; Class I of the family is comprised of HDAC/KDAC-1, -2, -3 and -8, all of which have the simplest structure; class II is subdivided into class IIa comprising HDAC/KDAC-4, -5, -7 and -9 and class IIb consisting of HDAC/KDAC -6 and -10; class IV

HDAC/KDAC is a single member family of HDAC/KDAC11. These sub-families are indicated in Figure 1.6.

HDACs/KDACs are expressed in different subcellular areas of the cell, with class I being expressed predominantly in the nucleus and playing a role in histone acetylation, acting as the 'conventional' HDAC with a primary role in epigenetic regulation (Delcuve, Khan, and Davie 2012). Class II HDACs/KDACs either remain in the cytoplasm wherein they post-translationally regulate activity of proteins, as demonstrated by class IIb HDAC6 mediated acetylation and stabilisation of tubulin, or shuttle between the cytoplasm and the nucleus wherein they regulate subcellular location of specific proteins and participate in macromolecular signalling pathways, demonstrated with HDAC4 and 5 (Toro and Watt 2020). A clear difference in function between class I and class IIa enzymes is also evidenced by the fact that class IIa enzymes demonstrate very little deacetylation activity, implying their primary role is unlikely to be primarily enzymatic in nature (Parra 2015). With regards class IV (HDAC/KDAC 11), despite having similarity to class I and class II and weak deacetylase activity, its role is believed to be primarily as a fatty-acid deacylase enzyme rather than a deacetylase (Kutil et al. 2018). Taken together, further to the differential roles and sub-cellular localisation of the HDACs/KDACs, emerging evidence increasingly now suggests that due to their complex regulatory and multi-functional roles, HDACs/KDACs should be considered as subunits of large regulatory complexes, facilitating a plethora of cellular activities (Toro and Watt 2020). For the purposes of this thesis, these enzymes will be termed HDACs rather than KDACs, due to the predominant use of this nomenclature within the literature.

The ever-increasing association between HDAC expression and activity and development and progression of a wider number of diseases, especially cancers, led to development of inhibitors of HDACs as a therapeutic strategy. However, despite considerable efforts and many putative inhibitors being produced, only a very small number of pan-class inhibitors have actually progressed into the clinic to date as anticancer agents most notably the hydroxamates vorinostat, panobinostat and belinostat (R. R. Shah 2019). The improved and evolving appreciation of the role of specific deacetylase enzymes and sub-classes, and their associations with other non-cancer diseases, is however reinvigorating excitement in the

development of class or isoform-selective deacetylase enzyme inhibitors, with several such therapeutics in advanced clinical trials (Kulka et al. 2020).

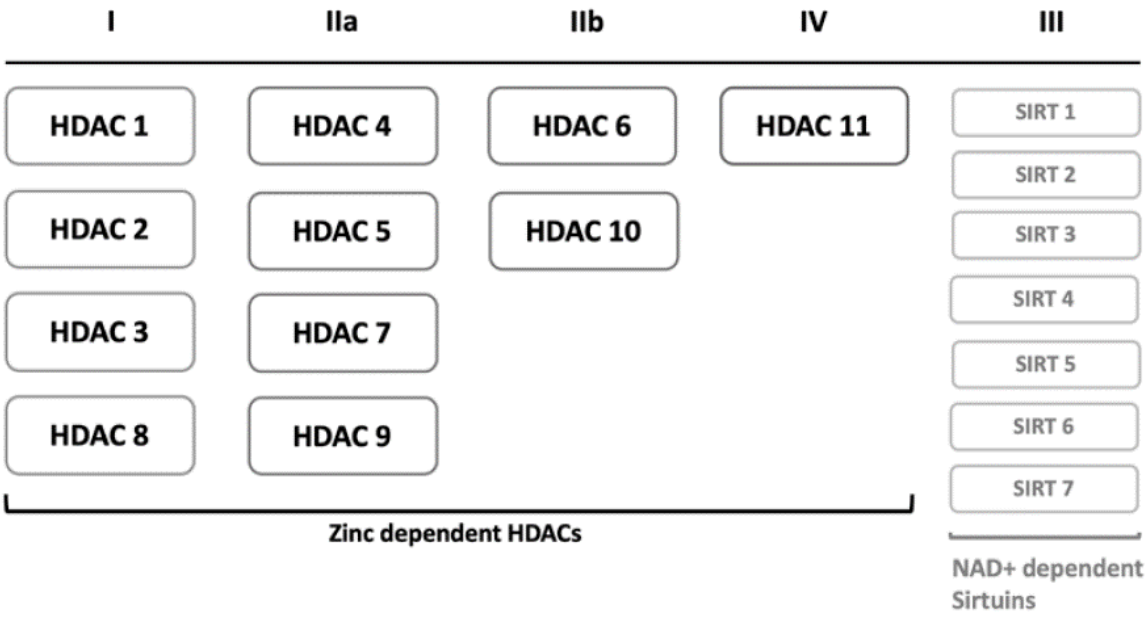

Figure 1.7. Classification of histone deacetylase family members.

1.3.2 Cardiotoxicity of HDACi

Inhibition of HDAC activity is showing significant promise as a therapeutic strategy, initially in cancer but now also in a range of other diseases including neurodegenerative disorders amongst others (Rodrigues et al. 2020). Since entry to the clinic, an increasing number of reports suggest an association with the development of cardiac adverse reactions , and there are now several reports of acute adverse effects in patients undergoing treatment with HDACis (M. H. Shah et al. 2006; R. R. Shah 2019). In patients undergoing HDACi treatment, a number of ECG changes, including QT prolongation and ST wave changes were observed (R. R. Shah 2019). In the case of the HDACi depsipeptide, during clinical trials alongside asymptomatic cases of ventricular tachycardia and delayed cardiac repolarisation, a case of fatal ventricular arrhythmia was reported (Lane and Chabner 2009; Gryder, Sodji, and Oyelere 2012b; R. R. Shah 2019). Similarly, asymptomatic delayed cardiac repolarisation, ventricular tachycardia and unsustained torsade de pointes, was detected during clinical trial of the HDACi LAQ824 (Rowinsky et al. 2004). During preclinical studies of this depsipeptide, although moderate cardiomyopathy, elevated serum cardiac enzymes, and prolonged cardiac

repolarisation were detected in dogs, there was no evidence to support drug-induced cardiac dysrhythmia and associated risk of fatality (M. H. Shah et al. 2006). This observation raises a question as to predictability of QT-prolongation for detection of life-threatening dysrhythmias with these drugs, with involvements of other ion channels or molecular factors potentially implicated (Noonan et al. 2013).

At present there are four HDACi currently approved in the clinic, vorinostat (SAHA), Romidepsin (FK228), belinostat (PXD101) and panobinostat (LBH589) for cancer therapy, predominantly against non-solid haematological malignancies (Kulka et al. 2020; R. R. Shah 2019). All of these HDACi are linked to potential development of cardiotoxicity, with Panobinostat (the most potent of the approved HDACi) carrying a black box warning for severe cardiac abnormalities. As was the case with depsipeptide and LAQ824, several other similar pan-HDACi were also developed but failed to progress due to concerns regarding drug-induced cardiotoxicity (Suraweera, O'Byrne, and Richard 2018; Gryder, Sodji, and Oyelere 2012b; Shultz et al. 2011). The underlying cause of the cardiotoxicity observed with these pan-HDACi hydroxamate-containing drugs is as yet still unresolved. It is unclear whether the adverse cardiac effects are a consequence of HDAC inhibition, a drug class effect or are due to the specific chemical structure in light of all these drugs containing highly reactive hydroxamate active headgroups. A further complexity is the fact that significant cardiotoxicity with depsipeptide was detected in the clinic in patients with metastatic neuroendocrine tumours but not in patients with haematological malignancies, potentially implying the presence of 'hidden cardiotoxicity' as a contributory factor in this context (M. H. Shah et al. 2006; Cardinale et al. 2020).

In an effort to improve therapeutic efficacy, develop drugs against specific HDAC associated with a disease, and to reduce potential off-target toxicities and adverse effects, significant efforts have been focused on development of class-selective or isoform-selective HDACi (Kulka et al. 2020). The vast majority of the drugs under development being class I selective. Such drugs would be expected to exhibit differential effects upon the heart due to their involvements in cardiac hypertrophy and cardioprotection. Class I HDACs are reported to demonstrate pro-hypertrophic effects (Morales et al. 2016). Therefore, specific inhibition of class I HDACs would be hypothesised to retard cardiac hypertrophy. In contrast, the class IIa HDAC, HDAC4, which is protective against cardiac hypertrophy would potentially exacerbate cardiac hypertrophy if inhibited (Backs et al. 2006; Xian Zhang et al. 2018). The caveat being

that due to the limited deacetylase activity exhibited by class IIa HDAC, any effects of HDACi would not be a consequence of enzyme inhibition but rather a factor of its predicted nuclear-cytoplasmic transportation capacity. Evidence for potential reduced toxicity of class I selective HDAC-inhibition, relative to pan-HDACi, is provided by the observation that entinostat (MS-275), a benzamide rather than a hydroxamate HDACi, showed efficacy against breast cancer in the absence of detectable adverse cardiac toxicity (Yardley, Ismail-Khan, and Klein 2011). Additionally, class I selective HDAC have also been shown to exhibit very limited effects on cardiac sodium currents and gap junctions, unlike pan HDACI, offering an additional advantageous mechanism to support the potential for reduced cardiotoxicity of class I selective HDACi (Xian Zhang et al. 2018) . Interestingly, the class IIb HDAC6 has been implicated in modulation of acetylation of the cardiac sodium channel Nav1.5 restricting its surface translocation and subsequent function, implying that specific inhibition of this isoform may be beneficial to prevention of cardiac arrhythmias (Xian Zhang et al. 2018). However, the significance of this for HDAC-selective drug development is as yet uncertain. Greater understanding the underlying mechanisms that contribute to cardiotoxicity of HDACi and the involvement of specific sub-classes and isoforms is necessary to mitigate putative HDACi-induced cardiotoxicity in the clinic and development of HDACi with an improved therapeutic index. Evaluation of HDACi against relevant cellular cardiac models is therefore necessary to identify and improve our understanding in this context.

1.4 Preclinical assessment of drug safety

In the drug development process, early decision-making is essential to avoid progression of detrimental compounds which could result in significant liabilities and financial loss. Early identification of safety issues is therefore a fundamental process that begins at the early stages of project development, as early as at target validation stages, and continues through to *in-vivo* studies and clinical development stages (figure 1.8) (Bendels et al. 2018; Bowes et al. 2012; Hornberg et al. 2014). In this context, early *in-silico* and *in-vitro* pharmacological profiling was shown to provide major improvements towards the successful progression of late-stage clinical development (Bowes et al. 2012). In particular, *in-vitro* pharmacology profiling is increasingly implemented to assist with specific phases of the drug development process, and this can be categorised into three main objectives specific to each project phase:

- hazard identification through early target identification/validation stages,
- hazard elimination through hit-to-lead and lead optimisation stages,
- mechanistic toxicology studies through candidate selection, preclinical and clinical development phases (Bowes et al. 2012).

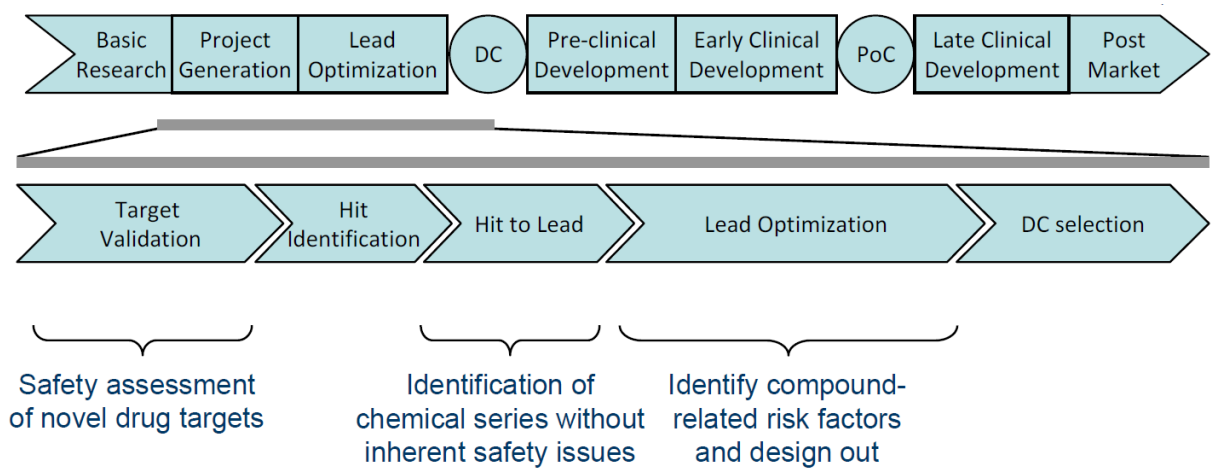

Figure 1.8 Stages and scope of safety assessments in relation to the drug discovery pipeline. The drug discovery timeline is shown left to right**.** DC = development candidate, PoC = proof of concept.

The alignment of *in-vitro* pharmacology and toxicology profiling to the drug development process allows to obtain a more comprehensive mechanistic understanding of the drug candidate before its introduction to first-in-human-trials. However, target assessment panels adopted across the industry have been designed to only cover a limited range of essential key targets, with the main rationale reflecting the cost-to-benefit ratio of an assessed target compared to the magnitude of the impact resulting from its hit (Bowes et al. 2012). Nonetheless, the development and integration of *in-vitro* models with the potentiality to screen for a wider array of targets would facilitate not only the understanding of the drug candidate pharmacological profile with a higher level of confidence, but also help address the translation of *in-vitro* findings to the clinic, whilst retaining cost feasibility. Additionally, effective *in-vitro* profiling has the potential of significantly improving the design of *in-vivo* studies, ultimately providing improvements towards the NC3R principles (Replacement, Reduction and Refining) for the use of animals in research (Https://nc3rs.org.uk/the-3rs 2020).

The routine implementation of various *in-vitro* methodologies in the drug discovery pipeline is a constantly evolving area, reliant on the continuous commitment and collaboration of regulatory, industry, government and academic experts to achieve scientific consensus. To ensure this, the International Council for Harmonisation of Technical Requirements for Pharmaceuticals for Human Use (ICH) has gradually established a set of ICH guidelines to promote the adoption of updated research methodologies and common standards (Https://www.ich.org/ 2020). While the establishment of such guidelines has allowed to considerably improve the introduction of safe and effective medicines onto the market, improvement and optimisation of new safety guidelines are still required, particularly in the nonclinical evaluation of cardiotoxicity.

1.4.1 Preclinical detection of drug-induced cardiotoxicity

Current methods used in regulatory-compliant preclinical cardiotoxicity screening do not fully reflect the complexity of the human heart as they generally rely on overly-simplistic techniques and models, with significant limitations in the detection of both functional and

structural cardiotoxicity (Gintant, Sager, and Stockbridge 2016a). These methods involve varying models that differ in terms of complexity ranging from highly complex *in-vivo* models to simpler tissue sections and simple single-cell electrophysiology studies. Several clinical cases in the last three decades, starting in the 1990s, linked the prolongation of QT interval to the development of life-threatening arrhythmias (Pollard et al. 2010; Redfern et al. 2003), particularly the rare and potentially fatal arrhythmia TdP, leading to the withdrawal of several compounds (R. R. Shah 2005). Consequently, the establishment of non-clinical guidelines for assessing the potential of a chemical entity to delay ventricular repolarisation was implemented by regulatory bodies in 2005. These regulatory guidelines are known as ICH S7B, and are complementary to the ICH S7A guidelines on safety pharmacology studies for human pharmaceuticals (E14/S7B 2005; Darpo, Nebout, and Sager 2006); the principles of the ICH S7B guidelines rely fundamentally on the study of hERG in *in-vitro* I_{kr} assays as well as *in-vivo* QT prolongation assessments.

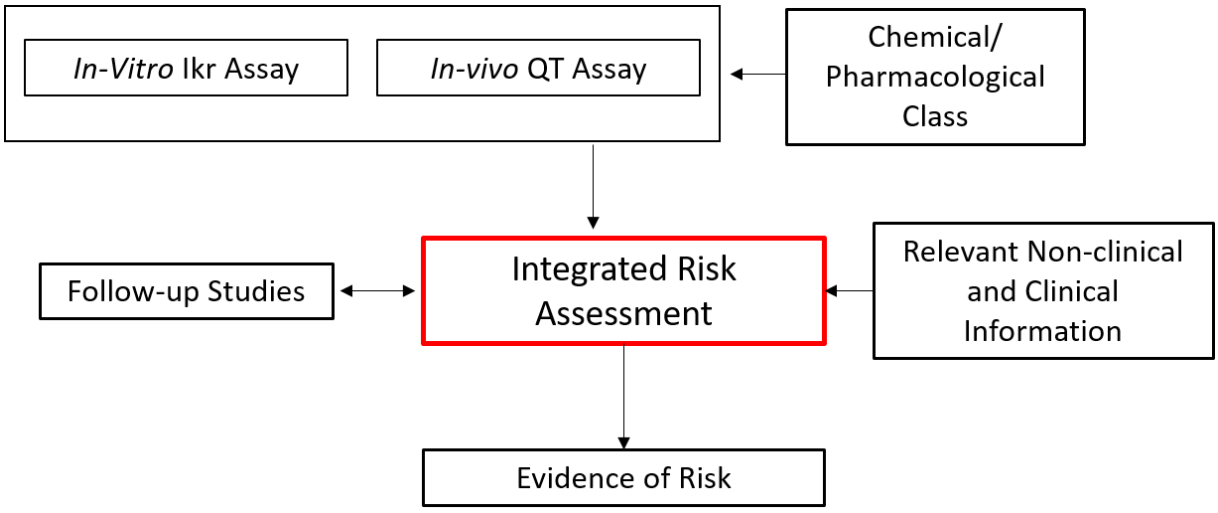

Figure 1.9 Nonclinical integrated testing strategy based on ICH guidelines.

At present, detection of markers of cardiac damage and telemetry monitoring in animals are still the principal nonelective methods used to screen for drug-induced cardiac effects *in-vivo*, looking primarily for the development of hazardous arrhythmias and QT interval prolongation, particularly focusing on avoidance of TdP. Considering the complexity of cardiac anatomy and physiology, it is evident that these methods offer insufficient predictivity and a generally

limited overview of the mechanisms involved in drug-induced cardiac damage. The increasingly evident limitations of current ICH guidelines for cardiac toxicity assessments have recently led to the re-contextualisation of the current pharmaceutical/bioindustrial needs (Sager et al., 2014). Several assays have been designed in order to detect hERG channel blockade in the early stages of compound development: currently, these assays mainly rely on *in-vitro* assessments of the I_{Kr} current in mammalian cell lines expressing recombinant hERG (Grilo et al., 2010). Since the ICH guidelines are non-prescriptive, this is achieved using a number of different protocols. The disadvantages of these type of assays firstly lie in their non-native nature, as recombinant hERG channels often do not comprise all the subunits observed in native hERG expression: despite some evidence suggesting that not all subunits are routinely needed for the purpose of the assay (Cavero et al. 2016), more physiologically-relevant cardiac tissue models would provide improved pharmacological insights. A second major disadvantage lies in the lack of standardisation of these types of assays, consequently leading to the production of highly variable data. Factors such as conditions settings and measurement methods vary between different pharmaceutical laboratories, and have been proven to heavily affect the safety evaluations and regulations for a given novel compound (Sager et al. 2014).

The development of novel technologies, including the advent of induced pluripotent stem cell derived cardiomyocytes (hiPSC-CM) and three-dimensional tissue culture techniques, has opened opportunities in terms of improving current preclinical cardiotoxicity screening. As one of the major issues in current cardiac safety testing is the high variability of data and biological platforms, industrially manufactured iPSC models offer a more robust alternative, suitable for high throughput screening (Clements et al. 2015). These advances have led to the establishment of the Comprehensive *In-vitro* Proarrhythmia Assay (CIPA) project, with the overall aim to facilitate the implementation of a new paradigm for assessment of TdP through the integration of novel *in-vitro* technologies with predictive in-silico methodologies (“Https://Cipaproject.Org/” n.d.). In particular, the CIPA initiative was designed to involve multiple working streams, each focusing on a core aspect of Proarrhythmia evaluation. These working streams involve the integration of individual ion channel studies, in-silico electrophysiology modelling, use of human stem-cell derived cardiomyocyte platforms and relevant assays, and use of ECG monitoring in humans. Among the CIPA main objectives are i) the standardisation and integration of these different streams, and ii) the subsequent

application of such standardised protocols to guide the clinical assessment of compounds (Fermini et al. 2016; Vicente, Stockbridge, and Strauss 2016). The substantial progress of the CIPA initiative and ICH safety guidelines to date have very recently led to the revision of some of the ICH S7B guidelines (E14/S7B 2020). While these important improvements are expected to positively impact preclinical cardiotoxicity screening in the near future, effective methodologies for the detection of structural cardiotoxicity currently remain mostly unsolved.

1.4.2 In-vitro cardiac cell models

Preclinical cardiotoxicity screening studies are typically focused on individual aspects of drug-induced events, where only a few will result in a significant association with TdP (Poluzzi et al. 2017), making current preclinical predictive evidence largely incomplete or not fully reliable. Whilst the assessment of specific proarrhythmic factors can be informative in relation to the most severe acute cardiotoxic events such as TdP and sudden cardiac death (SCD), novel preclinical predictive methods should be focused on a more inclusive and high-throughput screening, directed at the detection of sub-acute and structural effects. A limited number of cardiac cell-based *in-vitro* platforms is available, including isolated *ex-vivo* whole tissue perfused preparations, and primary CMs from medium and large animals (i.e. Rabbits, dogs) which are currently considered the gold standard for pharmacological target and proarrhythmia investigations (Sala, Bellin, and Mummery 2017). Despite recapitulating cardiac physiology with a high degree of complexity, primary perfused tissues and isolated CMs retain substantial inter-species differences, and are not scalable to support high-throughput screening (Sala, Bellin, and Mummery 2017). Similarly, primary CMs derived from human cardiac tissue obtained from surgical procedures, whilst providing a phenotypically mature and relevant model cannot be harvested on a large scale, and as such their use for standardised preclinical screening is very limited. The advent of human induced pluripotent stem cell derived CMs has drastically improved the scalability and standardisation of *in-vitro* cardiac models: hiPSC-CMs are currently increasingly implemented in preclinical cardiotoxicity screening, and are one of the pillar models within the CIPA paradigm. While the potential of hiPSC-CMs for use in preclinical screening has been abundantly documented, a number of limitations associated with this model remain unresolved, particularly in relation to its immature phenotype, electrophysiological differences and, not least, high maintenance costs

(Garg et al. 2018; Magdy et al. 2018). A limited number of immortalised cardiac cell lines is available, including the rat H9C2 non-contractile cardiomyoblast cell line, the HL-1 contractile murine atrial cell line and the non-contractile AC10/AC16 human ventricular cell line. Cell lines, unlike primary and hiPSC models, present the distinctive advantage of being continuously expandable, thus providing an unlimited and scalable source of CMs at relatively low maintenance costs. These models, particularly the HL-1 murine cardiomyocyte cell line and the AC10/AC16 human cardiomyocyte cell lines, have not been fully investigated for their potential in high throughput preclinical cardiotoxicity applications. Given the established limitations of the currently implemented models for the detection of sub-acute and structural cardiotoxicities, cell lines represent a potential source of relevant models for early toxicity screening. A full appraisal of hiPSC-CMs, HL-1 and AC10 cell models is discussed in chapters 3, 4 and 5, respectively.

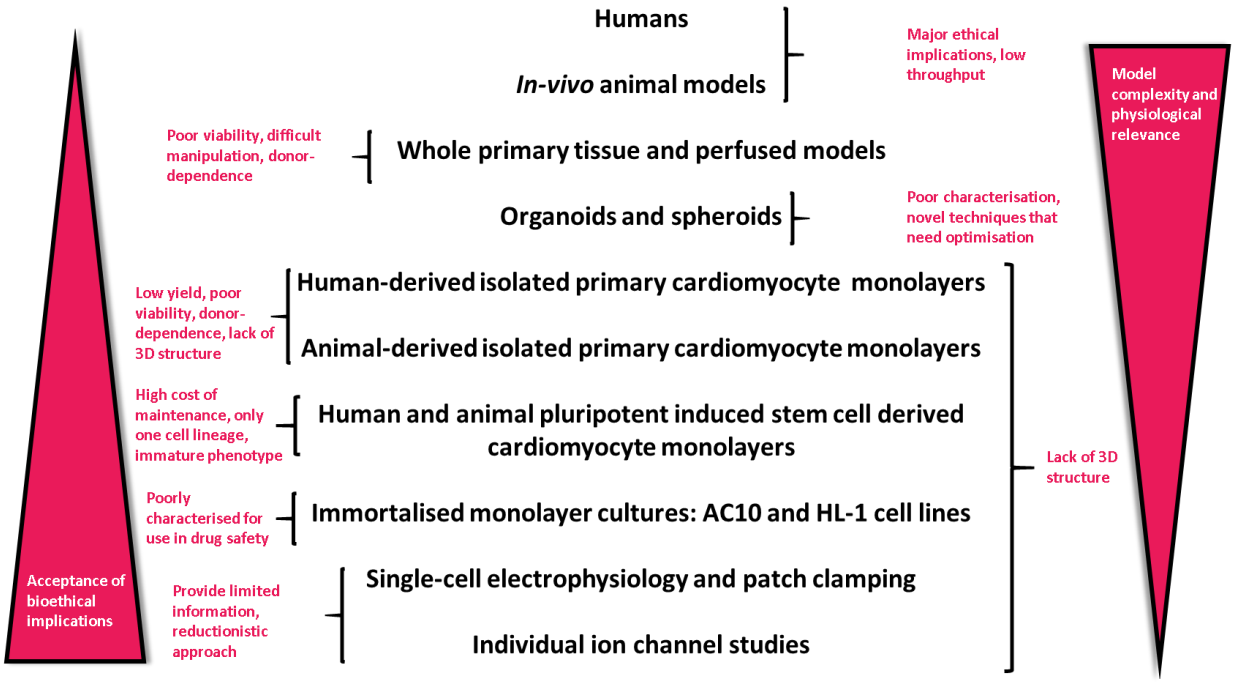

Figure 1.10 Range of cardiac models. Cardiac models ranked based on model complexity and physiological relevance vs model acceptance and bioethical implications.

1.5 Thesis aims and objectives

The overall aim of this thesis is the characterisation and evaluation of the predictive potential of *in-vitro* cardiac cell models for the assessment of drug-induced structural and functional cardiotoxicity, and the subsequent model qualification for preclinical drug-induced cardiotoxicity screening. Specifically, this research builds upon previous studies utilising hiPSC-CM models and is aimed at qualifying and integrating the HL-1 murine atrial cell line and the AC10 human ventricular cell line as additional screening tools within the drug safety assessment pipeline.

In addition to evaluation of 'standard' and known cardioactive drug panels with cardiotoxicity liability, this study aims to evaluate the potential for, and mode-of-action of, acute and longer-term cardiotoxicity of the histone deacetylase inhibitor (HDACi) class of molecular-targeted therapeutics, which have recently progressed into clinical use. Through the integrated use of 'conventional' cell and molecular biology methodologies with state-of-the-art real-time impedance-based technologies (xCELLigence RTCA), drug-induced effects upon cardiomyocyte viability and functional contractility, hyperplasia, and hypertrophy will be discussed. Additionally, the project evaluates the development of *in-vitro* three-dimensional cardiac models using these cell lines, in combination with cardiac fibroblasts and endothelial cells, and compares their potential to detect drug-induced cardiotoxicity to two-dimensional cardiac cell models. Furthermore, considering the current inadequacy and lack of preclinical *in-vitro* models for the detection of structural liabilities, this project additionally addresses currently unmet needs by qualifying cell line-based models for the detection of structural perturbations.

The overall objectives for this project are as follows:

- Characterisation of *in-vitro* growth and cardiac phenotype of HL-1 and AC10 cell line models, with subsequent establishment of protocols for use in high-throughput drug toxicity studies
- Evaluation of drug-induced functional and contractile alterations of hiPSC-CM, and HL-1 cellular monolayers, using the xCELLigence real-time analyser (RTCA) systems

- Evaluation of drug-induced cellular structural alterations of hiPSC-CM, HL-1 and AC10 cellular monolayers, using the xCELLigence real-time analyser (RTCA) systems
- Characterisation and evaluation of structural drug-induced cardiotoxicity in cell line-based three-dimensional spheroid models
- Application of the cardiac cell models characterised within this project to identify and predict the potential for drug-induced cardiotoxicity of the HDAC drug class, appraising differences between pan-isoform and isoform-selective inhibitors.

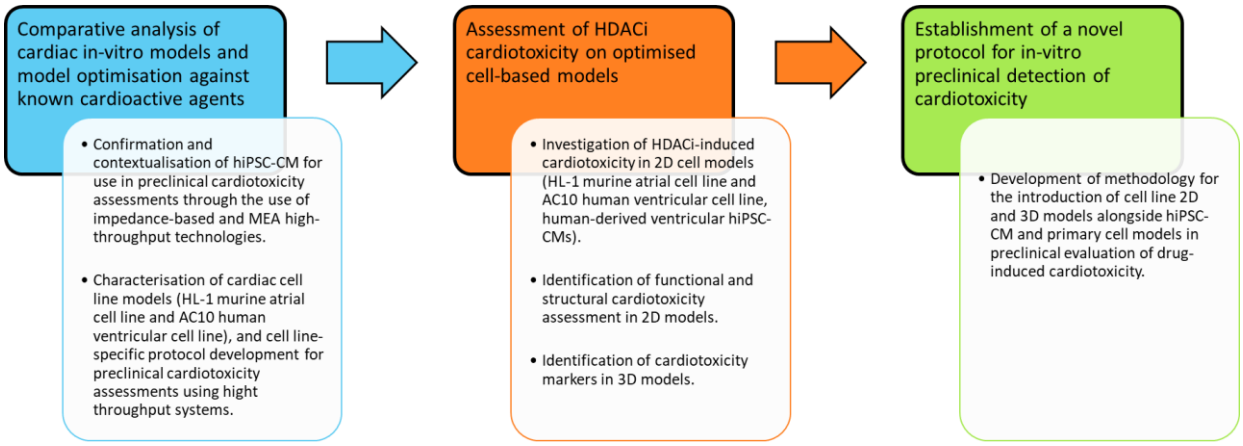

Figure 1.11 The project phases. Outline of the different project phases, aiming at the characterisation of *in-vitro* cardiac cell models for assessments of drug-induced structural and functional cardiotoxicity, and their subsequent implementation in preclinical evaluation of cardiotoxicity.

2 General materials and methods

2.1 Material source

Unless otherwise stated, all reagents were purchased from Sigma - Merck, UK.

2.2 Drug and compound treatment

All tested compounds were weighted in a high precision analytical balance and diluted in 100% dimethylsulfoxide (DMSO) unless otherwise specified, with a final concentration that never exceeded 0.1% DMSO.

2.3 Two-dimensional adherent tissue and cell culture

All cell and tissue cultures were routinely maintained in CO_2 incubator at 37°C and 5% CO_2 under humidified atmosphere. All culture vessels were purchased from Sarstedt, Germany, and Corning, UK.

Cell line/ Cell model	*Species*	*Complete culture medium*	*Source*
AC10/ventricular	**Human**	**DMEM-F12, 10% (v/v) FCS, 2 mM L-Glutamine, 80 U/ml Penicillin/Streptomycin**	**Donated by Dr Barbara Savoldo, Baylor College of Medicine, Houston TX, USA**
HL-1/atrial	**Mouse**	**Claycomb, 10% (v/v) HL-1-screened FCS TMS016B, 2mM L-Glutamine, 80 U/ml Penicillin/Streptomycin**	**Donated by Dr Michael Dodd, University of Oxford, Oxford, UK**
hiPSC-CM /ventricular	**Human**	• **Cor4U. / Axiogenesis hIPSC-CM maintenance medium** • **iCell^2/ Fujifilm Cellular Dynamics maintenance medium**	**Purchased from Axiogenesis and Fujifilm CDI**
Cardiac fibroblast	**Human**	**DMEM-F12, 10% (v/v) FCS, 2 mM L-glutamine, 80 U/ml Penicillin Streptomycin**	**Donated by Dr Parveen Sharma, University of Liverpool, Liverpool, UK**
Cardiac endothelial	**Human**	**PromoCell endothelial cell kit (Basal Growth Medium MV + SupplementMix)**	**Donated by Dr Parveen Sharma, University of Liverpool, Liverpool, UK**

Table 2-1 Cardiac cell cultures, origin, cell culture conditions and source. DMEM, Dulbecco's Modified Eagle's Medium; FCS, foetal calf serum.

2.3.1 AC10 human ventricular cell line culture

The AC10 cell line is a proliferative human cardiomyocyte cell line derived from non-proliferative primary adult ventricular cardiac tissue (Davidson et al. 2005). The AC10 cells were originally immortalised by fusing the primary cardiomyocytes with SV40 transformed uridine auxotroph human fibroblast, devoid of mitochondrial DNA, and removing unfused fibroblasts (Davidson et al. 2005). The resulting AC10 cell line is therefore a suitable cardiomyocyte ventricular cell model that can be passaged and maintained under simple culture conditions. AC10 cells were routinely cultured in Dulbecco's Modified Eagle's medium (DMEM) F-12 supplemented with 10% foetal calf serum (FCS), 80U/ml penicillin/streptomycin and 2mM L-glutamine. AC10 cells were passaged after reaching a confluency of 80-100%. Briefly, media was aspirated from the flask and cells were washed with 5ml of Hank's Balanced Salt Solution (HBSS, Sigma, UK) before incubation with 0.25% trypsin-EDTA solution (Sigma, UK) at 37°C for 5 minutes. Upon successful detachment of cells, trypsin was inactivated by adding FCS-containing media to the suspension. The suspension was transferred to a sterile centrifuge tube and centrifuged at 500 RCF for 5 minutes to pellet the cells. After centrifugation, supernatant was discarded, the cell pellet was re-suspended in fresh media and seeded accordingly. Cells were supplemented with fresh complete DMEM-F12 medium every 2-3 days.

2.3.2 HL-1 murine atrial cell line culture

The HL-1 cell line is a proliferative murine atrial cardiomyocyte cell line first isolated by Dr Claycomb and his team (Claycomb et al. 1998). The HL-1 cell line has the unique ability to maintain a contractile cardiac phenotype upon extended culture. Hl-1 cells were originally derived from a precursor cardiac SV40-transformed tumour cell line known as AT-1, which cannot be passaged in culture but is routinely passaged *in-vivo* subcutaneously (Claycomb et al. 1998). The subcutaneous AT-1 tumours were originally excised and cells digested and isolated on gelatin/fibronectin coated flasks (Claycomb et al. 1998). The resulting HL-1 cell line

maintains an atrial phenotype and can be serially passaged in culture. HL-1 cells were passaged only after reaching a confluency of 100%, observable by formation of contractile syncytia. Briefly, cells were washed twice with 5ml HBSS before incubation with 1X 0.025% trypsin-EDTA solution (0.05% trypsin in 0.02% EDTA-Na) (Sigma, UK). An equal volume of soybean trypsin inhibitor was added to inactivate trypsin digestion, and FCS-free and norepinephrine-free Claycomb medium were added to the cell suspension. The cell suspension was then transferred to a sterile centrifuge tube and centrifuged at 500 g for 5 minutes to pellet the cells. The supernatant was discarded and the remaining HL-1 cell pellet was resuspended in complete Claycomb medium. Cells were supplemented with fresh complete Claycomb medium daily.

The composition of complete Claycomb medium is detailed in the table below (Table2.2).

Claycomb medium formulation	
Total protein	261 mg/l
Bovine albumin	48.85 mg/l
Nonessential amino acids	0.1mM
Fetuin	165 mg/l
Transferrin	31.8 mg/l
Retinoic acid	300 µg/l
Human insulin (recombinant)	15 µg/l
LONG®R3IGF-1 (recombinant)	0.1 µg/l
LONG® EGF (recombinant)	0.1 µg/l
Cholesterol	1.96 mg/l
Linoleic acid	0.78 mg/l
1-Oleoyl-2-palmitoyl-sn-glycero-3-phosphocholine	1.96 mg/l
Ascorbic acid	0.3 mM
Norepinephrine	100 µM
L-glutamine	2 mM
Penicillin/Streptomycin	100 µg/ml
FBS	10%

Table 2-2 HL-1 Claycomb media formulation.

2.3.3 Human Induced Pluripotent Stem Cell-derived cardiomyocyte culture

Throughout this project, hiPSC-CMs were sourced commercially, and used exclusively in combination with xCELLigence-based analysis. hIPSC-CMs were cryogenically stored under liquid nitrogen until use, and were therefore thawed and seeded as per manufacturer's instructions prior to each experiment. Briefly, this involved quick thawing in a water bath at 37°C. Under sterile conditions, hiPSC-CMs were then transferred dropwise to a small commercial Plating medium aliquot to minimise osmotic shock. The cells were counted and assessed for viability using the trypan blue method described in section 2.3.6, and immediately seeded onto an xCELLigence Cardio ECR E-plate precoated with a 0.1% gelatin solution (Stem Cell Technologies, Cat. No. 07903). hiPSC-CMs were subsequently incubated at 37°C and 5% CO_2 under humidified atmosphere for 30 minutes before being transferred into the xCELLigence Cardio ECR cradle unit for continuous monitoring of contractility. hiPSC-CMs were supplemented with fresh commercial Maintenance medium daily, until stable contractility was attained (approximately 5 days from seeding).

2.3.4 Human cardiac fibroblast culture

Primary human cardiac fibroblasts were sourced from PromoCell (PromoCell, Heidelberg, Germany) and they were routinely cultured in DMEM-F12 medium supplemented with 10% FCS, 80U/ml penicillin/streptomycin and 2mM L-glutamine. Cells were passaged when reaching a confluency of 50%, for a maximum of 5 passages from thawing. Briefly, media was aspirated from the flask and cells were washed with 5ml of Hank's Balanced Salt Solution (HBSS, Sigma, UK) before incubation with 0.25% trypsin-EDTA solution (Sigma, UK) at 37°C for 5 minutes. Upon successful detachment of cells, trypsin was inactivated by adding FCS-containing media to the suspension. The suspension was transferred to a sterile centrifuge tube and centrifuged at 500 RCF for 5 minutes to pellet the cells. After centrifugation, supernatant was discarded, the cell pellet was re-suspended in fresh media and seeded accordingly. Cells were supplemented with fresh complete DMEM-F12 medium daily.

2.3.5 Human cardiac endothelial cell culture

Primary human cardiac endothelial cells were sourced from PromoCell (PromoCell, Heidelberg, Germany). ECs were routinely cultured in Endothelial Cell Growth MV medium kit (PromoCell), consisting of a basal growth medium supplemented with SupplementMix (PromoCell). Pre-mixed supplements are listed in table 2.3. Cells were passaged at sub-confluency levels of approximately 20%, for a maximum of 5 passages from thawing.

Endothelial cell medium formulation	
Basal Growth Medium MV	500 ml
Fetal Calf Serum	0.05 ml / ml
Endothelial Cell Growth Supplement	0.004 ml / m
Epidermal Growth Factor (recombinant human)	5 ng / ml
Heparin	90 µg / ml
Hydrocortisone	1 µg / ml

Table 2-3 Cardiac endothelial cell media formulation.

2.3.6 Assessment of cell viability and cell number determination

Cell cultures were regularly inspected using bright field microscopy on a Zeiss inverted light instrument (AxioVert, Zeiss, Germany). Overall cell health, viability and confluency were monitored on a regular basis. For experimental purposes, cells were trypsinised and counted using either a manual Neubauer haemocytometer, or an automatic cell counter (Countess Automated Cell Counter, ThermoFisher Scientific, USA). To assess viability whilst counting cells, trypan blue dye exclusion was used. After trypsinisation, centrifugation and cell resuspension in fresh media, an aliquot of cells was diluted in a ratio of 1:1 (v/v) with 0.4% Trypan blue dye. The dyed cell suspension was counted using a haemocytometer, where non-viable cells were identifiable due to their blue dye uptake. Viability was determined as follows:

$$\%\ cell\ viability = 100\ \mathrm{x}\left(\frac{Average\ number\ of\ viable\ cells}{Total\ cell\ number}\right)$$

2.3.7 Long-term cell storage

All cell lines for long-term storage were stored in stocks in liquid nitrogen. Generally, confluent cells were trypsinised under sterile conditions, and transferred to an FCS and DMSO-based freezing medium formulation (medium composition 10% DMSO in FCS). The suspension was then transferred to a sterile cryovial and left to gradually cool within a freezing container filled with isopropanol, at -80°C for 24h. The vial was finally removed from the freezing container and stored in a liquid nitrogen tank under vapour phase.

2.3.8 Cell stock revival

Cryogenically preserved cell line stocks were regularly revived. This involved a rapid 37°C water bath thawing, and transfer of the thawed cell suspension to fresh supplemented media. Centrifugation at 500 RCF was usually performed to pellet the cells in order to discard the DMSO-containing freezing media residues. Cells were then resuspended in fresh supplemented media and seeded onto appropriate culture vessels as per required experimental needs.

2.4 Three-Dimensional Tissue and Cell Culture

2.4.1 Materials

For the formation and long-term culture of spheroids, ultra-low adhesion (ULA) 96-well round-bottomed culture plates were used (Corning, NY, USA). All 3D cell and tissue cultures were routinely maintained in CO_2 incubator at 37°C and 5% CO_2 under humidified atmosphere. All culture vessels were purchased from Sarstedt, Germany, and Corning, UK.

2.4.2 Monoculture spheroid seeding and culture

Spheroids constructed using exclusively a single source of cardiomyocytes, and therefore containing only one main cell lineage, were referred to as monoculture spheroids. Monocluture spheroids for this thesis were constructed using cardiomyocyte cell lines, including the HL-1 atrial cell line and the AC10 ventricular cell line. 2D cultures were normally established and expanded a prior to spheroid construction. Cardiomyocytes were trypsinised and centrifuged at 500 RCF for 5 minutes before being counted using a manual haemocytometer. A number of 500 cells/100 µl complete media was added to each low-adhesion plate well, as this quantity was previously optimised in the Sharma Lab (University of Liverpool) for the formation of 1 spheroid per well. The plate was briefly centrifuged at 182 RCF for 5 minutes at room temperature to allow an even deposition of the cells towards the centre of the round bottomed well. The culture was subsequently left in a CO_2 incubator at 37°C and 5% CO_2 under humidified atmosphere for a minimum of 48 hours to avoid any disruption to the early stages of spheroid formation. Spheroid formation was subsequently confirmed by brightfield microscopy, and complete medium was changed every 72 hours thereafter.

2.4.3 Triculture spheroid seeding and culture

Spheroids constructed using a combination of cardiomyocytes, cardiac fibroblasts and cardiac endothelial cells were referred to as Triculture spheroids. For this project, triculture spheroids were constructed using cardiomyocyte cell lines (AC10 or HL-1), in addition to commercially sourced primary human cardiac fibroblasts (Promocell) and primary human cardiac endothelial cells (Promocell). All cell lineages were cultured in advance in regular 2D culture vessels as per specific protocols (described in section 2.2) until required. Cells were trypsinised and counted using a manual haemocytometer. A total number of 500 cells/well was considered optimal as established by (Ravenscroft et al. 2016), where different cell lineages were diluted using the proportion 1:2:4, where 1=cardiac endothelial cells, 2=cardiac fibroblasts and 4=cardiomyocytes. Triculture dilutions were added to ultra-low adhesion round-bottomed 96 well plates and spun at 182 RCF for 5 minutes at room temperature to allow an even deposition of the cells towards the centre of each well. The culture was subsequently left in a CO_2 incubator at 37°C and 5% CO_2 under humidified atmosphere for a minimum of 48 hours to avoid any disruption to the early stages of spheroid formation. Spheroid formation was subsequently confirmed by brightfield microscopy, and complete medium was changed every 72 hours thereafter. Tricultures were supplemented with complete cardiomyocyte-specific medium and cardiac endothelial cell-specific medium in a 50:50 proportion.

2.5 Cell viability assays

2.5.1 MTT: 3-(4,5-dimethylthiazol-2-yl)-2,5-diphenyltetrazolium bromide assay

MTT is a colourimetric assay used to assess cell viability. This assay relies on the conversion of MTT into purple formazan crystals by mitochondrial reductases in viable cells; these crystals are subsequently dissolved and can be quantified by measuring the absorbance of the resulting solution. The amount of solubilised product correlates with the number of viable cells. Typically, cells were seeded onto 96-well flat-bottomed plates and treated with the required compounds prior to the experiment (typically for 24 hour or 96 hours unless otherwise specified). Media was then removed from the culture plate, and 5mg/ml MTT in dH_2O diluted 1:10 in cell medium was added in equal quantity (100µl) to each well. After a 4 hour incubation at 37°C and 5% CO_2 under humidified atmosphere, the MTT/medium was discarded. The remaining formazan crystals were solubilised using DMSO, and absorbance was measured at 550nm. Cell viability was calculated as a percentage relative to control.

2.5.2 ATP Cell Titre Glo 2.0 and Cell Titre Glo 3D assays

Cell Titre-glo assays (Promega, USA) are luminescent assays used to assess cell viability. These assays rely on the mono-oxygenation of luciferin by luciferase in the presence of adenosine triphosphate (ATP) in viable cells, which generates luminescence quantifiable by luminometry. Luminescence intensity therefore correlates with the number of viable cells. For two-dimensional cell monolayers, Cell Titre-glo 2.0 (Promega, USA) was used. For three-dimensional spheroid cultures, cell Titre-glo 3D was used (Promega, USA). Cells or spheroids were seeded onto 96-well plates (flat bottom for 2D, and ULA for 3D spheroids according to protocols described in section 2.3 and 2.4 respectively), and exposed to the compound of interest (typically for 24 or 96 hours unless otherwise specified). The plates were left to equilibrate at room temperature for 30 minutes prior to the addition of cell Titre-glo reagent. An equal amount of cell Titre-glo reagent was therefore added to each well, and mixed by manual pipetting to promote cell lysis. After a 10 minute incubation at room temperature, the

cell lysate was transferred to a white polystyrene plate suitable for measurement of luminescence (Fisher Scientific, UK), and measured on a luminometer (Thermo Fisher Scientific, UK). Cell viability was calculated as a percentage relative to control.

2.6 Live-cell metabolic assays: Seahorse XF analysis

Live-cell metabolic assays were performed using a Seahorse XFe96 instrument (Agilent, Santa Clara, USA). The Seahorse instrument was used to measure oxygen consumption rates (OCR) and extracellular acidification rates (ECAR) in live cells to give an indication of mitochondrial activity, respiration and glycolysis.

Mitochondrial stress tests were performed using Seahorse XF Mito Stress Test kits (Agilent, USA), and were used to assess mitochondrial activity and respiration in the cells of interest. The method relies on the use of electron transport chain-specific modulators (ETC), including oligomycin, carbonyl cyanide-4 (trifluoromethoxy) phenylhydrazone (FCCP), rotenone and antimycin A. The experimental principles are illustrated in figure 2.1.

A fresh XF sensor cartridge was rehydrated using Seahorse XF calibrant solution 24 before the start of each experiment, and left to incubate at 37°C in a non- CO_2 incubator. Cells were plated directly in a Seahorse XF microplate according to individual experimental needs. Prior to the start of the Mito stress test, cells were washed twice in Seahorse assay medium (pH 7.4, 5.5 mM glucose, 1mM pyruvate, 2mM l-glutamine, Seahorse XF base medium). 180µl assay medium were added to each microplate well and incubated at 37°C in non- CO_2 incubator for 1 hour prior to analysis. Following cartridge rehydration, ETC modulators and other compounds of interest were loaded into the injection ports into the cartridge in a specific order, as illustrated in table 2.3. The cartridge was then loaded in the Seahorse XF analyser for calibration before the addition of the microplate containing cells. Based on the required experimental design, the duration and number of analytical cycles were selected on the instrument.

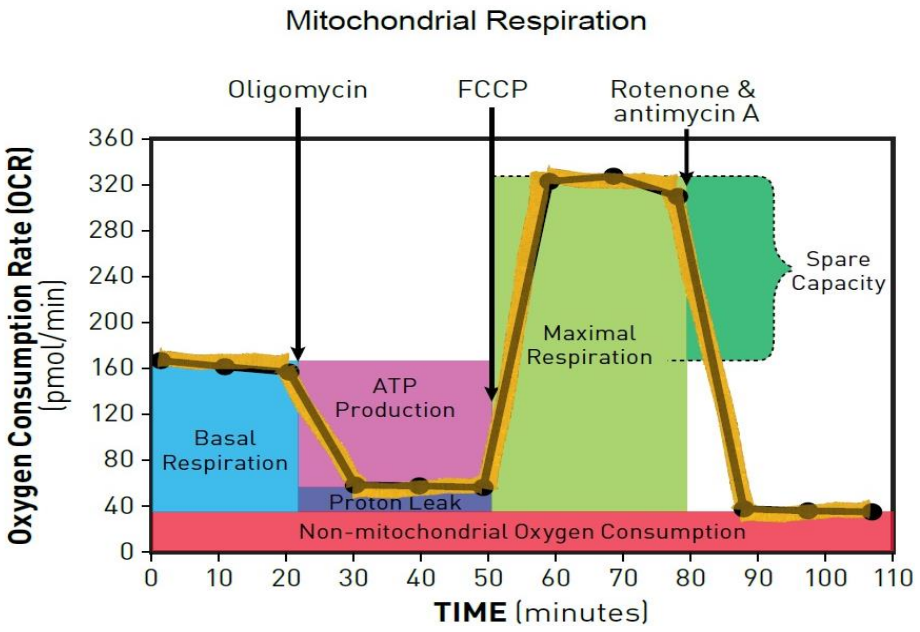

Figure 2.1 Principles of a Mito Stress test using Seahorse XF analysers (adapted from Agilent, Mito stress test). Illustration of the parameters assessed throughout the test including basal respiration, ATP production, maximal respiration, and spare respiratory capacity.

Compound	*Injection port*	*Concentration in port (µM)*	*Final concentration (µM)*
Chemical of interest	A	Various	Various
Oligomycin	B	10	1
FCCP	C	50	5
Rotenone/Antimycin A	D	30	3

Table 2-4 Compound and relevant port injection preparation for the Seahorse XF Mito Stress test.

2.7 Impedance-based real time cell analysis

Impedance-based cell analysers were used to monitor different cellular parameters, including cell viability, cell morphology and contractility over time, in real-time. The instruments used for impedance-based analysis were the xCELLigence DP16 instrument (ACEA Biosciences, Agilent, San Diego, USA) for the assessment of non-contractile cell models, the xCELLigence Cardio and Cardio ECR instruments (ACEA Biosciences, Agilent, San Diego, USA) for the assessment of contractile cell models.

Impedance-based cellular monitoring is a non-invasive technology that relies on the use of special electrode-coated cell culture vessels and microtiter plates (E-Plates, ACEA Biosciences, USA), and the application of a non-invasive electric potential. The presence of adherent cells actively impedes the electron flow, and therefore the generated impedance is quantified and correlated with high sensitivity to the presence, adherence, size and morphology of the cells (Figure 2.2, Agilent, USA). The recorded impedance measurements are reported using the unitless variable Cell Index (CI), where

$$CI = \frac{(Impedance\ at\ time\ point\ n\ (\Omega) - impedance\ in\ the\ absence\ of\ cells\ (\Omega))}{Nominal\ impedance\ value}$$

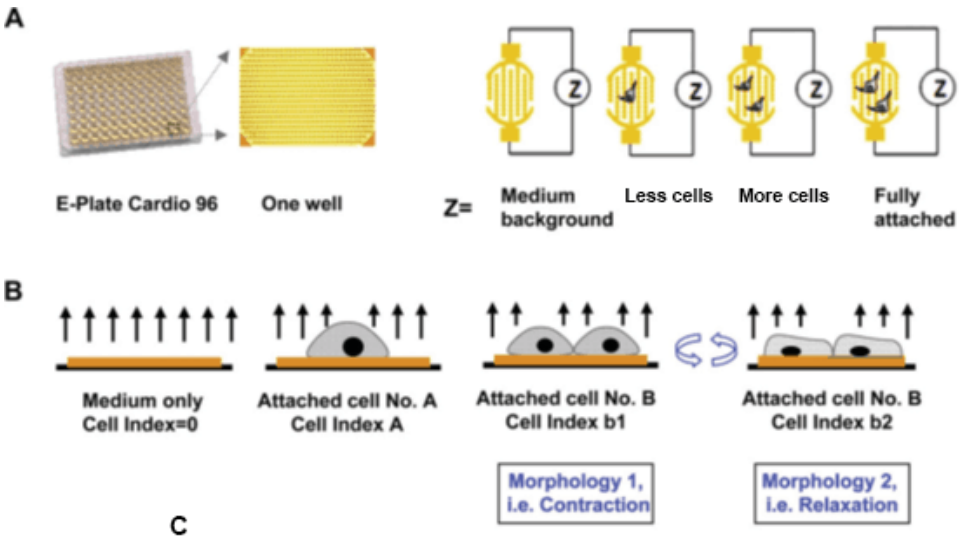

Figure 2.2 Principles of impedance-based cellular analysis (adapted from ACEA biosciences, Agilent).

A more detailed overview of how a typical xCELLigence trace is generated is represented in figure 2.3. Prior to cell seeding the CI is close to a value of 0. As cells are seeded onto the E-plate electrodes, the CI gradually increases in value reflecting cell adhesion, and cell growth kinetics in the case of proliferative cells. Typically, the CI reaches a plateau stage once all non-proliferative cells are adhered, or, in the case of proliferative cells, once all cells have achieved a stationary phase. The dynamic monitoring of the cells allows to detect alterations to impedance throughout the experiment, therefore compounds and cytotoxic agents can be added at any experimental time point. For most studies in this thesis, cytotoxic compounds and drugs were added at plateau phase. Decrease of CI value reflects cell detachment from the electrodes or modifications in terms of cell size and/or morphology.

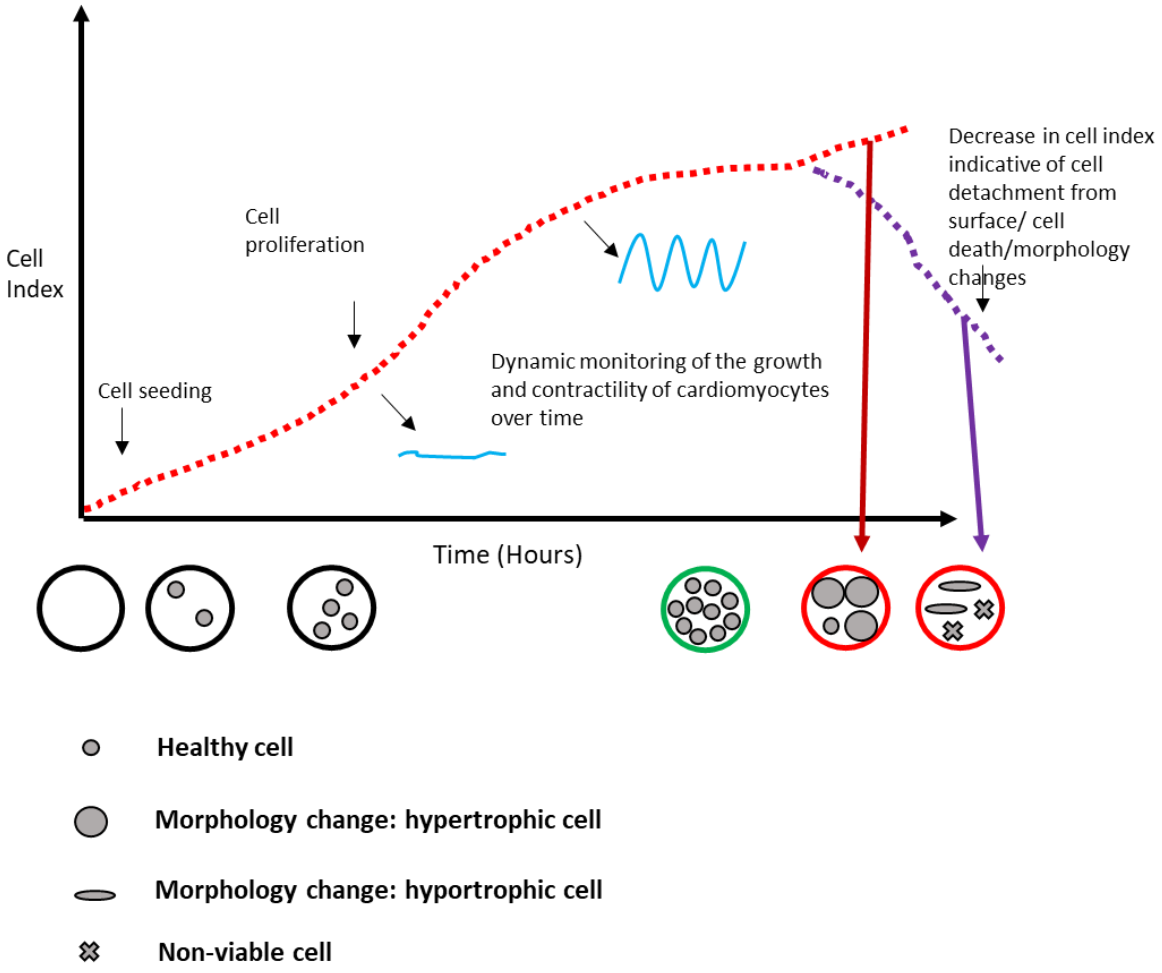

Figure 2.3 Principles of xCELLigence impedance-based data acquisition. Impedance measurements are plotted as y=Cell Index over x=time. Cell Index values reflect cell growth, size, morphology and death.

2.7.1 Overview and workflow of xCELLigence DP16 instrument

The xCELLigence DP (Dual Purpose) instrument was used to monitor adherent non-contractile cells (Table 2.5). The typical experimental workflow was based on manufacturer's instructions (ACEA Biosciences, USA) and was adapted in accordance with specific experimental needs. Briefly, a DP16 electrode-coated E-plate was selected and, if required, pre-coated with the desired agents (a list of precoating agents is illustrated in table 2.5). Experimental medium was added to the plate wells and a background scan was performed prior to cell seeding. The required amount of cells was added to the E-plate according to the appropriate experimental protocol and incubated at room temperature in the laminar flow hood for 30 minutes to allow even deposition of the cells onto the electrode surface. The E-plate was subsequently placed into the xCELLigence instrument cradle situated in a CO_2 incubator at 37°C and 5% CO_2 under humidified atmosphere. Duration and frequency of impedance recordings (sweeps) were selected and modified using xCELLigence RTCA PRO software version 2.3.2.

2.7.2 Overview and workflow of xCELLigence Cardio instrument

The xCELLigence Cardio instrument was used to monitor adherent contractile cells (Table 2.5). As well as recording overall cell generated impedance values as described in section 2.5.1, the Cardio instrument is designed to detect rapid changes in impedance, such as those resulting from physical movement of the cells on the electrode surface. Specifically, data acquisition occurs at a rate of 12.9ms for contractility parameters (ACEA Biosciences, Agilent, USA). The typical experimental workflow depended on the origin of the cells used, but was essentially based on manufacturer's instructions (ACEA Biosciences, USA). Briefly, this involved pre-coating of a Cardio E-plate with a suitable matrix (pre-coating information for each cell model is in table 2.5). Experimental medium was added to the plate wells and left to achieve equilibrium at room temperature under laminar flow hood. Prior to cell seeding, a background scan was performed. Depending on the cardiomyocyte origin (i.e., hiPSC-CM, cell lines etc.) cells were either thawed prior to seeding or trypsinised, and subsequently counted using trypan blue exclusion technique on a manual haemocytometer. Cells were seeded onto the cardio E-plate at the desired density and left to incubate at room temperature under laminar flow hood for 30 minutes to allow even deposition of the cells onto the electrode surface. The E-plate was then inserted in the Cardio system cradle situated in a CO_2 incubator at 37°C and 5% CO_2 under humidified atmosphere. Duration and frequency of impedance recordings (sweeps) were selected and modified using xCELLigence RTCA Cardio software version 1.2. Cardiomyocyte medium was changed based on the specific cardiomyocyte model needs, ranging from 12 to 48 hourly media changes on average. Media changes were usually performed in a 4-step process, ensuring the electrodes in the E-plate wells never remained dry. Prior to compound addition, baseline contractility parameters were recorded to exclude intrinsic beat rate irregularities

The xCELLigence Cardio-generated impedance waveform was analysed for two parameters: beat rate and beat amplitude (Figure 2.5). These parameters were used to define the characteristics of contractile myocytes. Beat rate was calculated as the number of positive peaks per minute. Beat rate changes were double-normalised (ΔΔ) to baseline and vehicle control and are expressed as percentage change, with baseline values being 100%. Beat amplitude was calculated as whole peak counts from each negative peak to the following

positive peak, and are expressed as a percentage change, double-normalised to baseline and vehicle control.

Impedance values were exported using the RTCA Cardio ECR software (Beta), and parameters were subsequently analysed as follows:

$$Normalisation\ to\ baseline\ (\Delta\%) = (Treatment\ \ Impedance\ /Baseline\ Impedance)x100$$

$$Double\ normalisation\ to\ vehicle\ control\ (\Delta\Delta\%) = (\Delta\%\ of\ sample - \ \Delta\%\ change\ of\ control)$$

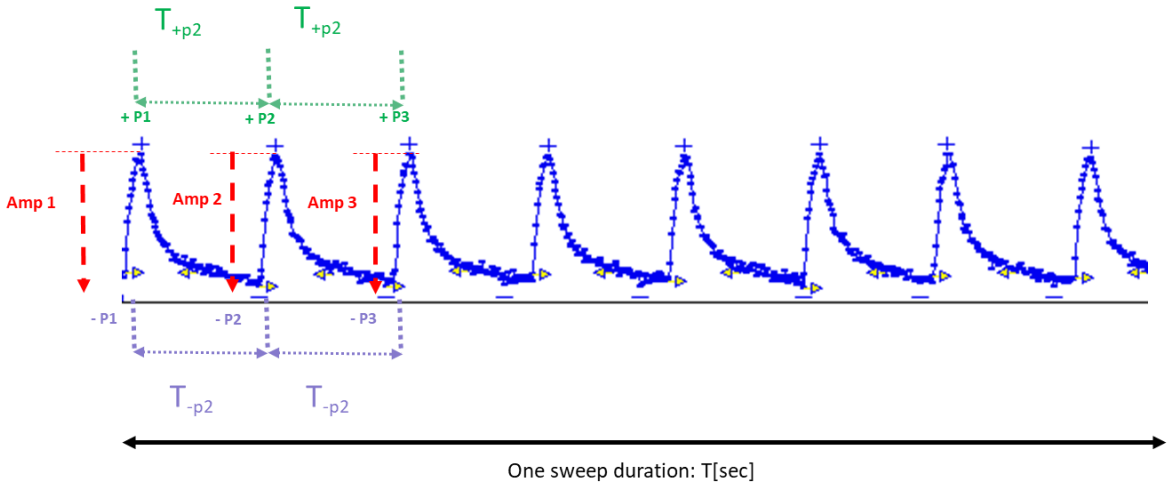

Figure 2.4: xCELLigence Cardio system impedance trace of cardiac cell contractility. Each beating corresponds to the excitation-contraction coupling of cardiomyocytes. These beats are defined as a sequence of positive peaks and negative peaks (+P and –P as labelled). Impedance beat rate was analysed based on the total number of positive peaks in one minute. Impedance beat amplitude analysis was performed on Whole Peak (WP) counts, from each negative peak to the following positive peak.

2.7.3 Overview and workflow of xCELLigence Cardio ECR instrument

The xCELLigence Cardio ECR instrument (ACEA Biosciences Agilent, USA) was used to monitor hiPSC-CMs. This instrument is designed to combine the previously described xCELLigence Cardio impedance technology (section 2.6.2) with multielectrode array (MEA) technology to assess electrophysiological cell properties. The xCELLigence Cardio ECR instrument has a faster impedance data acquisition rate of 1 millisecond compared to the 12.9 milliseconds achieved with the xCELLigence Cardio instrument, which allows for an extremely sensitive detection of dynamic changes in cell behaviour. In addition to the impedance data acquisition, the ECR Cardio instrument simultaneously acquires electrophysiology measurements which allow to assess parameters such as spike amplitude and field potential duration (FPD). The typical experimental workflow was essentially similar to the xCELLigence Cardio instrument protocol, and was based on manufacturer's instructions. Briefly, hiPSC-CMs were thawed and counted before being seeded onto a fibronectin-coated Cardio ECR E-plate (ACEA). The Cardio ECR E-plate had a 48-well capacity, where each well included a flat surface lined with impedance electrodes, and two electrodes for electrophysiology data acquisition. Cells were seeded onto the cardio E-plate at a density of 30,000 cells/well and left to incubate at room temperature under laminar flow hood for 30 minutes to allow even deposition of the cells onto the electrode surface. The E-plate was then inserted in the Cardio ECR system cradle situated in a CO_2 incubator at 37°C and 5% CO_2 under humidified atmosphere. Duration and frequency of impedance recordings (sweeps) were selected and modified using xCELLigence RTCA Cardio ECR software (Beta). Prior to compound addition, baseline contractility parameters were recorded to exclude intrinsic beat rate irregularities.

Data generated with the xCELLigence Cardio ECR system was analysed for the impedance parameters described in section 2.7.1 and 2.7.2, including CI variations, beat rate (BR) and beat amplitude (BA). Additionally, electrophysiological parameters were analysed and included Field Potential Duration (FPD) and Spike amplitude (SA) (Figure 2.5).

Specifically, FPD was calculated from FP baseline to FP wave end, and was corrected for beat rate using Fredericia's correction formula:

$$FPDc = \frac{FPD}{\sqrt[3]{\frac{RR}{1s}}}$$

Where:

- FPDc= corrected Field Potential Duration
- FPD= non-corrected Field Potential Duration
- RR= Interval between two FP- peaks

Step-by-step FPDc analysis:

- Obtained raw FPD data values from RTCA software
- Obtained raw Beat rate data values from RTCA software as beats/minute (BPM)
- Used $\frac{60}{BPM}$ to obtain beat period interval as BP/1s
- Applied Fridericia's correction formula to obtain FPDc where: $FPDc = \frac{FPD}{\sqrt[3]{\frac{RR}{1s}}} = \frac{FPD}{\sqrt[3]{BP}}$

Spike amplitude defines the voltage (mV) difference between each FP+ positive and FP- peak, and this parameter was double-normalised to baseline and vehicle control, and is expressed as a percentage change.

All xCELLigence raw data analysis was carried out using RTCA software (ACEA Bioscience Agilent, San Diego, CA). Statistical analysis was done using GraphPad Prism (GraphPad Software, San Diego, CA), Microsoft Excel (Microsoft, Washington, USA) and Visual Studio (Microsoft, USA) written in Python.

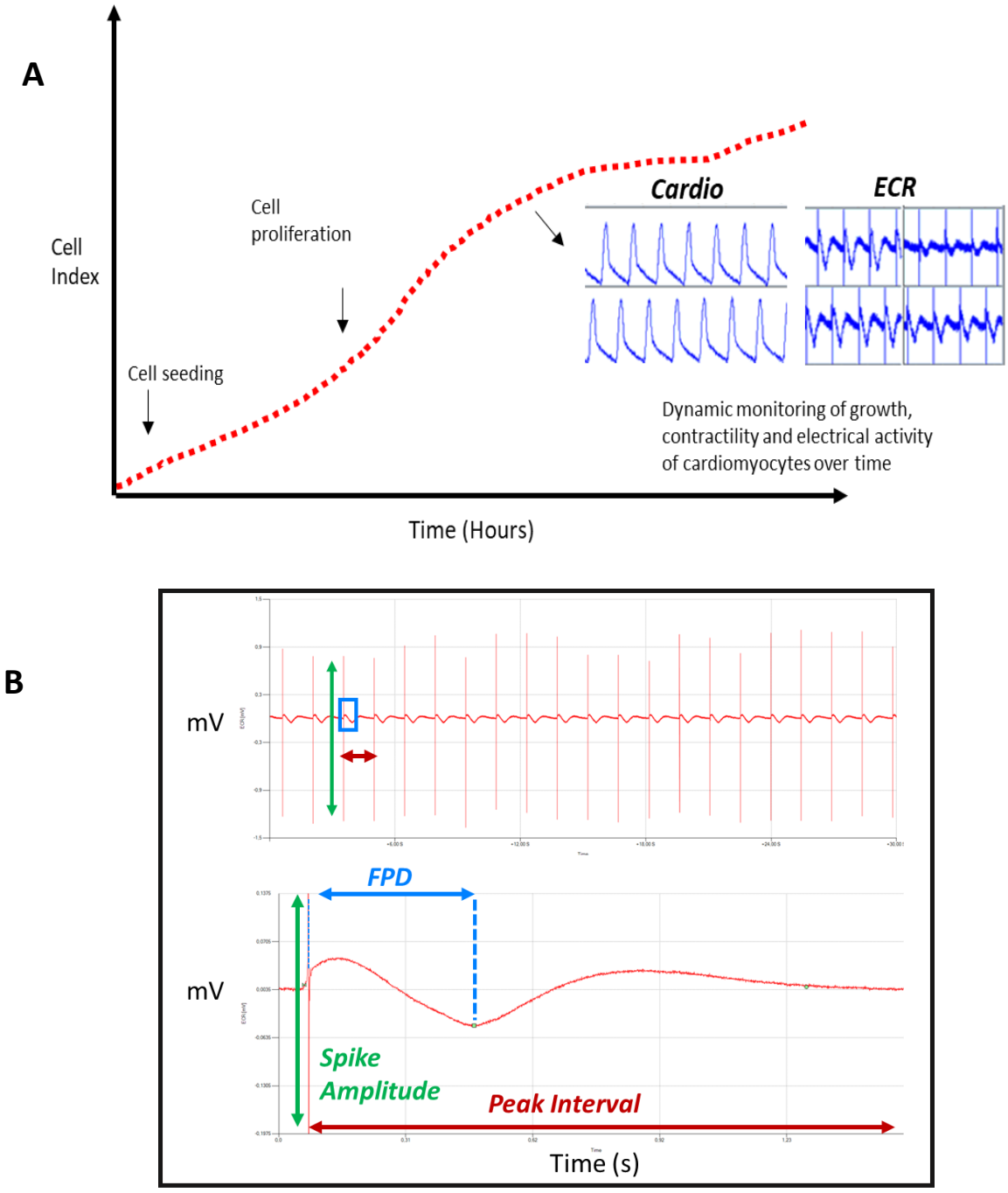

Figure 2.5. xCELLigence Cardio ECR system dual impedance/multi electrode array technology measurements. A. CI impedance is monitored in real-time, along with dynamic monitoring of cell contractility and electrical activity.**B**. ECR measurements including spike amplitude (mV), Field Potential Duration (ms) and Peak Interval (s).

Cell Model	*Contractile*	*Impedance instrument used*	*Parameters assessed*	*E-plate pre-coating*
hiPSC-CM	yes	xCELLigence Cardio and xCELLigence Cardio ECR	CI, BR, BA, SA, FPD	0.1% gelatin solution, (Stem Cell Technologies No. 07903)
HL-1 murine atrial cell line	yes	xCELLigence Cardio	CI, BR, BA	0.5µg/ml in 0.02% gelatin (Merck G9391)
AC10 human ventricular	no	xCELLigence DP	CI	Not required

Table 2-5 Cardiac cell models appraised in this thesis used in combination with impedance-based analysers. Analysed parameters included cell index (CI), beat rate (BR), impedance beat amplitude (BA), spike amplitude (SA) and field potential duration (FPD).

2.8 Protein analysis assays

2.8.1 Preparation of cell protein extracts

Cells were harvested for protein at exponential or plateau phase according to experimental needs. Media was aspirated and discarded from the culture vessel and cell monolayers were rinsed twice with 1-5ml of sterile PBS. Cells were scraped directly into 250 µl of Tris-Triton lysis buffer (50mM Tris Cl, 1mM EGTA, 1mM EDTA, 1mM sodium orthovanadate, 10mM β-glycerol phosphate, 50mM sodium fluoride, 5mM sodium pyrophosphate, 0.27M sucrose, 1% triton x100) and transferred into a clean microcentrifuge tube. Samples were centrifuged at 1300 rpm for 10 minutes at 4°C. Pelleted samples were kept on ice throughout the sample preparation process or kept at -20°C for long-term storage.

2.8.2 Bradford protein assay

Cell lysate total protein was quantified using the Bradford assay. Bovine serum albumin was used to make a set of known protein standards ranging from 0 µg/ml to 1000 µg/ml in sterile PCR-grade water. After centrifugation, the supernatant obtained from the cell lysates was transferred to a clean microcentrifuge tube. For the Bradford assay, an amount of unknown sample was diluted 1:20 in sterile PCR-grade water. 10 µl of known BSA standards and unknown diluted sample were added in triplicates into the wells of a clean 96-well flat-bottomed plate (Sarstedt, Germany). Bradford reagent (Bio-Rad, UK) was added to each well and incubated at room temperature for 5 minutes to allow development of the colour-changing reaction. Absorbance was measured at 595 nm using a plate reader (Thermo Fisher Scientific, MA. USA). A standard curve was plotted from the absorbance values of the BSA standards and used to quantify the tissue protein extracts.

2.8.3 Sodium-dodecyl sulphate polyacrylamide gel electrophoresis (SDS-PAGE)

Sodium-dodecyl sulphate polyacrylamide gel electrophoresis (SDS-PAGE) is a technique that allows to separate and identify proteins by molecular weight. After purification and quantification, extracted proteins were processed to undergo denaturation by addition of a thiol-reducing agent, such as 2-mercaptoethanol or dithiothreitol (DTT) that allow to break S-S bonds, and by heating to allow disruption of hydrogen bonds. The denatured proteins were then loaded onto a polyacrylamide gel matrix submerged in a running buffer solution (2.5M Trizma base, 1.9M glycine, 1%SDS, pH 8.3), and a voltage potential was applied at 100V promoting the migration of the negatively charged proteins through the gel towards the positively charged anode. Polyacrylamide gel composition was altered in accordance with the molecular mass of the protein of interest. The smaller the size of the protein of interest, the higher the gel percentage.

Gels were cast between glass plates using casting trays (Bio-Rad, UK). The separation gel was prepared by mixing dH2O, 30% acrylamide solution (Bio-Rad, UK), 1.5M Tris (pH 8.8), 10% SDS, 10% ammonium persulfate and 0.5% tetramethylethylenediamine (TEMED). For most experiments, a polyacrylamide gel of 10% was used for the protein separation. A stacking polyacrylamide 5% gel layer was used to form the wells for protein loading, and to ensure an even alignment of proteins prior to protein separation stage.

Before loading, proteins were diluted to 1-2µg/µl in a reducing sample buffer (dH2O, 0.5M Tris pH 6.8, Glycerol, 10% SDS, 0.5% bromophenol blue, 10% 2-mercaptoethanol).

2.8.4 Electrotransfer of proteins

After separation, proteins were transferred onto a positively charged polyvinylidene (PVDF) membrane (GE Healthcare Life Science, UK). Polyacrylamide gels were removed from the electrophoresis apparatus and left to briefly equilibrate in 4°C cooled transfer buffer solution (dH2O, 25mM Tris base, 192mM glycine, 20% v/v methanol) prior to being assembled onto PVDF for protein transfer. A schematic overview of transfer gel-PVDF set up is summarised in figure 2.6.

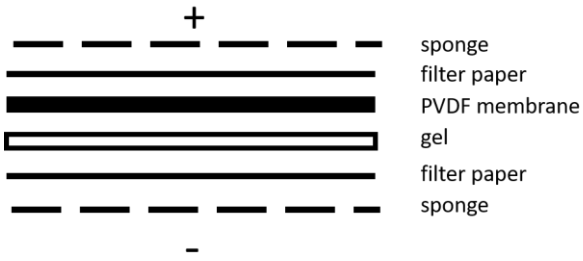

Figure 2.6. Transfer stack assembly used for protein migration from polyacrylamide gel to PVDF membrane.

The assembled membrane/gel stack was placed in an electrotransfer apparatus (Bio-Rad, UK), and protein transfer was carried out at constant 300mA for 1 hour on wet ice. After the transfer, PVDF membranes were blocked for non-specific binding in 5% skimmed milk in TBS-T (20mM Trizma base, 150mM NaCl, 0.1% Tween-20 detergent w/v) for 1 hour at room temperature.

Blocked membranes were therefore incubated with the appropriate primary antibody overnight at 4°C. Next, after removal of primary antibody by three consecutive washes in TBS-T, membranes were incubated with the relevant secondary horseradish peroxidase (HRP) conjugated antibody for 1 hour at room temperature. A list of primary and secondary antibodies used for immunoblotting purposes is illustrated in table 2-6.

2.8.5 Protein immunodetection

A luminol-based substrate (enhanced chemiluminescence solution, ECL) (ECL1: 2.5mM luminol, 0.4mM p-coumaric acid, 100mM Tris HCL pH 8.5; ECL2: Hydrogen peroxide 30% v/v, 100mM Tris HCL pH 8.5) was used to detect proteins on PVDF membranes. 1 ml of each ECL reagent was mixed and added to the membrane prior to immunodetection, and incubated for 3 minutes under dark conditions at room temperature. Proteins were visualised using a Bio-Rad ChemiDoc membrane imager (Bio-Rad, UK), where chemiluminescence image acquisition exposure times were set manually.

Antigen	***Raised in***	***Dilution used***	***Source***	***Molecular weight (kDa)***
Primary antibody				
Acetylated alpha tubulin	Mouse monoclonal	1:10000	Sigma Merck T6793	55
Acetylated histone H4	Rabbit monoclonal	1:500	CST 2594S	10
Beta actin	Mouse monoclonal	1:8000	Sigma Merck A5441	42
Secondary HRP conjugated antibody				
Anti-mouse	Horse	1:2000	Vector Laboratories	n/a
Anti-rabbit	Goat	1:2000	Vector Laboratories	n/a

Table 2-6 Specifications and source of antibodies used for immunoblotting.

2.9 Multiplex ELISA Immunoassay

Quantification of free cardiac troponin I (cTnI) in culture media was done using a multiplex MSD ELISA kit (Meso Scale Diagnostics LLC, USA) as per manufacturer's instructions. Briefly, a 96 well plate was pre-coated with a specific biotinylated capture antibody solution 24 hours prior to each experiment. Aliquots of assay diluent solution, desired samples and a set of known calibrator controls were added to the plate, subsequently sealed and incubated at room temperature for 1 hour. Next, the plate was washed with an MSD supplied wash buffer, and aliquots of detection antibody solution were added. Antibody incubation was done at room temperature with shaking for 1 hour. Following washing with 1X MSD wash buffer, aliquots of MSD GOLD Read buffer were applied to each well prior to immunodetection using a plate reader instrument. A standard curve of known controls was plotted to calculate cTnI values.

2.10 Spheroid imaging and immunocytochemistry

To examine their internal structure and cellular organisation, spheroids were imaged using immunocytochemistry, a technique which allows to locate specific antigens/proteins in fixed tissues using targeted fluorophore-conjugated antibodies or fluorescent stains.

2.10.1 Spheroid fixation, permeabilisation and staining

Following media removal, cultured spheroids were washed three times with PBS before being fixed with 4% paraformaldehyde (PFA) (pH 7.2) for 1 hour at 4°C. After fixation, spheroids underwent permeabilisation to allow subsequent efficient stain/antibody penetration through the tissue. 100 µl permeabilisation buffer (PBS containing 0.5 v/v Tween 20, 0.2% v/v Triton X-100) were added and spheroids were incubated at 4°C overnight. After removal of permeabilisation buffer, spheroids were blocked for nonspecific binding using bovine serum albumin (BSA) for 2 hours at room temperature, and then incubated with a primary antibody solution overnight at 4°C (primary antibodies with respective dilutions used are illustrated in table X). Spheroids were therefore washed with an immunofluorescence wash buffer (PBS containing 0.1% Tween, 0.2% Triton-X 100) three times, each time left for 1 hour at room temperature. Next, spheroids were incubated with relevant secondary antibodies conjugated with fluorescent components as well as specific stains to highlight selected spheroid structures (relevant antibodies and stains used are illustrated in table 2.7), with incubation occurring overnight at 4°C.

Antibody/Stain	*Raised in*	*Dilution used*	*Source*
Primary antibody			
CTnI	Rabbit polyclonal	1:1000	Abcam
CD31	Rabbit polyclonal	1:1000	Abcam
Secondary conjugated antibody			
Anti-rabbit Alexa Fluor 488	Goat polyclonal	1:1000	Thermo Fisher
Anti-rabbit Alexa Fluor 568	Goat polyclonal	1:1000	Thermo Fisher
Stain			
Phalloidin	n/a	1:250	Sigma Aldrich
Hoechst	n/a	1:5000	Sigma Aldrich

Table 2-7 Specifications and source of antibodies and stains used for immunocytochemistry.

2.10.2 Spheroid mounting

To allow immunofluorescence visualisation, spheroids underwent mounting onto microscope slides as follows. After washing with 1X PBS for 1 hour at room temperature, spheroids were transferred to a Superfrost microscope slide, and subsequently covered with 10 µl Prolong Gold Antifade Mountant solution. A glass coverslip was then carefully positioned over the slide, and sealed using clear nail polish. Slides were left to dry under dark conditions for 30 minutes at room temperature, and subsequently stored at 4°C until bioimaging acquisition.

2.10.3 Spheroid fluorescence bioimaging

Spheroids were imaged using a Zeiss AxioObserver (Zeiss, Germany) inverted fluorescence microscope with Apotome platform, and acquired using Zeiss Zen software. To attain an accurate visualisation of 3D structures, images were acquired using a z-stack approach and visualised as maximum intensity projections (figure 2.8). To enable subsequent image analysis and signal intensity comparisons between spheroid subsets, images were acquired at equal exposure times. Immunofluorescent signal analysis was done using ImageJ software.

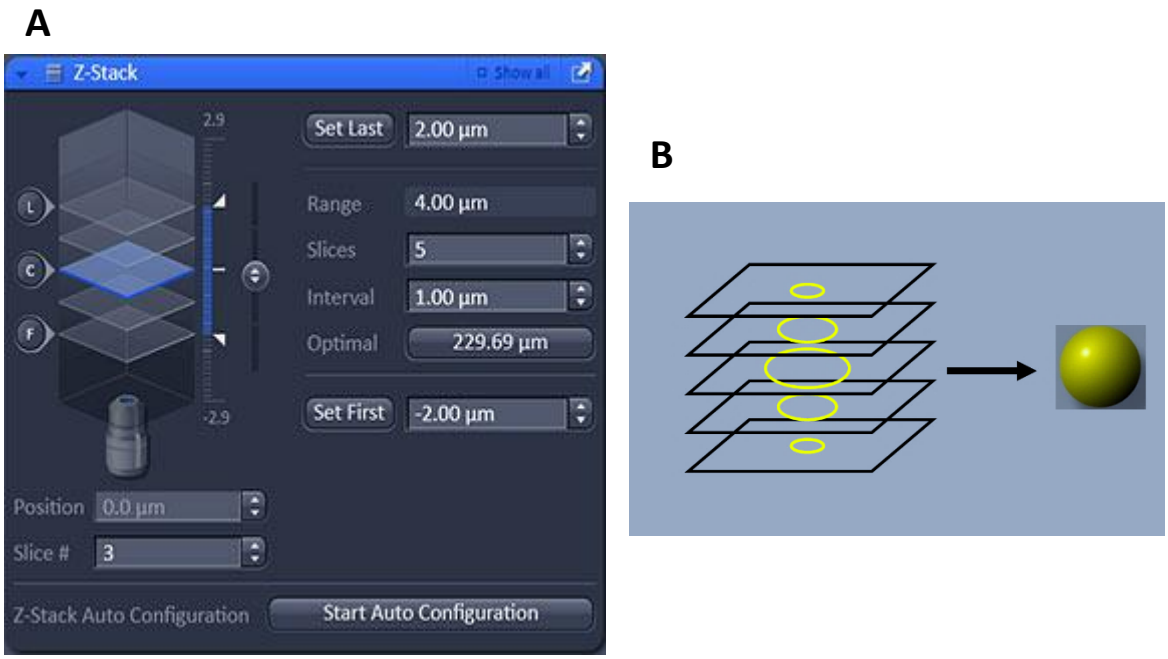

Figure 2.7 Z-stack image acquisition of 3D structures. 3D spheroids were imaged using a Zeiss AxioObserver inverted fluorescence microscope with apotome platform. The visualisation of internal spheroid structures occurred through the acquisition of image slices (z-stacks), subsequently combined into maximum intensity projection images. **A.** User interface for z-stack image acquisition on Zen software where number of slices, range, interval and position parameters were set (Zeiss, Germany). **B**. Principle of z-stack image composition (adapted from Northwestern University *Z Stack | Center for Advanced Microscopy*, no date)

2.11 Statistical analysis

Where required, statistical analysis was applied using a software combination that included Microsoft Office Excel (Microsoft, USA), Graph Pad Prism (Graph Pad Software, USA) and Visual Studio (Microsoft, USA) written with Python.

For comparison of group means, the Shapiro-Wilk test was performed to ascertain normal distribution of samples. The appropriate tests were then applied for comparative purposes. For comparisons of multiple means that did not violate normality assumptions, the parametric one way or two-way analysis of variance (ANOVA) tests were applied as necessary, following appropriate post hoc modifications which included Bonferroni's modification and Dunnett's modification.

For group means that rejected the normal distribution hypothesis, appropriate non-parametric tests were applied.

Where required, confidence intervals are provided in lieu of p values to quantify the uncertainty of an estimate. Where this applies, a level of confidence of 95% was chosen.

3 Characterisation and validation of hiPSC-CMs for *in-vitro* preclinical cardiotoxicity studies

3.1 Introduction

Over the last few decades, cardiac drug safety in preclinical settings has been cantered on the evaluation of acute electrophysiological alterations, primarily in relation to hERG inhibition and detection of cardiac dysfunctions translatable to proarrhythmic risk (Gintant, Sager, and Stockbridge 2016b). Typically, preclinical drug development involves a set of standardised assessments that are streamlined to provide critical safety evaluations in the early drug development project stages. These evaluations have been optimised to minimise hazard, and rely on in-silico and *in-vitro* approaches: the results derived from early-stage evaluations thus offer an improved tool to design subsequent preclinical evaluations, including *in-vivo* and ICH regulatory-compliant studies (Https://www.ich.org/ 2020; E14/S7B 2005; 2020).

The advent of pluripotent stem cell-derived technology has, under many aspects, revolutionised *in-vitro* organ modelling and preclinical research. Decades of ground-breaking research have provided crucial breakthroughs for the understanding of the molecular basis of hiPSC-to-cardiomyocyte re-differentiation (del Álamo et al. 2016). Recent hiPSC-CM differentiation protocols were optimised and developed to produce cell lineages yielding as much as 90-95% pure, highly enriched cardiomyocytes, which are now more commonly available on the market and commercialised by several bio-companies (del Álamo et al. 2016; Koivumäki et al. 2018). The commercial availability combined with the increasing number of studies and recent publications has incentivised the use of hiPSC-CM-based models in preclinical drug safety studies (Cavero and Holzgrefe 2015). A review conducted in 2015 by the National Centre for the Replacement, Refinement and Reduction of Animals in Research (NC3Rs) among the global safety community, including EFPIA, BTS, BPS and EuroTox, showed that a significant proportion of respondents currently use human-derived assays for safety screening studies (Holmes, Bonner, and Jones 2015). More remarkably, a large proportion of participants expressed their interest and intention to implement and use human tissue-based assays in the future. It is therefore not surprising that new iPSC technologies represent an enormous potential for early-stage drug discovery and toxicology. Despite the well-documented limitations of hiPSC-CMs, particularly in relation to their functionally immature phenotype (Koivumäki et al. 2018; Knollmann 2013), these models have been extensively characterised and integrated in many nonclinical *in-vitro* high-throughput screens for the

evaluation of cardiotoxicity; in this context, they are considered the most advantageous *in-vitro* model and they demonstrated adequate utility for acute functional studies, and identification of highly torsadogenic compounds (Blinova et al. 2018). One of the key aspects for the integration of novel *in-vitro* technologies in preclinical setting is strictly attributed to the introduction of the CiPA initiative (discussed in section 1.4)("Https://Cipaproject.Org/" n.d.). Introduced with the intention to improve, refine and enhance current ICH S7B guidelines for the assessment of preclinical cardiotoxicity, the CiPA paradigm has invested on the development of *in-vitro* strategies, including the validation and implementation of hiPSC-CM-based platforms. Specifically, the *in-vitro* CiPA component aims at the investigation of electrophysiological effects using ventricular hiPSC-CMs (Cavero and Holzgrefe 2015). The understanding of the strengths and limitations of hiPSC-CM-based models is therefore critical for the successful identification of potential model-specific fallacies that could ultimately hinder early-stage predictability of adverse drug events. Not least importantly, the assessment of model-specific drawbacks also justifies opportunities for the integration and assessment of complementary models and methodologies (Schwach, Slaats, and Passier 2020; del Álamo et al. 2016).

3.1.1 Chapter aims and objectives

This chapter aims to assess commercially sourced hiPSC-CMs for their ability to detect functional and structural cardiotoxicity for nonclinical studies using xCELLigence ECR systems. In particular, validation and limitation studies of this model are presented through the following objectives:

1) Appraisal of the advantages and limitations of hiPSC-CMs screened against a panel of known functional and structural cardioactive compounds.
    a) Assessment of impedance and electrophysiological parameters including Cell Index (CI), Beat Rate (BR), impedance Beat Amplitude (BA), Spike Amplitude (SA), corrected Field Potential Duration (FPDc).
    b) Evaluation of instrument and method detection limits, and their implications on the detection of cardiotoxicity.
2) Detection of proarrhythmic events and structural cardiotoxicity associated with the HDACi class of drugs.
    a) Assessment of impedance and electrophysiological parameters in response to pan-HDACi, evaluating Cell Index (CI), Beat Rate (BR), impedance Beat Amplitude (BA), Spike Amplitude (SA), corrected Field Potential Duration (FPDc).
    b) Assessment of impedance and electrophysiological parameters in response to selective HDACi to investigate mechanisms of functional and structural cardiotoxicity.

3.2 Characterisation of hiPSC-CMs for studies of cardiotoxicity using xCELLigence systems

Commercially sourced hiPSC-CMs iCELL^2 (Fujifilm Cellular Dynamics International, Madison, USA) were thawed and plated on a fibronectin-coated Cardio ECR E-plates as described in the methods section 2.7.3, essentially based on manufacturer's protocols. Post seeding, cells were monitored for viability and early contractility every 2 hours on the xCELLigence Cardio ECR instrument for the first 72 hours, and every hour thereafter. Spontaneous hiPSC-CM activity was recorded and assessed for each batch in order to detect and exclude wells displaying spontaneous beat rhythm irregularities (BRI) (Figure 3.1).

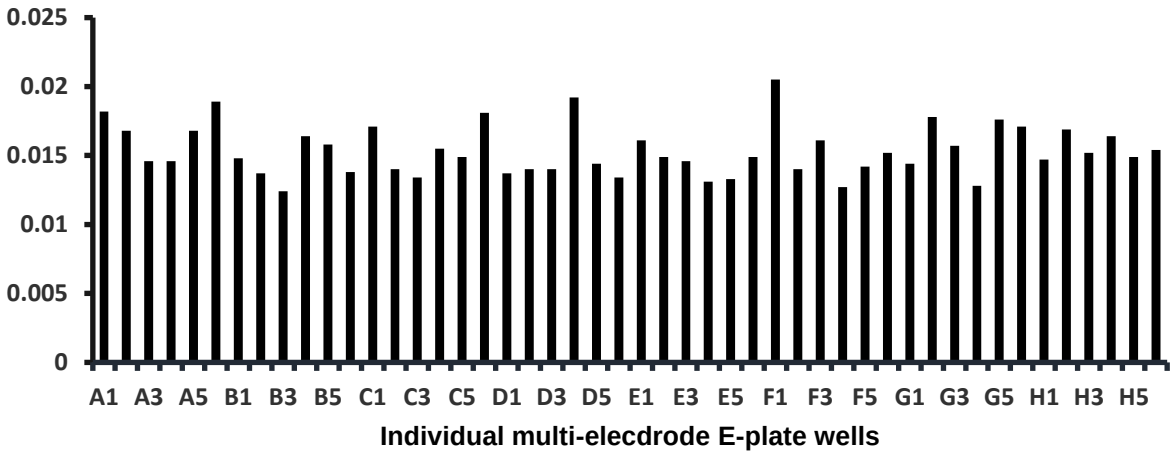

Figure 3.1 Assessment of spontaneous contractility iCELL^2 hIPSC-CMs following cryopreservation and revival recorded no significant beat rhythm irregularities (BRI) 5 days post seeding. Data is shown as ratio representing beat-to-beat variation recorded at baseline, where a value of < 0.1 for each E-plate well is indicative of no BRI. Data is representative of one typical xCELLigence Cardio ECR E-plate.

In order to validate different batches of hiPSC-CMs, for each experiment the cells were screened against a panel of compounds with known and well-defined cardioactive effects (Table 3.1). Analysed parameters included CI variations, beat rate, cell index (impedance) beat amplitude, spike amplitude and field potential duration. All parameters were determined and analysed as described in methods section 2.7.

3.2.1 hiPSC-CMs demonstrate inconsistencies in response to known cardioactive agents

Isoproterenol is an adrenoceptor agonist, which acts as a short-acting positive chronotrope without direct ion channel interaction, and selectively targets the β1 and β2 cardiac receptors. In this study, isoproterenol induced an expected transient increase in beat rate, with the highest peak resulting in a 40% beat rate increase 30 minutes post compound addition ($p<0.001$). Following the 30 minute time point post compound addition, beat rate showed a gradual decrease by 40% over 48 hours essentially returning to baseline values. Sodium spike amplitude was gradually increased with a maximum increase of 35% at 12 hours post compound addition, with a confidence interval of the mean (135%) [86.2% - 152%] for a 95% confidence level. The beat amplitude and cell viability were not affected and remained stable as expected. (Figures 3.3, 3.4).

Dofetilide blocks the α subunit of the delayed rectifier outward potassium current (I_{kr}), and is therefore classed as a hERG channel inhibitor. Dofetilide generally shows successful inhibitory activity at concentrations even in the nanomolar range, where the occurrence of early afterdepolarisation (EAD) and torsadogenic events that would render ineffectual data analysis is usually averted. In this study, dofetilide induced an expected significant and gradual decrease in beat rate, decreasing by 30% 30 minutes post compound addition, and resulting in a maximum 40% decrease 48 hours post compound addition. Beat amplitude was transiently affected with a 10 to 20% decrease in the first 24 hours post compound addition (Figure 3.5). A partial decrease in spike amplitude was detected, albeit showing considerable dispersion as reflected in the relevant SD values, with a confidence interval of the mean at 12 hours (99%) [59% - 141%] for a 95% confidence level (Figure 3.6). Dofetilide induced an

expected prolongation in FPD and FPDc, with marked T wave shifting and a reduction in repolarisation peak amplitude compared to baseline and vehicle control traces (Figure 3.6). Due to dofetilide being a well-established FPD altering compound, an in-depth analysis was carried out to assess FPD/FPDc parameters, comparing two different beat rate correction formulas to record any relevant differences. Interestingly, when FPD/FPDc parameters were corrected using the commonly accepted Frederica's formula, FPDc resulted in a higher change achieving a 20% prolongation, compared to the lower 14% prolongation achieved using Bazett's correction formula. This suggests that Frederica's correction could result in an overcorrection or miscorrection of FPD values (Figure 3.7).

Verapamil is an L-type calcium channel blocker with a relatively short-acting binding effect on the Cav1.2 calcium channel subunit, and as such it normally displays a negative inotropic activity resulting from the reduced calcium influx that propagates the AP signal in the heart. However, contrary to what expected, in this study verapamil induced a transient increase in beat rate, with a significant increase peak of 70% 30 minutes post compound addition. CI beat amplitude showed a mirrored transient percentage decrease, with the lowest values recorded as a 60% decrease 30 minutes post compound addition. Verapamil induced detectable variations in sodium spike amplitude. However, the confidence interval of the mean (145%) at 24h post compound addition is [32.4% – 256.9%] for a 95% confidence level, suggesting that any observed changes in spike amplitude are not deemed as necessarily significant in this case (Figures 3.8 and 3.9).

Doxorubicin is a cytotoxic anthracycline, and it is a well-established structural and functional cardiotoxicant. The known acute effects of doxorubicin include drug-induced cytotoxicity, depression of myocardial contractility, tachycardia, decreases in QRS complex and QT prolongation. As expected, doxorubicin induced a significant ($p<0.001$) decrease in CI 6 hours post compound addition indicating potential loss of cell viability or structural toxicity. Doxorubicin induced an expected significant ($p<0.001$) increase in beat rate 12 hours post compound addition, increasing by a further 44% by 48 hours post compound addition. CI beat amplitude was temporarily increased by 20 % 6 hours post compound addition before showing a decreasing trend 24 hours post compound addition, reaching an overall maximum decrease of 70% after 48 hours. Sodium spike amplitude was gradually decreased, resulting in an 80% decrease 48 hours post compound addition (Figures 3.10 and 3.11).

Compound	*Mechanism*	*Expected pharmacological effect*	*Detected effect on xCELLigence ECR Cardio system*
Isoproterenol	B-adrenoceptor agonist	BR↑ BA↑ SA↑	BR↑ **BA-** SA↑
Dofetilide	Potassium channel blocker	BR↓ SA↓ FPDc↑	BR↓ SA↓ FPDc↑
Verapamil	Calcium channel blocker	BR↓ BA↓ FPDc↓SA↓	**BR↑** BA↓ SA↑
Doxorubicin	Structural cardiotoxicant	CI↓ BR↑ BA↓ SA↓ FPDc↑	CI↓ BR↑ **BA↑↓** SA↓

Figure 3.2. Known cardioactive agent effects in hiPSC-CMs vs expected physiological effects detected using impedance-based technology. hiPSC-CMs iCELL^2 were screened against a panel of known cardioactive agents on the xCELLigence Cardio ECR system. The table shows expected drug-induced effects vs detected effects on multiple parameters. Analysed parameters are: Cell Index (CI), Beat Rate (BR), Cell Index Beat Amplitude (BA), Spike Amplitude (SA), corrected Field Potential Duration (FPDc). All parameters in this table are reported as an increase (↑) a decrease (↓) or unaffected (-).

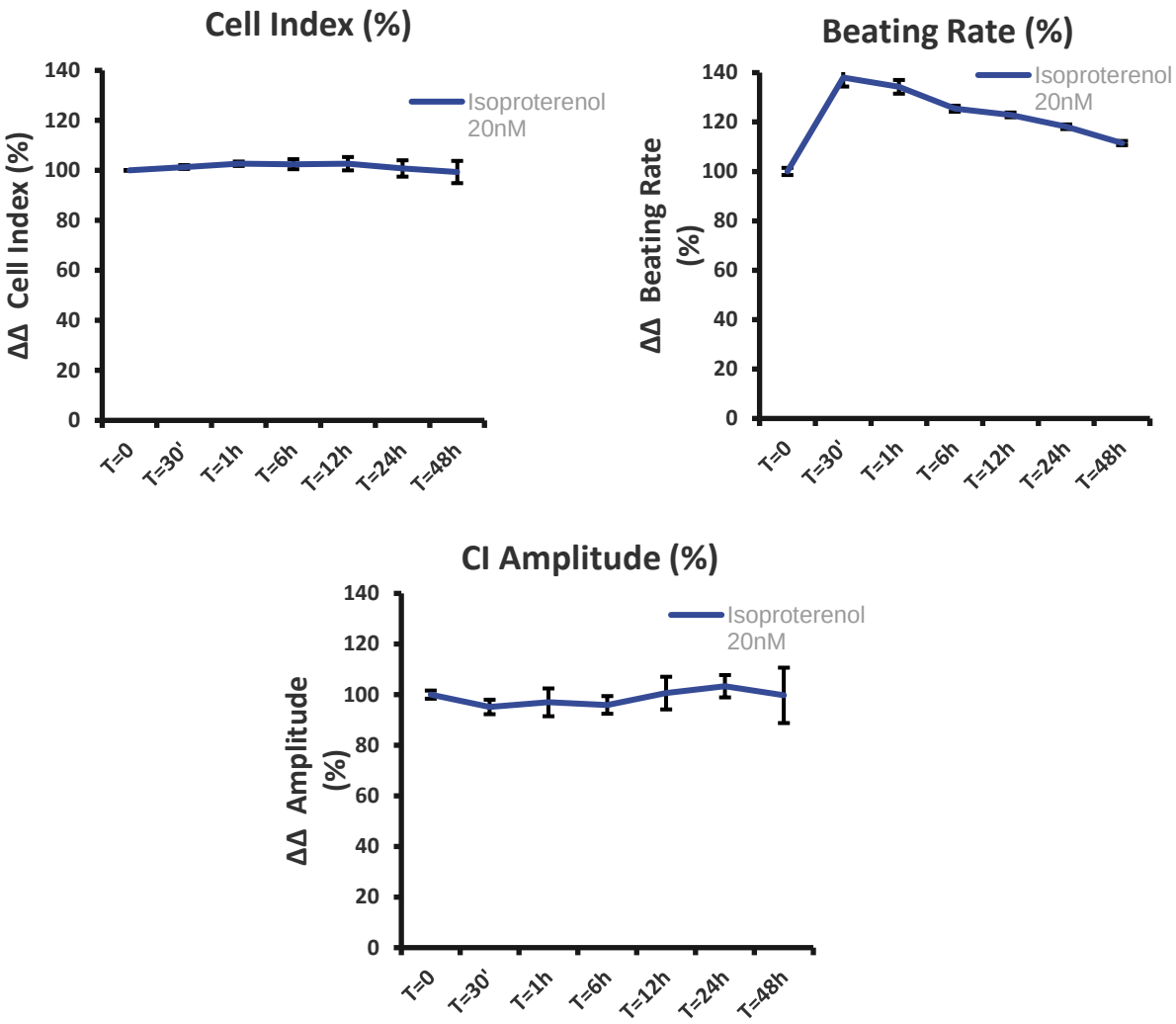

Figure 3.3. Isoproterenol induces transient contractile changes in hiPSC-CMs. hiPSC-CMs iCELL^2 were exposed to 20nM Isoproterenol for 48h in the Cardio ECR system. Isoproterenol did not affect cell viability and CI amplitude, but temporarily increased beat rate by 40%. Data are the average ± SD of at least 3 separate determinations, and are normalised to baseline and DMSO vehicle control (ΔΔ).

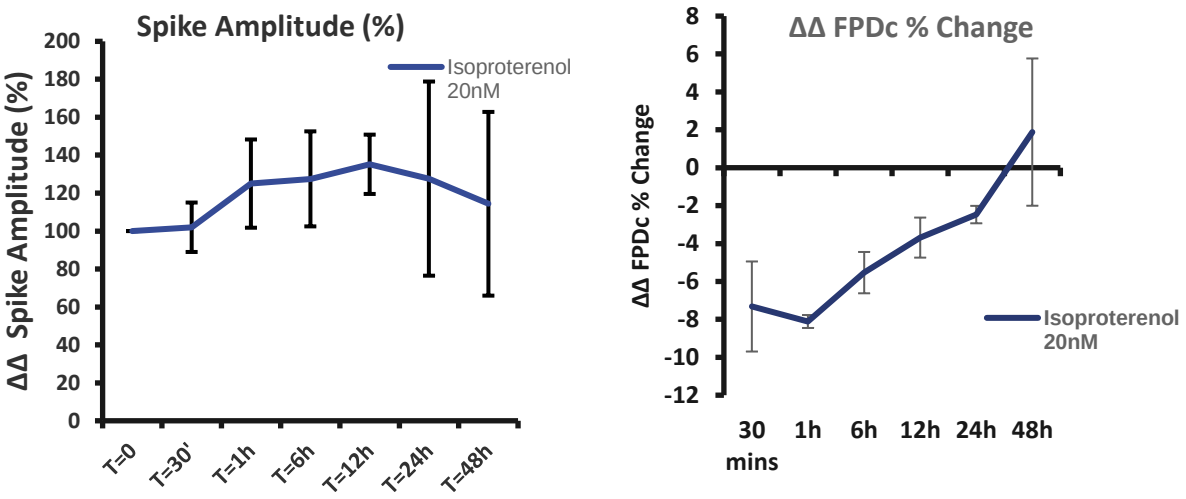

Figure 3.4 Isoproterenol induces transient electrophysiological changes in hiPSC-CMs. hiPSC-CMs iCELL^2 were exposed to 20nM Isoproterenol for 48h in the Cardio ECR system. Isoproterenol temporarily increased sodium spike amplitude by 20%. Isoproterenol induced transient non-significant FPDc shortening by 8% within 30 minutes post compound addition. Data shown for FPDc are corrected for beat rate using Fridericia's formula. Data are the average ± SD of at least 3 separate determinations, and are normalised to baseline and DMSO vehicle control (ΔΔ).

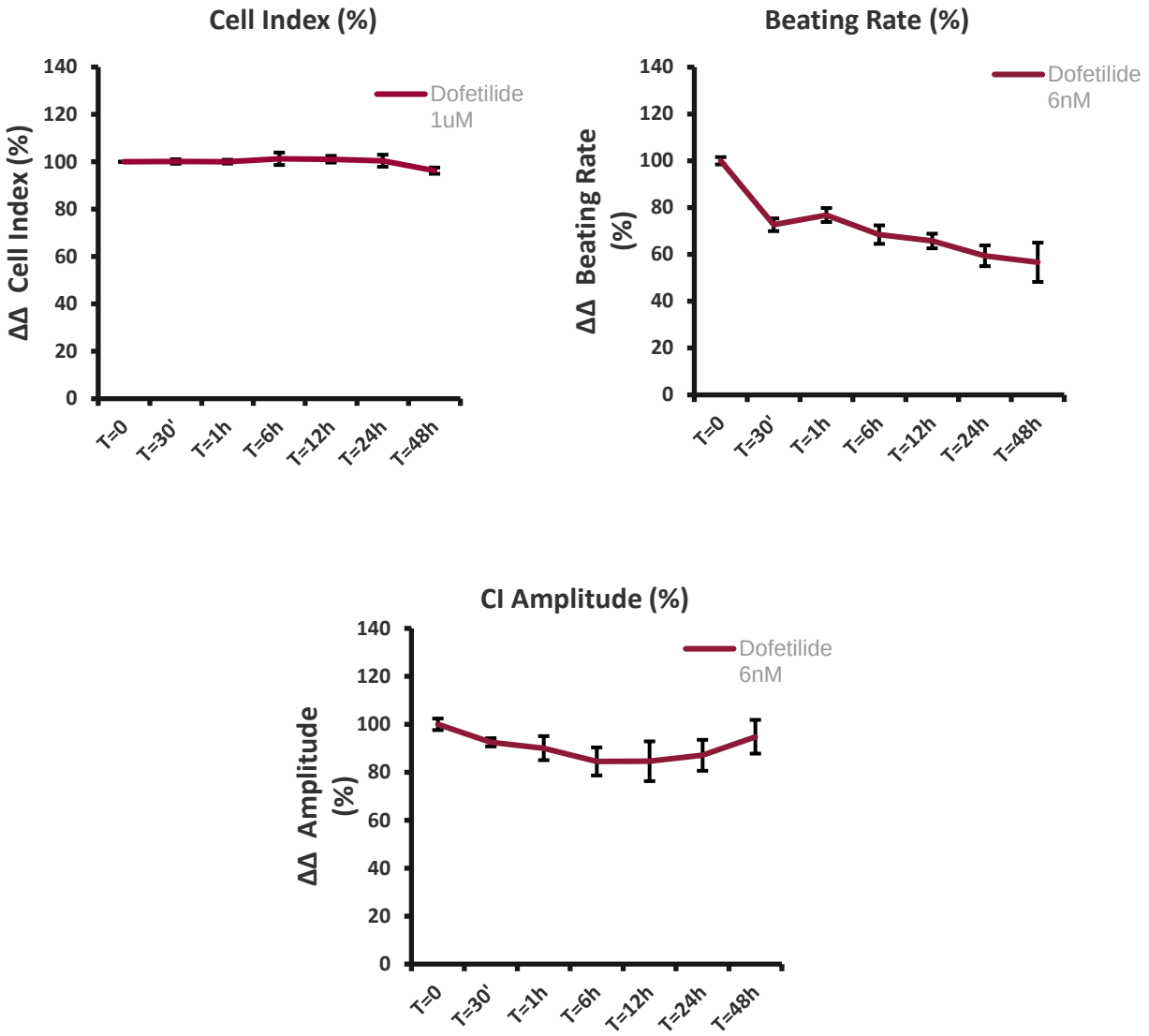

Figure 3.5. Dofetilide induces detectable contractile changes in hiPSC-CMs. hiPSC-CMs iCELL^2 were exposed to 6nM Dofetilide for 48h in the Cardio ECR system. Dofetilide did not affect cell viability. Beat rate was gradually decreased by 40% at 48h. CI amplitude resulted in a 10 to 20% transient decrease. Data are the average ± SD of at least 3 separate determinations, and are normalised to baseline and DMSO vehicle control (ΔΔ)*.*

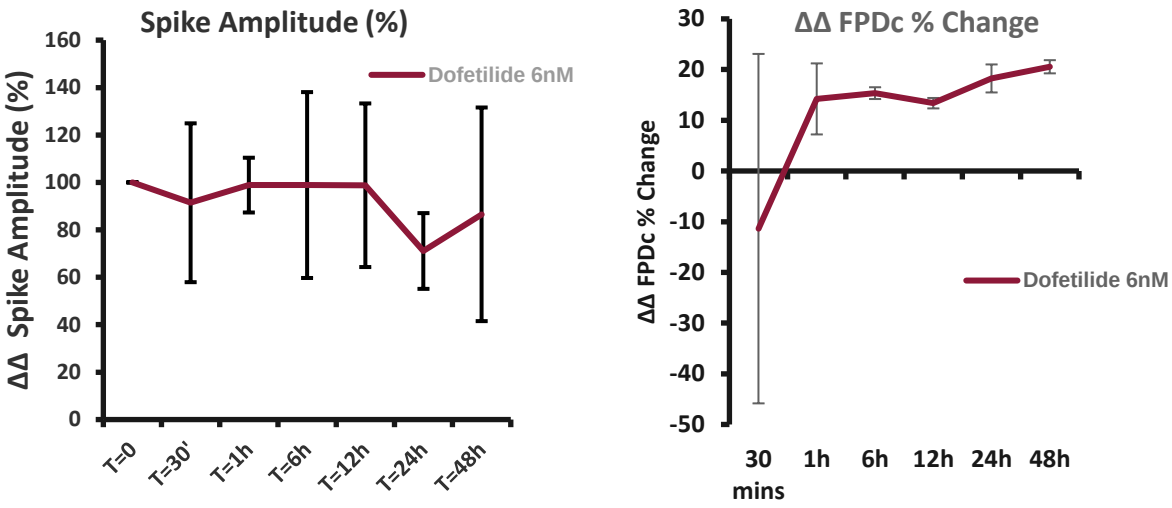

Figure 3.6 Dofetilide induces detectable electrophysiological changes in hiPSC-CMs. hiPSC-CMs iCELL^2 were exposed to 6nM Dofetilide for 48h in the Cardio ECR system. Spike amplitude was decreased at 24h and 48h, albeit with high dispersion. Dofetilide induced FPDc prolongation by 20% within 48h post compound addition. Data shown for FPDc are corrected for beat rate using Fridericia's formula. Data are the average ± SD of at least 3 separate determinations, and are normalised to baseline and DMSO vehicle control (ΔΔ)**.**

$$FPDc = \frac{FPD}{\sqrt[3]{\frac{RR}{1s}}}$$

$$FPDc = \frac{FPD}{\sqrt{\frac{RR}{1s}}}$$

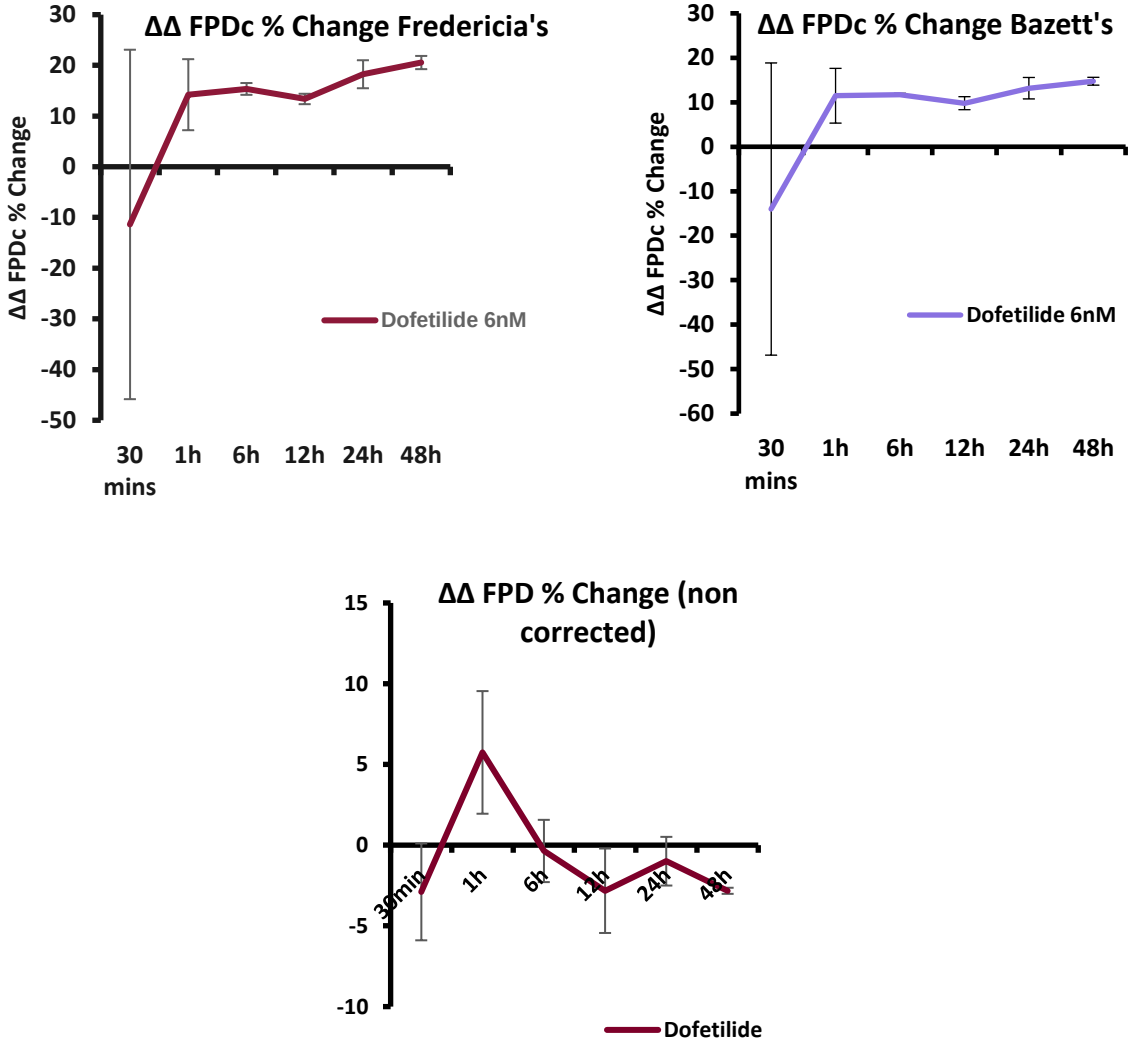

Figure 3.7. Fredericia's correction formula can result in overcorrection of FPDc parameters in hiPSC-CMs. hiPSC-CMs iCELL2 were exposed to 6nM Dofetilide for 48h in the Cardio ECR system. Data shown for FPDc are corrected for beat rate using Fridericia's formula and Bazett's formula, and are the average ± SD of at least 3 separate determinations, normalised to baseline and vehicle control. Data shown for FPD are not corrected for beat rate, and are the average ± SD of at least 3 separate determinations, normalised to baseline and vehicle control. Tested by ANOVA followed by Dunnet's post-hoc modifications.

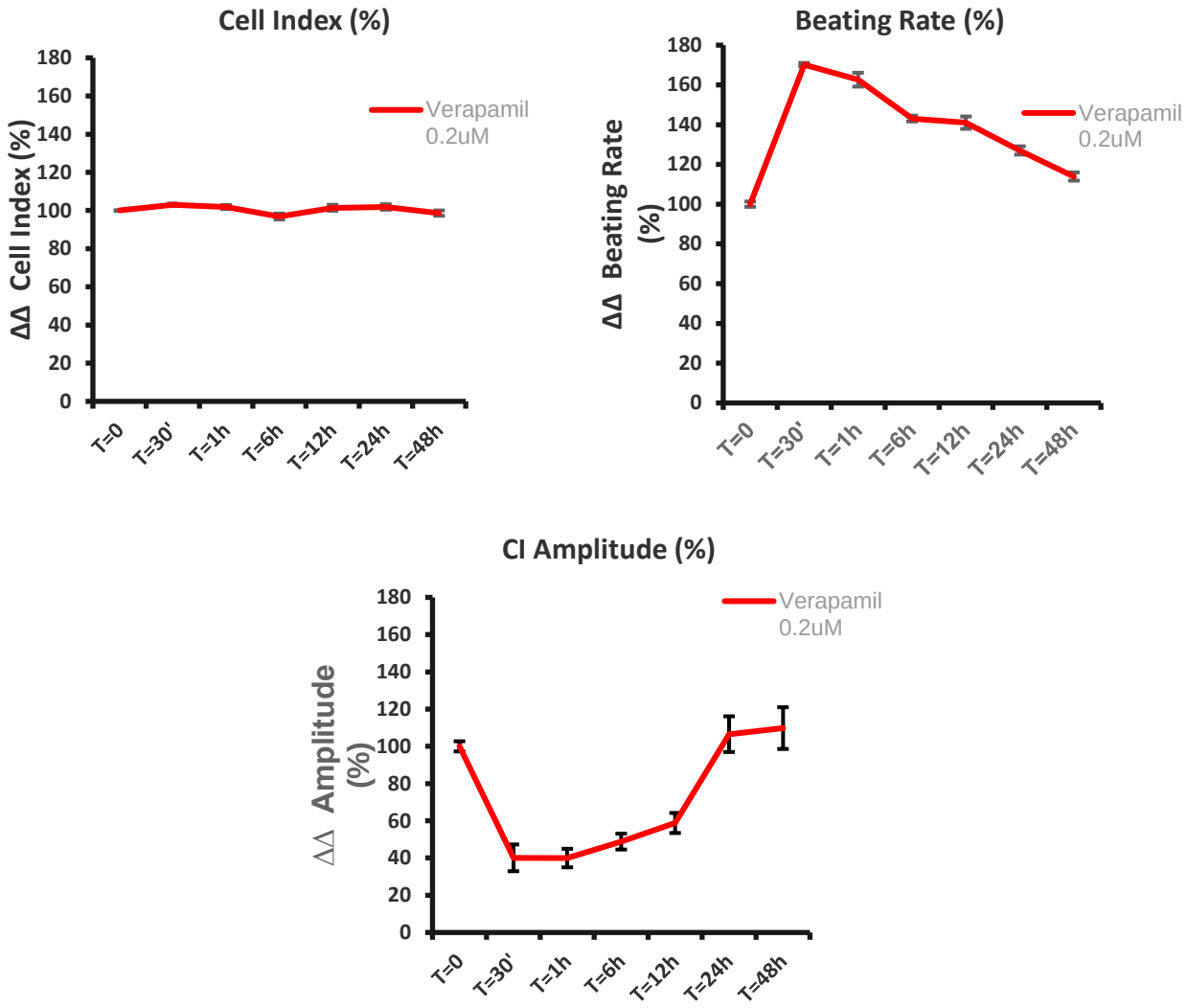

Figure 3.8. Verapamil induces transient contractile changes in hiPSC-CMs. hiPSC-CMs iCELL^2 were exposed to 0.2µM Verapamil for 48h in the Cardio ECR system. Verapamil did not affect cell viability, but increased beat rate by 60% whilst simultaneously decreased CI amplitude by 60%, in a mirrored manner. Data are the average ± SD of at least 3 separate determinations, and are normalised to baseline and DMSO vehicle control.

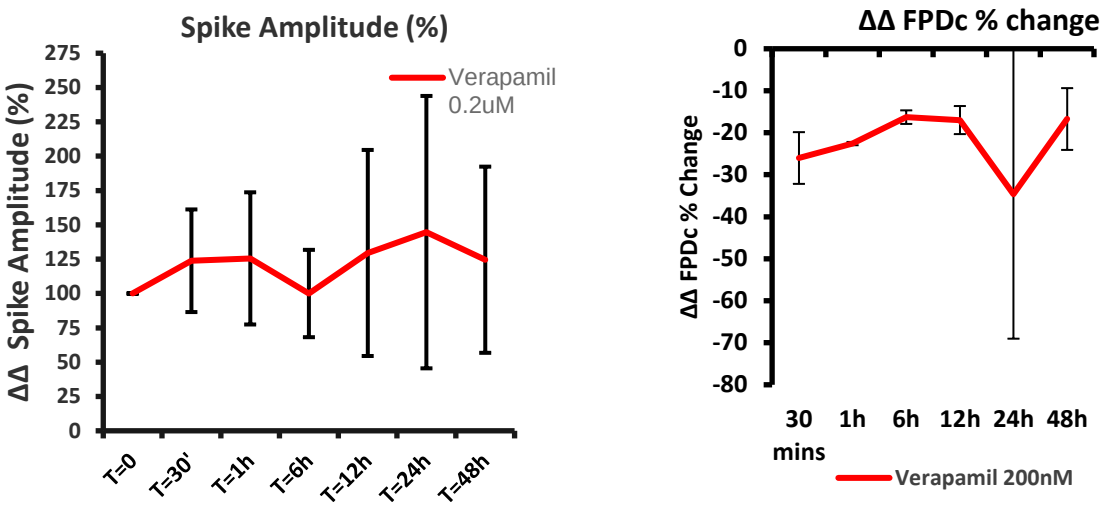

Figure 3.9 Verapamil induces transient electrophysiological changes in hiPSC-CMs. hiPSC-CMs iCELL^2 were exposed to 0.2µM Verapamil for 48h in the Cardio ECR system. Data shown for FPDc are corrected for beat rate using Fredericia's formula. Data are the average ± SD of at least 3 separate determinations, and are normalised to baseline and DMSO vehicle control (ΔΔ).

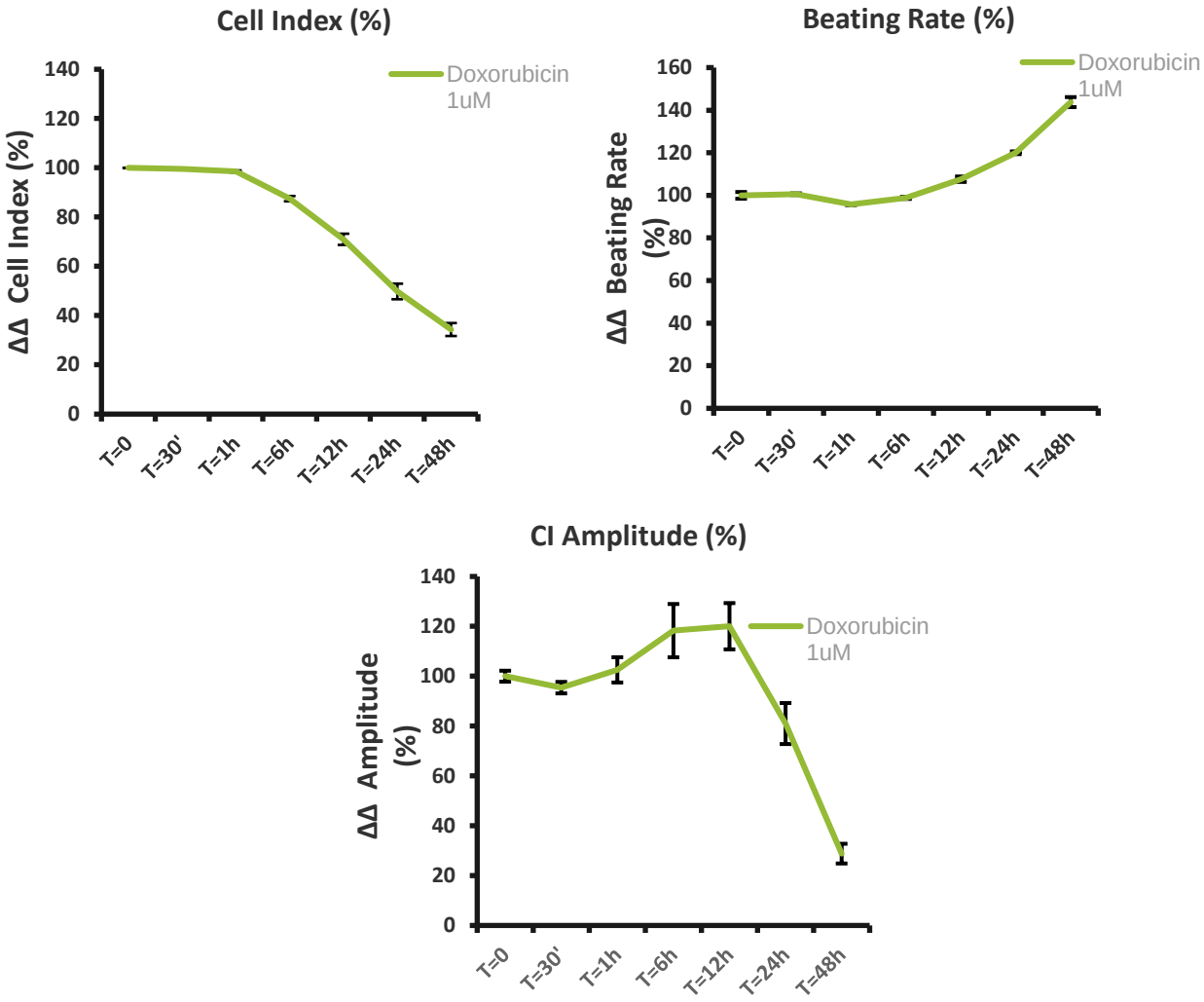

Figure 3.10. Doxorubicin induces permanent contractile changes in hiPSC-CMs. hiPSC-CMs iCELL^2 were exposed to 1µM Doxorubicin for 48h in the Cardio ECR system. Doxorubicin induced a 70% decrease in cell viability. Doxorubicin induced an increase in beat rate by 40% and a simultaneous decrease in CI amplitude by 70%. Spike amplitude was decreased by 80%. Data are the average ± SD of at least 3 separate determinations, and are normalised to baseline and vehicle control.

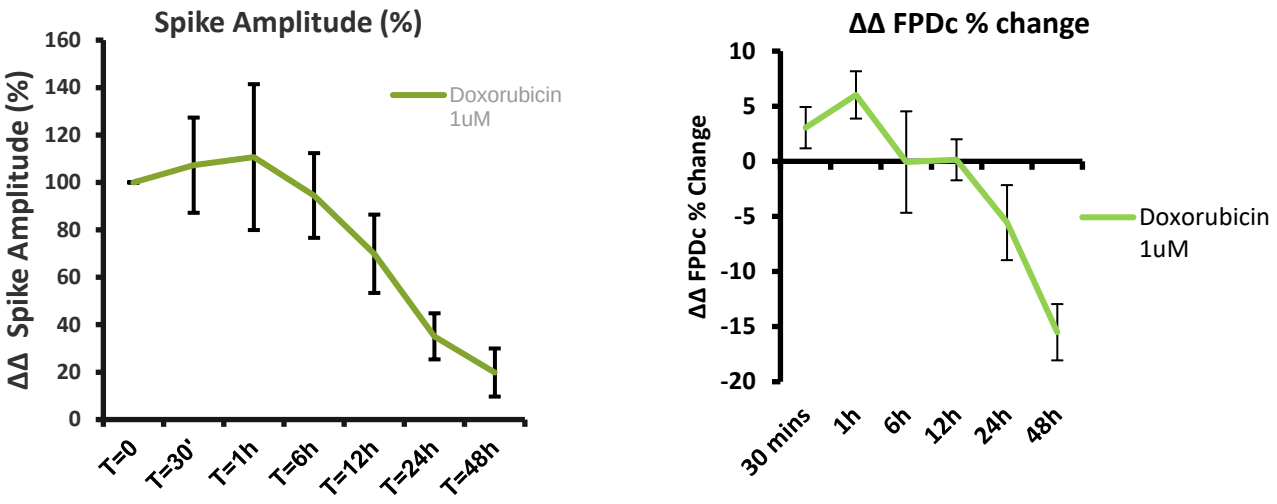

Figure 3.11. Doxorubicin induces permanent electrophysiological changes in hiPSC-CMs. hiPSC-CMs iCELL^2 were exposed to 1µM Doxorubicin for 48h in the Cardio ECR system. Doxorubicin induced a permanent decrease in spike amplitude and FPDc parameter. Data shown for FPDc are corrected for beat rate using Fridericia's formula. Data are the average ± SD of at least 3 separate determinations, and are normalised to baseline and DMSO vehicle control (ΔΔ).

3.3 Pan-HDAC inhibition induces perturbations in viability and functional parameters in hiPSC-CMs

The commercially-sourced hiPSC-CMs iCELL^2 were screened against the pan-HDACi SAHA at a range of concentrations, between 20 μM and 0.05 μM, representing clinically applicable concentrations (clinical plasma Cmax = 1.2 ± 0.53 μM). These studies were carried out using the xCELLigence Cardio ECR system, as previously described (section 2.7.3), and were focused on detection of acute structural and functional perturbations. The assessed parameters included impedance CI, beat rate, beat amplitude, sodium spike amplitude and FPD/FPDc. All parameters were monitored in real-time and analysed at multiple time points to gain an insight into parameter changes and fluctuations. In order to confirm and validate the representative function of each batch of hiPSC-CMs, cells were grown for 5 days post plating before drug exposures. Each validated batch of hiPSC-CMs were then exposed to a single dose of SAHA for a maximum of 48 hours. This limited exposure period being based on evidence in the literature suggesting that longer-term culture of hiPSC-CM associates with a permanent loss of cardiac phenotype through de-differentiation (Ebert et al. 2019).

In this study, SAHA did not induce proportional concentration-dependent changes in CI, with different responses observed at concentrations above the therapeutic range relative to those at or below the clinically-relevant concentrations. Double-normalised analysis showed a significant ($p<0.001$) progressive decrease in CI at concentrations greater than their therapeutic range (3 - 20 μM) from 12 hours post compound addition. In contrast, clinically relevant concentrations (0.05 - 0 1 μM) induced a 5 - 13% increase in CI by 24 hours post compound addition (Figure 3.12). To ascertain whether the differential correlations between CI variations and SAHA concentration were due to loss of cellular viability or induction of cell death, an ATP quantification assay was performed on the treated cells (methodology outlined in section 2.5) upon termination of the Cardio ECR assay. No significant loss of cell viability was detected within the therapeutic range of SAHA, up to the termination of the assay at 48 hours after drug addition. Within the concentration range 3-20 μM, associated with a 60-73% decrease in CI, only a 40% reduction in cellular viability was observed over the 48 hour exposure period, even at the highest concentration. Together, these results therefore suggest

that the reduction in CI is only partially due to cell death, with factors related to changes in cellular morphology or structural integrity playing a significant role.

SAHA induced dose-dependent effects on contractility parameters. Beat rate changes were recorded as early as 12 hours post compound addition for SAHA concentrations 0.2-1 µM, and at 6 hours post compound addition for SAHA concentrations 3-20 µM. All concentrations between 3 µM and 20 µM resulted in complete loss of contractility 24 hours post compound addition (figure 3.14). Impedance beat amplitude parameters were affected in a similar manner, with a decrease in amplitude observed 12 hours post compound addition for concentrations 3-20 µM, and a significant decrease for concentrations 0.2-1 µM (change > 20%; $p < 0.001$) decreased 12 hours post compound addition (Figure 3.15).

Analysis of electrophysiological parameters demonstrated that changes in spike amplitude voltage were triggered following treatment with SAHA at most concentrations in a dose-dependent manner (Figure 3.18). Depolarisation spike amplitude changes followed an increasing trend starting as early as 1 hour post SAHA exposure at most tested concentrations. After 12 to 24 hours post SAHA exposure, changes in spike amplitude demonstrated a decrease at all SAHA concentrations, with the exception of 0.05 µM and 0.2 µM where, on the contrary, both concentrations maintained an increasing trend.

Additionally, changes in FPDc followed a decreasing trend starting 12 hours post compound addition at SAHA concentrations 3-20 µM, and 24 hours post compound addition at SAHA concentrations between 0.02-1µM (Figure 3.17).

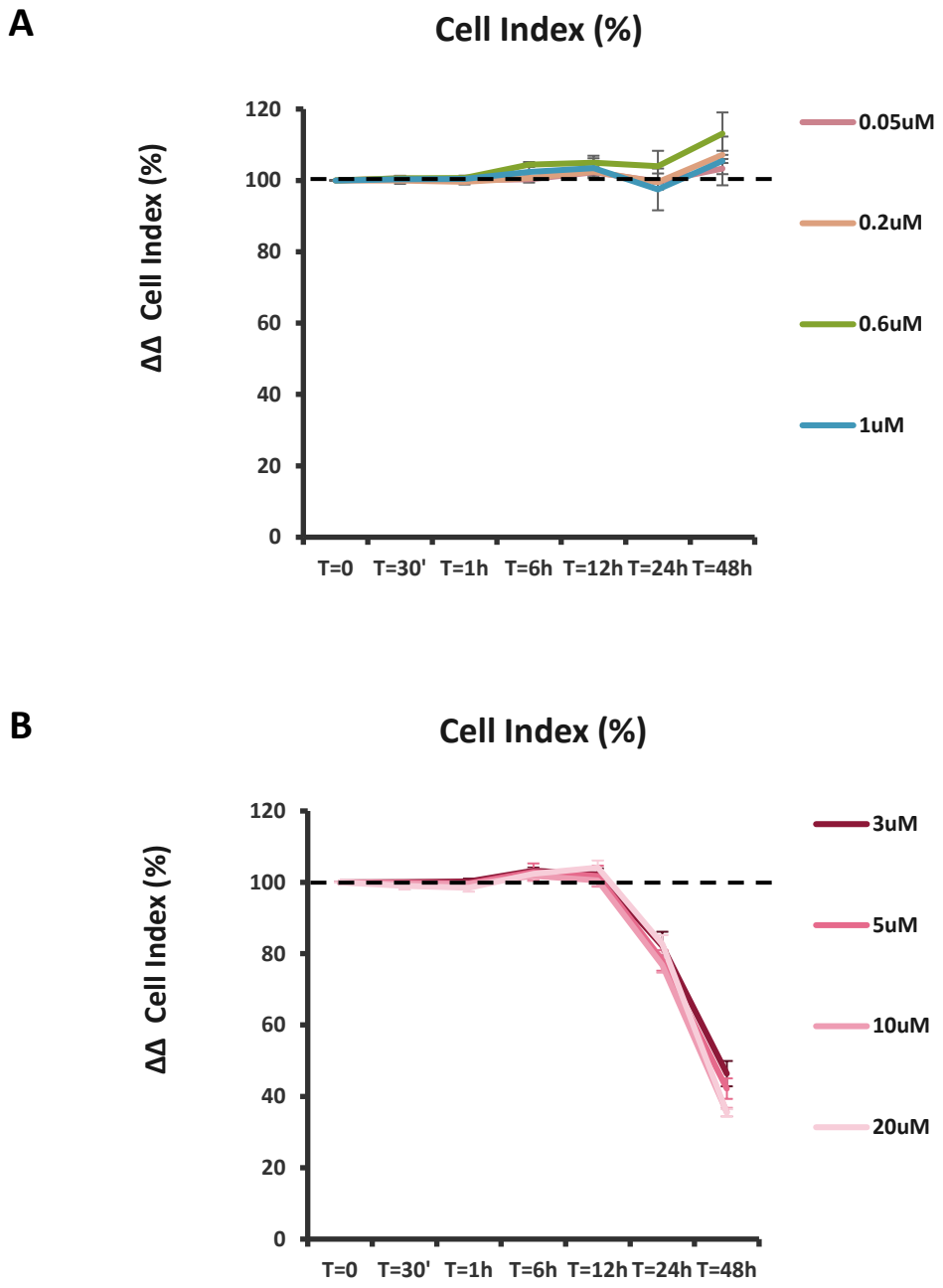

Figure 3.12 SAHA does not induce dose-dependent changes in CI. hiPSC-CMs in the Cardio ECR system were exposed to SAHA at a range of concentrations 0.05 µM to 20 µM for 48 h **A.** SAHA concentrations between 0.05 µM and 1 µM did not have effects on CI. **B.** SAHA concentrations between 3 µM and 20 µM induced a significant (% change > 20%, $p < 0.001$) decrease in CI from 12 h post compound addition. Data are the average ±SD of at least 3 separate determinations, and are normalised to baseline and vehicle control. Tested by ANOVA and Bonferroni post-hoc modifications.

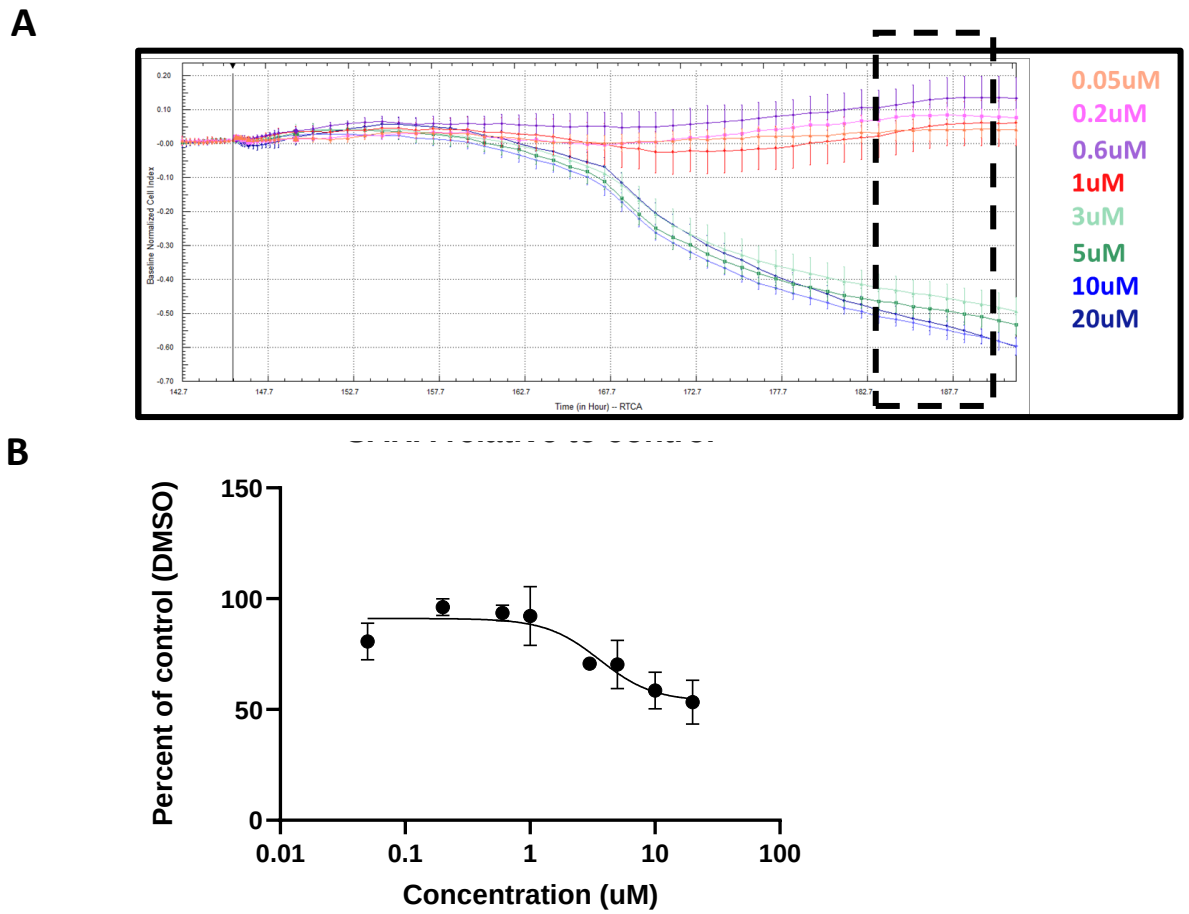

Figure 3.13 CI decrease induced by pan-HDACi SAHA at cytotoxic concentrations is not exclusively attributed to loss of cell viability in hiPSC-CMs. A. hiPSC-CMs were exposed to SAHA at a range of concentrations for 48h. SAHA induced a CI decrease by 70% 48h post compound addition at concentrations between 3 µM and 20 µM. Data are representative xCELLigence Cardio ECR traces showing CI vs Time (h) ±SD. **B.** The Cell-Titer Glo ATP luminescence assay was performed on hiPSC-CMs in the Cardio ECR E-plate following exposure to SAHA for 48h, results show a dose-dependent decrease in cell viability, where at the highest concentration 60% cells were viable. Data are normalised to vehicle control and are the average ±SD of at least 3 separate determinations.

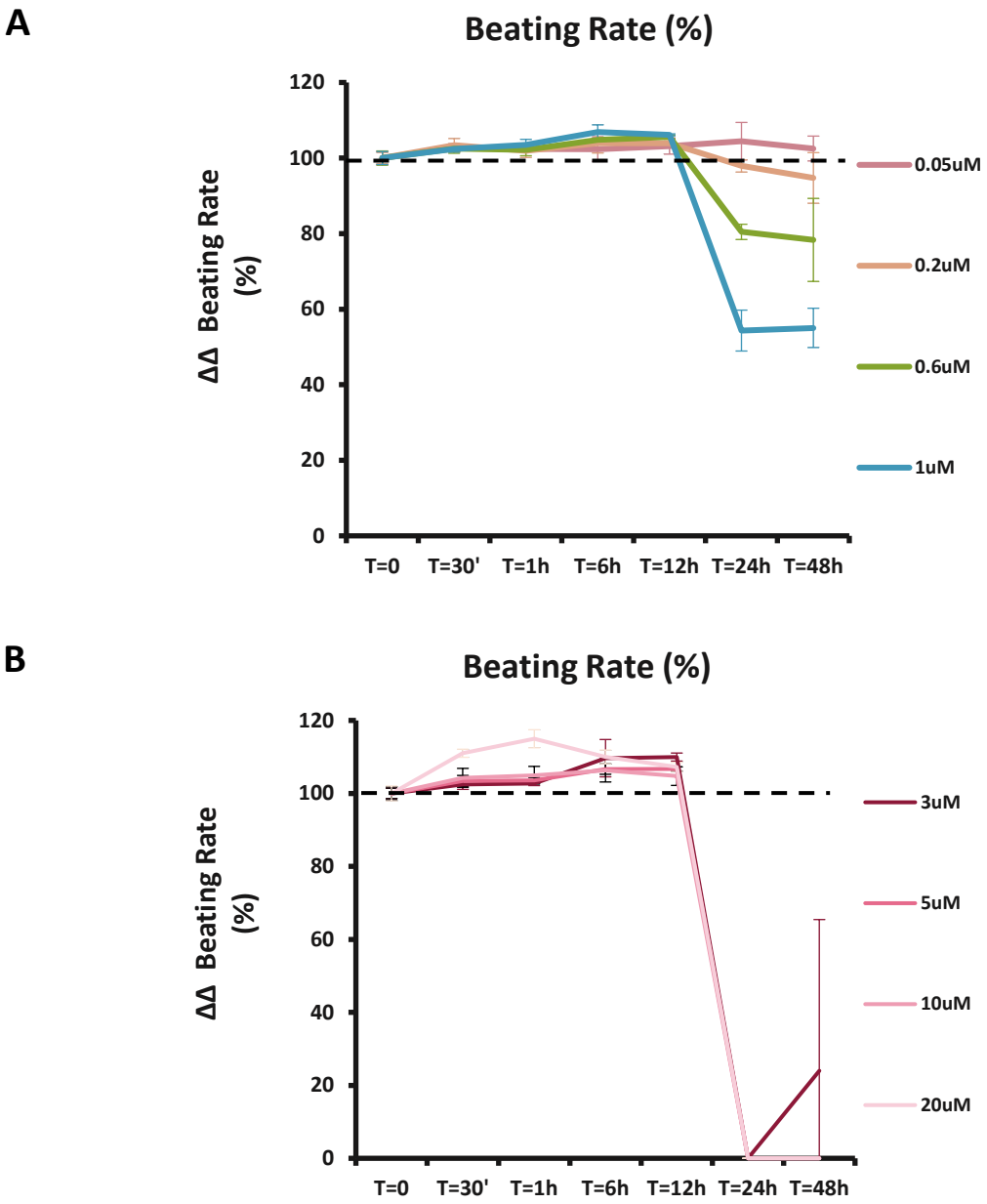

Figure 3.14 SAHA induces dose and time dependent changes in beat rate at clinical and toxic concentrations in hiPSC-CMs. hiPSC-CMs were exposed to SAHA at a range of concentrations for 48 h. SAHA induced significant beat rate changes starting from 12 h post compound addition at concentrations between 0.6 µM and 20 µM in a dose-dependent manner. Data are the average ±SD of at least 3 separate determinations, and are normalised to baseline and vehicle control. Tested by ANOVA and Bonferroni post-hoc modifications.

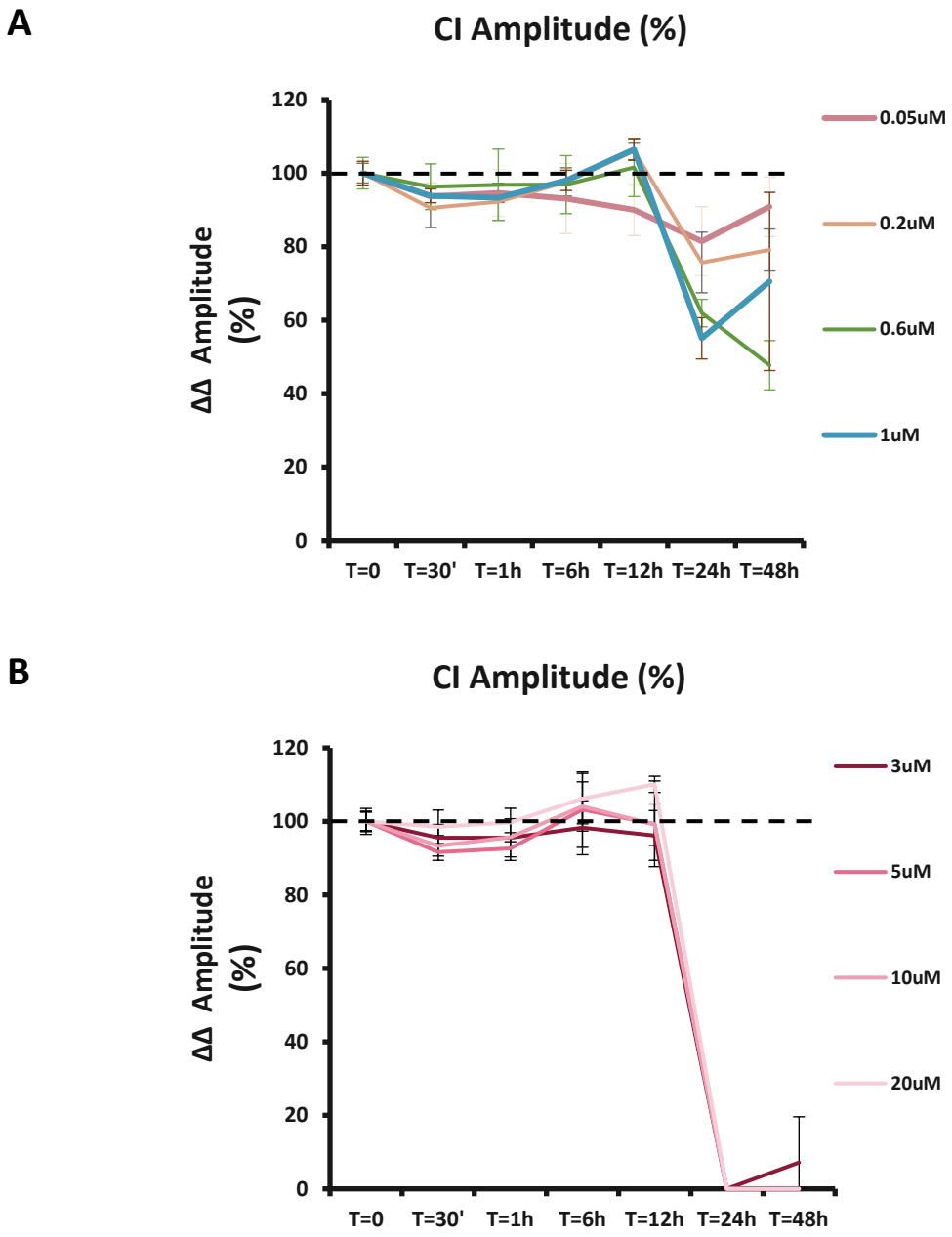

Figure 3.15 SAHA induces dose and time dependent changes in impedance beat amplitude at clinical and toxic concentrations in hiPSC-CMs. hiPSC-CMs were exposed to SAHA at a range of concentrations for 48 h. SAHA induced significant beat amplitude changes starting from 12 h post addition at concentrations between 0.6 µM and 20 µM in a dose-dependent manner. Data are the average ±SD of at least 3 separate determinations, and are normalised to baseline and vehicle control. Tested by ANOVA and Bonferroni post-hoc modifications.

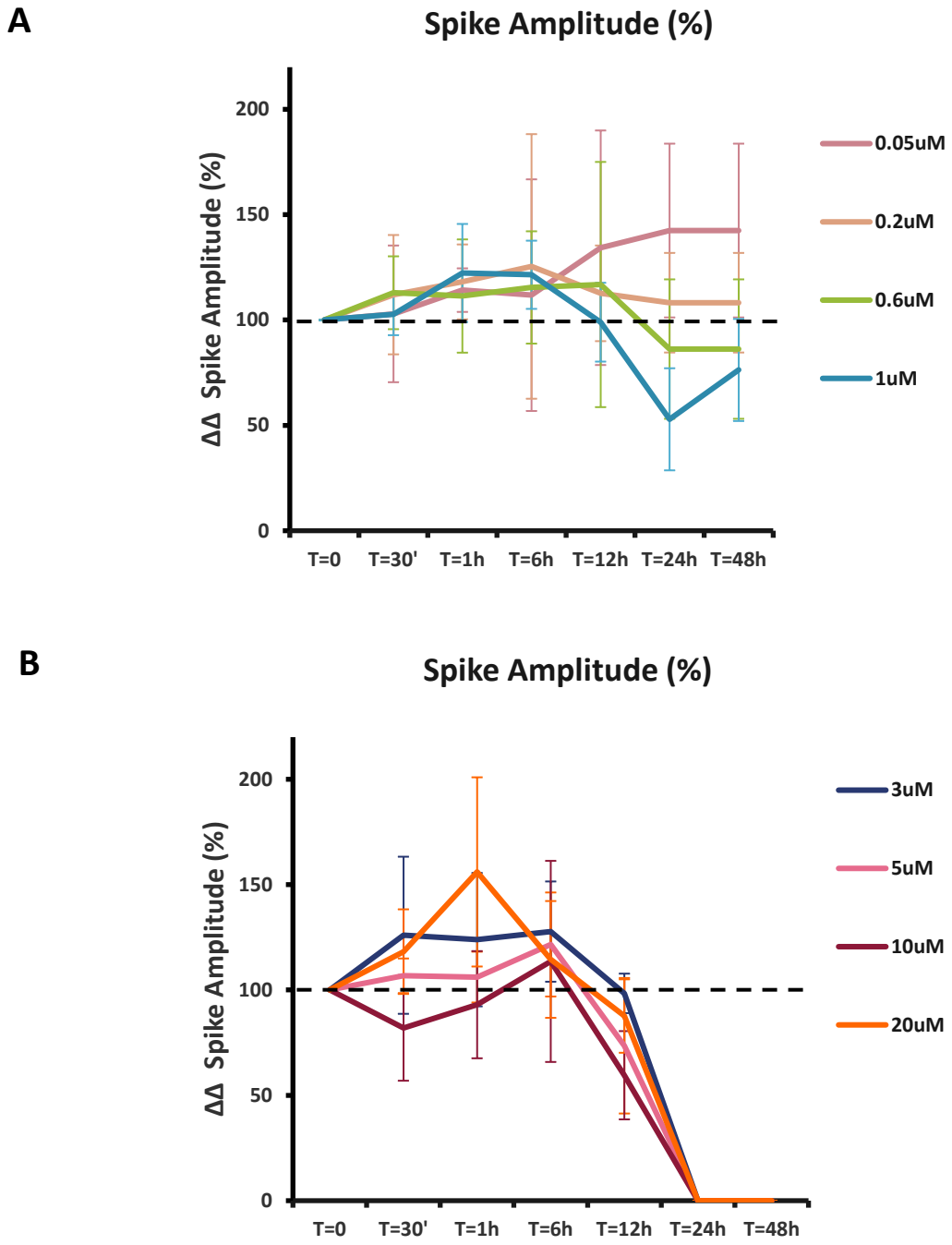

Figure 3.16 SAHA induces dose and time dependent changes in spike amplitude at clinical and toxic concentrations in hiPSC-CMs. hiPSC-CMs were exposed to SAHA at a range of concentrations for 48 h. SAHA induced significant spike amplitude changes starting from 6 h post addition, causing a decrease at concentrations between 0.6 µM and 20 µM, and an increase at 0.05 µM. Data are the average ±SD of at least 3 separate determinations, and are normalised to baseline and vehicle control. Tested by ANOVA and Bonferroni post-hoc modifications.

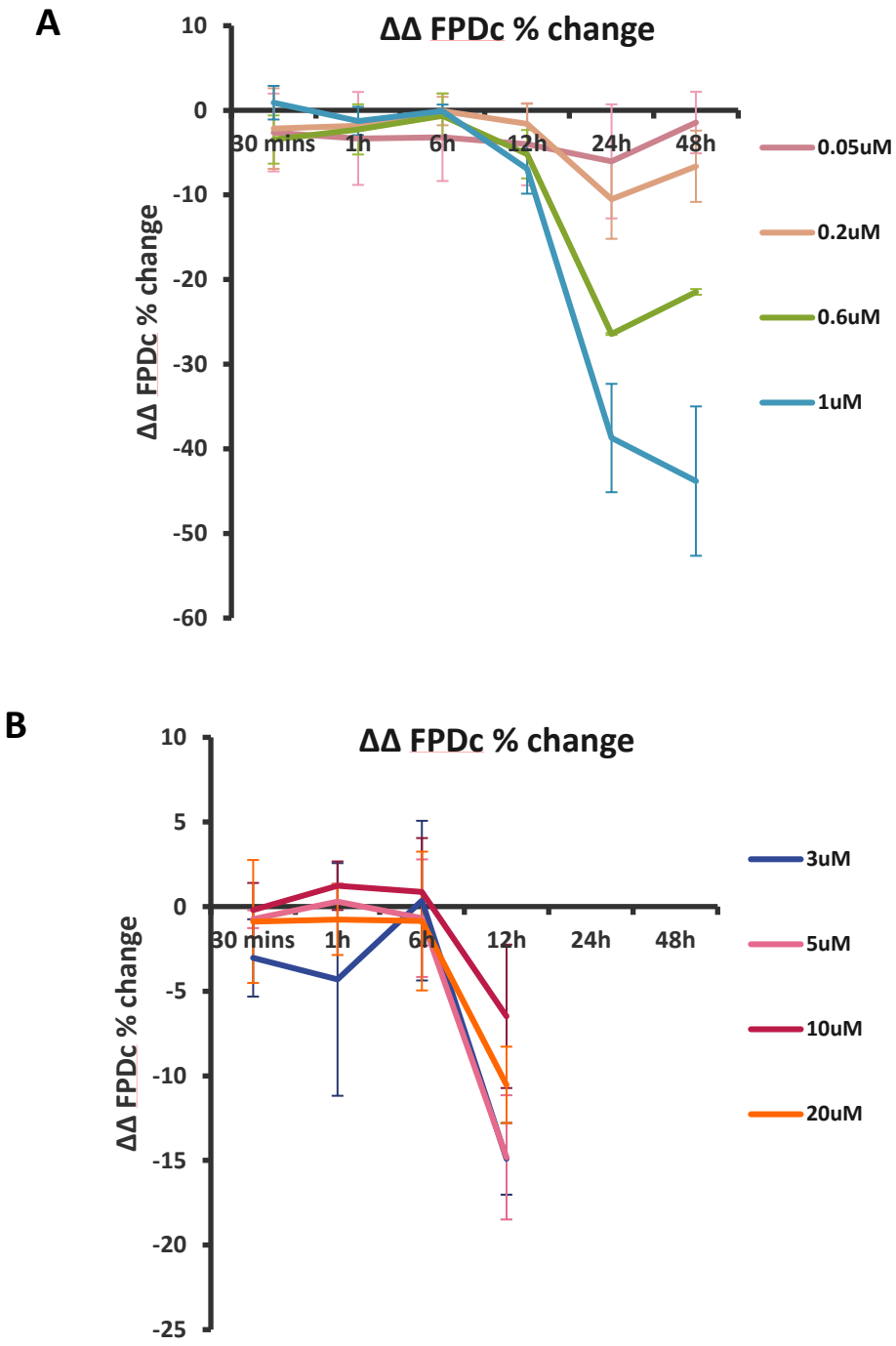

Figure 3.17 SAHA induces dose and time dependent changes in FPDc at clinical and toxic concentrations in hiPSC-CMs. hiPSC-CMs were exposed to SAHA at a range of concentrations for 48 h. SAHA induced a significant ($P<0.001$) decrease to FPDc starting from 6h post addition at concentrations between 3 µM and 20 µM, and from 12 h at concentrations between 0.05 µM and 1 µM. Data are the average ±SD of at least 3 separate determinations. Tested by ANOVA and Bonferroni post-hoc modifications.

Taken together, these results indicate that nearly all measured parameters consistently decreased in response to SAHA concentrations 0.6-20 µM, and for most parameters the maximum changes to baseline were recorded after 24 hours from initial compound addition (Figure 3.18). Overall, the study suggests that SAHA-induced toxicity in hiPSC-CMs is likely attributed to a combination of mechanisms, related to the concentration being at or below the therapeutic range, or above these concentrations. In this regard, normalised FPDc values demonstrated a significant shortening in field potential duration at SAHA concentrations within the therapeutic range, that did not induce significant changes to other parameters including beat rate and CI. This is suggestive of SAHA affecting propagation of the AP through modulation of specific ionic currents, possibly hERG. Additionally, the significant ($p< 0.05$) increase in spike amplitude recorded at 24 hours post compound addition with SAHA concentrations of 0.05 µM and 0.2, is indicative that SAHA may also interfere with sodium-related ion currents even at sub-clinical doses (Figure 3.20). Furthermore, the concomitant decrease in CI beat amplitude is also suggestive of a negative inotropic effect, imputable to either electrophysiological disruptions or structural cardiomyocyte disruptions, at a syncytial or metabolic level (Figure 3.18). Overall, this study demonstrates an acute effect of SAHA upon cardiac function at therapeutically relevant concentrations.

These data thereby support an effect of pan-HDACi upon cardiomyocyte contractility, viability, and structural integrity and morphology, with several potential mechanisms involved. Although these effects may relate to actions upon HDACs (or other secondary protein targets) *per se*, it is highly likely that effects can be attributed to modulation of specific classes or even individual HDACs themselves. Therefore, an investigation on the effect of sub-selective class specific HDACi is needed. Ultimately, further investigations designed to discern additional structural and functional endpoints would be required to provide a more defined mechanistic insight of HDACi-induced cardiotoxicity.

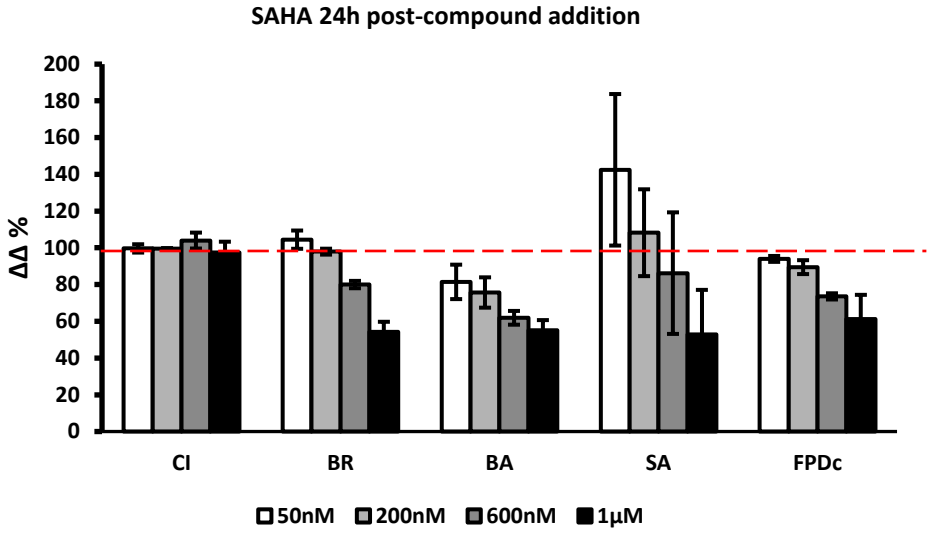

Figure 3.18 SAHA induces maximum acute cardiotoxic effects in hiPSC-CMs after 24 h exposure. hiPSC-CMs iCELL^2 exposed to SAHA on the xCELLigence Cardio ECR system detect maximum perturbations in BR, BA, SA and FPDc parameters 24 h post compound addition. Changes in BA and SA that did not otherwise induce significant perturbations are evident. Data are normalised to baseline and vehicle control (ΔΔ), and are the average ±SD of at least 3 separate determinations. Tested by ANOVA followed by Bonferroni post-hoc modifications.

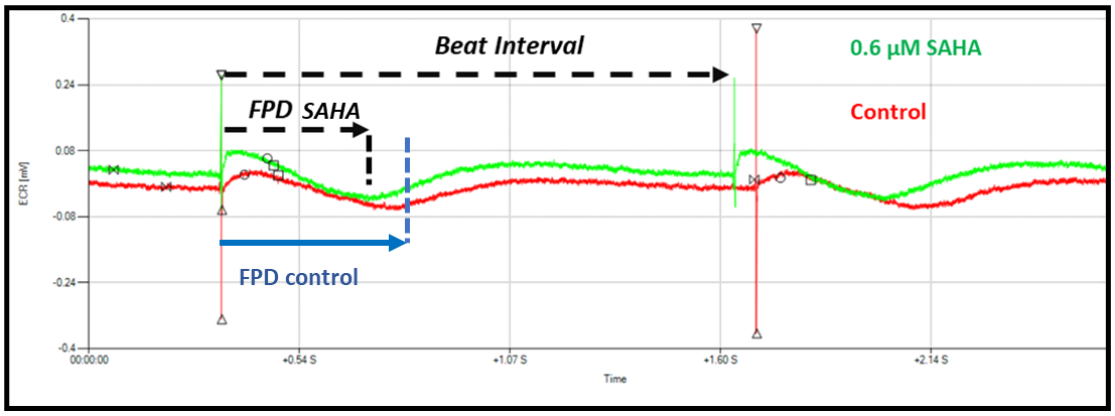

Figure 3.19 SAHA induces shortening of FPD at sub-clinical concentrations in hiPSC-CMs. hiPSC-CMs exposed to 50 nM SAHA display a shortening in FPD compared to vehicle control. Data shows selected representative ECR traces.

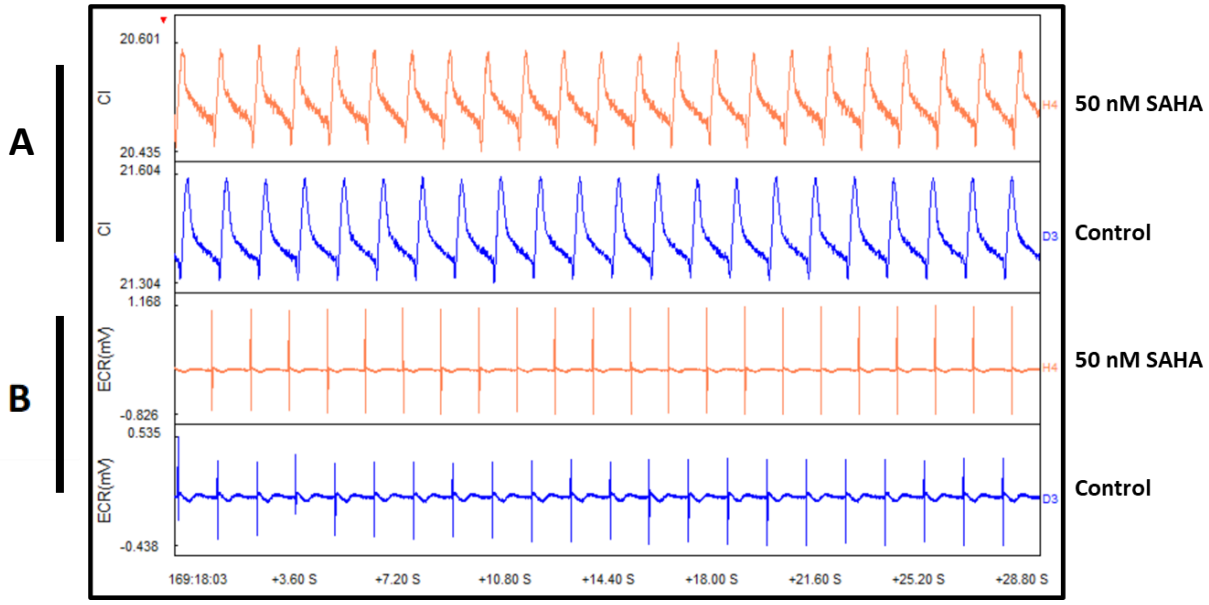

Figure 3.20 SAHA induces an increase in depolarisation spike amplitude (mV) at sub-clinical concentrations in hiPSC-CMs. hiPSC-CMs exposed to 50 nM SAHA result in an increased sodium depolarisation spike amplitude. This concentration did not elicit significant changes in other measured parameters (BR, BA, FPDc). Data shows selected representative traces of impedance contractility (A) and their respective ECR traces (B).

3.4 Selective HDAC inhibition in hiPSC-CMs elucidates different mechanisms of HDACi-induced cardiotoxicity

To establish whether HDACi-induced cardiotoxicity could be attributed to the inhibition of a specific sub-class of HDACs, an investigation into the effects of selective HDACi in hiPSC-CMs was carried out using the xCELLigence Cardio ECR system. The same experimental setup defined in section 3.3 was adopted, with the measured parameters being overall CI, beat rate, CI beat amplitude, spike amplitude and FPDc.

In these studies, iCELL^2 hiPSC-CMs were exposed to a class I-selective HDAC inhibitor (MS275) and a class IIb-selective HDAC inhibitor (Tubacin); MS-275 (Entinostat®) is currently in phase 3 clinical trials, whereas Tubacin is an experimental compound not currently used in a clinical setting. The evaluation of a specific involvement or role for class IIa HDACs in HDACi-induced cardiotoxicity is not yet feasible due to an absence of available selective agents. It is however of note that class IIa HDACs demonstrate very low enzymatic activity and are only weakly affected by pan-HDACis, such as SAHA, implying the effects of SAHA are unlikely to be attributed to class IIa HDACs (Hsu et al. 2017).

3.4.1 Class I selective HDACi induces changes in cardiomyocyte viability and functionality

The study evidenced that class I HDACi MS-275 induced dose-dependent changes in CI, resulting in cytotoxicity at a supra-therapeutic concentration of 5 µM and no detectable cytotoxicity at therapeutically relevant concentrations of 1 µM and 0.5 µM; (Clinical plasma C_{max} = 303 ± 223nM). Specifically, CI values were monitored for 48 hours, and a significant ($p<0.05$) increase in CI by 10% was observed in response to 1 µM and 0.5 µM MS-275 concentrations. Conversely, 5 µM MS275 induced a noticeable, albeit non-significant, 5% increase in CI between 6 and 12 hours post compound addition, before inducing a significant ($p< 0.001$) decrease by 60% 48 hours post compound addition.

MS-275 did not induce changes in beat rate until 24 hours post compound addition. In particular, a complete loss of contractility was observed 24 hours post compound addition

with 5 µM, and 48 hours post compound addition with 1 µM. Exposure to 0.5 µM concentration resulted in partial loss of contractility, significantly decreasing beat rate by 34% to baseline ($p<0.001$).

The effects of MS-275 on beat rate were reflected in a similar manner on CI beat amplitude. Similarly to beat rate, beat amplitude decreased 24 hours post compound addition, and reached a maximum decrease by 40% to baseline with a MS-275 concentration of 0.5 µM. Since 5 µM and 1 µM concentrations of MS275 induced a complete loss of contractility by 24 and 48hrs, respectively, beat amplitude parameters decreased accordingly.

In terms of ECR parameters, spike amplitude resulted in a significant ($p<0.001$) transient increase by 30% to baseline after exposure to 1 µM MS-275, 12 hours post compound addition. Spike amplitude resulted in a gradual decrease after 24 hours from initial exposure at all three tested MS-275 concentrations.

MS-275 did not induce significant changes to FPDc. The partial shortening in FPDc observed after 24 hours exposure to 1 µM MS-275 preceded the complete loss of cellular functionality and as such was not indicative of significance.

This study demonstrates that class I HDACi MS-275 affects cardiomyocyte viability and functionality in hiPSC-CMs, reflective of the effects observed with pan-HDACi SAHA. Remarkably, the sustained significant increase in depolarisation spike amplitude paired with the simultaneous decrease in CI beat amplitude is suggestive of a possible impairment of ionic currents, and is therefore in agreement with the similar effects described in section 3.3 with the use of pan-HDACi SAHA. However, specific assessments would be required to clarify the electrophysiological effects of class I inhibitors.

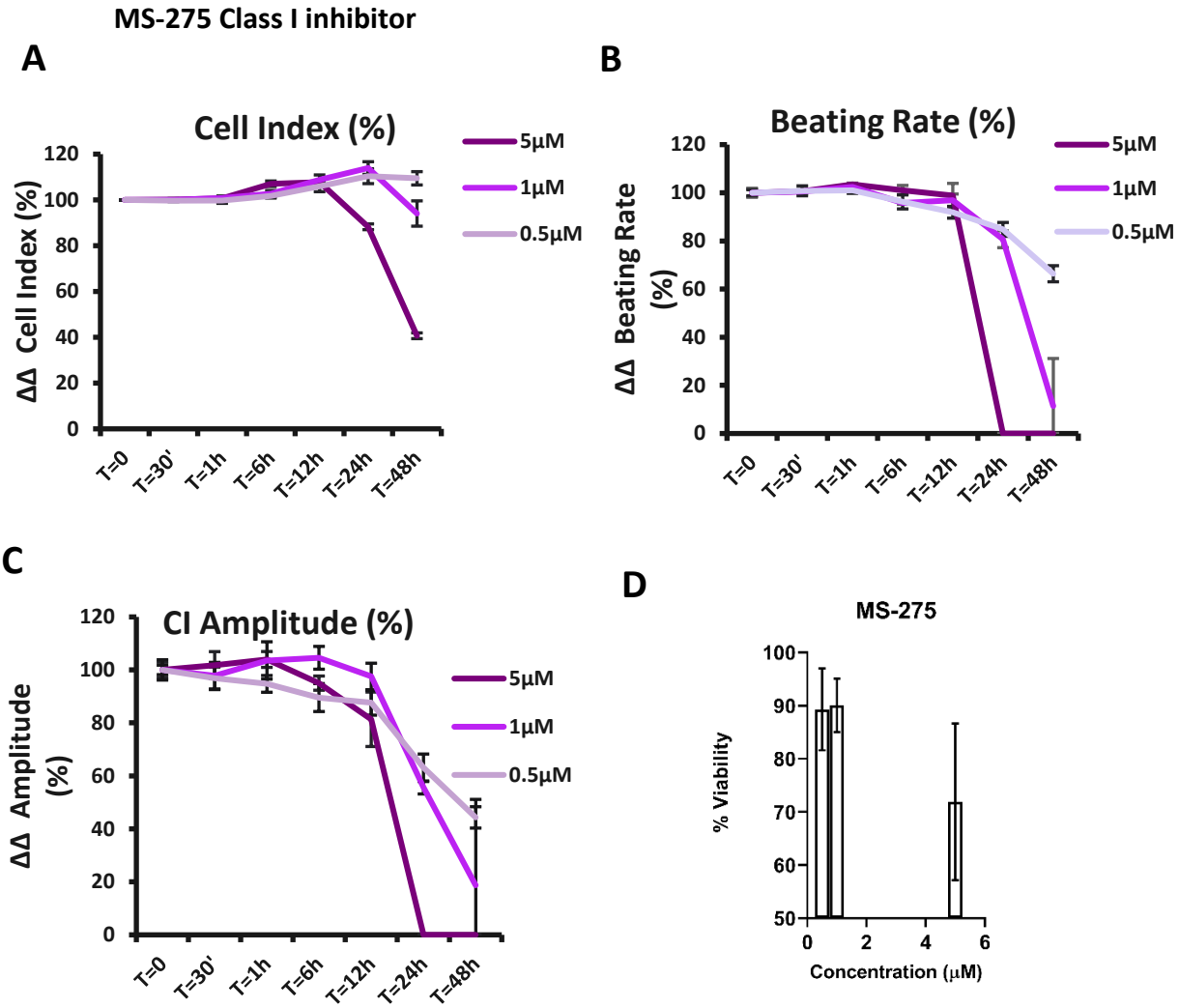

Figure 3.21 MS-275 class I inhibitor induces dose-dependent changes in impedance parameters at non-clinical and toxic concentrations in hiPSC-CMs. . hiPSC-CMs iCELL^2 were exposed to MS-275 at a range of concentrations for 48 h. **A.** MS-275 induced a significant decrease in CI at 5 µM. MS-275 induced significant ($p<0.001$) changes to beat rate(**B.**) and beat amplitude (**C.**) parameters at all used concentrations in a time and dose dose-dependent manner. Data are normalised to baseline and vehicle control (ΔΔ), and are the average ±SD of at least 3 separate determinations. Tested by ANOVA and Bonferroni post-hoc modifications. **D.** MTT assays evidenced a decrease in cell viability at 5µM but not at 1 and 0.5µM concentrations after 48 h post exposure.

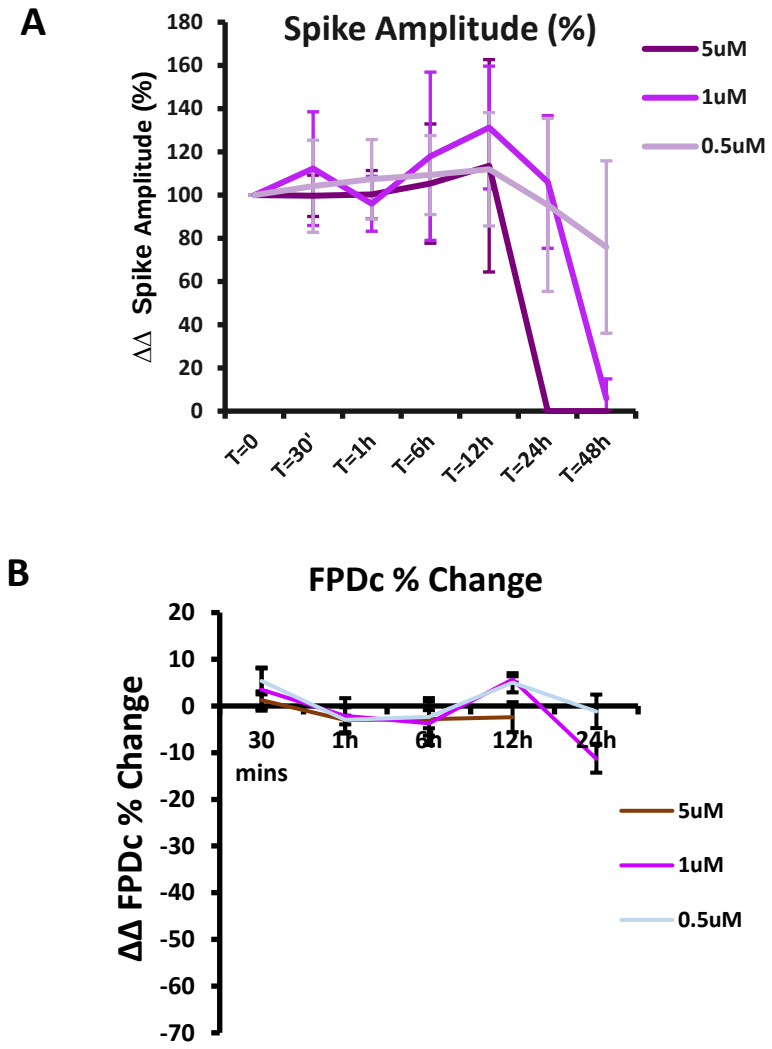

Figure 3.22 MS-275 induces time and dose-dependent changes in spike amplitude but not FPDc in hiPSC-CMs. hiPSC-CMs iCELL^2 were exposed to MS-275 at a range of concentrations for 48 h. **A.** MS-275 induced a significant (30% change $p<0.001$) increase in spike amplitude 12 h post compound addition, and a significant ($p<0.001$) decrease 48 h post compound addition. **B.** MS-275 did not induce significant changes in FPDc. Data are normalised to baseline and vehicle control (ΔΔ), and are the average ±SD of at least 3 separate determinations. Tested by ANOVA followed by Bonferroni post-hoc modifications.

3.4.2 Class IIb selective HDACi induces changes in cardiomyocyte functionality but does not alter cardiomyocyte viability

The Class II b-selective HDACi Tubacin did not induce detectable changes in overall CI at any of the tested concentrations.

Tubacin induced a significant ($p<0.05$) decrease in beat rate 12 hours post compound addition at 5 µM and 10 µM concentrations, however only a non-significant decrease in beat rate was observed post compound addition at 1µM.

No significant changes in CI beat amplitude were observed at 5 µM and 1 µM Tubacin concentrations, however a transient significant ($p<0.05$) increase by 20% was observed following exposure to 10 µM 12 hours post compound addition.

Tubacin induced multiple changes in ECR parameters. Specifically, non-significant perturbations in spike amplitude were observed within 6 hours post compound addition at 5 µM and 1 µM concentrations, before a gradual decrease 24 hours post compound addition. A significant ($p<0.001$) decrease in spike amplitude was observed at all used concentrations at 48 hours post compound addition.

Tubacin-induced perturbations in FPDc measurements, with a marked sustained significant ($p<0.05$) prolongation in FPD after 24 hours exposure to the higher concentration of 10 µM. Exposure to 5 µM and 1 µM concentrations did not induce significant changes to FPDc.

Overall, this study demonstrates that class IIb HDACi Tubacin does not significantly affect hiPSC-CM viability and syncytial morphology even at the highest tested concentrations. Conversely, Tubacin affects cellular functionality by slowing the beat rate, whilst also reducing depolarisation spikes and prolonging the FPD interval, suggesting a possible interaction with the K^+ channels or relevant channel subunits. These findings therefore also support the observations described in section 3.3 following exposure to pan-HDACi, however specific electrophysiological assessments would be required to clarify acute functional toxicity mechanisms off class IIb inhibitors

Tubacin class IIb inhibitor

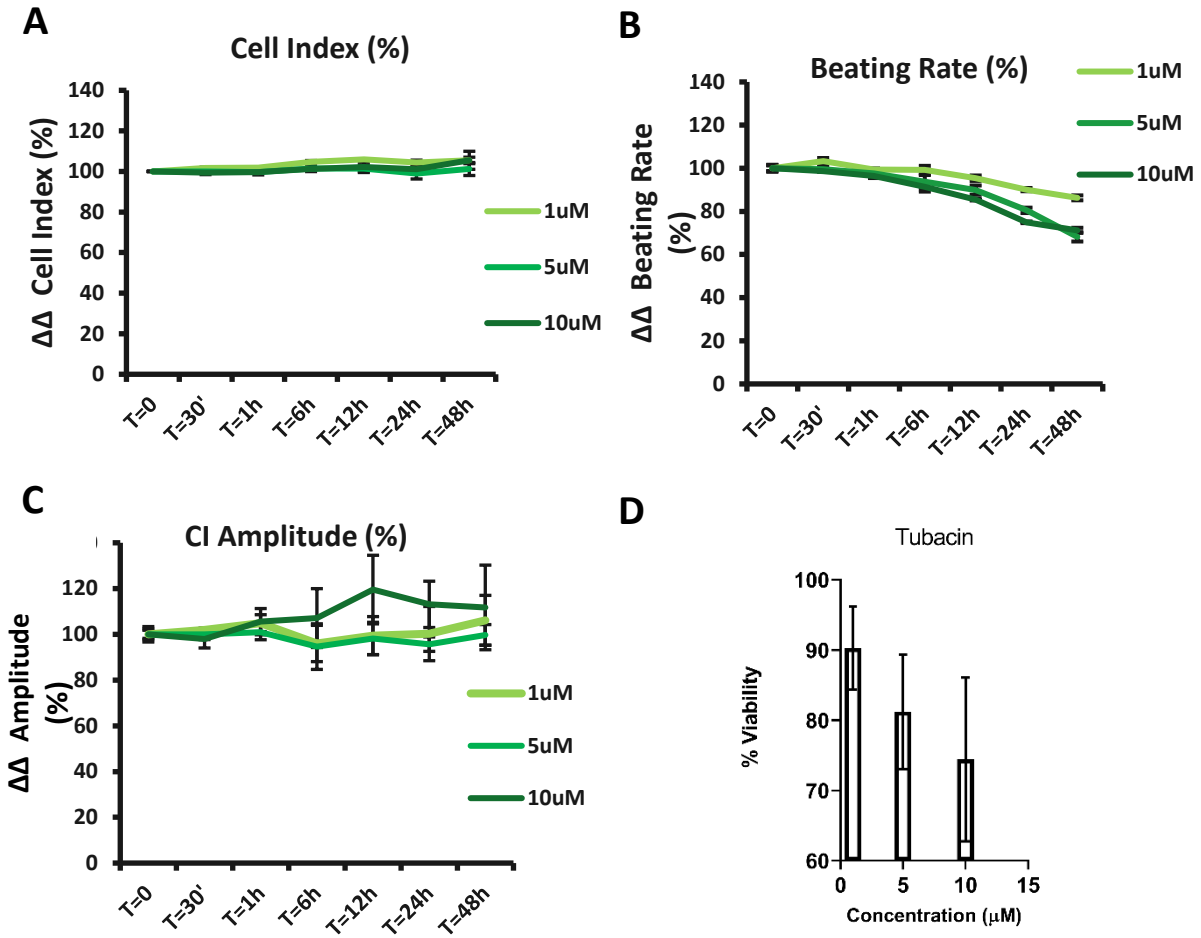

Figure 3.23 Tubacin induces changes in impedance contractility parameters but not CI. hiPSC-CMs iCELL^2 were exposed to tubacin at a range of concentrations for 48 h. **A.** Tubacin did not affect cell index. **B**. Tubacin induced a decrease in beat rate 48 h post compound addition ($p<0.05$ for 5-1- µM) at all tested concentrations**. C.** Tubacin did not affect beat amplitude between 1-5 µM but induced a 20% increase at 10 µM 12 h post addition. **D**. MTT assays evidenced a viability decrease between 5-10µM. Data are normalised to baseline and vehicle control (ΔΔ), and are the average ±SD of at least 3 separate determinations. Tested by ANOVA and Bonferroni post-hoc modifications

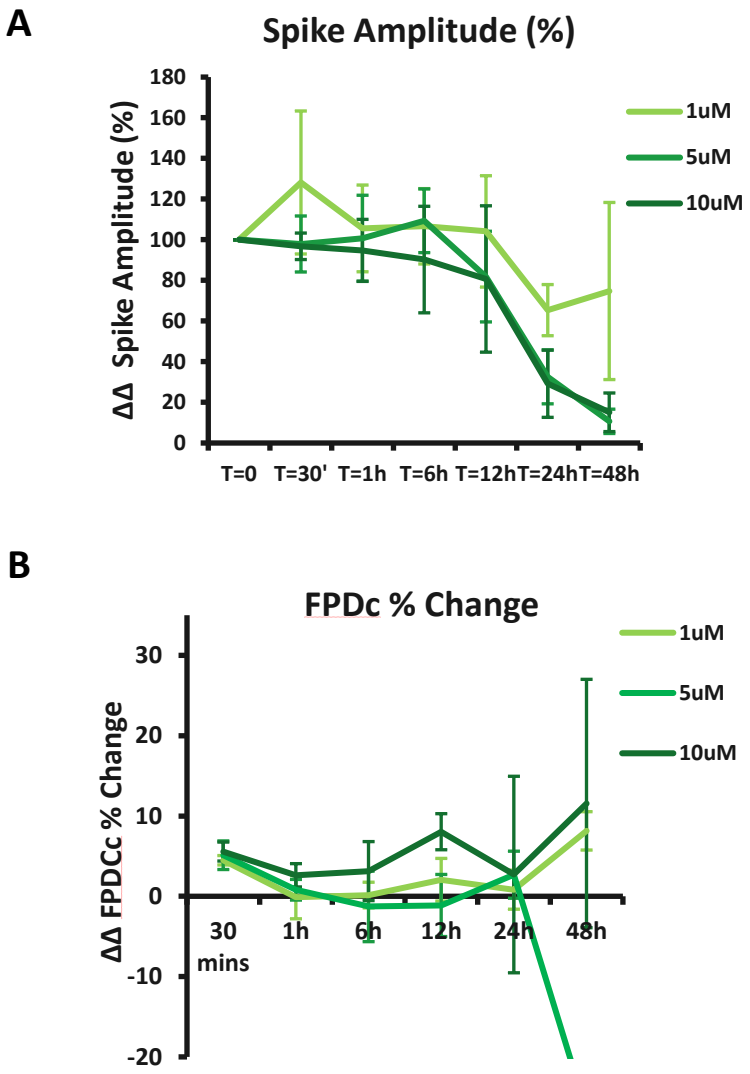

Figure 3.24 Tubacin induces changes in spike amplitude and FPDc parameters. hiPSC-CMs iCELL^2 were exposed to tubacin at a range of concentrations for 48 h. **A.** Tubacin induced a decrease in spike amplitude at all concentrations 24 h post compound addition. **B**. Tubacin induced an increase in FPDc at 10µM but not 1-5µM. Data are normalised to baseline and vehicle control (ΔΔ), and are the average ±SD of at least 3 separate determinations. Tested by ANOVA and Bonferroni post-hoc modifications

3.5 HDACis do not associate with an increased release of cardiac troponin I indicative of cardiomyocyte damage in hiPSC-CMs in-vitro

Release of cardiac troponin I (cTnI) into the bloodstream is a biomarker of cardiac damage and cardiomyocyte necrosis in the clinic, associated with cardiac remodelling and subsequent cardiac failure (Babuin and Jaffe 2005). In order to assess these effects preclinically, an *in-vitro* high-sensitivity multiplex assay was developed to detect cTnI levels in culture media of hiPSC-CM exposed to potential cardiotoxicants. This assay was utilised to evaluate whether HDACi induced damage to hiPSC-CMs, and thus whether they may associate with cardiac structural remodelling *in-vivo*. In this study, no elevation of cTnI levels were detected in the media of hiPSC-CMs exposed to HDACi at any of the concentrations tested (Figure 3.25). This contradicts the HDACi-induced loss of cellular viability detected by both impedance and ATP analyses. Consequently, this implies either the lack of sensitivity of the cTnI assay for detection of cardiomyocyte damage *in-vitro*, the inability of the cTnI assay to capture cumulative loss of cTnI, or HDACi-induced loss of cellular viability being due to an alternative non-necrotic mechanism of cell death. These findings suggest that detection of free cTnI alone is therefore not a reliable marker for detection of HDACi-induced cardiomyocyte cellular damage and the associated implied cardiac remodelling response.

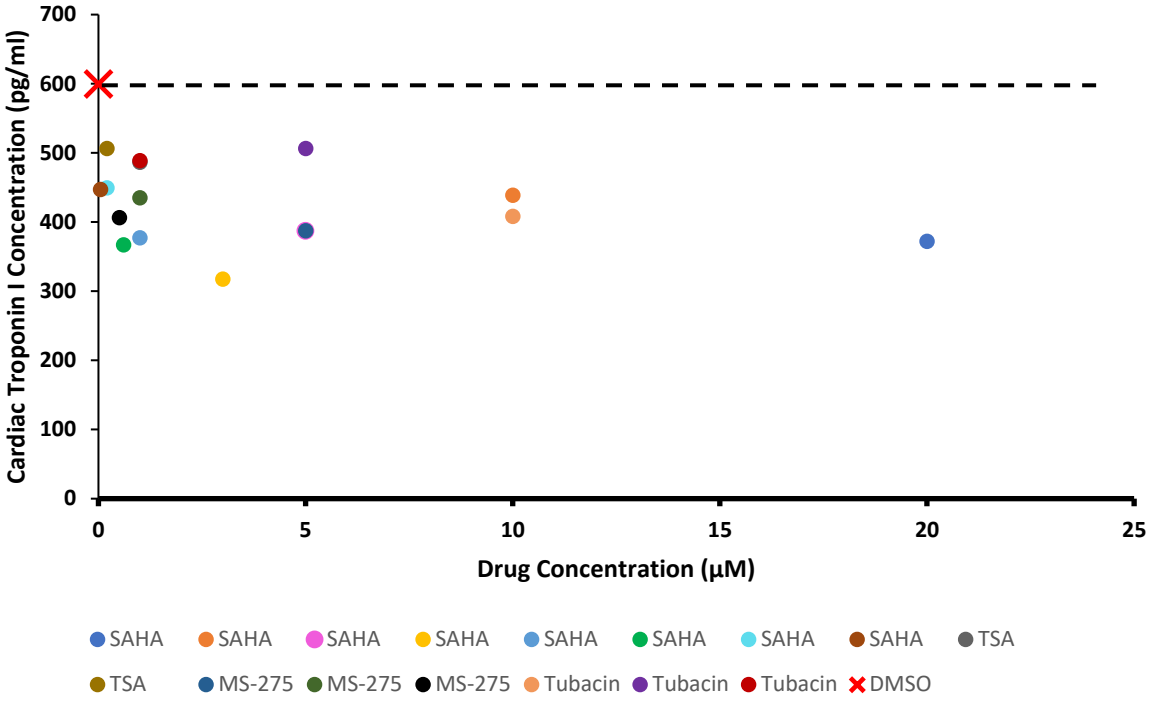

Figure 3.25 HDACi exposure does not cause an increase cTnI levels detectable in the culture media of hiPSC-CMs. . hiPSC-CMs iCELL^2 were exposed to various HDACi at a range of concentrations for 48 h. cTnI released in media was measured using multiplex assays. Detected levels of cTnI remained similar in HDACi-treated vs vehicle-treated hiPSC-CMs. Data are the average of at least 3 separate determinations. Dashed line indicates vehicle control maximum cTnI detection levels.

3.6 Discussion

Preclinical evaluation of the risk of drug-induced cardiac liabilities until recently was dependent upon the limited hERG screen, which utilised a non-cardiac cell line engineered to express a single ion channel. The poor predictivity of this model has led to endeavours to identify a more suitable and representative cell model for this purpose, with hiPSC-CMs now at the forefront in this context. However, a number of uncertainties still remain in terms of defining the morphological and electrophysiological predictivity potential of hiPSC-CM.

To characterise the limitations of hiPSC-CMs for detection of drug-induced cardiotoxicity, associated with different molecular mechanisms, these cells were first screened against a panel of known functional and structural cardioactive compounds. In this context, although commercially sourced hiPSC-CMs demonstrated the expected response to the majority of cardioactive agents, they exhibited a limited response to other agents (Table 3.1). Despite hiPSC-CMs showing a physiologically-relevant increase in beating contractility when exposed to the β-adrenoceptor agonist isoproterenol, no obvious increase in positive inotropy (recorded beat amplitude, a surrogate for contractile force) was detected (Figure 3.3) (Peters et al. 2015; Abassi et al. 2012). Likewise, the response to the L-type calcium channel blocker verapamil did not elicit a fully physiologically relevant response; shown by an increase in beat rate rather than the expected decrease (Figure 3.3). These consistent phenomena are potentially due to the immature phenotypic features of hiPSC-CMs and altered ion channel activity profiles (Xiaoyu Zhang and Abassi 2018; Koivumäki et al. 2018). Several studies have demonstrated that hiPSC-CMs possess ion currents necessary for membrane depolarisation (I_{Na};I_{CaL};I_f) and repolarisation (I_{to};I_{Kr};I_{Ks};I_{K1}) and express excitation-contraction coupling components including L-type calcium channels and the sodium-calcium exchanger pump NCX (Karakikes et al. 2015; Koivumäki et al. 2018; Ma et al. 2011). However, one particular challenging aspect relates to the lack of T-tubules in hiPSC-CMs (del Álamo et al. 2016). In the adult CM, T-tubules are found as a complex network built in connection with the sarcoplasmic reticulum (SR), where they mediate the calcium-induced calcium release (CICR) which is critical in the excitation-contraction mechanism observed in cardiac muscle cells. Albeit present, the hiPSC-CM CICR calcium handling mechanism relies on the slow influx of Ca^{2+} from the extracellular environment into the cytoplasm rather than on the rapid release mechanism

from the SR observed in healthy adult CMs. Evidence suggests that a certain degree of maturation allowing for the development of a CICR more representative of the adult cardiomyocyte is achievable via long-term culture, however the actual mechanism remains yet to be elucidated (Xiao hua Zhang and Morad 2020). A recent study by Zeng at al. describes a possible protocol for the resolution of the reversed rate effect of calcium channel blockers on hiPSC-CMs; this study relied on the partial blockade of sodium currents by either Na^+ channel blocker tetrodotoxin or by voltage-dependent mechanisms by increasing the extracellular potassium concentration, which allowed to correct the tachycardic effect to a physiologically relevant bradycardic response. Remarkably, Zeng et al.'s study highlighted that action potentials of hiPSC-CMs are primarily I_{Na} driven, thus directly underpinning the discrepancies observed with the use of known cardioactive agents (Zeng et al. 2019; 2018). Since hiPSC-CMs are often sourced commercially, problems arise as plating and maintenance media formulations are usually patented and undisclosed, and making additional corrections to the media formulation could pose problems in terms of correct supplementation and protocol standardisation.

In a bid to try and improve the accuracy and responsiveness of hiPSC-CMs to isoproterenol and FPD-altering compounds such as hERG blockers and calcium channel blockers, studies were reported on the effect of cardiomyocyte electrical pacing (E-pacing) (Wei et al. 2020). Electrical stimulation was hypothesised to induce hiPSC-CM maturation to a more adult-like phenotype, as well as reduce inter-batch baseline contractility variations by controlling AP firing (Wei et al. 2020). The study conducted by Feng Wei et al. showed a successful reduction in plate-to-plate baseline variations when cells were paced compared to spontaneous baseline activity. However, the study also indicated that E-paced cells exhibited reversed-rate effects and reduced sensitivity to I_{Kr} blockade, diminishing FPD prolongation in a pacing frequency-dependent manner. As such, E-pacing can be considered a suitable solution exclusively for the evaluation of compounds that do not interfere with FPD: given that FPD and FPDc evaluations are the *in-vitro* surrogate of QT prolongation assays, this might lead to missed detection of dangerous EADs and other proarrhythmic events. In relation to FPD parameters, the study presented in this chapter further highlighted the lability of FP/FPDc interpretations that originate from the application of a set of correction formulas to generate FPDc values. Throughout this study, Fredericia's correction formula was applied due to its widely accepted

application in similar contexts (Sala, Bellin, and Mummery 2017), however this formula was shown to result in possible overcorrection, thus leading to the misinterpretation of FPD-altering compounds (Fig 3.7). This is because commonly adopted FPD correction formulas, such as Fredericia's or Bazett's, were originally developed to correct clinical QT/QTc parameters, and were not directly intended for experiments using hiPSC-CMs, where electrophysiological properties differ (Izumi-Nakaseko et al. 2017). Recently, a study reported by Izumi-Nakaseko et al. has developed a non-linear equation for the correction of FPD parameters relevant to *in-vitro* applications, however the adoption of similar equations for FPD analysis is yet to be standardised before being commonly implemented (Izumi-Nakaseko et al. 2017). It is therefore evident that the concept of an individual/universal resolution that could overcome the limitations of hiPSC-CMs in response to known agents is not viable at the time of this writing.

Overall, data presented in the first phase of this study (figures 3.3 to 3.11) demonstrates that both the clinically representative responses and the unexpected reversed-rate effects and discrepancies observed with the use of known cardioactive compounds are consistent between different hiPSC-CM cell batches, and in line with the most recent literature (Zeng et al. 2018; Peters et al. 2015; Zeng et al. 2019). The appraisal of these limitations is fundamental for the interpretation and evaluation of new chemical entities (NCEs) in nonclinical drug screening.

The second objective of this study was to evaluate cardiotoxicity associated with the HDACi class of drugs using the hiPSC-CM model, particularly in terms of characterisation of the strengths and limitations of this model in the detection of functional and structural cardiotoxicity. HDACi are investigated for their therapeutic potential towards the treatment of oncological, immune, and inflammatory disorders (Falkenberg and Johnstone 2014; Gryder, Sodji, and Oyelere 2012b). Despite showing clinical promise, these agents have been associated with clinical cardiotoxicity, manifesting mainly through delayed arrhythmic events and sudden cardiac death (R. R. Shah 2019). HDACi-mediated functional cardiotoxicity has been documented in several studies (Xu et al. 2016; Schiattarella et al. 2016); a study conducted by Kopljar et al. identified transcriptional mechanisms induced by several HDACi compounds in a hiPSC-CM model, defining potential epigenetic changes linked to HDACi-mediated proarrhythmic effects. In particular, HDACis including SAHA and MS-275 were

reported to induce delayed contractile dysfunction in a hiPSC-CM model, resulting in loss of contractility, arrhythmic events and electrophysiological alterations in FPD manifesting as late as 72 hours post compound addition at clinically relevant concentrations (Kopljar et al. 2016). The pan-HDACi SAHA induced significant functional alterations in hiPSC-CM contractility and electrophysiology as early as 48 hours post compound addition at a range of concentrations (figures 3.14 to 3.17), including at high supratherapeutic concentrations (3-20 μM), and clinically relevant concentrations (≤1 μM). Whilst both supratherapeutic and therapeutic concentrations of SAHA resulted in acute arrhythmic events and progressive reduction of contractility in line with other reported findings, this study demonstrates that even sub-therapeutic concentrations (<0.6 μM) of SAHA induce delayed cardiotoxicity in hiPSC-CMs, resulting in both contractile and electrophysiological perturbations. Remarkably, sub-clinical non-cytotoxic concentrations were shown to induce FPDc shortening and SA alterations, indicative of electrophysiological disruptive mechanisms (figure 3.16 and 3.17). These FPDc and SA alterations were however not correlated with a concomitant decrease in beat rate, but only with a partial reduction in beat amplitude (figures 3.18 and 3.19). As beat amplitude is a surrogate for the evaluation of extent of cardiomyocyte contractility, a negative inotropic effect with no simultaneous alteration in beat rate indicates a potential disruption of cardiomyocyte morphology and structure, thus suggesting that cardiotoxicity associated with HDACi could be mediated by the modulation of specific structural molecular targets rather than purely ion channel disruption. In agreement with this proposition, a study by Kopljar et al. hypothesised that clinically relevant pan-HDACi at C_{eff} values affected the expression of genes associated with the structural organisation of the cardiomyocyte (Kopljar et al. 2016). Additionally, increasing accumulating evidence reported the use of HDACi as possible therapeutic agents for the treatment of some forms of heart failure (Weeks 2019; Wallner et al. 2020), including those with preserved ejection fraction (HFpEF); in particular Wallner et al. reported that the pan-HDAC inhibitor SAHA determined a reduction in left ventricular hypertrophy in a HFpEF model (Wallner et al. 2020), hence fully supporting not only the HDACi-mediated role in cardiac structural modifications, but also its translatability to the clinic. The investigation into sub-selective HDACi effects on hiPSC-CMs in this study additionally showed that class I HDAC inhibition elicited a moderate effect on functional and cell viability parameters, and although the effects largely reflected those observed with pan-HDACi exposure, they were not as prominent (figure 3.22-3.23). Furthermore, class I selective

inhibition was linked to more significant cardiomyocyte alterations compared to class IIb selective HDACi (figures 3.22-3.23 and 3.24-3.25). Similar findings were also reported in literature, where class I and class IIb selective HDACi evoked comparable effects to those observed in this study, which suggests that the HDACi cardiac safety profile could possibly be improved by targeting specific HDAC sub-sets (Kopljar et al. 2016). Further investigations in this study aimed at the quantification of HDACi-induced cardiomyocyte damage, specifically through the detection of release of cardiac troponin I, a validated clinical biomarker for detection of cardiomyocyte loss and subsequent cardiac remodelling (Adamcova et al. 2019). This study demonstrated no observable change in detectable levels of free cTnI in media upon HDACi exposure (figure 3.26), even at the highest tested HDACi concentrations. Although damage-dependent release of cTnI is conventionally correlated with loss of cardiomyocyte membrane integrity and cellular death, a recent study described the occurrence of additional drug-induced troponin-disruptive mechanisms whereby in response to the cardiotoxicant doxorubicin cTns undergo drug-induced structural rearrangements rather than extracellular release (Adamcova et al. 2019). Whilst the study presented in this thesis did not specifically investigate cTnI localisation and disruption at the cellular level following HDACi exposure, it is plausible to assume that the lack of detection of cTnI in media is not sufficient to exclude the eventuality of a structural cardiomyocyte alteration *per se*. Nonetheless, an important limitation of this study is the limited experimental timespan that hiPSC-CM-based models offer before undergoing de-differentiation and phenotypical alterations that would render them ineffectual, generally allowing a maximum of 48 to 72 hours for the assessment of drug-induced effects (Ebert et al. 2019). Given that structural cardiac cell modifications often occur with a delayed onset, manifesting several days or weeks after drug exposure, it is possible that any major structural HDACi-induced cardiomyocyte disruption involving the release of cTnI could not be detected within the 48 hour experimental timeframe used in this study.

Taken together, the results described in this study prove that despite providing a tangible improvement to the preclinical *in-vitro* screening scene, there are still numerous limitations that emerged with the use of standardised hiPSC-CM models for cardiotoxicity applications, not only in terms of physiological relevance but also in relation to the experimental and analytical methodologies. This supports the need for the investigation of a complementary repertoire of *in-vitro* cardiac models for use in preclinical toxicity screening, which could help

overcome some of the drawbacks associated with hiPSC-CM use, and ultimately facilitate cardiotoxicity screening.

4 Characterisation of the HL-1 murine atrial cell line for use in preclinical cardiotoxicity studies

4.1 Introduction

The lack of reliable and reproducible cardiac models for *in-vitro* preclinical screening is a well-established issue. While it is undeniable that hiPSC-CM technology represents a considerable step towards the improvement of these necessary models, a variety of limitations remain unresolved and ultimately contribute to the lack of standardisation of such models (Da Rocha et al. 2017; Koivumäki et al. 2018). Numerous studies have evidenced the variability that commercial hiPSC-CM models present in terms of baseline parameters, both in terms of contractility and electrophysiology (Feyen et al. 2020; Wei et al. 2020; Zeng et al. 2019). Not least of all, the high costs associated with the use of hiPSC-CM technology signify that *in-vitro* studies are often designed in a limited number, adding further limitations in terms of reliability due to the small sample size. Given that, over the last decade, as many as 27% cardiovascular adverse events are reported for NCEs discovery projects prior to entering phase I clinical trials (Roche et al. 2019; Valentin and Redfern 2017), the design of cost-effective, reproducible, and standardised tests that could enhance the utility of preclinical screening is of paramount importance. The availability of immortalised cells, such as the HL-1 murine atrial cardiomyocyte cell line, represents an unexplored source of cost-effective models that could aid in the design of more feasible preclinical cardiotoxicity studies.

Despite the inter-species differences that distinguish human-derived and mouse-derived atrial cells, murine models are widely accepted and are considered suitable for the study of cardiac electrophysiology and arrhythmic mechanisms (Kaese and Verheule 2012). The HL-1 cell line was first established from a genetically engineered atrial tumour grown in a transgenic mouse (Claycomb et al. 1998). The cell line was established to be immortalised, and as such it provides an expandable source of atrial-like cardiomyocytes. Several studies have demonstrated the cardiac phenotype of this cell line, which uniquely retains several cardiac markers as well as the ability to contract upon passaging (Claycomb et al. 1998) (Figure 4.1). HL-1 cells have been used in numerous electrophysiology studies due to the presence of native forms of several cardiac ion channels, making them a particularly suitable model for the study of atrial arrhythmias (Wiersma et al. 2019) (table 4-1). These features, coupled with the use of novel technologies such as high-throughput impedance-based cellular analysers, could offer additional screening methods to facilitate early-stage detection of cardiotoxicity.

Current	*Gene*	*Functional in HL-1 cells*	*Comments*	*Reference*
I_{kr}	hERG	☑	Encode α subunit of I_{kr}	(Claycomb et al. 1998)
I_f	HCN	☑	All 4 isoforms present, HCN1 and HCN2 at higher levels. Plausibly contributes to HL-1 spontaneous contractility	(Sartiani et al. 2002)
$I_{ca\text{-}L}$	Cav1.2 or CACNA1C	☑	Presence in HL-1 dependent on culture conditions (i.e. Norepinephrine)	(Xia et al. 2004)
$I_{ca\text{-}T}$	CACNA1G	☑	Present in HL-1 cells. Dependent on culture conditions. Characteristic of SA node	(Xia et al. 2004)

I_{Na}	Scn5a	☑	Present in HL-1 cells	(White, Constantin, and Claycomb 2004; Daimi et al. 2015)
I_{Na-Ca}	Ncx-1	☑	Present in HL-1 cells	(White, Constantin, and Claycomb 2004)
I_{KATP}	SUR1, SUR2, Kir2.6	☑	Present in HL-1 cells.	(Fatima et al. 2012; Seymour et al. 2003)

Table 4-1 Electrophysiological characterisation of the HL-1 murine atrial cell line. Previous studies reported in literature have described the presence of functional currents in the HL-1 cell model.

A

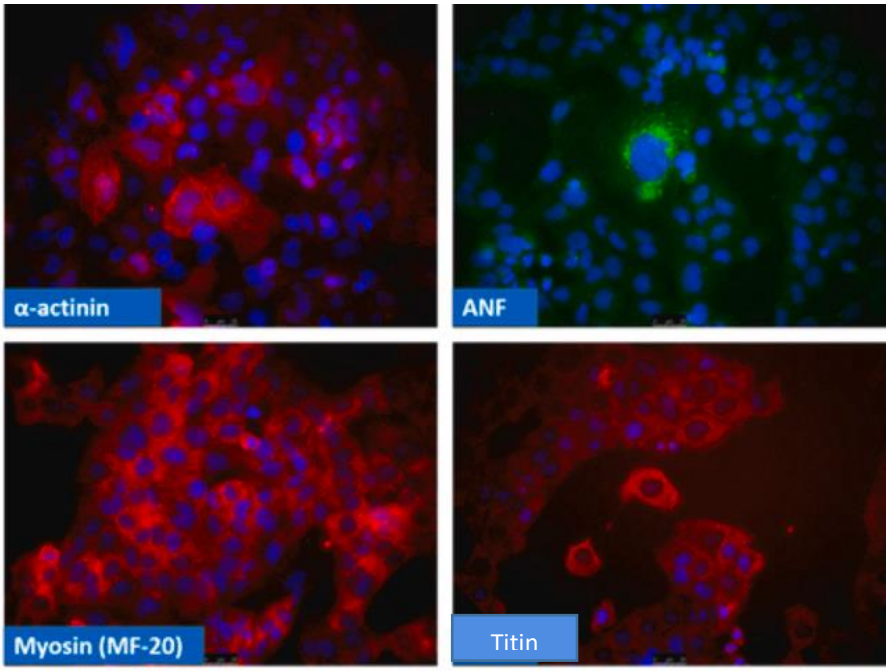

B

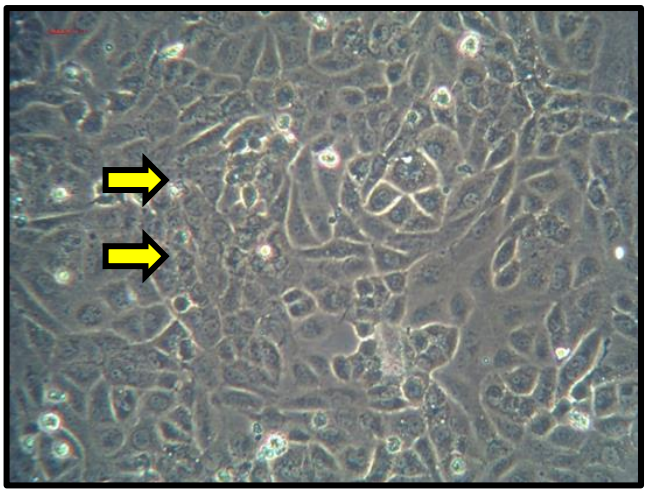

Figure 4.1 HL-1 cells express cardiac markers and display syncytial formation in culture. HL-1 cells retain a cardiac phenotype *in-vitro*. Figure **A.** shows positive immunofluorescence staining for α-actinin, atrial natriuretic factor, myosin and titin. (image adapted from Sigma-Merck). **B.** Typical morphology of HL-1 cells, with arrows indicating contractile syncytial structures.

4.1.1 Aims and Objectives

HL-1 cells express a range of cardiac markers and retain a contractile phenotype, however their use and characterisation for toxicological *in-vitro* applications has been very limited. For this reason, a set of studies is presented in this chapter, with the aim to characterise this cell line and determine the utility advantages and limitations of the HL-1 murine atrial cell model for use in early preclinical cardiotoxicity studies. Specifically, this is achieved through the following objectives:

1. Development of a protocol for the use and application of HL-1 murine atrial cell line paired with high throughput impedance assays (xCELLigence systems).
2. Characterisation and validation of the ability and limitations of the HL-1 cell line model to detect functional and structural drug-induced cardiotoxicity against a panel of known cardioactive agents.
3. Evaluation of the ability of the HL-1 model to detect structural and functional cardiotoxicity induced by HDACi *in-vitro*, utilising methodologies established in this thesis.

4.2 Determination and optimisation of HL-1 cell line culture conditions, growth kinetics and contractility

To develop and optimise a protocol for the use of HL-1 murine atrial cell line on impedance-based technology systems, the intrinsic properties of this cardiac cell model, including morphology, kinetics and contractile phenotype were studied and defined. Figure 4.2 shows growth characteristics of HL-1 cells seeded at different initial densities, and defines doubling time for each population. For the initial assessments, HL-1 cells were cultured in regular supplemented commercial Claycomb medium (Claycomb et al.) as described in section 2.2.2. and the experiment was performed using the xCELLigence Cardio system. HL-1 cells were seeded at 10,000, 5000, 2500 and 1250 cells/well, and at least 8 separate determinations in the same experiment were considered for significance. Determinations were averaged and data on exponential phase, plateau phase and monitoring of contractility were recorded. Cells seeded at 10,000 cells/well reached a cell index (CI) plateau stage 120 hours post-seeding, while early contractility was detected at 72 hours post-seeding, suggesting that the formation of functional syncytia occurred. Representative impedance traces of HL-1 contractility seeded at 10,000 cells/well are shown in figure 4.4A, where cells demonstrated early contractility at 72 hours post-seeding: the noise recorded in the impedance waveform signal suggests early contractility is characterised by unorganised syncytial structures. Following exponential cell proliferation, the CI reached a plateau phase at which the impedance traces of contractility resulted in improved definition and reduced noise in the signal, albeit beat amplitude and beat-rate were decreased compared to pre-plateau timepoints.

HL-1 cells seeded at an initial density of 5000 cells/well and 2500 cells/well reached a plateau phase at 150h and 170h post-seeding, respectively. Representative impedance traces of HL-1 cells seeded at 5000 cell/well and 2500 cells/well are shown in figure 4.4B and 4.5A, where early contractility was recorded at 96 and 110 hours post-seeding respectively. The impedance signal noise of contractility traces appeared more defined throughout the experiment in the cell group plated at 5000 cells/well compared to the group plated at 2500 cells/well.

HL-1 cells seeded at the lower initial density of 1250 cells/well reached a plateau phase at 212 hours post-seeding. Contractility for this group was first recorded 160 hours post-seeding, and

the noise recorded on the contractility impedance signal was consistent until a more stable contractility waveform was recoded at 250 hours post-seeding, as shown in figure 4.5B.

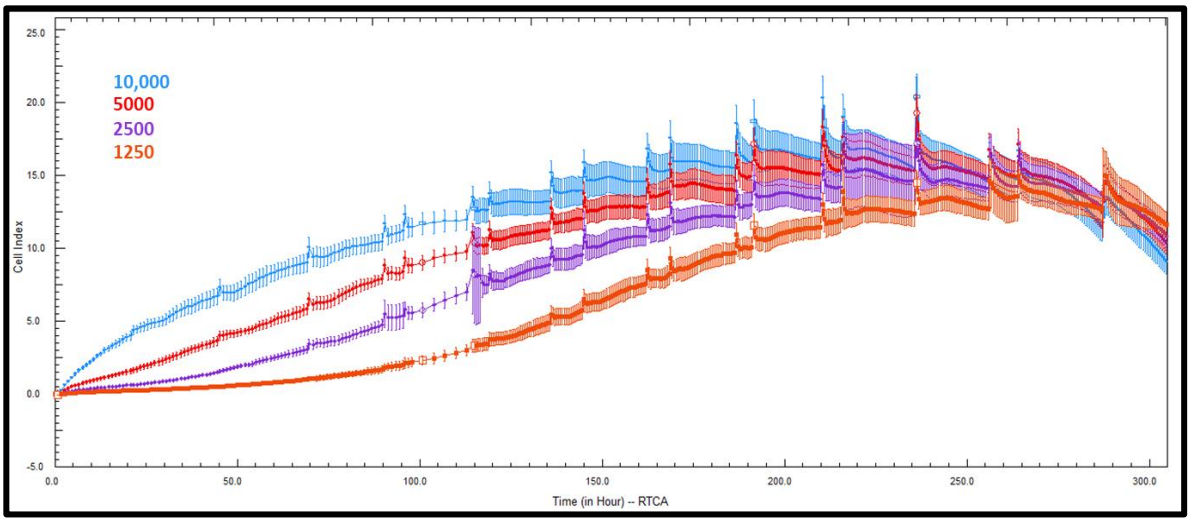

Figure 4.2. Growth kinetics of HL-1 cells plated at different seeding densities. HL-1 cells were plated on an xCELLigence Cardio E-plate and monitored over time. Exponential and plateau growth phases are attained at different points post-seeding, with a positive correlation between initiation of these phases and higher cell densities. Final cell density per well is comparable between all initial seeding densities. Data are mean ± SD of at least 8 separate determinations.

Seeding density (cells/well)	CI impedance plateaus at	Contractility first recorded at	Contractility stops at	Average duration of contractile activity, post media change
10,000	120h ±2h	70h post seeding	210h post seeding	2h ±0.5h
5,000	150h ±1.5h	96h post seeding	235h post seeding	4.5h ±1.7h
2,500	170h ±3h	110h post seeding	264h post seeding	5h ±1.3h
1,250	212h ±3.5h	160h post seeding	270h post seeding	4h ±1.2h

Table 4-2 Different initial seeding density determines differences in contractility consistency and duration in HL-1 cells. HL-1 cells were seeded at different initial densities and monitored on the xCELLigence Cardio System. Different parameters were recorded, including growth kinetics, start and end timepoints of contractility and average duration of contractile activity.

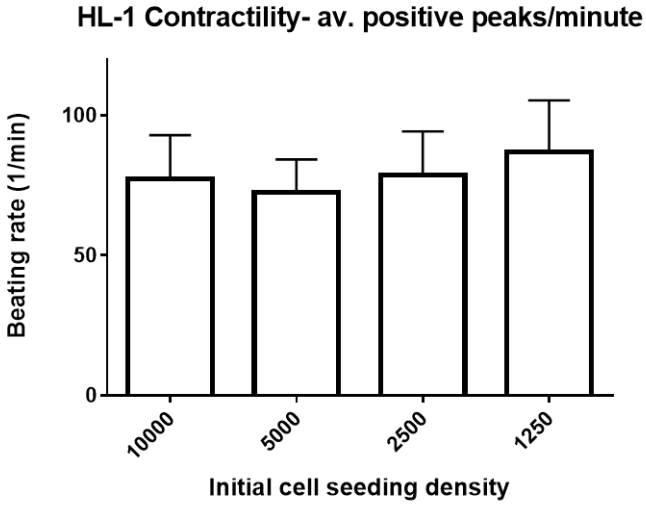

Figure 4.3 Native HL-1 average contractility analysed as beat rate/min. HL-1 cells were seeded at different initial densities and monitored on the xCELLigence Cardio system for early detection of contractility. Spontaneous beat rate/min is comparable between all initial seeding densities. Data represents average beat rate/min ±SD of at least 8 separate determinations.

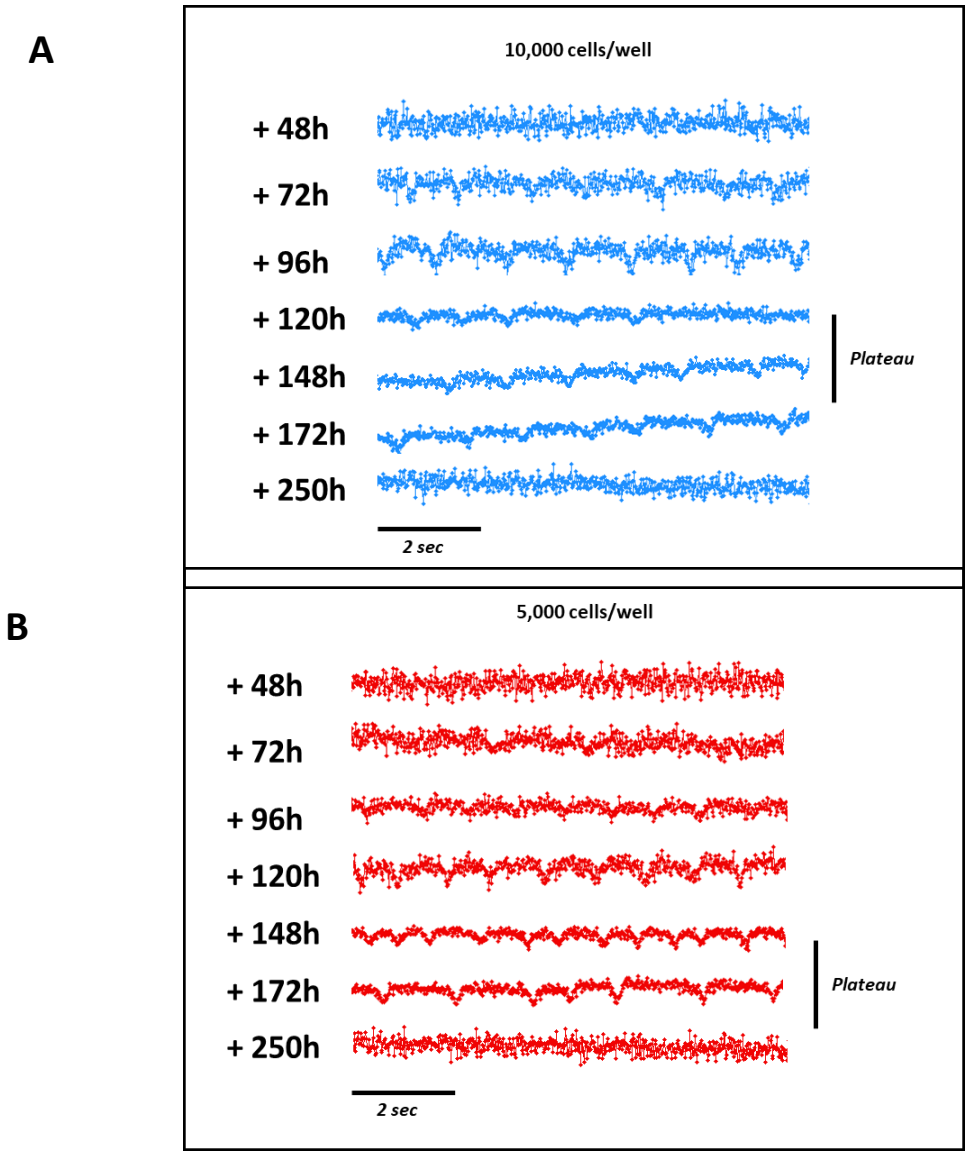

Figure 4.4. HL-1 cells seeded at different initial densities achieve contractility at different proliferation stages. HL-1 cells were seeded at different initial densities and monitored on the xCELLigence Cardio system for early detection of contractility. A. Representative contractility impedance traces for cells seeded at 10,000 cells/well and B. representative contractility impedance traces for cells seeded at 5,000 cells/well. All data are typical of at least 8 separate determinations.

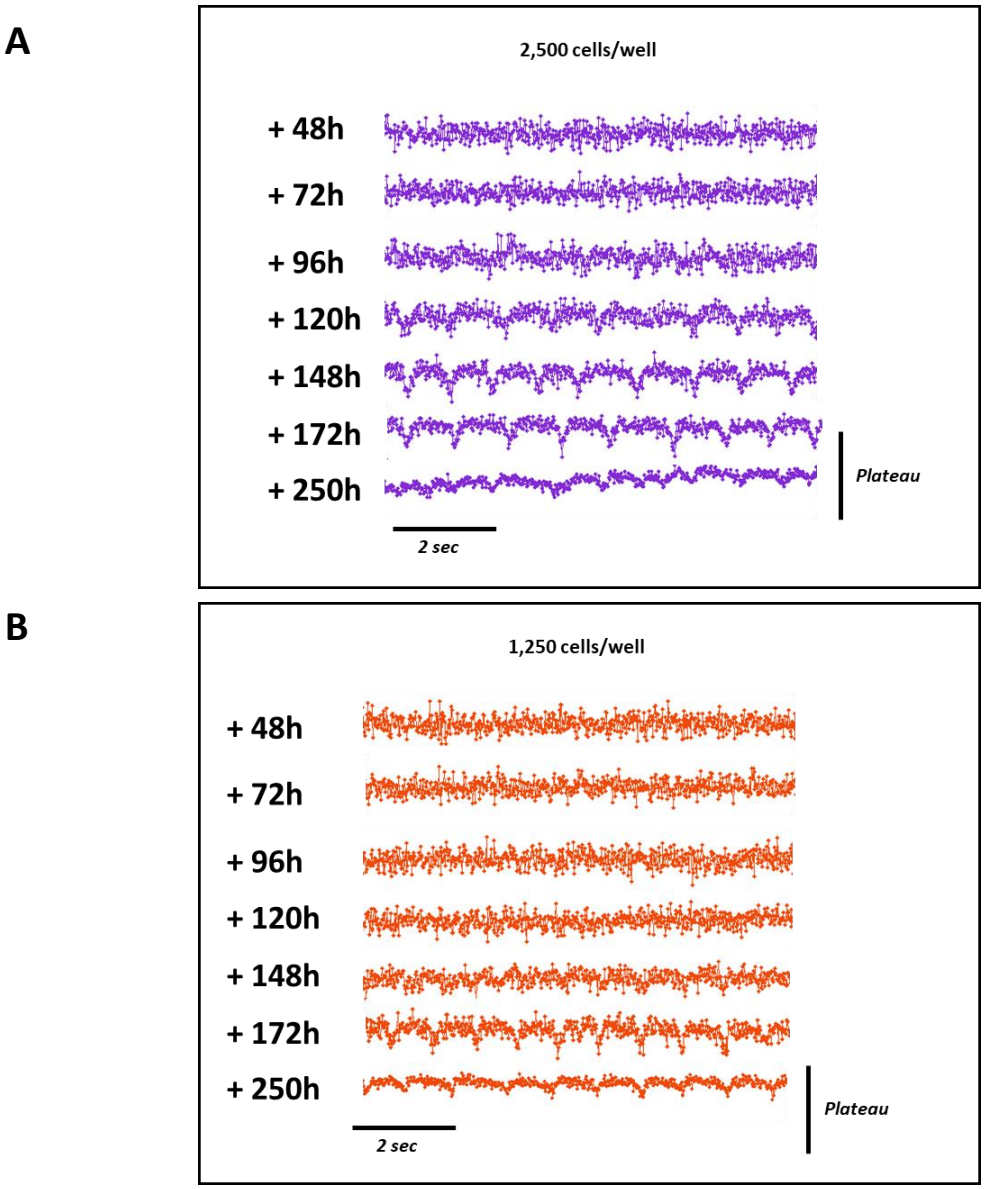

Figure 4.5. HL-1 cells seeded at different initial densities achieve contractility at different proliferation stages. HL-1 cells were seeded at different initial densities and monitored on the xCELLigence Cardio system for early detection of contractility. **A.** Representative contractility impedance traces for cells seeded at 2,500 cells/well and **B.** representative contractility impedance traces for cells seeded at 1,250 cells/well. All data are typical of at least 8 separate determinations.

Together, these data suggest that HL-1 cells cultured in standard supplemented commercial Claycomb medium achieve a fully contractile phenotype when grown between 80% and 100% confluency. Despite different initial seeding densities, each group displayed erratic and noisy early contractility waveform signals, indicative of a non-homogeneous syncytial formation as well as a non-coordinated conduction of the electrical signal; brightfield microscopy on live cells at different initial exponential growth stages confirmed the presence of separate cell colonies forming individual syncytial structures, which consistently formed a more synchronised monolayer at plateau stages, as reflected by impedance contractility traces.

Furthermore, the study demonstrated that consistent and stable contractility is maintained for a maximum of 4 to 5 hours on average after each complete media change and is subsequently progressively lost over time unless cell passaging occurs. This finding therefore suggests that HL-1 cells do not fully achieve complete contact inhibition upon syncytial monolayer formation.

To determine whether native HL-1 contractility performance could be improved to generate a more stable, synchronised and reproducible impedance waveform, DMEM-based medium was formulated to i) selectively exclude individual components of the Claycomb growth medium to identify those indispensable for the induction and maintenance of HL-1 contractility, and ii) optimise medium formulation and increase availability of key contractility components. All recordings were performed using the xCELLigence Cardio system where HL-1 cells were grown to confluency in supplemented commercial Claycomb medium until contractility was detected. Cell media was then replaced with DMEM-based medium specifically excluding one of the following components: growth factors, retinoic acid, oleic and linoleic acids, cholesterol, Insulin-Transferrin-Selenium complex (ITS), ascorbic acid, and norepinephrine (NE). Changes in impedance and contractility were recorded and are described in figures 4.6 to 4.8.

Figure 4.6 shows the overall effects on cell viability following selective omission/depletion of specific components and factors from the cellular media, relative to complete media containing all of the stipulated additional additives. No significant differences in viability were recorded at 24 hours post exposure to the modified media, for all formulations. However, at

48 hours, significant decreases in CI were observed associated with omission of specific components. A lack of the ITS complex or growth factors (both EGF and R3IGF-1) resulted in approximately a 30% decrease, omission of cholesterol or ascorbic acid caused a 20% increase, and absence of linoleic/oleic acid associated with a 13% decrease in CI. As expected, HL-1 cells plated directly in multi-factor-depleted media formulations did not achieve successful growth and proliferation (Figure 4.8).

However, whilst a decrease in CI gave was indicative of reduced cell viability, there was no observable direct correlation between decrease of CI and loss of contractility. Figure 4.7A illustrates representative impedance traces of contractility for each depleted component group, and figure 4.7B shows raw beat-rate changes at 24, 48 and 120 hours post deconstructed media addition. Notably, commercial Claycomb and in-house reconstructed Claycomb media formulations resulted in a beat-rate increase 48 hours post media addition. Conversely, a beat-rate decrease was detectable within 48 hours of changing to a factor-depleted media, with the exception of omission of growth factors for which beat-rate remained stable throughout the study. Although omission of these factors from the media did not result in loss of contraction up to 48 hours, contractility ceased in all factor-depleted media conditions apart from growth-factors and ascorbic acid by 120 hours. Whilst beat-rate remained constant for growth-factor deficient media, a decrease in beat-rate was observed following omission of ascorbic acid (figure 4.7A and B).

Data from this study demonstrates that selective depletion of key Claycomb media components does not result in complete loss of HL-1 contractile phenotype. Once cellular confluency and cell index plateau were achieved, the overall contractile stability and duration was improved in the absence of growth factor components (EGF and 3IGF-1) . Furthermore, maintenance of HL-1 contractility was shown to be dependent upon both retinoic acid and norepinephrine, with omission of the other constituents having only minor effects upon the HL-1 contractile phenotype. This thereby opens new dimensions and opportunities for utility of HL-1 cells as a model for study of drug-induced cardiotoxicity and cellular contractility.

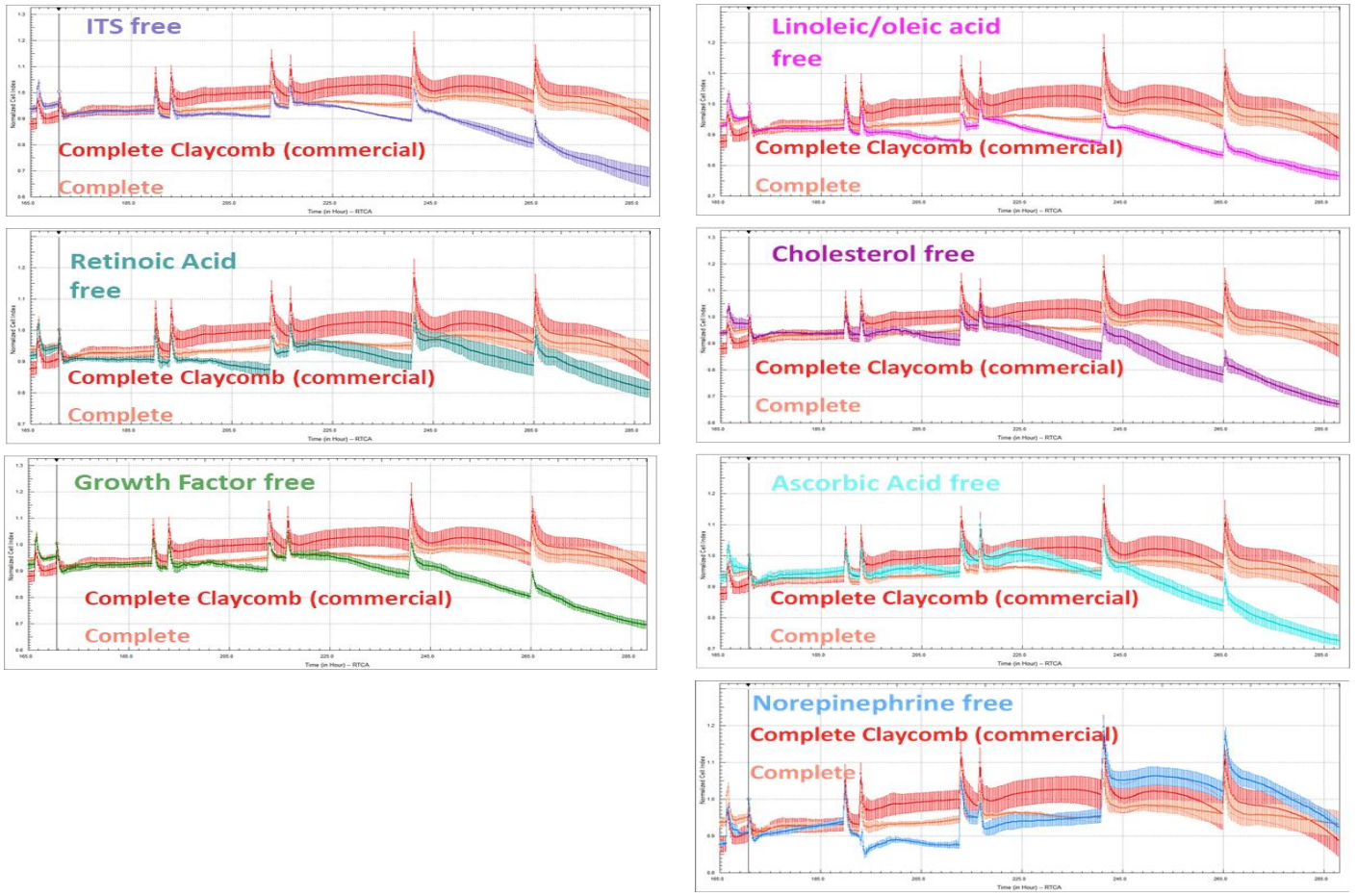

Figure 4.6: Omission of supplements to growth medium affects HL-1 cell viability. HL-1 cells were grown in an xCELLigence Cardio E-plate in complete Claycomb medium until confluency was attained, thereafter exposed to deconstructed and supplement-omitted media formulations. Data shows normalised CI variations over time.Significant decrease in CI was observed in the absence of several supplements, including ITS complex, growth factors, linoleic/oleic acid, cholesterol and ascorbic acid. Data are the average ±SD of at least 8 separate determinations.

A

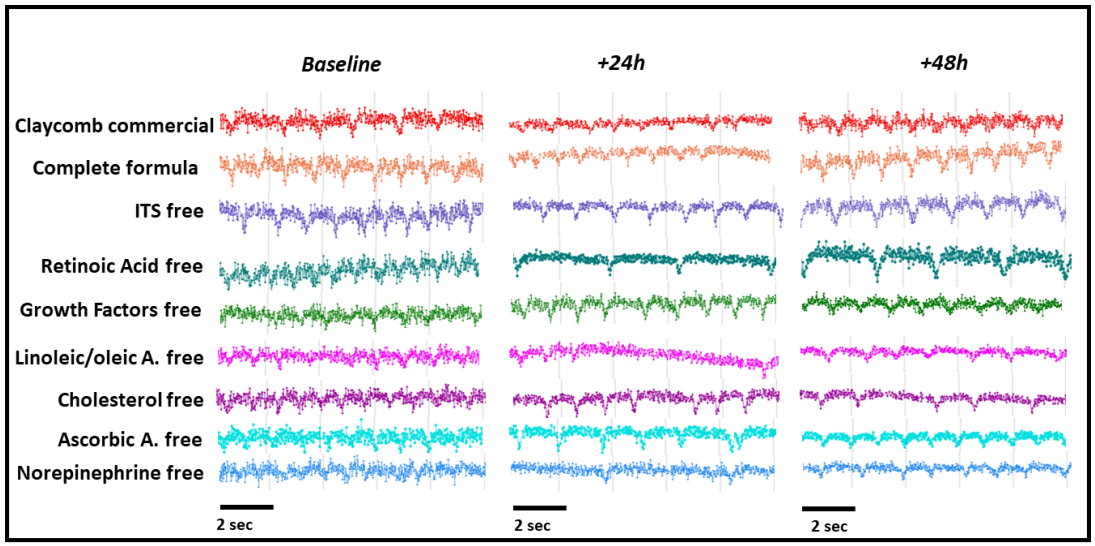

B

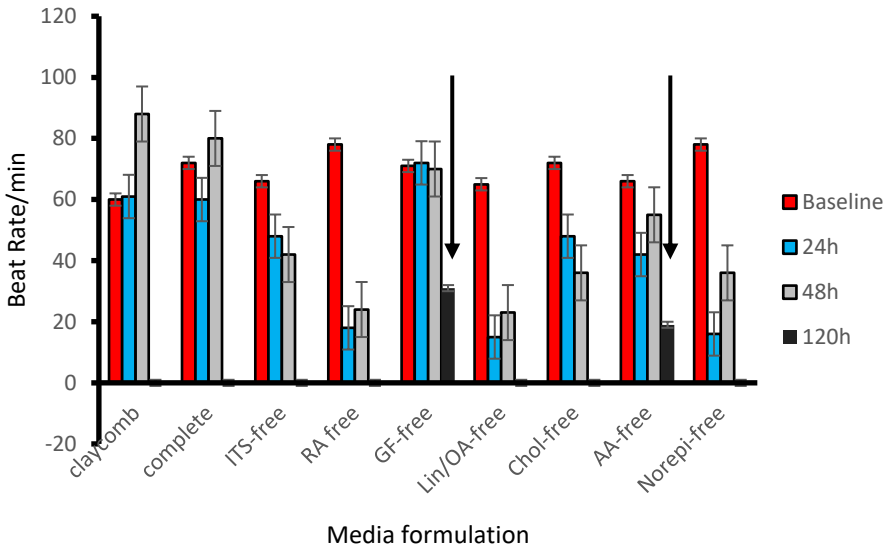

Figure 4.7. Omission of selected Claycomb medium components does not prevent contractility (A) of HL-1 cells but affects beat-rate duration and stability (B). HL-1 cells were grown in an xCELLigence Cardio E-plate in complete Claycomb medium until confluency was attained, thereafter exposed to deconstructed and supplement-omitted media formulations. A) impedance contractility waveform traces at baseline, 24h and 48h; B) mean beat-rate/min, where data are the mean ±SE of at least 8 separate determinations of 3 independent experiments. Contractility remained observable at 120h in the absence of growth factors (GF) and ascorbic acid (AA). Significance defined as $p<0.05$ from baseline using one-way ANOVA with Bonferroni post-hoc modifications.

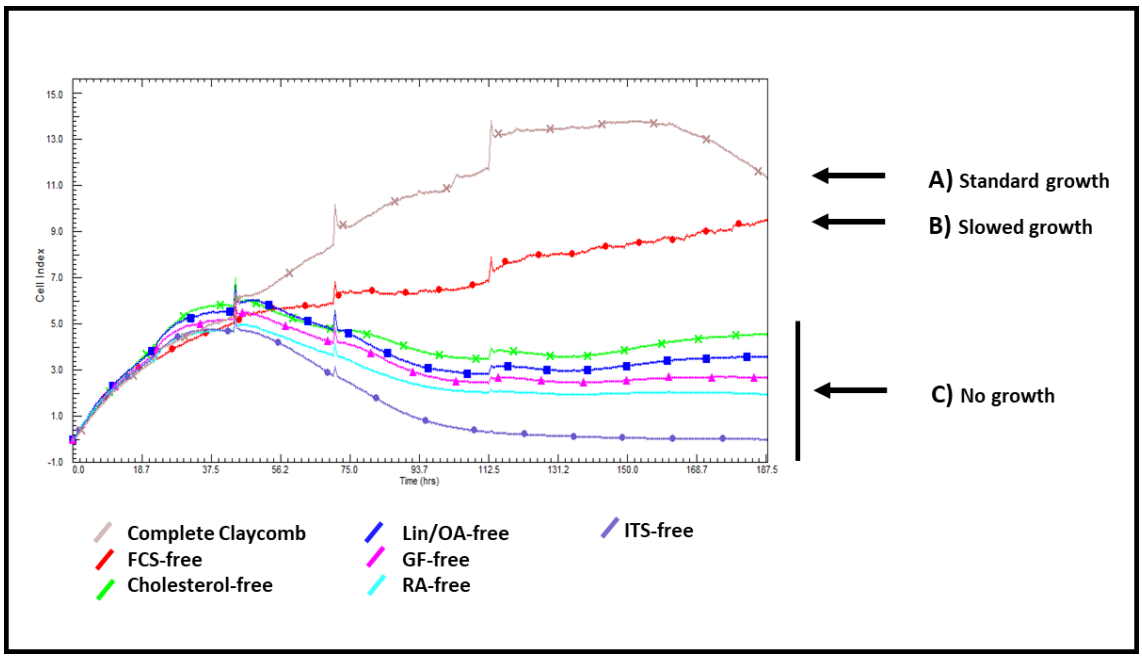

Figure 4.8 Omission of selected Claycomb medium components halts HL-1 early-stage proliferation. HL-1 cells were plated in an xCELLigence DP E-plate and exposed directly to deconstructed and supplement-omitted media formulations. **A**. Cells grown in complete Claycomb formulation achieved standard proliferation. **B.** Cells grown in FCS-depleted medium achieved a slowed proliferation. **C.** Cells grown in supplement-omitted media formulations did not proliferate.

4.3 Medium-induced inhibition of cellular proliferation associates with improvement of HL-1 cellular contractility.

Previous experiments suggested HL-1 cells reach optimal contractility when 80-95% confluent (just prior to reaching plateau) and evidenced their inability to achieve contact inhibition following the formation of functional syncytia, thus resulting in loss of contractility over time due to overcrowding of the culture vessel. Retinoic acid and norepinephrine are both confirmed as key components for maintenance of HL-1 cellular contractility (section 4.2.1), whereas omission of EGF from the growth media promoted stable contractility. This thereby implies that inhibition of cellular proliferation, without impacting cell viability, would improve consistency and robustness of HL-1 contractility. To address this assumption, a study was performed with the aim to optimise a medium formulation that would permit the maintenance of the contractile and differentiated phenotype of HL-1 cells, as well as inhibit their ability to proliferate. To achieve this, several formulations of basal media were tested (Table 4-3). For these studies, HL-1 cells were grown to confluency in complete Claycomb medium on the xCELLigence Cardio system, and at plateau stage the complete Claycomb formulation was substituted with the modified basal media batches. Cell viability and contractility were monitored using the xCELLigence Cardio system (figure 4.9).

Basal Medium	*NE*	*RA*	*Additional Supplements*
Claycomb Media	✓	✓	10% FCS
Claycomb Media	✓	✓	1% FCS
Claycomb Media	✓	✓	None
DMEM high glucose Media	✓	✓	None
Advanced DMEM Media (Thermo-Fisher)	✓	✓	None

Table 4-3. Media formulations evaluated for improvement of HL-1 cell contractility.

No consistent contractility baseline was observed in HL-1 cells grown in complete Claycomb medium prior to reaching 80% confluency (Figure 4.9A and 4.9B). Remarkably, HL-1 cells that were subsequently exposed to Claycomb media in the absence of FCS and growth-factors exhibited successful contractility, as opposed to cells that were kept in FCS-containing Claycomb media. However, the CI value decreased by 20% in Claycomb media devoid of growth factors and FCS, relative to FCS-containing Claycomb media.

A change from complete Claycomb media to a base media of either DMEM or advanced DMEM, devoid of any supplements apart from norepinephrine or retinoic acid, resulted in steady and consistent contractility over time as demonstrated by beat-rate and beat amplitude uniformity, suggesting that proliferative inhibition resulted in the stabilisation of contractile syncytia. These results therefore indicate that growth factor -depleted medium, including only norepinephrine, retinoic acid, alongside the standard L-glutamine and penicillin/streptomycin can be used to maintain consistent contractility in HL-1 cells without significantly affecting cell viability for as long as 120h.

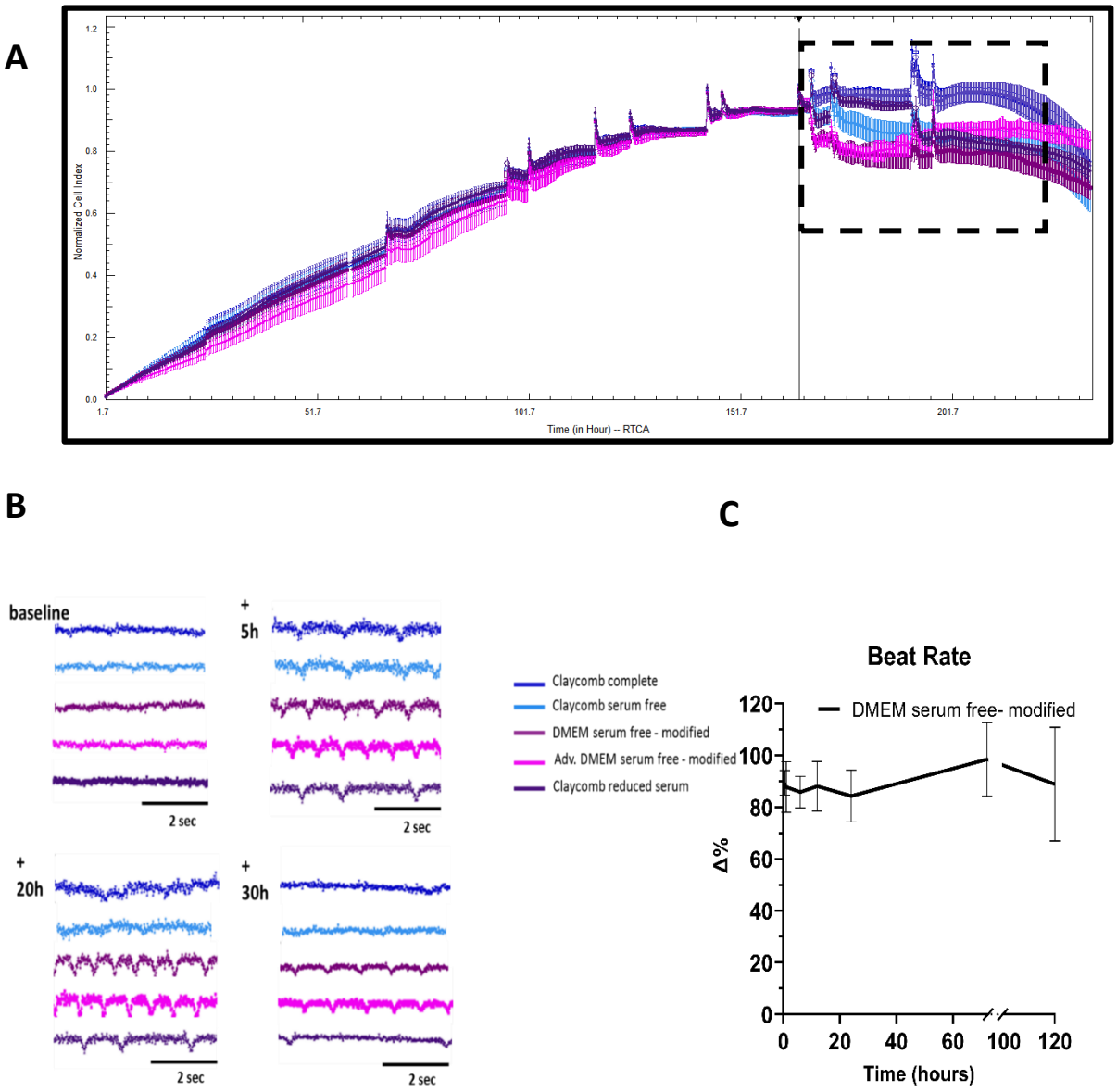

Figure 4.9 Inhibition of HL-1 proliferation is associated with improved contractility. HL-1 cells were grown in an xCELLigence Cardio E-plate in complete Claycomb medium until confluency was attained, thereafter exposed to various growth factor-depleted media formulations. HL-1 cells exposed to growth factor-depleted media formulations resulted in improved contractility at plateau resulting in stabilised contractility over time. Data shows normalised CI variations (**A**) and representative impedance contractility traces(**B**), typical of at least 8 separate determinations. **C.** Illustrates continuous beat rate changes over 120 hours using serum-free DMEM formulation, data is normalised to baseline (Δ) ±SE from three different experiments.

4.4 Growth supplement depleted medium does not alter the bioenergetic profile of HL-1 cells

To maximise HL-1 contractility at confluency, the study described in section 3.2.2. identified standard DMEM medium supplemented with only norepinephrine and retinoic acid as effective for maintenance of viability and contractility. However, to ascertain whether omission of the other factors from the growth media had an effect upon cellular energetics or introduced cellular stress, mitochondrial function of HL-1 cells in these growth media were evaluated using Seahorse XF analysis (defined in section 2.6). Following initial growth in complete Claycomb media and establishment of cell confluency and a functional syncytia, the media was either retained as complete Claycomb media or changed to HL-1 optimised DMEM medium (devoid of FCS and supplemented with only norepinephrine and retinoic acid) for 48 hours. Mitochondrial function and respiration were then assessed by modulation of complexes in the Electron Transport Chain (ETC) by the consecutive addition of specific compounds, and the subsequent assessment of Oxygen Consumption Rate (OCR), as detailed in section 2.6. The sequence of added compounds is listed in table 2.4 and included: oligomycin as a mitochondrial complex V inhibitor, FCCP as a proton uncoupler, rotenone and antimycin-A as inhibitors of complex I and complex III respectively. In both media, addition of the complex V inhibitor, oligomycin, promoted ATP synthase inhibition and resulted in an expected decrease in OCR from baseline level. Subsequent addition of the proton uncoupler, FCCP, resulted in the expected increase of OCR above baseline level due to the proton uncoupling mechanisms that allow mitochondrial membrane permeabilization to protons, indicative of the maximum respiratory capacity of HL-1 cells. Final addition of the complex I and III inhibitors, rotenone and antimycin-A, decreased the OCR below baseline level, as expected due to the inhibition of the respiratory chain. Additionally, no differences were observed in basal rate, proton leak and ATP production rates (Figure 4.11A and4.11B). Together this confirms that there was no significant difference in HL-1 bioenergetics between those incubated in the DMEM formulation as opposed to complete Claycomb media (figures 4.10 and 4.11), further supporting the use of the modified DMEM media for assessment of functional contractility studies in this cell line.

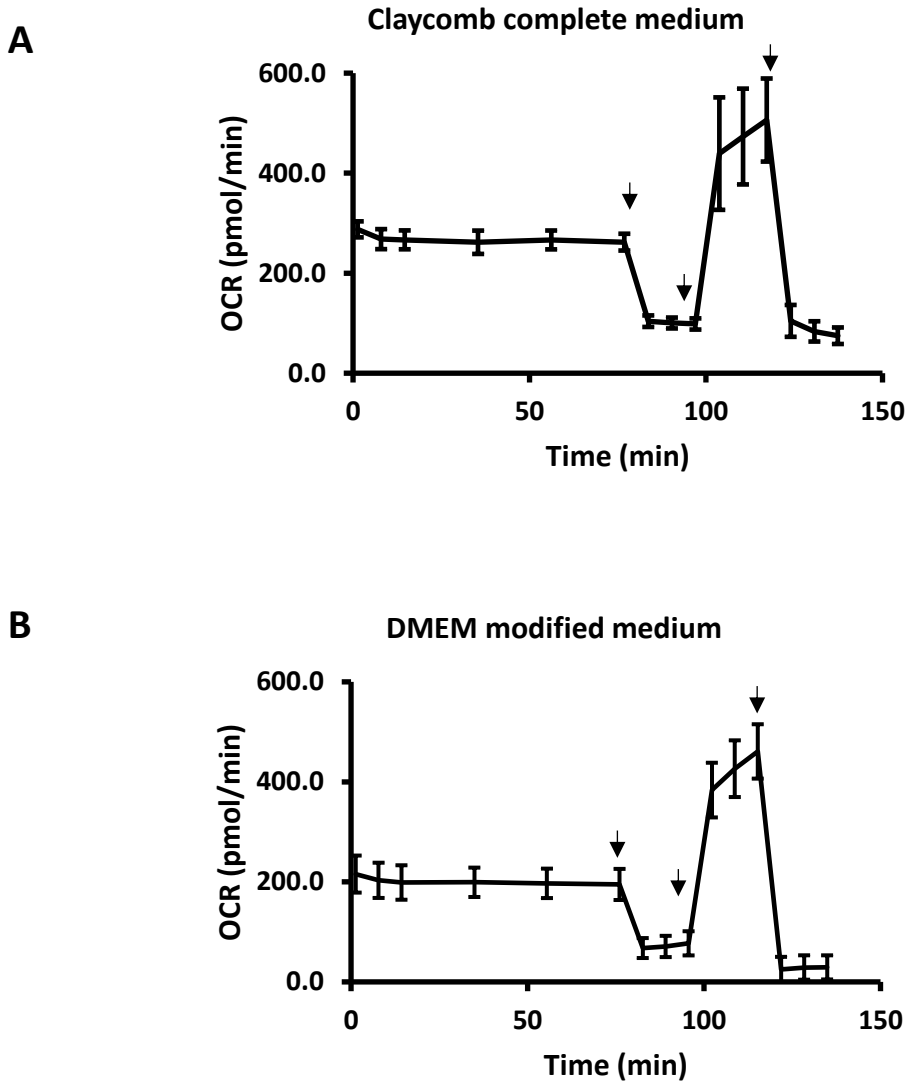

Figure 4.10 Exposure to complete Claycomb and modified DMEM media formulations does not affect mitochondrial oxygen consumption rate of HL-1 monolayer cultures. HL-1 cells were grown to functional confluency and subsequently exposed to different media conditions **A.** complete commercial Claycomb medium and **B.** modified DMEM medium for 48 h prior to testing. OCR was measured using a Seahorse analyser. Data shows OCR measurements over time in response to electron transport chain modulators. Arrows indicate injection of electron transport chain complex modulators, oligomycin, FCCP, rotenone/antimycin A in order of injection. Data are mean ±SD of at least 10 separate determinations from the same experiment, typical of 3 separate experiments.

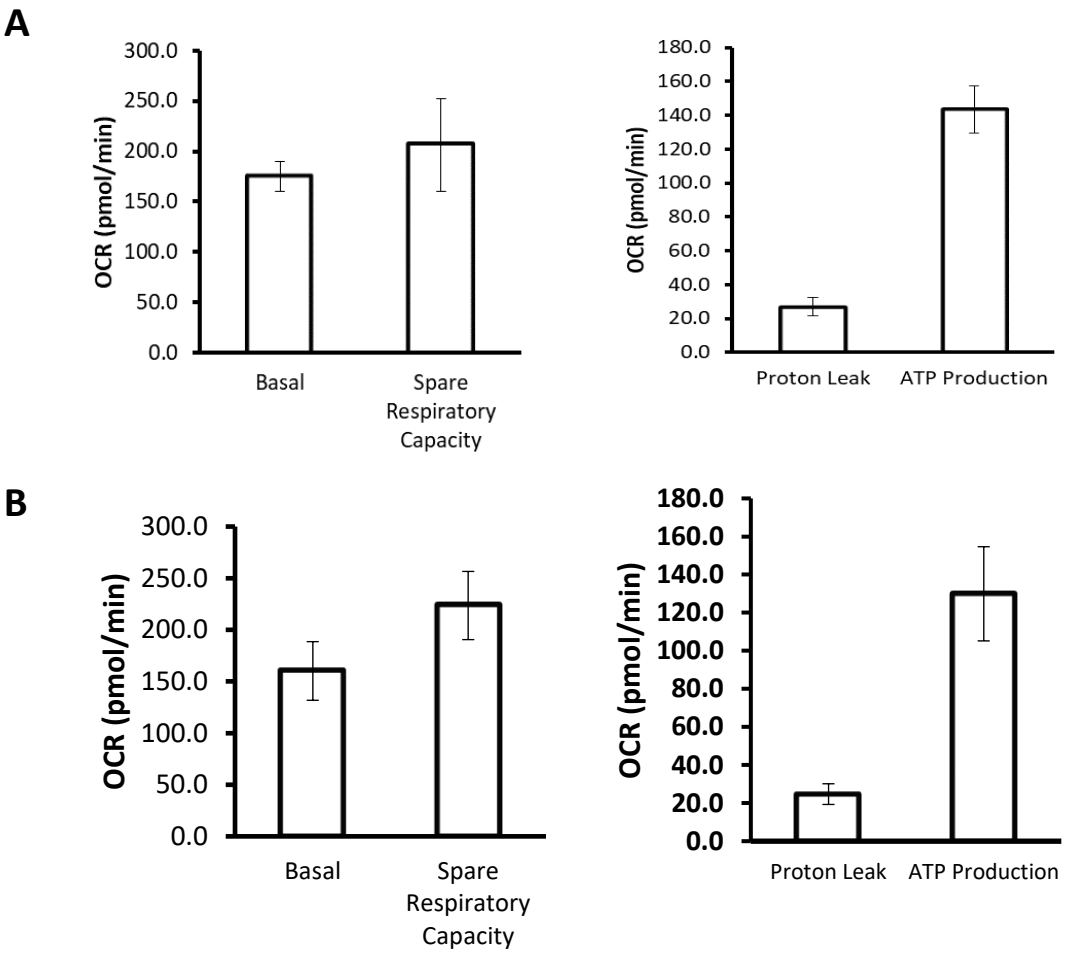

Figure 4.11 Exposure to complete Claycomb and modified DMEM media formulations does not alter the bioenergetic profile of HL-1 cells. HL-1 cells were grown to functional confluency and subsequently exposed to different media conditions **A.** complete commercial Claycomb medium and **B.** modified DMEM medium for 48 h prior to testing. Data shows comparable rates of basal and spare respiratory capacity, proton leak and ATP production. Data are mean ±SD of at least 10 separate determinations from the same experiment, typical of 3 separate experiments.

4.5 Implications of norepinephrine supplementation upon HL-1 cell bioenergetics and contractility

The inclusion of norepinephrine in growth media is established as a necessity for maintenance of HL-1 contractility in monolayer culture (Claycomb et al. 1998). However, norepinephrine acts as a α1/α2-adrenergic agonist and as such activates functional signalling in HL-1 cells, and therefore may interfere with subsequent analyses of drugs interacting with this pathway, with implications for determination of drug-induced cardiotoxicity. Consequently, the effects of norepinephrine upon HL-1 cellular bioenergetics and spontaneous contractility were evaluated using a combination of Seahorse technology and xCELLigence Cardio systems.

4.5.1 Norepinephrine-supplemented media formulations do not alter the HL-1 basal bioenergetic profile

The analysis of mitochondrial stress tests reported in figure 4.12 shows OCR fluctuations in response to known electron transport chain complex modulators oligomycin, FCCP, and rotenone/antimycin A. Confluent cells that were not supplemented with norepinephrine exhibited a similar respiration profile compared to confluent cells that were supplemented with norepinephrine, thus corroborating the fact that the bioenergetic profile of HL-1 cells was not affected by the presence or absence of norepinephrine. (Figure 4.12).

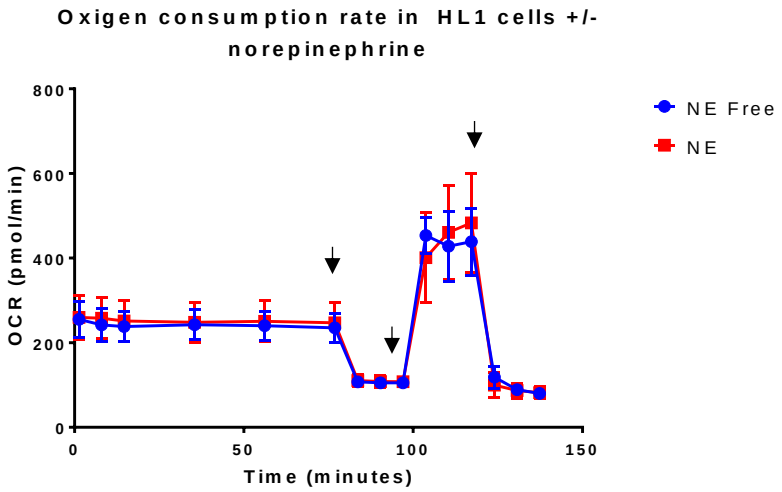

Figure 4.12 The presence or absence of norepinephrine as a medium supplement for confluent HL-1 cells does not alter cellular bioenergetic profile. HL-1 cells were grown to functional confluency and subsequently exposed to media formulations supplemented with and without norepinephrine for 48 hours prior to testing. Data shows OCR measurements over time in response to electron transport chain modulators. Arrows indicate injection of electron transport chain complex modulators, oligomycin, FCCP, rotenone/antimycin A in order of injection. Data are mean ±SD of at least 10 separate determinations from the same experiment, typical of 3 separate experiments.

4.5.2 Norepinephrine-supplemented media formulations are essential for the maintenance of HL-1 synchronous contractility

Following confirmation that the presence or absence of norepinephrine does not alter HL-1 mitochondrial respiration, the effects of norepinephrine upon HL-1 baseline contractility was carried out. HL-1 monolayers were grown to contractile confluency in the xCELLigence Cardio system, and subsequently exposed to media formulations with or without norepinephrine. Contractility baseline readings were monitored 24 hours post media substitution. Data presented in figure 4.13 demonstrates that HL-1 cells exposed to norepinephrine-depleted medium exhibited an unstable baseline contractility pattern (figure 4.13). Conversely, HL-1 cells in media supplemented with norepinephrine achieved a stable and synchronised contractile pattern, indicating the importance of norepinephrine for maintenance of cell-cell interactions and functional contractility. This study therefore suggests that norepinephrine depletion leads to altered cell-cell interactions within HL-1 syncytia, possibly due to disturbances in AP conduction.

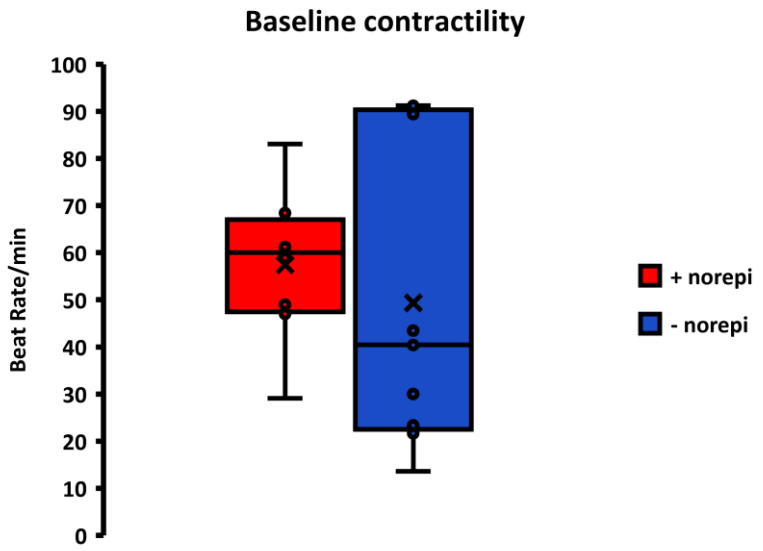

Figure 4.13 Medium supplementation with norepinephrine leads to improved stabilisation of HL-1 baseline contractility. HL-1 cells kept in norepinephrine supplemented medium achieved stable contractility, while norepinephrine depleted HL-1 cells displayed an uneven and erratic baseline contractility pattern. Data are the distribution of beat-rate at baseline of at least 8 separate determinations, typical of 3 separate experiments.

4.6 Implications of norepinephrine supplementation upon response of HL-1 to cardioactive agents

The inclusion of norepinephrine in growth media is established as a necessity for maintenance of HL-1 contractility in monolayer culture (section 4.5). However, norepinephrine acts as a α1/α2-adrenergic agonist and as such may interfere with subsequent analyses of drugs interacting with this pathway, with implications for determination of drug-induced cardiotoxicity. To address this concern, the effects of a known panel of cardioactive agents on HL-1 contractility in the presence or absence of norepinephrine using the xCELLigence Cardio system were evaluated.

4.6.1 Norepinephrine-supplemented media has minimal effect upon impedance determination of the drug-induced effects of cardioactive agents

Norepinephrine acts as a positive chronotropic stimulant via its affinity to cardiomyocyte adrenergic receptors, with potential implications for impeding detection of cardioactive compounds with comparable properties and targets; this is particularly evident with the drug isoproterenol, a norepinephrine analogue. In order to appraise this issue, the effects of a panel of cardioactive agents (table 4.4, including isoproterenol) upon confluent contractile HL-1 cells were assessed in the presence and absence of norepinephrine. For these studies, once satisfactory cell growth and stable contractility were achieved, cells were exposed to the growth-factor depleted DMEM medium formulation with or without norepinephrine supplementation. A panel of known cardioactive agents (table 4.4) was then evaluated through the assessment of contractility parameters.

The study described in section 4.5.2 highlighted the inability of norepinephrine-free HL-1 cells to achieve a stable contractility baseline. This finding was further confirmed in this study, where only a small proportion of norepinephrine-free HL-1 plate wells showed a measurable impedance contractility waveform; selected representative contractility waveforms are shown in figure 4.14 A, where baseline and 2 hours post-treatment traces are compared. Contractility parameters were assessed as beat rate/ minute.

In the presence and absence of norepinephrine supplementation, isoproterenol was still able to elicit an increase in contractility beat-rate. Exposure to the β-adrenoceptor antagonist Carvedilol should theoretically counteract the effect of norepinephrine, an activity evident in this study with a decrease in beat-rate only observed in the absence of norepinephrine. In the case of the calcium channel blocker verapamil, a non-significant change in beat-rate was observed in both the presence and absence of norepinephrine (figure 4.14). Taken together, this study indicates that media supplementation with norepinephrine has little effect upon detectability of cardioactive agents. While the absence of norepinephrine in the growth factor-depleted DMEM medium formulation seemed to elicit more physiologically relevant effects in HL-1 contractility parameters in response to specific agents, the overall functionality and stability of HL-1 contractility was compromised as demonstrated in the baseline readings. For this reason, norepinephrine exclusion from media formulations was deemed disadvantageous for HL-1 cardiomyocyte studies.

Name	*Structure*	*Comments*
Norepinephrine	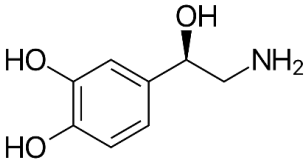	Adrenergic receptor agonist
Isoproterenol	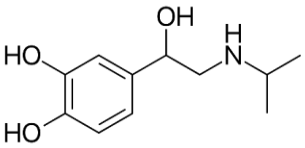	Norepinephrine analogue and adrenergic receptor agonist
Carvedilol	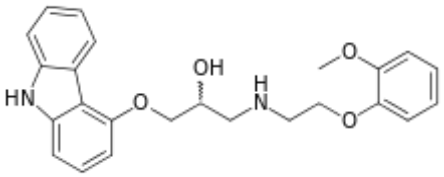	Beta-adrenoceptor antagonist
Verapamil	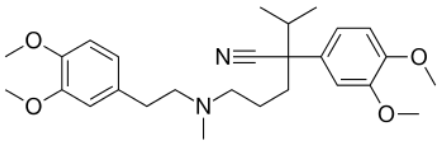	Calcium channel blocker

Table 4-4 Chemical structures of known cardioactive agents that may interfere with drug-induced cardiotoxicity determinations.

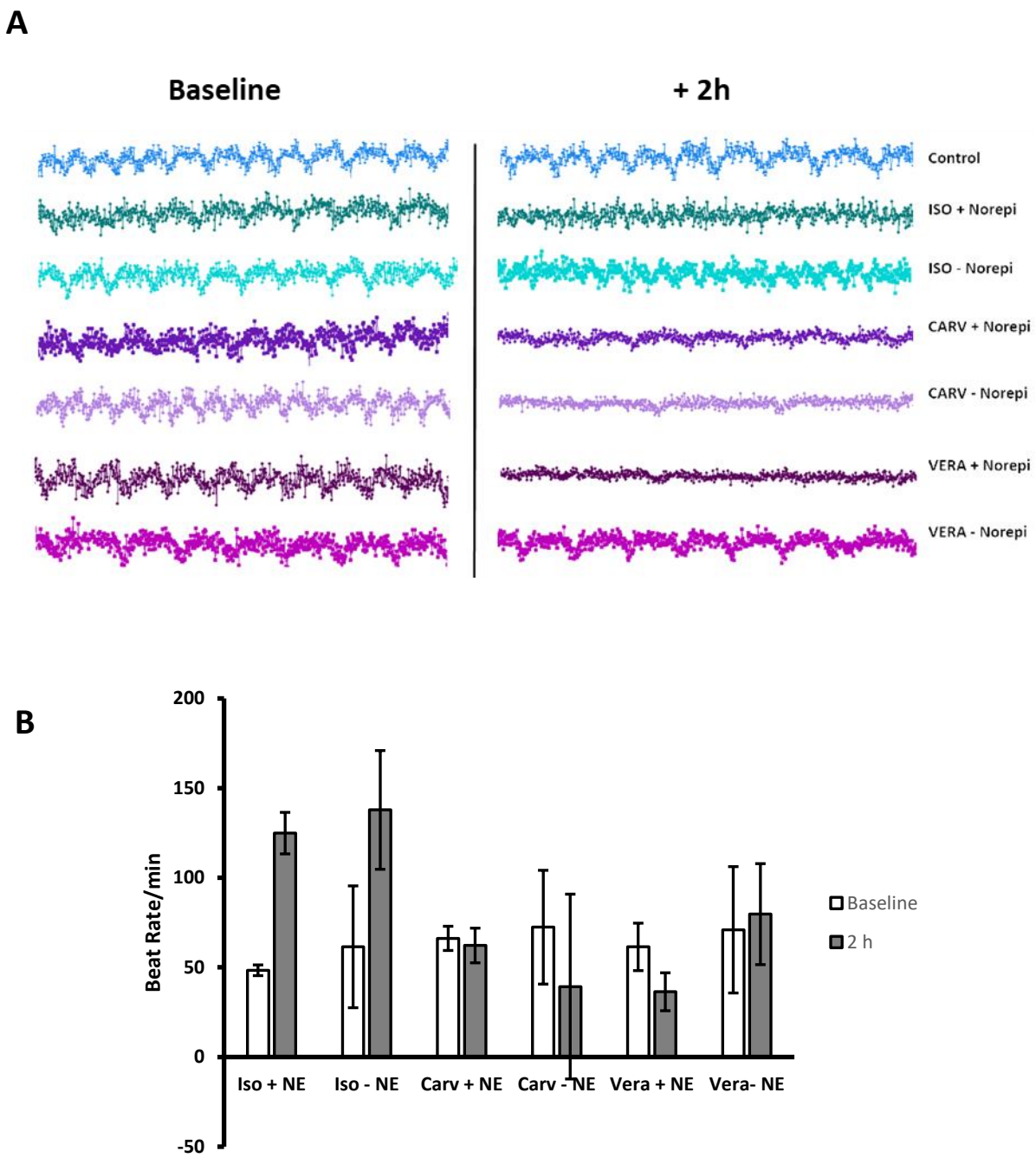

Figure 4.14 Norepinephrine-supplemented HL-1 medium stabilises baseline contractility, and exerts little effect upon detectability of cardioactive agents.

HL-1 cells were grown to contractility on the xCELLigence Cardio system and exposed to a set of known cardioactive agents in the presence or absence of norepinephrine. Data shows **A)**. representative raw impedance traces of contractility at baseline and 2h post compound exposure, and **B)**. beat-rate expressed as beat/minute ±SD, corrected for vehicle control. Data are derived from > 4 independent determinations.

4.7 HL-1 cell line demonstrates consistent responses to known cardioactive and antiarrhythmic agents

In order to establish the suitability of the HL-1 cell line model for the detection of drug-induced functional and structural effects, a panel of known cardioactive agents (Table 4.4) was screened using the xCELLigence Cardio system.

For these studies, once stable contractility was detected, medium was substituted with the growth factor-depleted DMEM medium formulation supplemented with norepinephrine, retinoic acid, l-glutamine and penicillin/streptomycin, and contractility was monitored for 24 hours every 30 minutes thereafter. Spontaneous HL-1 activity was recorded and assessed for each experimental batch in order to detect and exclude wells displaying spontaneous beat rhythm irregularities prior to compound addition with compounds. To validate different batches of HL-1 cells, the cells were screened against a panel of compounds with well-defined cardioactive effects (Table 4-5). Analysed parameters included CI variations, beat rate, and cell index (impedance) beat amplitude.

The class I antiarrhythmic agents quinidine, lidocaine and propafenone elicited consistent detectable effects in HL-1 cells. Quinidine induced a transient decrease in beat rate, as expected due to its effects on AP prolongation by Na^+ channel blockade, resulting in a 60% total decrease in beat rate within 24 hours post compound addition. Additionally, quinidine resulted in a transient 20% decrease in CI beat amplitude (BA) within 6 hours post compound addition. Similarly, lidocaine induced a marked decrease in beat rate, resulting in a 40% decrease 1 hour post compound addition, and a concomitant 20% decrease in BA 6 hours post compound addition. Propafenone exerted a 45% decrease in beat rate, and a 20% decrease in BA 1 hour post compound addition.

Exposure of contractile HL-1 cells to either of the class II β-adrenergic blockers, Metoprolol and Carvedilol, did not result in any detectable effects upon HL-1 contractility and CI parameters. Conversely, exposure to the β-adrenoceptor agonist isoproterenol induced a detectable effect on HL-1 contractility parameters, causing an 82% increase in beat rate 0.5 hours post compound addition.

Exposure to the non-selective potassium channel blocker amiodarone did not exert a detectable effect in HL-1 contractility parameters. On the contrary, the experimental selective potassium hERG channel blocker E-4031 elicited an expected marked response in contractile parameters, with beat rate decreasing by 74% within 0.5 hours post compound addition. Beat amplitude was decreased 0.5 hours post compound addition, and increased 6 hours post compound addition.

The class IV antiarrhythmic compound verapamil induced detectable effects on HL-1 contractility. Verapamil however exerted an unexpected transient increase in beat rate by 50% 0.5 hours post compound addition, therefore inducing a diametric effect. Beat amplitude was temporarily decreased by 24% 1 hour post compound addition.

The structural cardiotoxic anthracycline doxorubicin induced an expected significant ($p<0.001$) initial increase in beat rate, followed by a steady decrease of the parameter within 24 hours post compound addition. Similarly, changes in beat amplitude resulted in an acute temporary increase of the parameter by 250%, before undergoing a steady decline and contractility arrest within 24 hours post compound addition. As predicted, doxorubicin induced a significant ($p<0.001$) decrease in CI, inducing a 66% decrease of the parameter within 24 hours.

Overall, these results demonstrate that the HL-1 cell line steadily responds to a wide panel of functional and structural cardioactive agents. This study therefore serves as proof of concept validating the suitability of HL-1 cell line use in combination with impedance RTCA systems.

Compound	*Mechanism*	*Expected effect*	*Detectable effect in HL-1 cell line using xCELLigence Cardio*
Class I antiarrhythmic agents: Voltage-gated Sodium Channel Blockade			
Quinidine	Class Ia: Nav1.5 open state inhibitor with rapid dissociation rate (& K^+ channel blockade)	BR↓ BA↓ CI-	☑
Lidocaine	Class Ib: Nav1.5 open state inhibitor with intermediate dissociation rate	BR↓ BA↓ CI-	☑
Propafenone	Class Ic: Nav1.5 inactivated state inhibitor with slow dissociation rate	BR↓ BA↓ CI-	☑
Class II antiarrhythmic agents: Autonomic inhibitors and activators			
Metoprolol	Selective β-adrenergic blocker	BR↓ BA↓ CI-	**X**
Carvedilol	Non-selective β-adrenergic blocker	BR↓ BA↓ CI-	**X**
Isoproterenol	β-adrenergic receptor activator	BR↑ BA↑ CI-	☑
Class III antiarrhythmic agents: Potassium channel blockers			
Amiodarone	Nonselective K^+ channel blocker	BR↓ BA- CI-	**X**
E-4031	Kv11.1 (hERG) channel (IK_r) blocker	BR↓ BA- CI-	☑
Class IV antiarrhythmic agents: Calcium channel blockers			
Verapamil	L-type Ca^{2+} channel blocker	BR↓ BA- CI-	☑
Structural Cardiotoxicants			
Doxorubicin		BR↑ BA↑ CI↓	☑

Table 4-5 Known cardioactive agent effects in HL-1 cells vs effects detected using impedance-based technology. All parameters in this table are reported as an increase (↑) a decrease (↓) or unaffected (-).

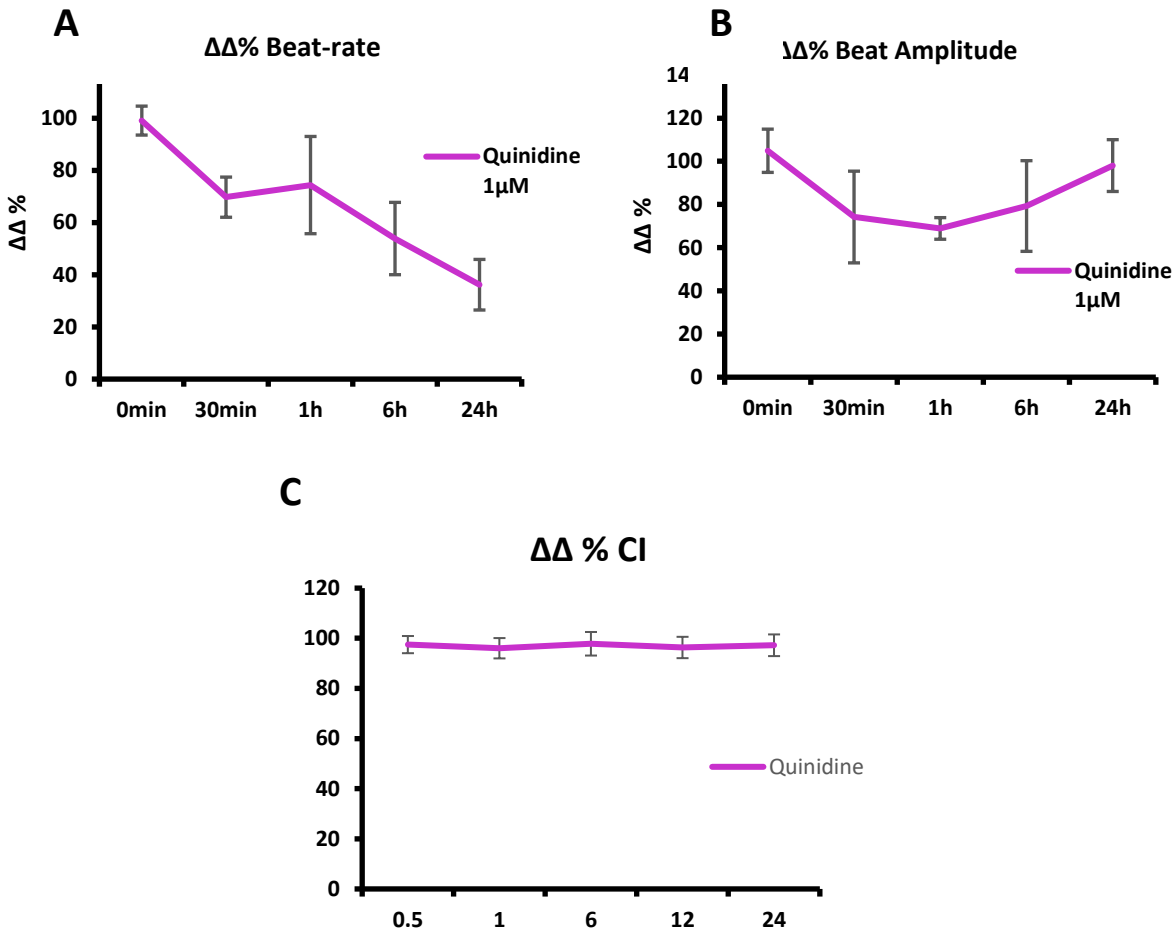

Figure 4.15 Quinidine induces contractility changes in HL-1 cells. HL-1 cells were grown to contractility on the xCELLigence Cardio system and exposed to 1µM quinidine for 24 hours. Beat rate was significantly decreased ($p<0.001$) by 60 % within 24 h. CI beat amplitude was transiently affected showing a 20% decrease 1 h post dosing and restored to baseline levels at 24 h post dosing. Impedance cell index was unaffected. Data are normalised to baseline and vehicle control (ΔΔ), and are the average ±SD of at least 3 separate determinations. Tested by ANOVA and Dunnet's post-hoc modifications.

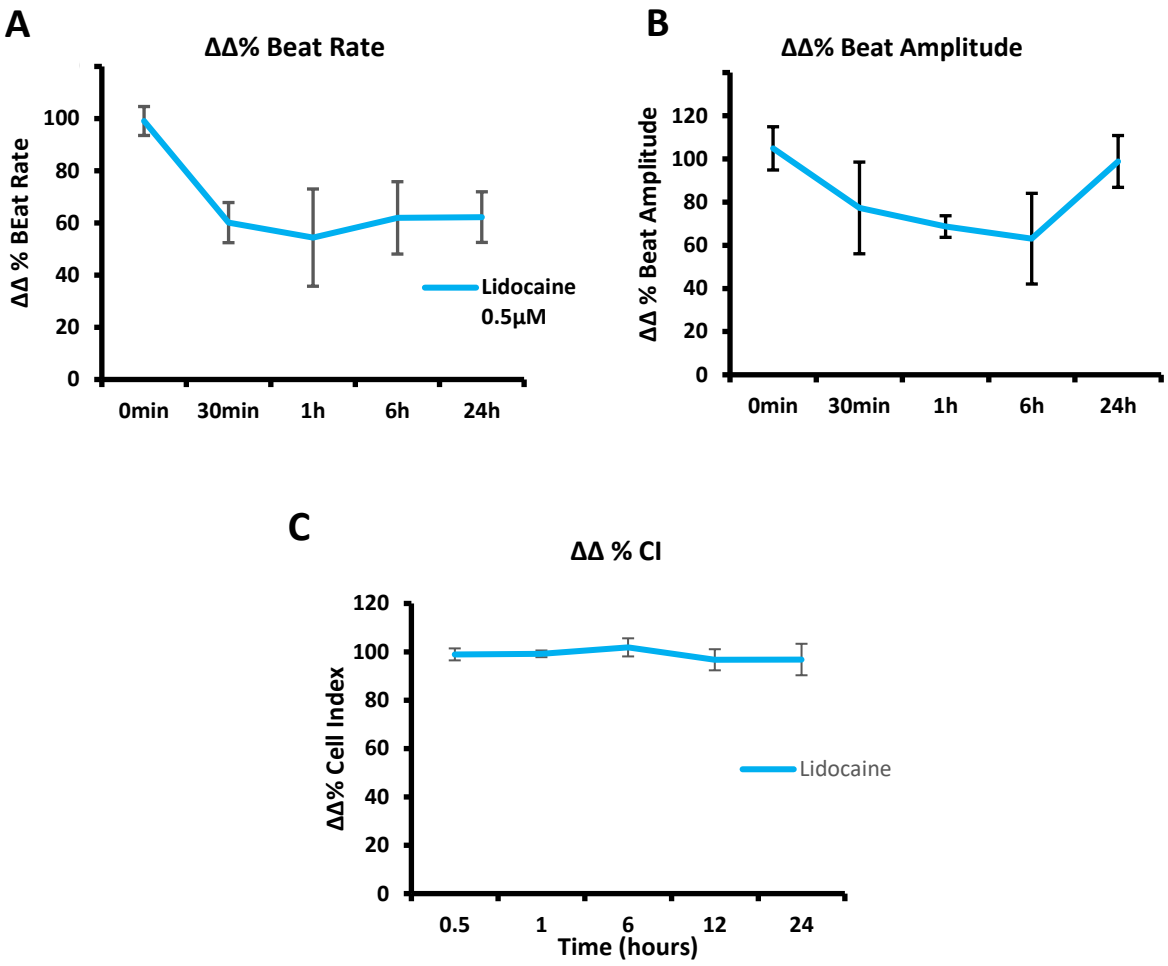

Figure 4.16 Lidocaine induces contractility changes in HL-1 cells. HL-1 cells were grown to contractility on the xCELLigence Cardio system and exposed to 0.5µM lidocaine for 24 hours. Beat rate was significantly decreased ($p<0.001$) by 40 % within 24 h. CI beat amplitude was transiently affected showing a 20% decrease 1 h post dosing and restored to baseline levels at 24 h post dosing. Impedance cell index was unaffected. Data are normalised to baseline and vehicle control (ΔΔ), and are the average ±SD of at least 3 separate determinations. Tested by ANOVA and Dunnet's post-hoc modifications.

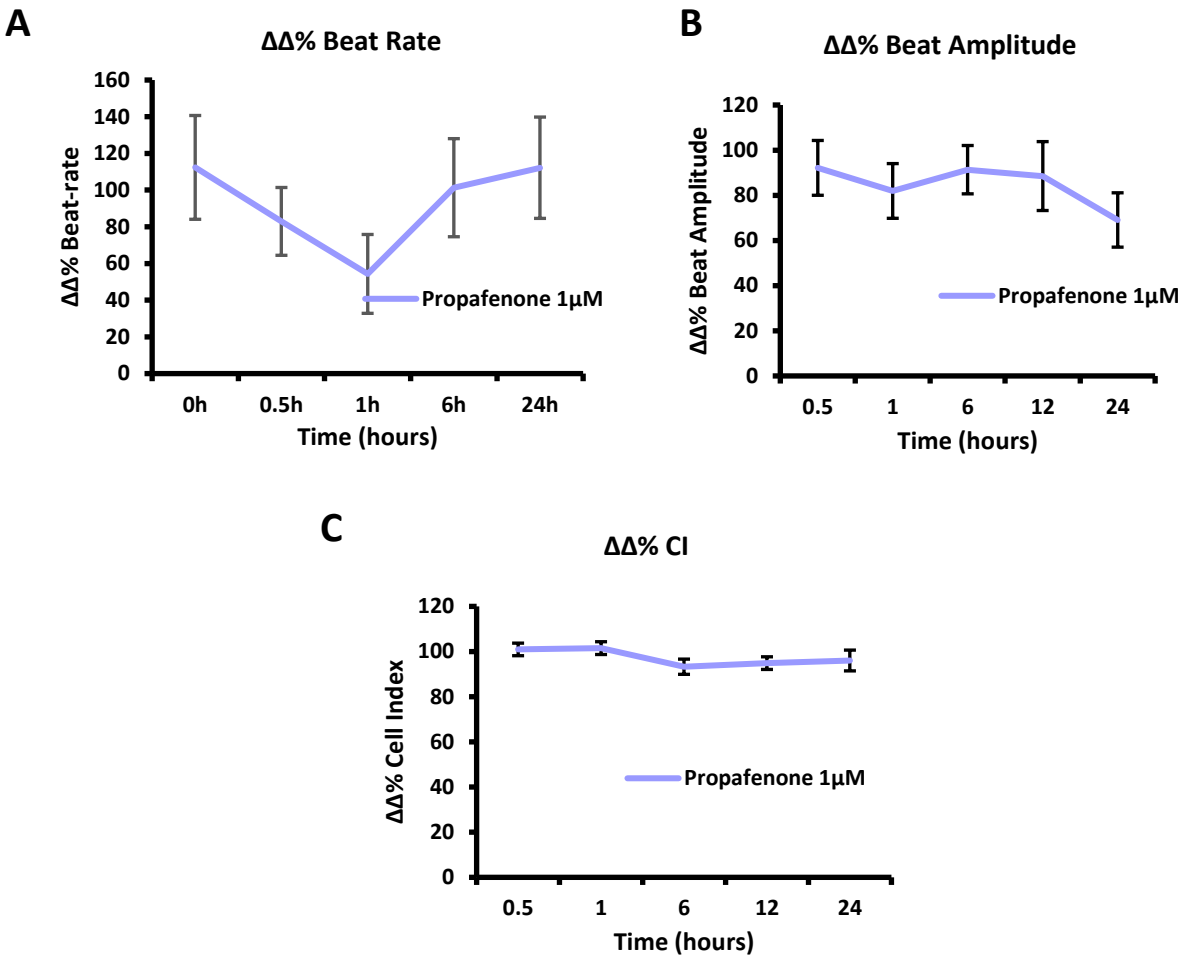

Figure 4.17 Propafenone induces contractility changes in HL-1 cells. HL-1 cells were grown to contractility on the xCELLigence Cardio system and exposed to 1µM propafenone for 24 hours. Beat rate was significantly decreased ($p<0.001$) by 40 % within 24 h. CI beat amplitude was affected showing a 20% decrease within 1 h and a further decrease 24 h post drug addition. Impedance cell index was unaffected. Data are normalised to baseline and vehicle control (ΔΔ), and are the average ±SD of at least 3 separate determinations. Tested by ANOVA and Dunnet's post-hoc modifications.

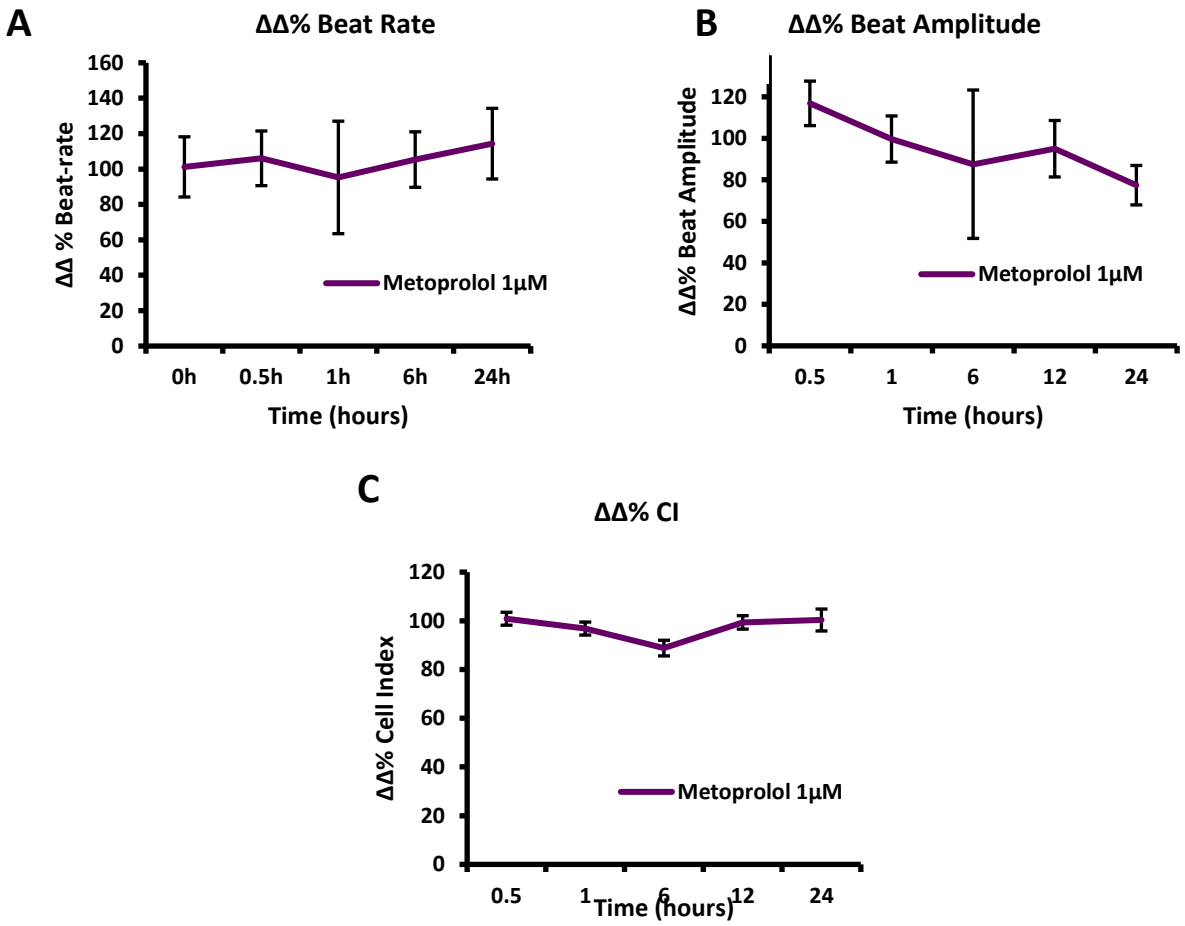

Figure 4.18 Metoprolol does not induce detectable contractility changes in HL-1 cells. HL-1 cells were grown to contractility on the xCELLigence Cardio system and exposed to 1µM metoprolol for 24 hours. Beat rate, CI beat amplitude and. impedance cell index were unaffected. Data are normalised to baseline and vehicle control (ΔΔ), and are the average ±SD of at least 3 separate determinations. Tested by ANOVA and Dunnet's post-hoc modifications.

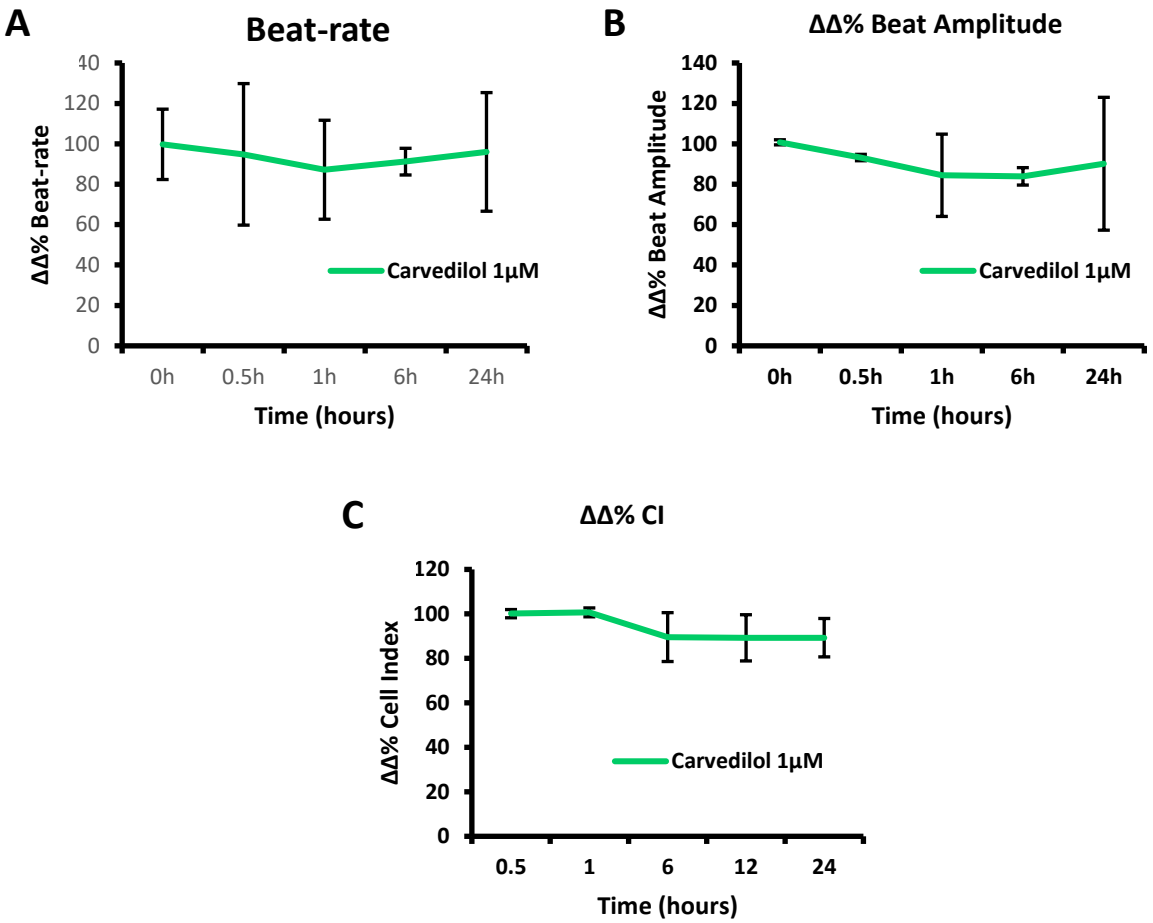

Figure 4.19 Carvedilol does not induce detectable contractility changes in HL-1 cells. HL-1 cells were grown to contractility on the xCELLigence Cardio system and exposed to 1µM carvedilol for 24 hours. Beat rate, CI beat amplitude and impedance cell index were unaffected. Data are normalised to baseline and vehicle control (ΔΔ), and are the average ±SD of at least 3 separate determinations. Tested by ANOVA and Dunnet's post-hoc modifications.

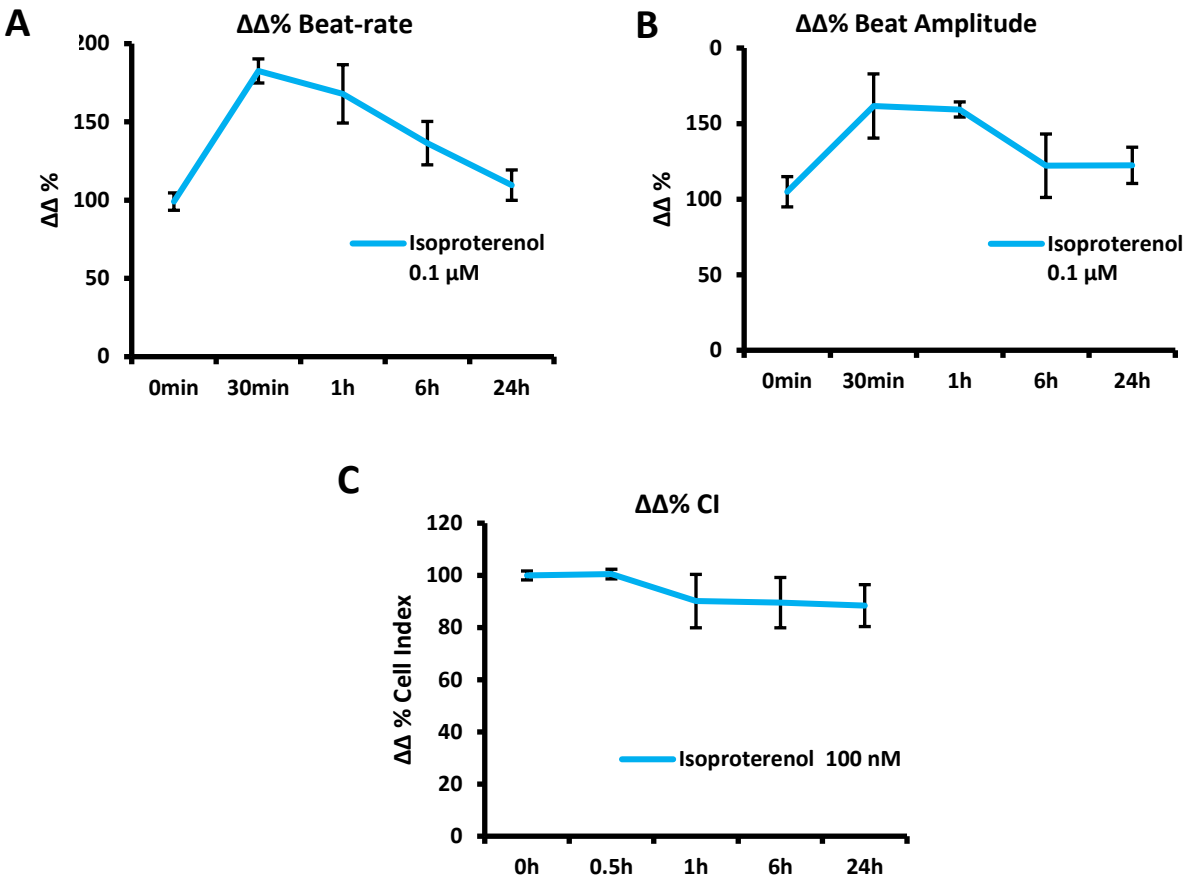

Figure 4.20 Isoproterenol induces contractility changes in HL-1 cells. HL-1 cells were grown to contractility on the xCELLigence Cardio system and exposed to 100nM isoproterenol for 24 hours. Beat rate was significantly increased ($p<0.001$) by 82 % within 0.5 h. CI beat amplitude was affected showing a 60% increase 1 h post drug addition. Impedance cell index was unaffected. Data are normalised to baseline and vehicle control (ΔΔ), and are the average ±SD of at least 3 separate determinations. Tested by ANOVA and Dunnet's post-hoc modifications.

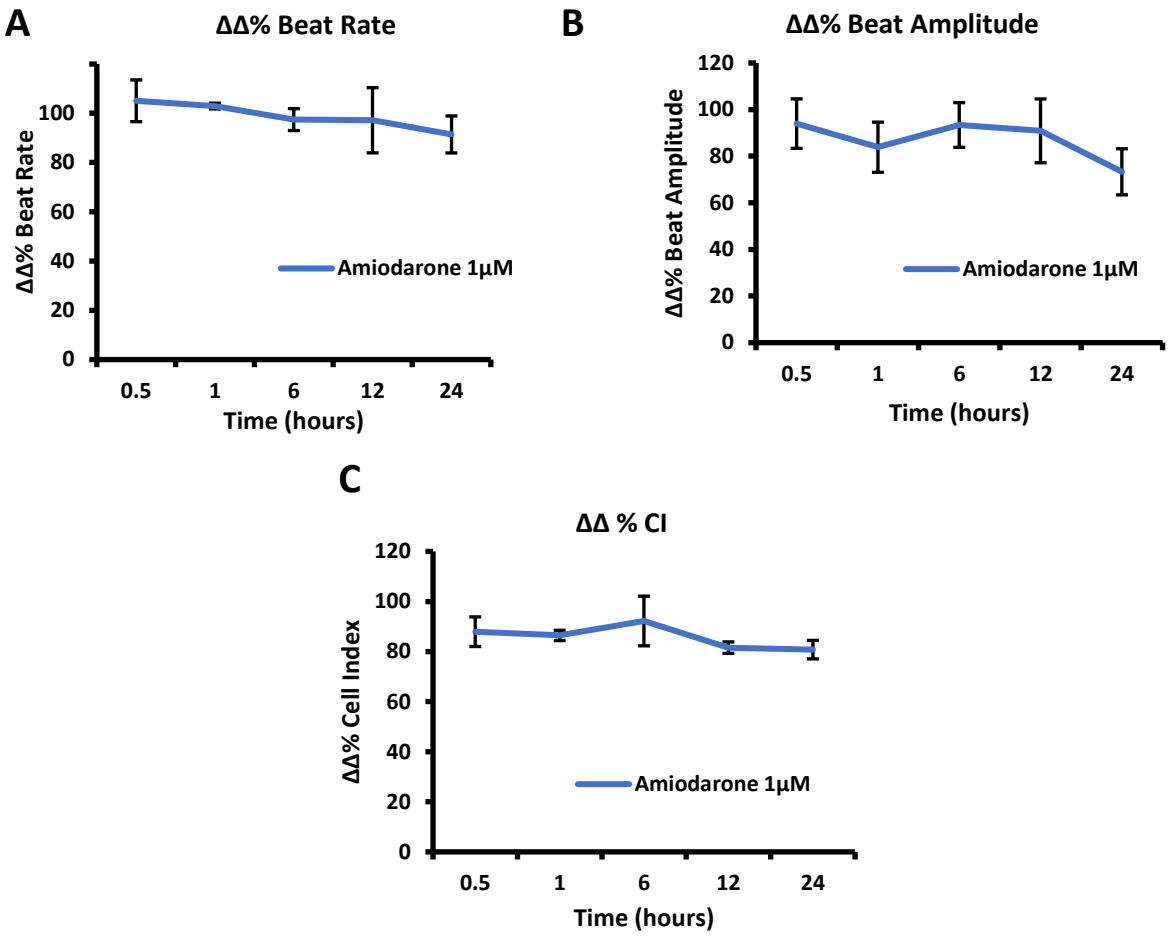

Figure 4.21 Amiodarone does not induce detectable contractility changes in HL-1 cells. . HL-1 cells were grown to contractility on the xCELLigence Cardio system and exposed to 1µM amiodarone for 24 hours. Beat rate, CI beat amplitude and impedance cell index were unaffected. Data are normalised to baseline and vehicle control (ΔΔ), and are the average ±SD of at least 3 separate determinations. Tested by ANOVA and Dunnet's post-hoc modifications.

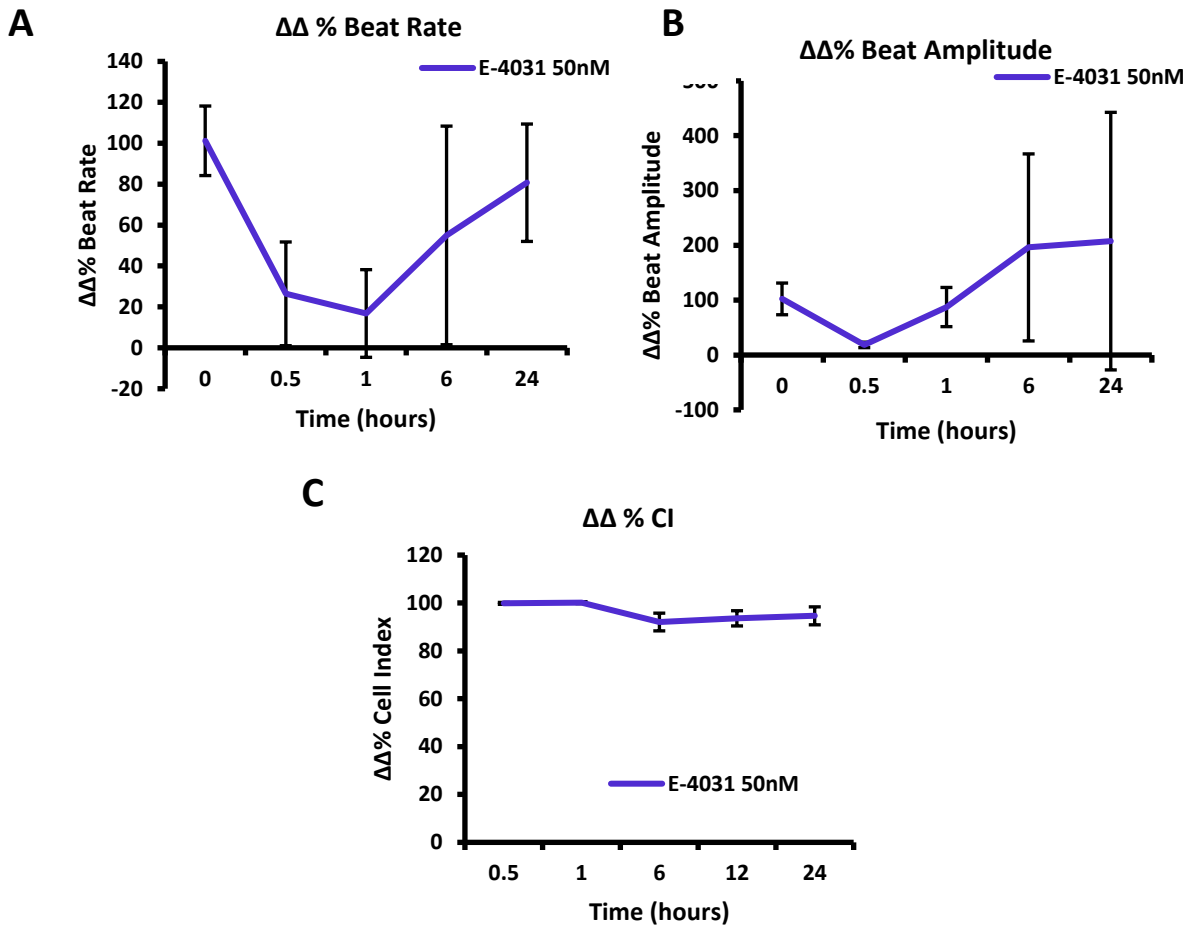

Figure 4.22 E-4031 induces contractility changes in HL-1 cells. HL-1 cells were grown to contractility on the xCELLigence Cardio system and exposed to 50nM E-4031 for 24 hours. Beat rate was significantly decreased ($p<0.001$) by 84 % within 1 h. CI beat amplitude was affected showing an 82% decrease 0.5h post drug addition. Impedance cell index was unaffected. Data are normalised to baseline and vehicle control (ΔΔ), and are the average ±SD of at least 3 separate determinations. Tested by ANOVA and Dunnet's post-hoc modifications.

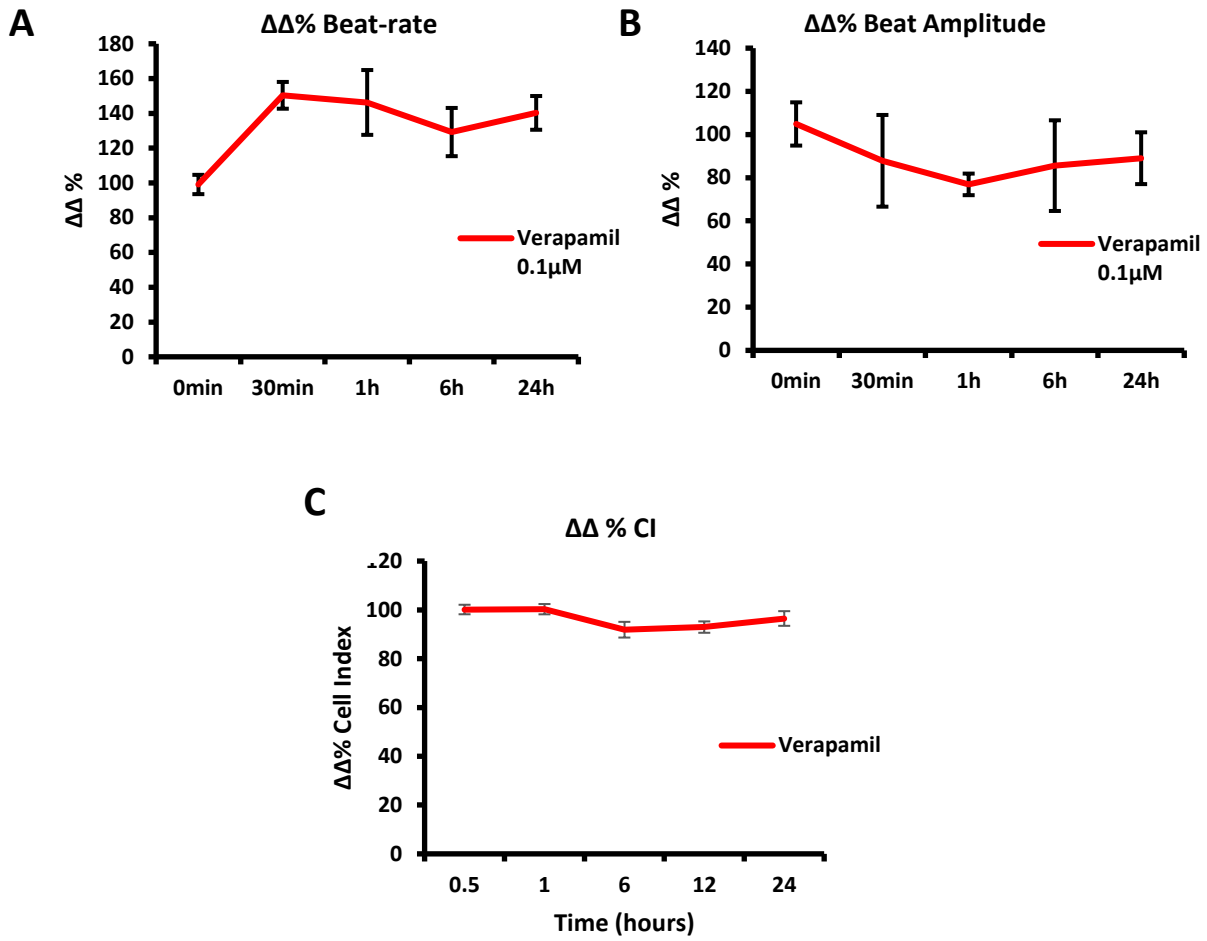

Figure 4.23 Verapamil induces contractility changes in HL-1 cells. HL-1 cells were grown to contractility on the xCELLigence Cardio system and exposed to 0.1µM verapamil for 24 hours. Beat rate was significantly increased ($p<0.001$) by 50 % within 0.5 h. CI beat amplitude was affected showing a 24% decrease 1h post dosing. Impedance cell index was unaffected. Data are normalised to baseline and vehicle control (ΔΔ), and are the average ±SD of at least 3 separate determinations. Tested by ANOVA and Dunnet's post-hoc modifications.

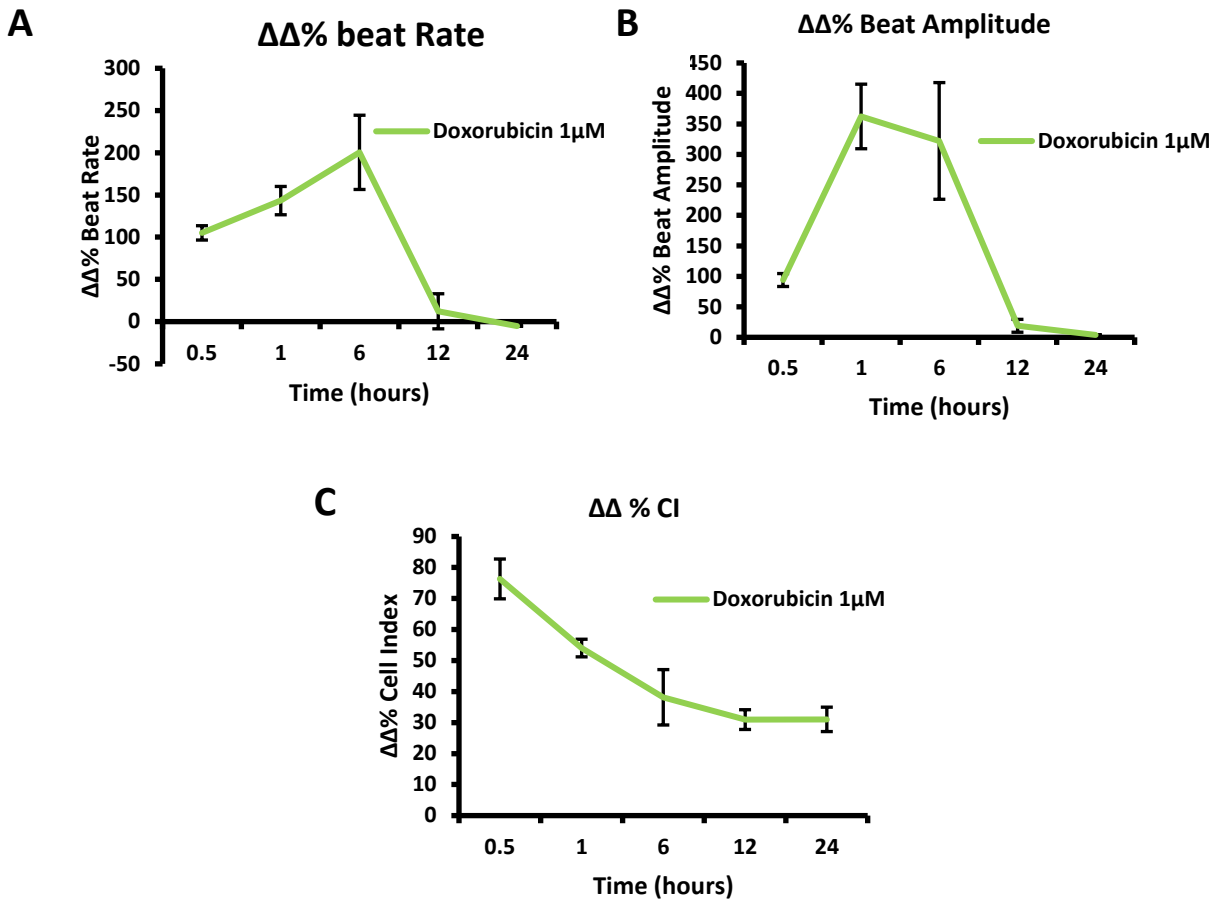

Figure 4.24 Doxorubicin induces contractility changes in HL-1 cells. HL-1 cells were grown to contractility on the xCELLigence Cardio system and exposed to 1µM doxorubicin for 24 hours. Beat rate was significantly increased ($p<0.001$) by 100 % within 6 h. CI beat amplitude was affected showing a 250% increase ($p<0.001$) 1h post drug addition. Impedance cell index was decreased by 66% ($p<0.001$) within 24 h. Data are normalised to baseline and vehicle control (ΔΔ), and are the average ±SD of at least 3 separate determinations. Tested by ANOVA and Dunnet's post-hoc modifications.

4.8 Pan-HDAC inhibition induces perturbations in functional, structural and viability parameters in the HL-1 murine atrial cell line

Previous studies reported in section 3.3 indicated that pan-HDAC inhibition at sub-clinically relevant concentrations induced proarrhythmic events and permanent contractility changes in a hiPSC-CM model. Following validation of the HL-1 cells as a suitable model for the detection of functional and structural changes in this study, the effects of the pan-HDAC inhibitors SAHA and TSA were evaluated in this model using the xCELLigence Cardio system, with a focus on sub-clinical concentrations (methods described in section 2.7). Impedance cell index (CI) beat rate and beat amplitude changes were evaluated with the aim of detecting acute and late-onset cardiotoxicity.

SAHA at both 600 nM and 200 nM induced a marked 110% increase in beat rate 12 hours post drug addition, before steadily decreasing and resulting in complete contractility arrest 100 hours after drug exposure. HL-1 cells exposed to 50 nM SAHA maintained a stable beat rate until 105 hours after drug addition, before displaying an abrupt decline leading to total cessation of contractility by 120 hours (Figure 4.25 A). Contractility was not restored upon fresh media supplementation, thus indicating the occurrence of a permanent damage.

Similarly to SAHA, TSA resulted in contractility arrest at all tested concentrations (1 µM, 200 nM and 50 nM), displaying functional cardiotoxicity in a dose-dependent manner (Figure 4.25 B). TSA induced significant ($p < 0.001$) beat rate changes 5 hours post drug exposure, with 1µM TSA resulting in a 55% decrease, in contrast to 200 nM which resulted in a 46% increase in beat rate. Exposure to 50 nM TSA resulted in a delayed effect upon beat rate of the HL-1 cells, presenting as an initial 26% increase after 12 hours exposure, followed by a steady decline within 24 hours (Figure 4.25 B). Contractile activity did not resume upon fresh media supplementation.

At the higher concentrations of SAHA and TSA (600 nM and 1 µM, respectively) a positive inotropic effect upon cellular beat amplitude was detected ($p < 0.05$) (Figure 4.26 A and 4.26 B). However, at the lower drug concentrations no significant inotropic effect upon beat amplitude was observed, and a steady reduction in the parameter was recorded, as reflected in beat rate analysis.

Remarkable changes were observed in cell index (CI) in the presence of both SAHA and TSA. SAHA induced a dose-dependent CI decrease, resulting in a maximal decrease of 34%, 52% and 69% at 48 hours for 50 nM, 200 nM and 600 nM, respectively (Figure 4.27 A). These CI changes remained stably decreased, albeit showing a marginal restoration towards baseline levels between 72-84 hours after drug addition. Upon compound removal, CI changes remained unaffected and were not restored to baseline levels. This decline in Cl is indicative of either cell death/detachment, cellular hypotrophy, or a morphological change. To determine whether it was attributed to cellular death/detachment, a parallel MTT assay was performed alongside the xCELLigence assay. This showed that HL-1 cell viability and thus cell number were not diminished at any of the SAHA concentrations evaluated, coinciding with the decline in Cl values, and therefore the changes were a result of structural modifications of cellular/syncytial morphology.

In a similar fashion to SAHA, TSA also induced a decrease in CI following drug addition (Figure 4.27 C). Effects with 1 µM TSA were noticeable as early as 1 hour post compound addition and exposure to 200 nM TSA resulted in a significant ($p < 0.001$) CI decrease culminating 12 hours after drug addition. In the case of the lower 50 nM TSA concentration, a non-significant decline in Cl was observed by 24 hours after drug exposure. As with SAHA, removal of TSA did not affect CI levels, which remained at their reduced levels and did not return to baseline levels indicating the occurrence a permanent change. Assessment of drug-induced cytotoxicity by the MTT assay indicated a significant effect with 1 µM, supporting the drop in Cl being a consequence of primarily cell death/detachment (figure 4.27D). On the contrary, no cytotoxicity was observed with TSA concentrations of 200 nM or 50 nM (figure 4.27D), and therefore any changes in CI can also be plausibly linked to changes in cell morphology and structural cardiotoxicity.

To further confirm that the effects of pan-HDACi at sub-cytotoxic concentrations were dependent on structural changes, and not on cellular death or reduction in cellular metabolic activity, manual cell counts were performed to ascertain that cell numbers in treated and untreated cells remained similar. Results shown in figure 4.28A and 4.28B demonstrate that cell numbers were unaffected by sub-clinical and sub-cytotoxic concentrations of SAHA and TSA, thus further corroborating the conclusion that changes in CI are dependent on structural cytotoxicity and morphological changes

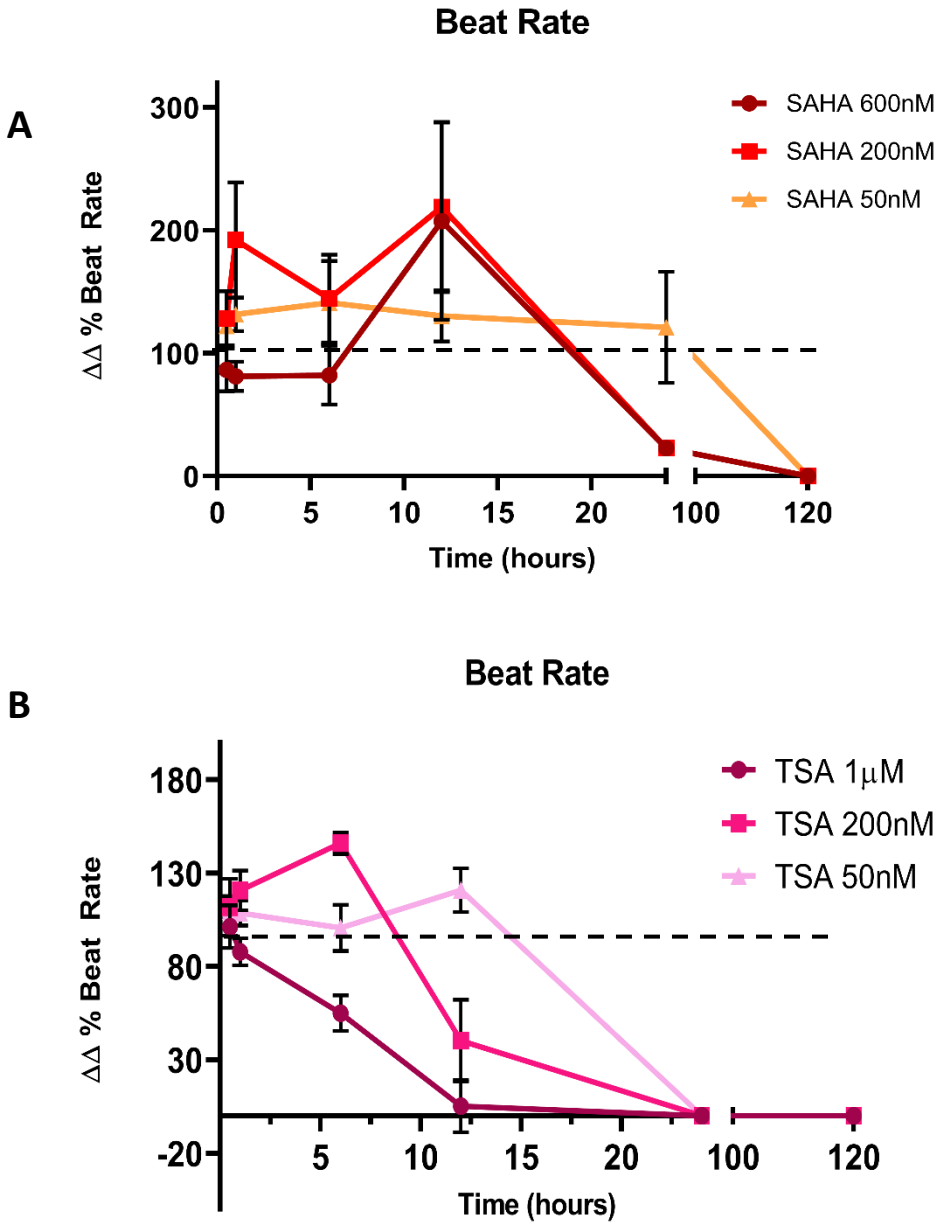

Figure 4.25 Pan-HDACis induce time-dependent changes in beat rate at clinical and sub-clinical concentrations in HL-1 cells. HL-1 cells were exposed to SAHA and TSA at a range of concentrations for 120 h. **A.** SAHA induced significant beat rate changes starting with an increase 12 h post addition at concentrations between 200 nM and 600 nM before a late-onset contractility arrest within 48 h post exposure B. TSA induced significant beat rate changes starting from 5 h post compound addition at concentrations between 1 µM and 50 nM, starting with an initial increase and followed by contractility arrest in a time-dependent manner. Data are the average ±SD of at least 3 separate determinations, and are normalised to baseline and vehicle control. Tested by ANOVA and Bonferroni post-hoc modifications.

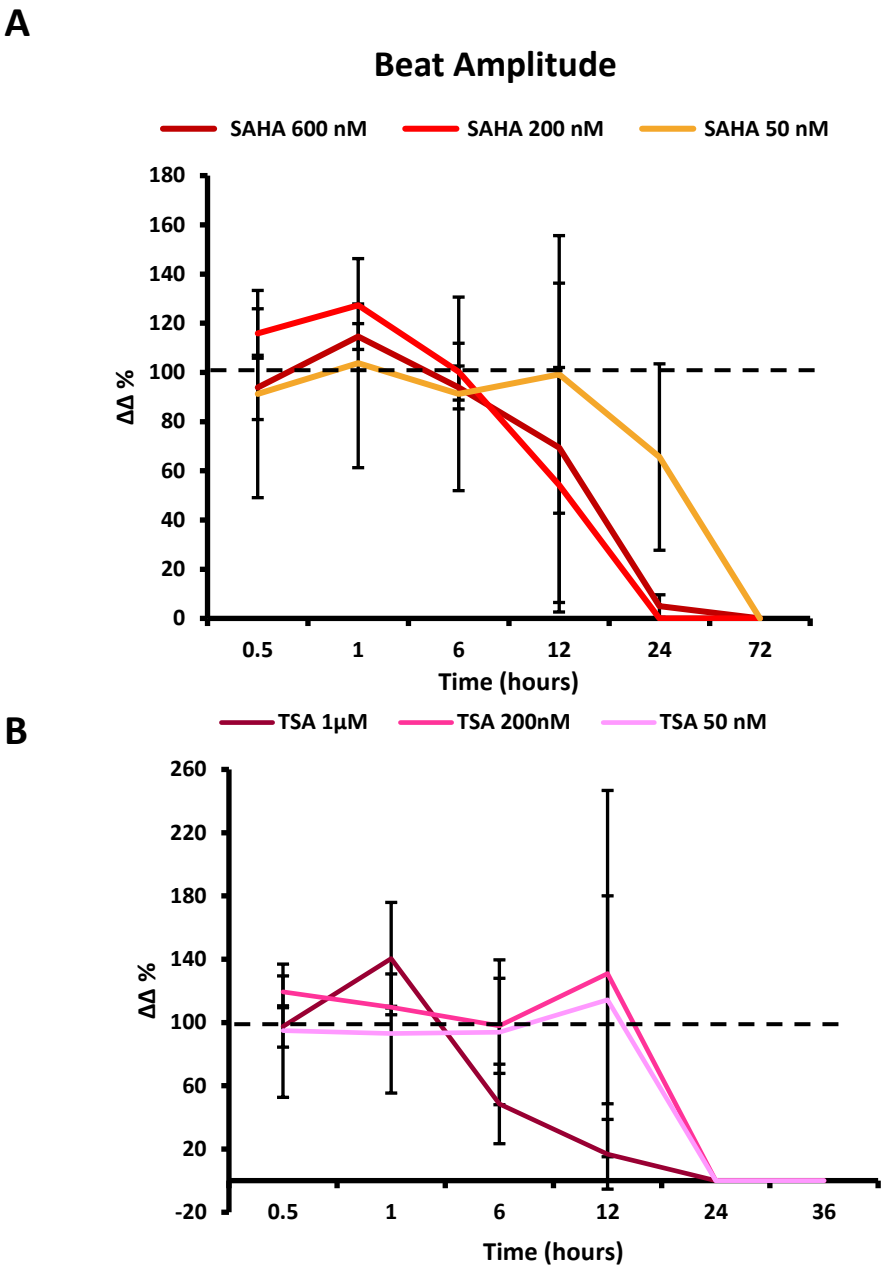

Figure 4.26 Pan-HDACis induce time-dependent changes in beat amplitude at clinical and sub-clinical concentrations in HL-1 cells. HL-1 cells were exposed to SAHA and TSA at a range of concentrations for 120 h. **A.** SAHA induced significant beat amplitude changes starting from 12 h post addition at concentrations between 600nM and 50nM in a time-dependent manner. B. TSA induced significant beat amplitude changes starting from 5 h post compound addition at concentrations between 1 µM and 50 nM in a time-dependent manner. Data are the average ±SD of at least 3 separate determinations, and are normalised to baseline and vehicle control. Tested by ANOVA and Bonferroni post-hoc modifications

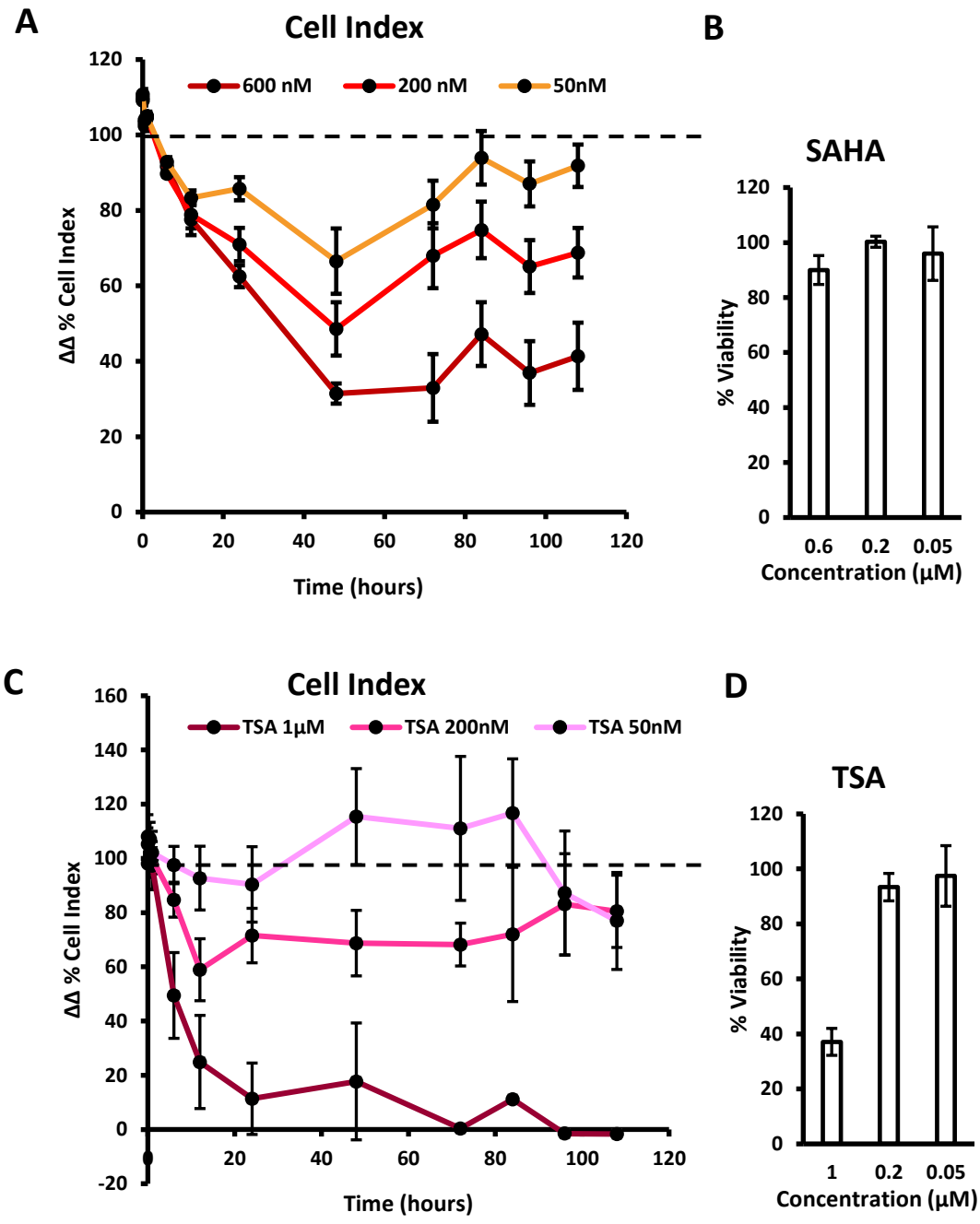

Figure 4.27 Pan-HDACIs induce dose and time-dependent permanent changes in cell index and viability at clinical and subclinical concentrations in HL-1 cells. HL-1 cells were exposed to SAHA and TSA at a range of concentrations for 120 h. **A.** SAHA induced a significant decrease in CI at all tested concentrations starting 12 h post compound addition. **B.** MTT assays did not evidence any reduction in cell viability following SAHA addition. **C.** TSA induced a significant decrease in CI starting 12 h post compound addition. **D.** MTT assays did not evidence any reduction in cell viability at 200 nM and 50nM TSA concentrations. Data are the average ±SD of at least 3 separate determinations. Tested by ANOVA and Bonferroni post hoc modifications.

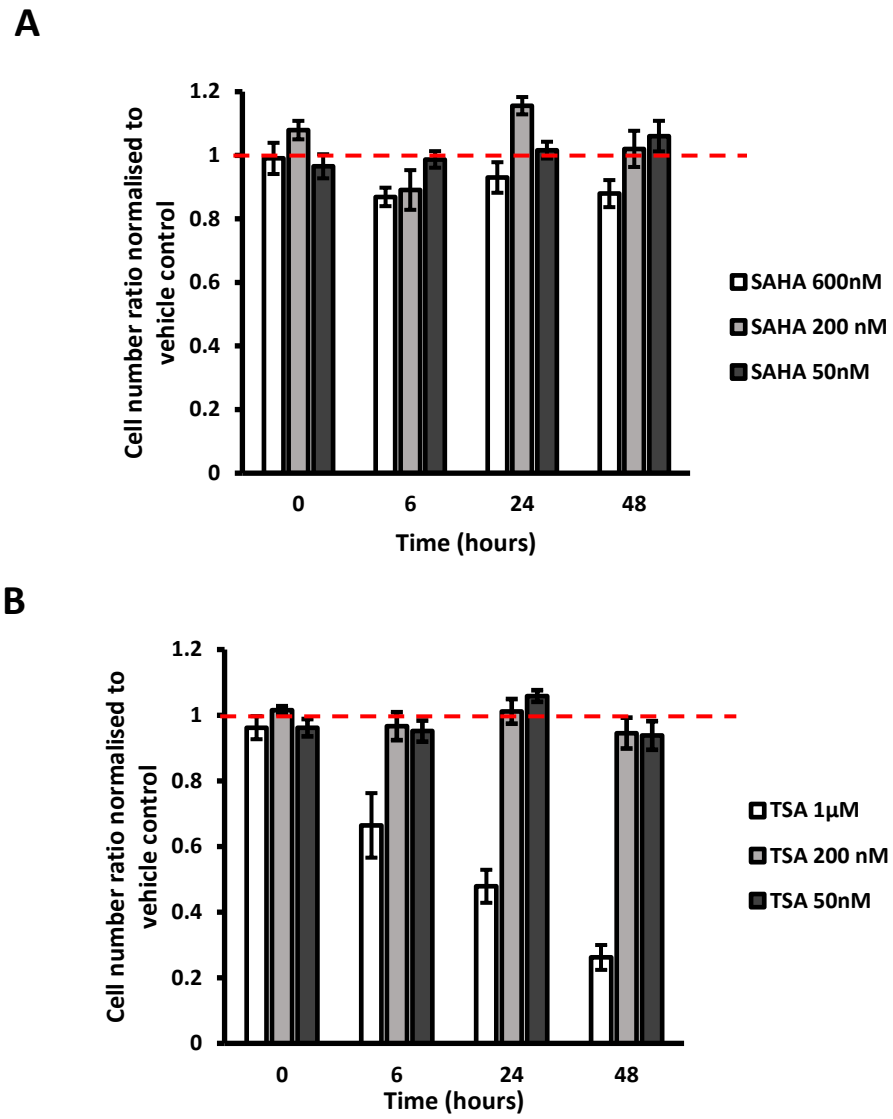

Figure 4.28 Pan-HDACIs at sub-cytotoxic concentrations do not affect cell viability. Functional HL-1 cells were exposed to SAHA and TSA at a range of concentrations and counted using a haemocytometer after 6, 24 and 48 h compound exposure. **A.** sub-clinical concentrations of SAHA did not affect average cell numbers. **B.** TSA at sub-cytotoxic concentrations did not affect average cell numbers. Data are normalised to time-matched vehicle control and are the average ±SE of at least 3 different experiments. Tested by ANOVA with Bonferroni post-hoc modifications.

4.9 Determination of pan-HDACI pharmacological targets in HL-1 cells

Following the confirmation that pan-HDACI compounds induce functional and structural alterations in HL-1 cells at sub-clinical and non-cytotoxic concentrations, a study was designed to ascertain whether these drugs induced their reported pharmacological activity in these cells at these concentrations. Specifically, the protein acetylation of two main pan-HDACI molecular targets was assessed (methodology detailed in section 2.8). Acetylation of histone H4, as a primary HDACI pharmacological target was assessed in HL-1 cells. Additionally, the HDACI-mediated inhibition of HDAC6 α-tubulin deacetylation was assessed. Given that α-tubulin is a protein found in the cytoskeleton, where it has fundamental roles in maintaining cellular structural features, an investigation into the HDACI-induced effects upon α-tubulin acetylation were hypothesised to define potential mechanisms of HDACI-induced structural cardiotoxicity.

Treatment of HL-1 cells with 1 μM TSA, shown to be cytotoxic, caused an increase in both α-tubulin and histone H4 acetylation levels in a time-dependent manner. Conversely, no change in acetylation patterns was observed with the non-cytotoxic 200 nM concentration of TSA, suggesting that TSA concentrations ≤ 200 nM are not-pharmacologically active in this cell type (Figure 4.29B). As SAHA is an analogue of TSA, with lower pharmacological activity, it is assumed this is also the case for this drug. Overall, these findings implicate that any functional or structural effects upon HL-1 cells evidenced with sub-cytotoxic pan-HDACi concentrations are unlikely to be a result of the reported pharmacological mechanism of action. It is therefore likely that the effects of sub-pharmacologically active pan-HDACI concentrations could be attributed to additional secondary pharmacology effects.

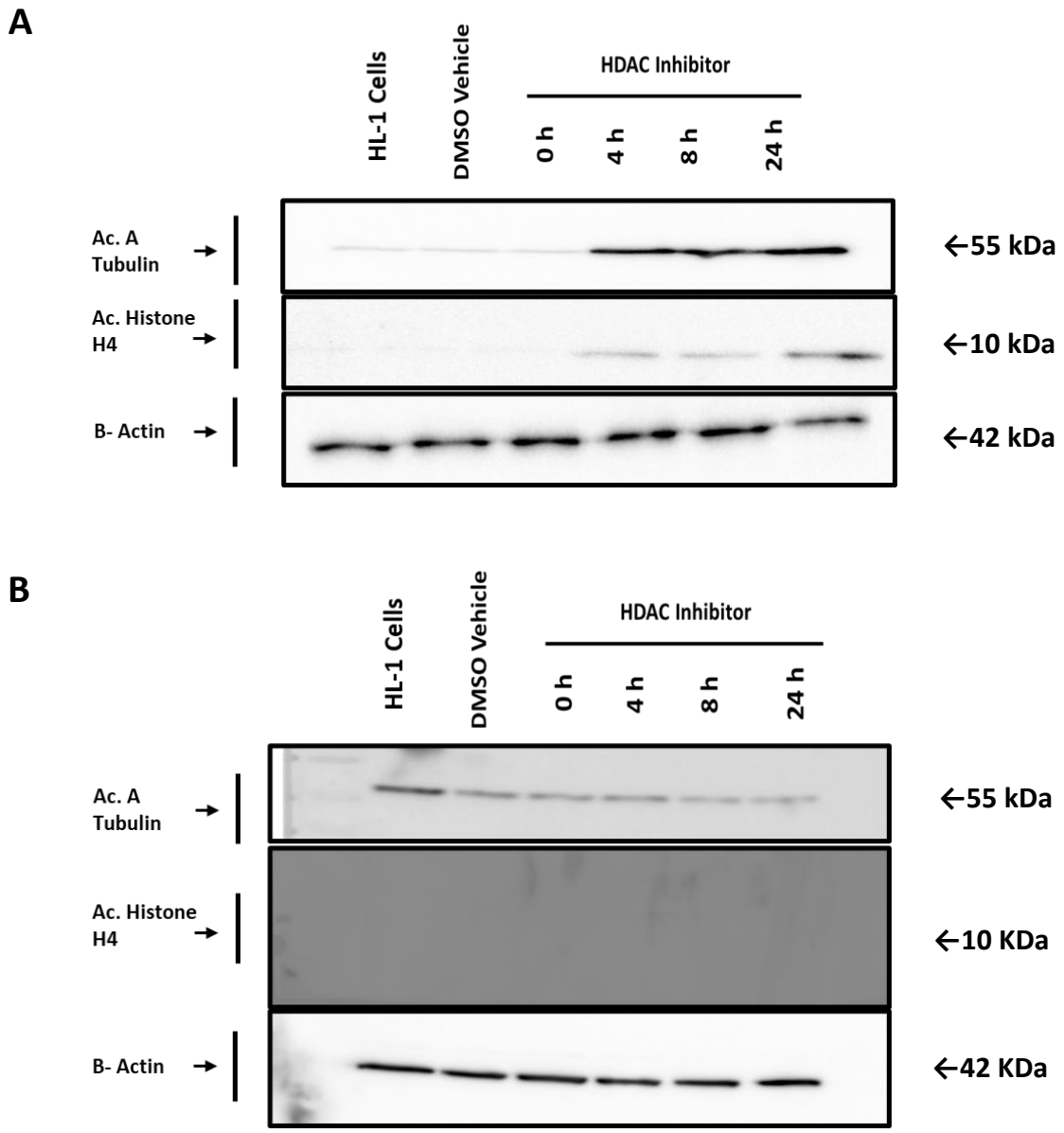

Figure 4.29 Determination of pan-HDACi pharmacological targets in HL-1 cells. Western Blot analysis of HL-1 whole protein extracts assessing levels of acetylated α tubulin (55 kDa) and acetylated histone H4 (10 kDa) following treatment with **A.** 1μM and **B.** 200 nM concentrations of Pan-HDACi TSA. Each lane contained 20μg protein/lane. Results are representative of one typical experiment of at least 3 separate experiments.

4.10 Pan-HDAC inhibition increases mitochondrial spare respiratory capacity in HL-1 cells

In order to elucidate potential additional mechanisms underpinning HDACI-induced cardiotoxicity, the effects of the pan-HDACI TSA on HL-1 metabolic respiration were assessed using Seahorse XF technology (methods detailed in section 2.6). The mitochondrial stress test results reported in figure 4.30A indicate that treatment with 1 µM TSA induced a significant ($p<0.05$) acute increase in HL-1 spare respiratory capacity, observable upon oligomycin and subsequent FCCP exposure, compared to vehicle treated cells. Remarkably, TSA treated cells displayed a 200% increased spare respiratory capacity under stressed conditions, leading to an overall 400 pmol/min increase (from 200 to 600 pmol/min) in OCR compared to endogenous OCR values.

Overall, these results suggest that HDACi-mediated bioenergetic changes could alter cardiomyocyte functionality thus leading to functional and structural cardiotoxicities.

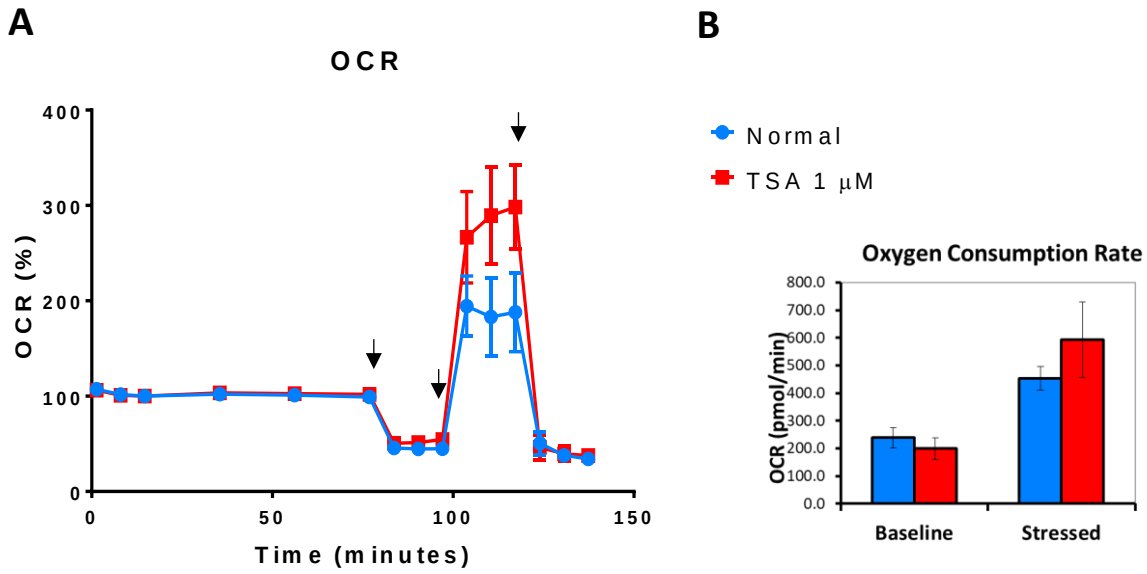

Figure 4.30 Treatment with pan-HDACi increases spare respiratory capacity in HL-1 cells. HL-1 cells were grown to functional confluency before being exposed to 1µM TSA. Data shows **A.** Oxygen consumption rate (OCR) measurements over time in response to electron transport chain modulators. Arrows indicate injection of electron transport chain complex modulators, oligomycin, FCCP, rotenone/antimycin A in order of injection. And **B.** pmol/min changes in OCR at baseline and stressed conditions in treated cells. Data are mean ±SD of at least 10 separate determinations from the same experiment, typical of 3 separate experiments.

4.11 Selective HDAC inhibition elicits functional and structural cardiotoxicity in HL-1 cells

To define whether HDACi-induced cardiotoxicity could be attributed to the inhibition of a specific sub-class of HDACs, thus confirming the findings observed in the hiPSC-CM model (chapter 3.4), an analogous investigation into the effects of selective HDACi in HL-1 cells was carried out using the xCELLigence Cardio system. Measured parameters included beat rate, beat amplitude and cell index.

4.11.1 Class I selective HDACi induces changes in HL-1 cardiomyocyte functionality

The class I selective HDACI MS-275 (Entinostat) induced permanent contractility changes in HL-1 cells. At clinically relevant concentrations (1.2µM and 0.5 µM) complete loss of contractility within 48 hours post compound addition was observed (Figure 4.31). Similarly to the effect induced by pan-HDACIs, MS-275 induced a significant ($p < 0.001$) increase in beat rate prior to contractility arrest. Upon compound washout, contractility did not resume. Beat amplitude was not affected until 12 hours post compound addition, where a constant decline in the parameter was initiated, decreasing by 63% and 56 % after exposure to 1.2µM and 0.5 µM, respectively. MS-275 therefore induced acute functional cardiotoxicity in HL-1 cells.

A significant ($p<0.001$) change in CI was observed starting 24 hours post MS-275 addition, at both tested concentrations of 1.2µM and 0.5 µM, resulting in a total 44% and 36% CI decrease, respectively (Figure 4.32). Upon compound removal, CI values were not restored to baseline values. Assessment of cellular viability by the MTT assay however showed no significant cytotoxicity, thus supporting the conclusion that class I HDAC selective inhibition could mediate morphological changes in HL-1 cardiomyocytes.

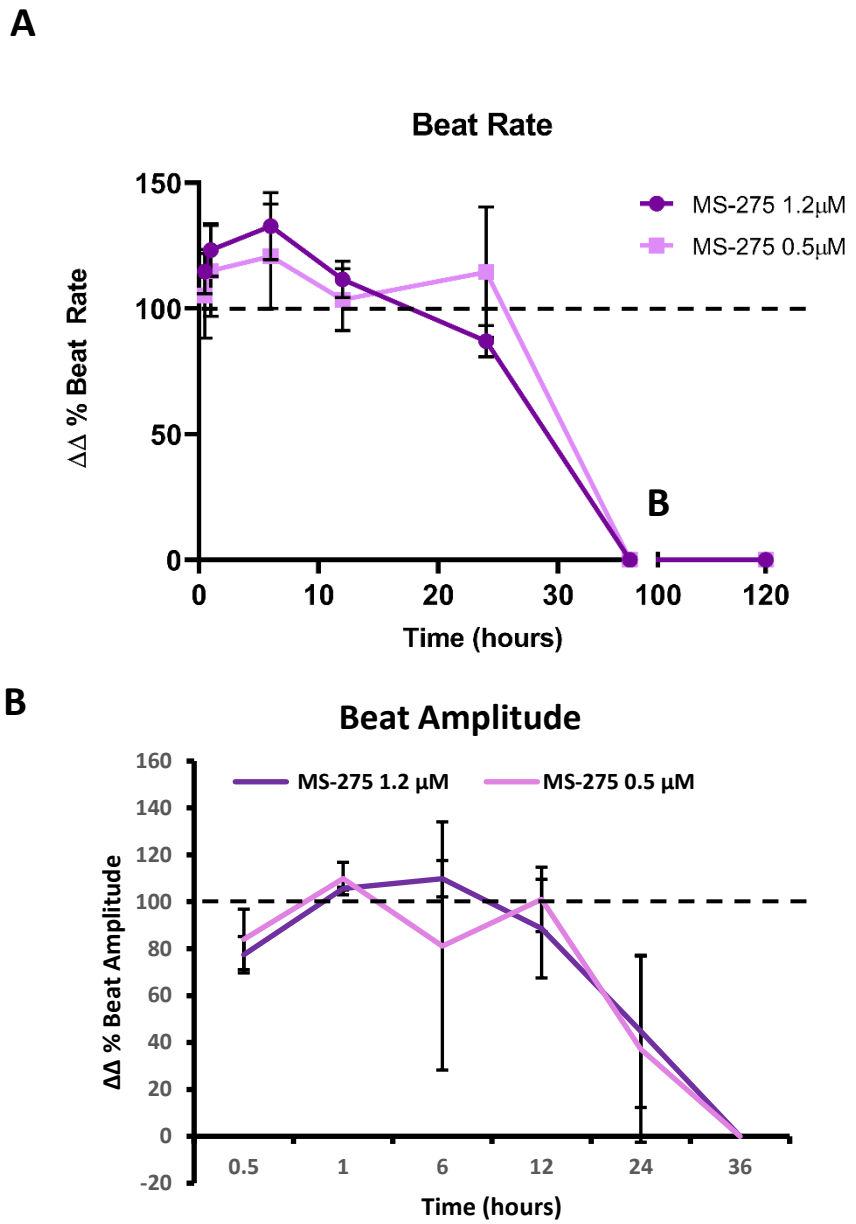

Figure 4.31 MS-275 class I inhibitor induces changes in contractility parameters at clinically-relevant concentrations in HL-1 cells. HL-1 cells were exposed to MS-275 at different concentrations for 120 h. **A.** MS-275 induced a significant decrease in beat rate and **B**. Beat amplitude Data are normalised to baseline and vehicle control (ΔΔ), and are the average ±SD of at least 3 separate determinations. Tested by ANOVA and Bonferroni post-hoc modifications.

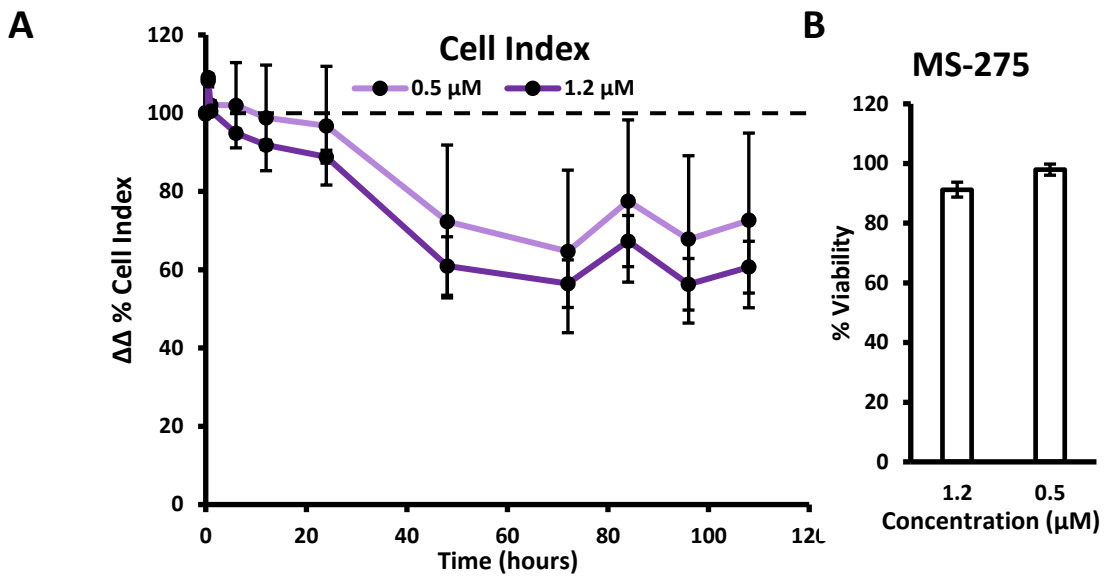

Figure 4.32 MS-275 class I inhibitor induces permanent changes in cell index at clinically-relevant concentrations in HL-1 cells. HL-1 cells were exposed to MS-275 at different concentrations for 120 h. **A.** MS-275 induced a significant decrease in CI starting 24 post compound addition. Data are normalised to baseline and vehicle control (ΔΔ) **B**. MTT assays did not evidence a significant decrease in cell viability. Data are normalised to control and are the average ±SD of at least 3 separate determinations. Tested by ANOVA and Bonferroni post-hoc modifications.

4.11.2 Class IIb selective HDACi induces temporary changes in HL-1 cardiomyocyte functionality

The class IIb selective HDACi tubacin induced transient contractility changes in HL-1 cells. Both tested concentrations of 5 µM and 1 µM resulted in a temporary acute increase in beat rate within 6 hours post compound addition, before returning to baseline levels within 12 hours.

Changes in impedance beat amplitude were only recorded with the use of 5 µM tubacin, where an increase of the parameter was observed between 1 and 12 hours post compound addition. No significant changes of the parameter were recorded following treatment with 1 µM tubacin.

A non-significant decrease in CI was observed with both tested concentrations, resulting in a total 19 % decrease of the parameter 72 hours post compound addition.

Overall, these results suggests that class IIb-selective HDAC inhibition are not associated with functional or structural perturbations in HL-1 cells at these tested concentrations.

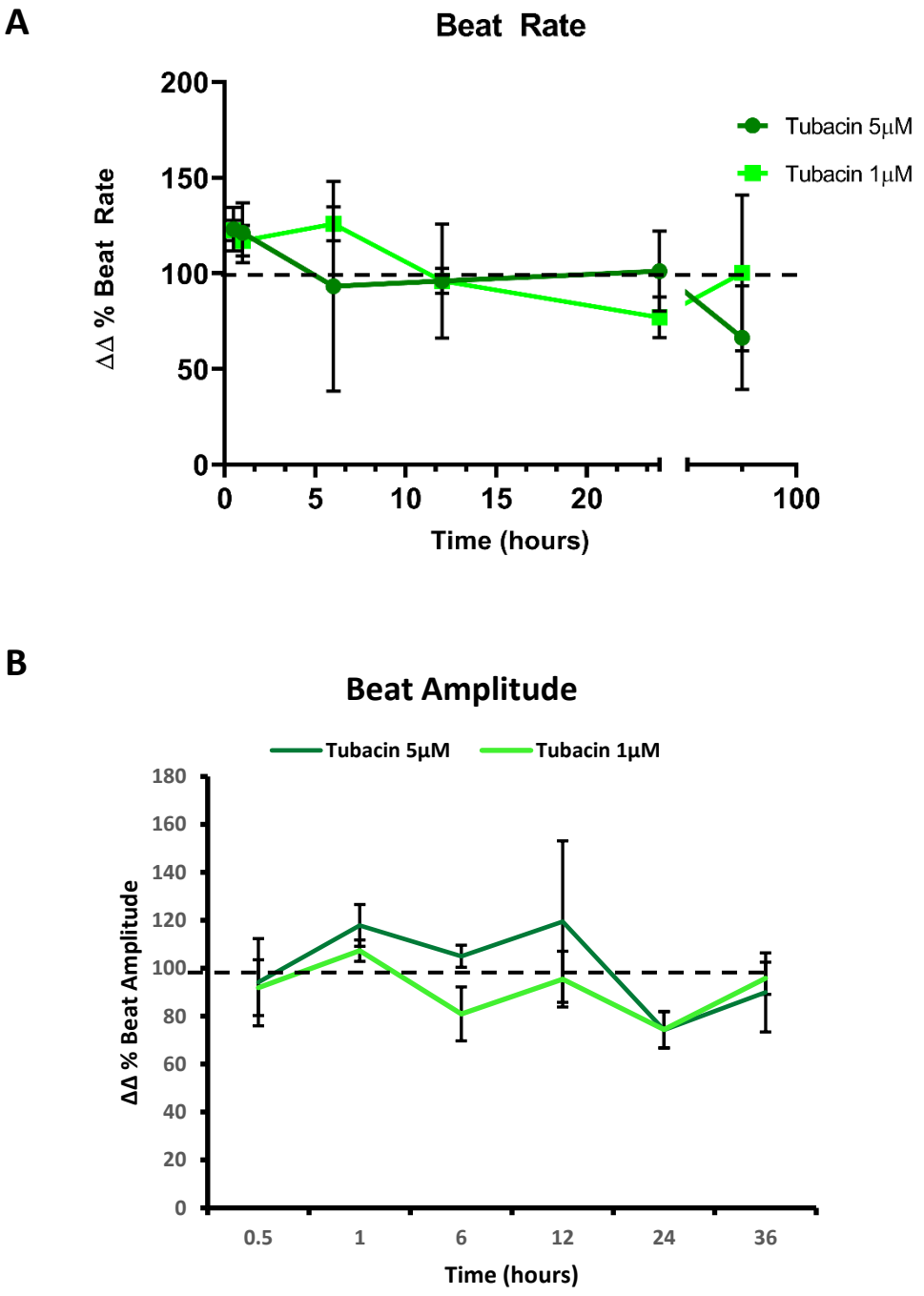

Figure 4.33 Tubacin class IIb inhibitor does not induce major changes in contractility parameters in HL-1 cells. HL-1 cells were exposed to tubacin at different concentrations for 120 h. **A.** Tubacin induce a transient beat rate changes in HL1 cells by 20% 6 h post compound addition. **B.** Tubacin did not induce significant beat amplitude changes in HL-1 cells. Data are normalised to baseline and vehicle control (ΔΔ) and are the average ±SD of at least 3 separate determinations typical of 3 different experiments. Tested by ANOVA and Bonferroni post-hoc modifications.

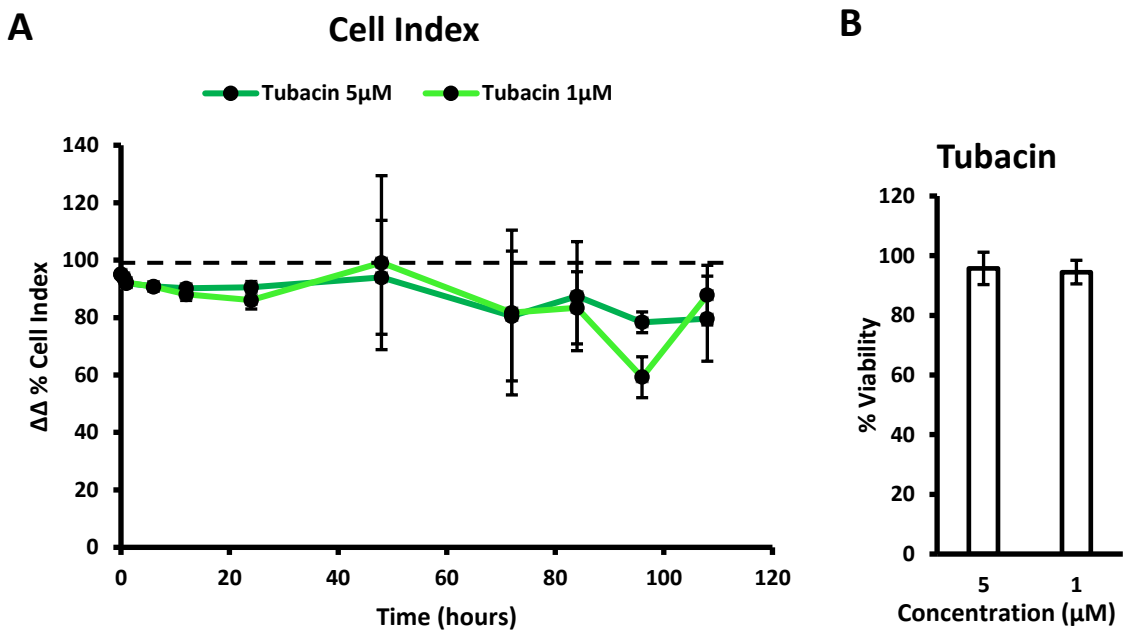

Figure 4.34 Tubacin class IIb inhibitor does not induce significant changes in viability parameters in HL-1 cells. HL-1 cells were exposed to tubacin at different concentrations for 120 h. **A.** Tubacin did not induce significant variations in CI. Data are normalised to baseline and vehicle control (ΔΔ) and are the average ±SD of at least 3 separate experiments **B.** MTT assays did not evidence a significant reduction in cell viability. Data are normalised to control and are the average ±SD of at least 3 separate determinations. Tested by ANOVA and Bonferroni post-hoc modifications**.**

4.12 Discussion

Current methods used in preclinical cardiotoxicity screening involve *in vivo* models complemented by *in-vitro* cell models. Current cell models are limited by a lack of capacity for expansion and finite lifespan in culture, high cost and requirements for complex culture conditions, poor representation of the cardiac phenotype, or focus on specific cardiac ion channels or molecular pathways. As such these current models generally provide limited insights into toxicological investigations (Ando et al. 2017; Obergrussberger et al. 2016). The availability of an expandable and reproducible source of cardiomyocytes with applicability for screening of compounds for cardiotoxicity potential would undoubtedly improve this area. However, attempts to create fully functional cardiac immortalised cell lines with applicability (and compatibility) for evaluation of mechanistic cardiotoxicity have not been successful to date. The HL-1 atrial murine-derived cell line is unique in that it remains the only expandable *in-vitro* model that is cardiac in origin, retains a cardiac phenotype, and an ability for functional contractility in culture (Claycomb et al. 1998). The aim of this chapter was to assess and characterise the HL-1 cell line in terms of its utility as a model for evaluation of drug-induced cardiotoxicity and its potential for inclusion in non-clinical studies for assessment of cardiac liabilities.

The initial stage of this study focused on defining the intrinsic growth properties and native contractility characteristics of the HL-1 cell line. In addition to elucidating culture and growth parameters, this study also uniquely utilised impedance-based technologies, specifically the xCELLigence Cardio real-time cell analysis (RTCA) system, to non-invasively and continuously evaluate growth kinetics and *in-vitro* contractility parameters of the Hl-1 cell line. Previous studies had reported the HL-1 model to be heterogeneous in terms of its contractile phenotype, particularly a lack or presence of contractility in sub-clones of the HL-1 cell line despite expression of specific ion channel and cardiac markers (Dias et al. 2014). In this study, HL-1 cells were shown to consistently retain the ability for contractility, albeit asynchronously and differentially across the culture vessel, suggesting that previous studies involving selective cloning of contractile sub-populations may be somewhat ambiguous and misleading in this regard and assumptive of uniform clonal contractility. Nonetheless, as demonstrated in this study, intrinsic HL-1 contractility is

time-limited and strictly dependent on regular media supplementation, only displaying consistent rhythmicity for up to 4 hours after each media change. This factor of HL-1 cell contractility had not been incorporated into earlier reported studies of this cell line (Eimre et al. 2008; Dias et al. 2014). Furthermore, an additional hindrance to HL-1 contractility is the persistent proliferative nature of this immortalised cell line (section 4.2). Based on these findings, it is perhaps not surprising in hindsight that most previously reported HL-1 based studies addressing contractile effects were restricted to either single endpoint assays or assessment of short-term acute electrophysiological effects, a consequence of a lack of longevity or appreciation of contractility *in-vitro* (Wiersma et al. 2019; Z. Dong et al. 2017; Darpo et al. 2014; White, Constantin, and Claycomb 2004). Consequently, the next aim of this phase of the study was focused toward utilisation for this cell line for acute and long-term cardiotoxicity evaluations. The objective being to develop a novel methodology to improve the HL-1 contractility timespan, and to optimise the use of this model on the xCELLigence system. Several studies focused on culture of cardiomyocytes and their maintenance *in-vitro* have demonstrated the requirement of specific media supplements for maintenance of a cardiac phenotype, albeit these primary cell models are limited by their post-mitotic non-proliferative nature for longer-term evaluations (Callaghan et al. 2020; Fiegle, Volk, and Seidel 2020; Tomsits et al. 2020). Similarly, media for maintenance of stem-cell derived cardiomyocytes is also highly dependent on a panel of supplements and other biological factors (Correia et al. 2017). With respect to HL-1 cells, their *in vitro* culture was established through the development of a specialised media termed 'Claycomb media' supplemented with a series of growth factors and supplements (Claycomb et al. 1998). However, the derivation of this media was focused on growth and survival of this immortalised cell line, alongside maintenance of a defined set of cardiac-specific phenotypic parameters, rather than establishment of consistent contractility and longer-term studies cardiac-selective effects (Claycomb et al. 1998). An important approach was thus to deconstruct the Claycomb media to gain an insight into the role and importance of media components towards growth, maintenance and contractility of the HL-1 cell line. The outcome of this investigation demonstrates that although most included factors are required for growth and maintenance of this cell line, inclusion of specific factors are crucial to establishment and continuation of contractility, particularly norepinephrine and retinoic acid. Supplementation with norepinephrine was previously

shown to be essential for the expression of Cav1.2 and CACNA1C genes during cardiomyogenesis, thus regulating the presence of L-type voltage-dependent calcium channels (Lehmann et al. 2013). Physiologically norepinephrine is released by sympathetic neurons wherein it activates beta-1 adrenoceptors on cardiac myocytes to facilitate chronotropic, inotropic and lusitropic effects upon the heart. This is counterbalanced by the greater parasympathetic effects mediated at the sinoatrial and atrioventricular node by acetylcholine to cause negative chronotropy and regulate cardiac contraction (Gordan, Gwathmey, and Xie 2015). However, cardiac cells cultured *in-vitro* lack innervation and the majority do not exhibit autonomous pacemaker capability, therefore relying on norepinephrine supplementation to promote contractility. The observations in this study thereby not only corroborate a requirement of norepinephrine for the correct formation of HL-1 syncytial structures, but evidence that continuous supplementation with norepinephrine is decisive in the stabilisation of HL-1 contractility, without impacting cell viability and bioenergetics. Retinoic acid plays multiple roles during heart development and is an important factor in subtype differentiation of cardiomyocytes, particularly promotion of atrial-like or sinoatrial-like differentiation (Stefanovic and Zaffran 2017; Protze et al. 2017). Furthermore, exposure of stem-cell derived cardiomyocytes to retinoic acid promotes their electrophysiological maturation and calcium handling (Gassanov et al. 2008). It is not unconceivable to expect a similar effect occurs with the HL-1 cell model. Consequently, both norepinephrine and retinoic acid were therefore identified as essential components for the long-term maintenance of HL-1 functionality.

One of the aforementioned issues that impact the timespan of HL-1 contractility was attributed to the immortalised nature of these cells, as observed in the xCELLigence studies, with cellular proliferation progressing in spite of the formation of functional syncytial structures in HL-1 cells. In this regard, effort was focused on identification of a media formulation unsupportive of cellular proliferation once cellular confluency was obtained, whilst simultaneously preserving syncytial integrity. Unsurprisingly, HL-1 cells do not achieve successful proliferation when seeded in growth factor-depleted media formulations. Nevertheless, HL-1 cells that are initially grown in fully supplemented Claycomb formulations until syncytial formation, and only thereafter depleted of growth factor and other supplemental agents, retained a stable contractile phenotype whilst

lacking support factors for proliferative growth. Several supplements found in Claycomb media formulations, including cholesterol, oleic and linoleic acids, were reported to play a critical role in the formation of cardiomyocyte cellular membranes, cell-cell interaction and assembly of mitochondrial complex subunits (Maekawa et al. 2019; Haque et al. 2016). Therefore, after ensuring the successful formation of HL-1 syncytial structures using complete Claycomb media formulations, depletion of selected supplements including growth factors, cholesterol, oleic and linoleic acids allowed cessation of further cellular proliferation, and led to a functional improvement of the existing HL-1 monolayers without hampering viability and metabolic functionality (sections 4.3 and 4.4). Consequently, these studies allowed to design a novel optimised protocol for long-term HL-1 studies, whereby cells are initially plated and grown to functionality, and thereupon maintained in growth-factor depleted medium, with the addition of norepinephrine and retinoic acid, with twelve-hourly media changes for up to 120 hours.

After the establishment of a novel effective protocol for the use of HL-1 cells on the xCELLigence RTCA systems, the second phase of the study was dedicated to the validation of the HL-1 model for its use in nonclinical cardiotoxicity studies. Initially this involved evaluation of the effects of a panel of known cardioactive agents upon HL-1 cells using the xCELLigence Cardio RTCA system. The HL-1 model consistently and reproducibly responded to the majority of tested cardioactive agents, demonstrating for the first time that the analysis of impedance functional parameters can successfully detect arrhythmic and proarrhythmic effects in this model. Early investigations reported by Claycomb et al indicated the presence of functional ion channels in HL-1 cells, describing the expression of fully functional I_{Kr} currents, I_{Na} and L-type calcium currents (Claycomb et al. 1998; White, Constantin, and Claycomb 2004). Further studies supported this through the ability of HL-1 cells to respond to specific ion channel interactive agents using various electrophysiological techniques, including manual and automated patch clamping (White, Constantin, and Claycomb 2004; Toyoda et al. 2010; Kammonen et al. 2017). In particular, potassium channel blocker compounds E-4031 and dofetilide were reported to elicit strong responses by successful blockade of HL-1 endogenous I_{kr} currents (Toyoda et al. 2010). Conversely, the sodium channel blocker lidocaine and the β-adrenergic agonist isoproterenol were not reported to elicit detectable effects in patch clamping studies

(Kammonen et al. 2017). In the study presented herein, I_{kr} blockade with E-4031 resulted in a marked effect on beat rate and beat amplitude impedance parameters, agreeing with the previously reported electrophysiological endpoint studies. On the contrary, the non-selective potassium channel blocker amiodarone did not elicit detectable effects on impedance parameters; recent studies on beat rate variability in a murine embryonic stem cell-derived cardiomyocyte model have documented a similar response to amiodarone, whereby no detectable variations in beat parameters were recorded (Niehoff et al. 2016). Even though amiodarone is classified as a class III antiarrhythmic compound, its effects are notoriously complex and can affect a wide array of mechanisms: amiodarone was in fact shown to elicit structural effects, as well as sodium and calcium current blockade in a rate-dependent manner (Riedel et al. 2014). The resulting competing effects could therefore underpin the undetected response to this compound in HL-1 cells. Relevant cardioactive effects via voltage-gated sodium channel blockade were consistently achieved, with significant effects on beat rate and beat amplitude impedance readings (figures 4.15, 4.16 and 4.17). Exposure of the HL-1 cells to the calcium channel blocker verapamil also induced a significant response, which rather than the expected bradycardic response observed *in vivo* was the converse, and resulted in an increase in beat rate. This effect is not exclusive to this model but is also observed in hiPSC-CM models (Zeng et al. 2019). This paradoxical response of hiPSC-CMs to verapamil and other calcium channel blockers was confirmed as being the net effects of other cardiac ion currents, with action potentials of hiPSC-CMs shown to be sodium channel driven (Zeng et al. 2019). By reducing sodium channel availability in hiPSC-CMs, such as via modulation of potassium ion levels in growth media, the response to calcium channel blockers was reversed, reflecting the bradycardic effect observed *in vivo* and clinically (Zeng et al. 2019). This has implications for safety assessment of drug candidates with multiple effects, including calcium channel inhibition, wherein results *in vitro* may contrast the actual *in vivo* response and thus a misleading result. Therefore, adaption of the monovalent concentrations of growth media may be required to address this issue. It remains to be determined whether further configuration of Claycomb media would also circumvent this issue in HL-1 cells.

Overall, the detection of functional effects through the use of impedance-based systems was in line with the findings obtained with the considerably more costly hiPSC-CM model.

While HL-1 cells retain atrial characteristics, they have the advantage of expressing native forms of various ionic currents (Claycomb et al. 1998); this study proves that HL-1 monolayers can therefore be useful not only for the investigation of atrial-linked dysfunctions, such as atrial fibrillation, but also for the detection of more general aspects of functional early cardiotoxicity studies.

Following the successful validation of the HL-1 model for use in cardiotoxicity studies, this model was applied to the evaluation of cardiotoxic potential of the epigenetic modulating histone deacetylase (HDAC) inhibitor class of drug, implicated as a therapeutic approach for a range of conditions (Gryder, Sodji, and Oyelere 2012b; Lopez et al. 2016). Exposure of HL-1 cells to clinically relevant concentrations the pan HDAC inhibitors, SAHA and TSA, caused consistent functional changes. Marked increases in beat rate and beat amplitude parameters were elicited with both compounds, followed by a complete cessation of contractility by 100 hours after drug addition. These findings are in agreement with those obtained with hiPSC-CMs (Chapter 3), where a marked decrease in contractility was observed by approximately 48 hours post compound addition. These effects mirror the detection of delayed cardiac dysrhythmias, including atrial fibrillation, in clinical studies (Kopljar et al. 2016; Subramanian et al. 2010). Importantly, detection of these functional abnormalities several hours after drug exposure in the HL-1 model offers a distinct advantage over the majority of current preclinical cardiac screening methodologies which often focus on acute (≤ 1 hour) effects. These observations thereby support the utility of the HL-1 model as a screening tool for drug-induced functional cardiac disturbances.

Alongside identification of effects upon cardiomyocyte contractility, these studies also indicated effects upon cardiomyocyte structure or morphology following exposure to the pan-HDACi SAHA. Of note is the fact that decreases in cell index were recorded even at drug concentrations below those that induced cytotoxicity. A lack of loss of cellular viability coupled to maintenance of cell number, alongside these declines in cell index, strongly implicated these changes were imputable to structural cardiomyocyte changes. This effect of pan-HDACi upon cardiac cells is supported by a recent study using hipSC-CMs *in-vitro* which showed transcriptional changes induced by these compounds were associated with structural cardiac changes (Kopljar et al. 2016). Moreover, several recent studies have investigated the role of HDACi as possible treatments for various forms of

heart failure, primarily involving the reversal of cardiac hypertrophy (McKinsey 2012; Wallner et al. 2020). This implicates that HDACi additionally cause structural changes in cardiomyocytes, involving cellular hypotrophy or atrophy, although it remains to be determined whether these effects are mirrored in toxicity of these drugs in the clinic.

The investigation into pan-HDACi pharmacological activity in HL-1 cells revealed that both functional changes in contractility, as well as structural/morphological changes reflected in CI changes, were elicited at HDACi concentrations that did not initiate histone acetylation. This finding implicates that HDACi-mediated cardiotoxicity could depend on additional secondary pharmacology effects. Several studies have linked the involvement of class I HDACs with mitochondrial alteration in cardiomyocytes (Herr et al. 2018; Lkhagva et al. 2018). Additionally, recent studies have observed that treatment with pan-HDACis is correlated with an improvement of mitochondrial bioenergetics, particularly when investigated in relation to cardiac oxidative stress dysfunctions as well as ischemia-reperfusion myocardial injuries (Lkhagva et al. 2018; Wallner et al. 2020). In this study, pan-HDAC inhibition resulted in significant changes in mitochondrial respiration, with a marked augmentation of spare respiratory capacity levels of HL-1 cells, therefore confirming the contribution of HDACi activity to mitochondrial impairment. While the improvement of mitochondrial oxygen consumption rate (with the subsequent increase in respiratory capacity levels) can be considered as a potentially cardioprotective effect in a pathological context, this study suggests that further elucidation of the interplay between HDACi and cardiac mitochondria is needed to determine possible cardiotoxic consequences associated with the use of this class of compounds.

The selective inhibition of HDAC sub-classes provided an additional insight into the mechanisms of HDACi-mediated effects on cardiomyocytes. Similar to the effects observed with the use of pan-HDACis SAHA and TSA, the class I selective inhibitor MS-275 resulted in delayed functional and structural alterations in HL-1 cells. Remarkably, the delayed onset of functional perturbations was concomitant with perturbations in CI that were not associated with decreased cellular viability, and thus indicative of morphological changes even at sub-clinical concentrations. Conversely, the class IIb inhibitor tubacin did not induce major detectable changes in either functional or structural parameters. These findings therefore indicate that HDACi-associated cardiotoxicity might be partly mediated

by class I HDAC selective inhibition, but not class IIb. There may be an involvement for class IIa in these effects, but based on the fact they show little HDAC enzymatic activity and inhibitory response to SAHA or TSA, this is unlikely (Bü et al. 2013). The involvement of class I HDAC inhibition with structural cardiac alterations has been well documented in literature: class I HDAC inhibition has in fact been shown to blunt cardiac pathological hypertrophy by epigenetic modifications that suppress a cell growth-associated gene through the mTOR pathway (Morales et al. 2016). However, further investigations are needed to understand whether class I HDACi induces cardiomyocyte perturbations at sub-pharmacologically active levels, or whether HDACi-mediated cardiotoxicity is due to an integrative combination of epigenetic and off-target effects.

5 Characterisation of the AC10 human ventricular cell line for use in preclinical structural cardiotoxicity studies

5.1 Introduction

At present, effective approaches for *in-vitro* preclinical detection of structural cardiac liabilities are lagging, leading to most drug-induced structural perturbations either being detected at late-stage project phases during final trials, or post-marketing, usually manifesting in the clinic as a result of latent late-onset effects (Schwach, Slaats, and Passier 2020; J. Dong and Chen 2018). Currently, hiPSC-CMs are considered the most relevant *in-vitro* model used for preclinical cardiotoxicity screening applications. However, several limitations still remain unresolved with this model, as detailed in chapter 3. Two major limitations include I) the reliability for detection of structural liabilities, and II) high maintenance and experimental cost. The availability of cost-effective and representative models that could aid in the detection of structural cardiotoxicity at the early stages of drug development, would therefore offer important improvements in this area. Due to their simplicity and ease of use, the AC10 and AC16 human-derived ventricular cardiomyocyte cell lines could represent an accessible and pragmatic candidate model for this purpose.

The AC cell lines are derived from the fusion of SV40 transformed immortalised human fibroblasts with primary human cardiomyocytes (Davidson et al. 2005). The resulting immortalised AC cell lines (AC1, AC10, AC12 and AC16) retain a cardiac phenotype, albeit remaining in a pre-contractile state (Davidson et al. 2005). AC cell lines express relevant cardiac features, displaying tropomyosin protein structures, as well as expressing cardiac troponin I and troponin C (Figure 5.1, Rockley 2018). Additionally, AC10 cells exhibit expression of the cardiac transcription factor NKX2.5, as well as the presence of alpha-actinin in a non-striated fashion, confirming the unique pre-contractile phenotype of these cells (Figure 5.1). Since their development, the AC16 and AC10 cell lines have been used for developmental studies of the human heart, evaluation of myocardial cell injury, post-ischaemia cardiac remodelling, and molecular studies of myocardial inflammatory responses, fibrosis and cardiomyopathies (Ontoria-Oviedo et al. 2018; Hirai et al. 2020; Wen et al. 2020; Yuan et al. 2016). Therefore, despite their inability to form functional syncytia, they could provide a simple and cost-effective model for the mechanistic early detection of structural drug-induced perturbations of cardiac cells.

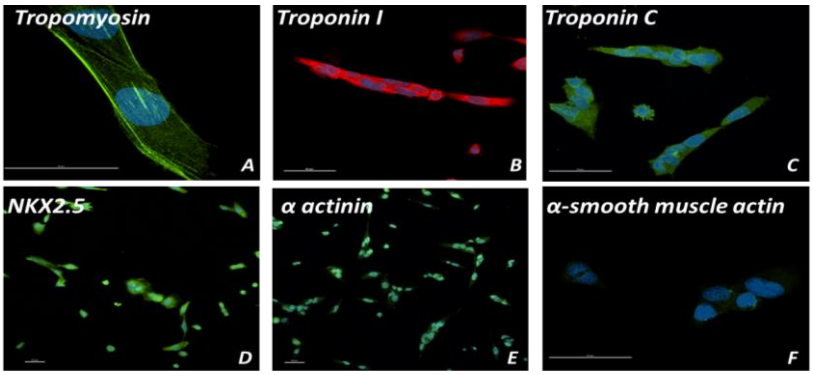

Figure 5.1 AC10 cells retain cardiac phenotype features. AC10 are a human ventricular-derived cell line that shows different levels of expression of cardiac markers: tropomyosin, cardiac troponin I, cardiac troponin C, cardiac transcription factor NKX2.5, alpha actinin. (Image courtesy of Dr Richardson and Dr Rockley)

5.1.1 Use and relevance of three-dimensional modelling in preclinical cardiotoxicity

The optimisation and use of three-dimensional *in-vitro* culture techniques has gained increasing momentum in recent years. The use of spheroids and organoids is particularly appealing for use in *in-vitro* drug safety screening, as three-dimensional models have the potential of providing better in-vivo-like and physiologically relevant tissues, thus providing enhanced predictivity profiles compared to two-dimensional platforms (Wrzesinski et al. 2014). Such is the case of various hepatic 3D models derived from hepatocyte cell lines, which have been successfully established and implemented for drug safety and toxicology applications (Gaskell et al. 2016; Kyffin et al. 2019).

Cardiac spheroids have recently been established, utilising hiPSC-CMs in co-culture with primary cardiac fibroblasts and cardiac endothelial cells (Ravenscroft et al. 2016). This particular triculture combination of cell lineages, representative of the adult human cardiac composition, has enabled the generation of reproducible and contractile cardiac 3D models which demonstrated good predictivity against acute functional cardiotoxicants (Tomlinson et al. 2019; Ravenscroft et al. 2016). Furthermore, 3D cultured hiPSC-CMs have been shown to enhance non-myocyte cell functionality, as well as enhance overall microtissue maturity (Ravenscroft et al. 2016).

The utility of cardiomyocyte cell lines, including the AC10 cell line, has not been assessed for use in 3D scaffold free microtissue applications. Given the remarkable advantages of 3D microtissues in terms of improvement of CM functionality, phenotype maturation and prolonged culturing lifespan, the AC10 cardiomyocyte cell line could provide a more accessible, scalable and cost-effective model for acute and sub-acute structural cardiotoxicity screening, with possible advantages over hiPSC-CM-based models.

5.1.2 Aims and Objectives

The AC10 cardiomyocyte cell line provides a readily expandable source of cells that retain several relevant cardiac markers. The use of this cell line paired with high-throughput and advanced culture technologies for early preclinical cardiotoxicity screening has not been fully explored to date. For this reason, a set of studies is hereby described with the aim to characterise the AC10 cell line for use in structural toxicology applications through the following objectives.

1) Assess the suitability of the AC10 human ventricular cell line for preclinical cardiotoxicity studies in two-dimensional monolayers
    (a) Assess the utility of the AC10 cell line in combination with xCELLigence RTCA impedance systems
2) Evaluate and characterise the suitability of AC10 cells for preclinical cardiotoxicity studies in three-dimensional spheroid cultures
3) Evaluate the utility of the AC10 model in the detection of structural cardiotoxicity induced by the HDACi class of drugs.
    (a) Assess the ability of AC10 cells to detect structural cardiotoxicity in 2D platforms using impedance-based systems.
    (b) Assess the ability of AC10 cells to detect structural cardiotoxicity in 3D spheroid models.

5.2 AC10 cell line characterisation for structural cardiotoxicity studies

5.2.1 AC10 cell line characterisation of growth kinetics for studies in two-dimensional cultures

To optimise a protocol for AC10 cell cardiotoxicity using two-dimensional platforms, cellular proliferative and kinetic characteristics were assessed. A set of studies combining the use of xCELLigence DP16 system and MTT assays were designed to gain an insight into the optimal seeding densities of AC10 cells required for cardiotoxicity detection experiments using these methodologies.

To determine the limitations of the MTT assay for cellular quantitative purposes of AC10 cells, an investigation into the relationship between manually determined cell number and detectable absorbance was carried out, in cells cultured in a 96-well plate. The lower and upper absorbance detection thresholds, whereby cell numbers were either insufficient to allow a quantifiable MTT formazan crystal reduction or were too elevated leading to colourimetric saturation were determined (Figure 5.2). Specifically, the lower detection limit was identified as ≤ 1 X 10^3 cell/mL and the upper detection limit was identified as ≥ 1 x 10^5 cell/mL. A linear relationship between cell number and detection by the MTT assay was therefore confirmed for AC10 cells within these identified limits (1 X 10^3 - 1 x 10^5 cell/mL).

In terms of determination of cellular responses using the xCELLigence methodologies, AC10 cells were plated on a DP16 E-Plate at a range of seeding densities, and cell index was monitored over time (method, section 2.7.1). Specific growth and kinetics parameters were identified for each initial seeding density, allowing to identify the optimal cell growth stage in relation to impedance values (Figure 5.3). Since AC10 cells do not form contractile syncytia, a suitable initial seeding density necessary to attain a stable cellular monolayer was extrapolated from the impedance traces. For subsequent cytotoxicity studies combined with the xCELLigence DP16 system, an initial seeding density between 1 x 10^5 and 2 x 10^5 cells/mL was deemed optimal, as it allowed AC10 cells to reach a stable impedance value within 36 hours post-seeding. The impedance cell index values further suggest that a confluent cellular monolayer was achieved and sustained for ≥48 hours post plateau, demonstrating suitability for the design of long-term cytotoxicity studies.

To confirm viability of AC10 cells during assessment by xCELLigence, cells were plated at a range of seeding densities, with cell viability subsequently evaluated using the MTT assay (methodology described in section 2.5.1) (figure 5.2A). A steady increase in absorbance was detected with AC10 cells plated at initial seeding densities between 1×10^3 and 1×10^5 cell/mL, demonstrating successful survival of AC10 cell monolayers over the course of 96 hours. On the contrary, cells plated at initial seeding densities between 1×10^2 and 1×10^3 did not determine a detectable increase in absorbance over time, in agreement with the previously defined limitations of the MTT assay stated above.

Overall, these experiments allowed to validate the use of MTT assays for AC10 quantitative investigations of cytotoxicity.

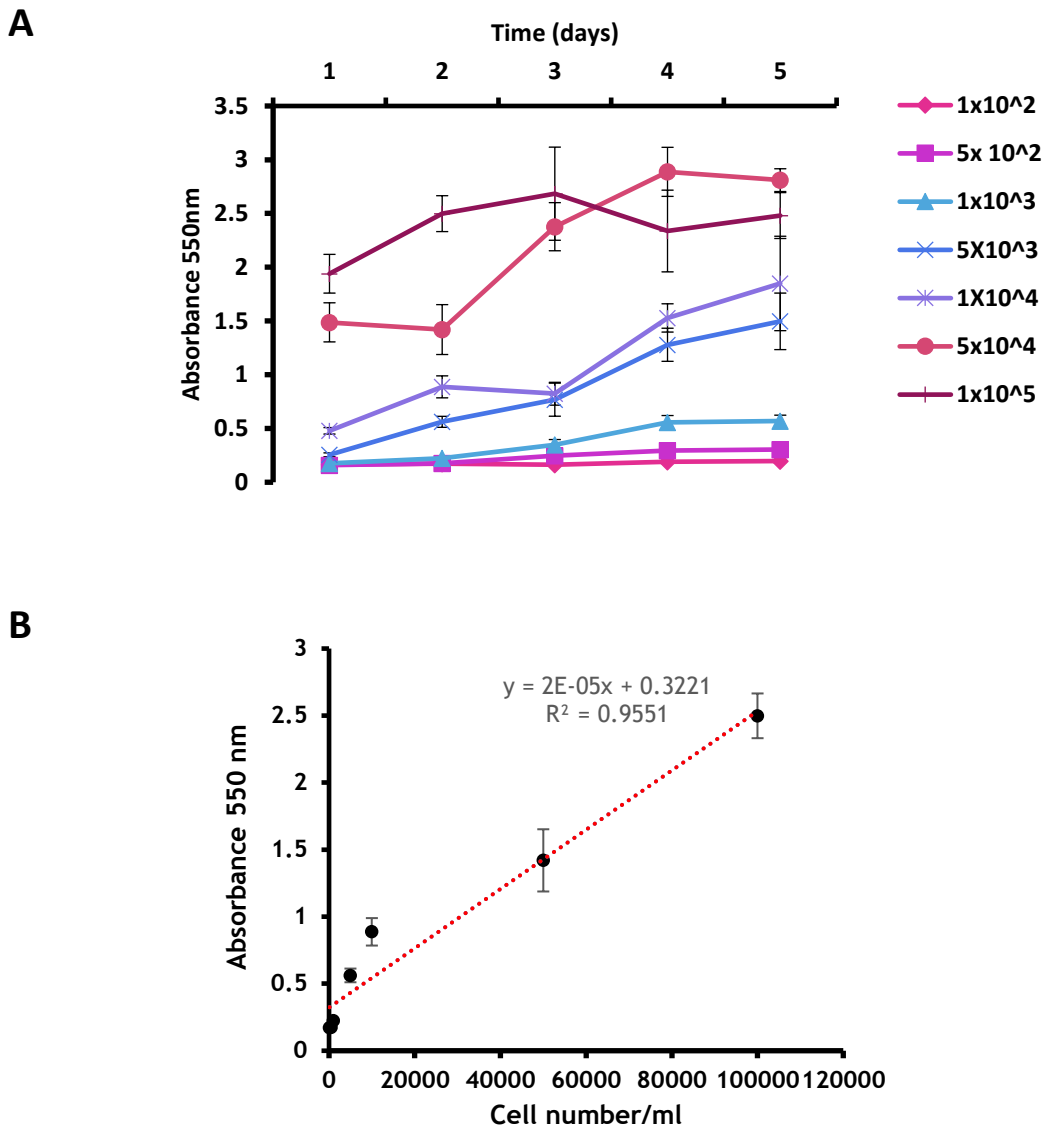

Figure 5.2 MTT assay as a quantitative method to assess AC10 cell viability over time. A. MTT assay to assess AC10 cell growth and survival over time. B. relationship between cell number and MTT colorimetric absorbance values at 550 nm. Data are the mean and SEM of at least 3 independent experiments.

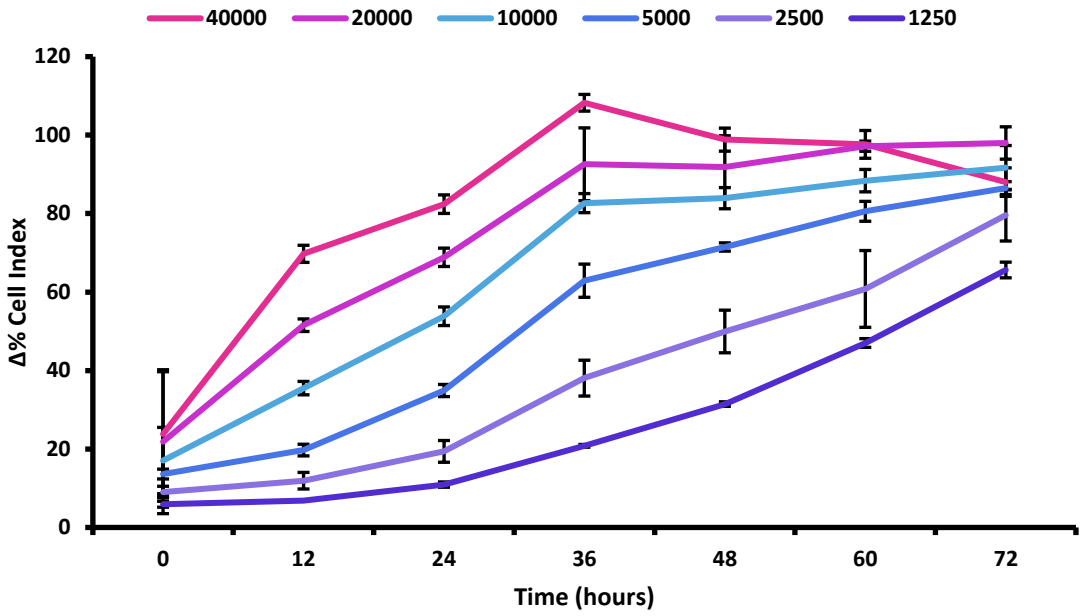

Figure 5.3 Growth kinetics of AC10 cells plated at different seeding densities. AC10 cells were plated on an xCELLigence DP E-plate at different densities and monitored over time. Impedance plateau was attained at different timepoints post seeding. Data are the mean ±SD of at least 4 different determinations from separate experiments.

5.2.2 AC10 cell line characterisation for structural cardiotoxicity studies in two-dimensional cultures

To assess the suitability of the AC10 cell line for the detection of drug induced structural perturbations, effects of the known structural cardiotoxicant doxorubicin were assessed using the xCELLigence DP system. For this study, AC10 cells were plated and monitored on a xCELLigence DP E-plate until confluency and cell index plateau were achieved, and subsequently doxorubicin was added at a range of concentrations.

Doxorubicin induced a significant ($P<0.05$) increase in cell index 24 hours post compound addition at 100 nM and 50 nM concentrations, suggesting AC10 cells underwent an acute hypertrophic morphological change (Figure 5.4A and 5.4B). Doxorubicin induced a steady significant ($P<0.001$) decrease in cell index at 1 µM concentration, indicating a reduction in cell viability.

A

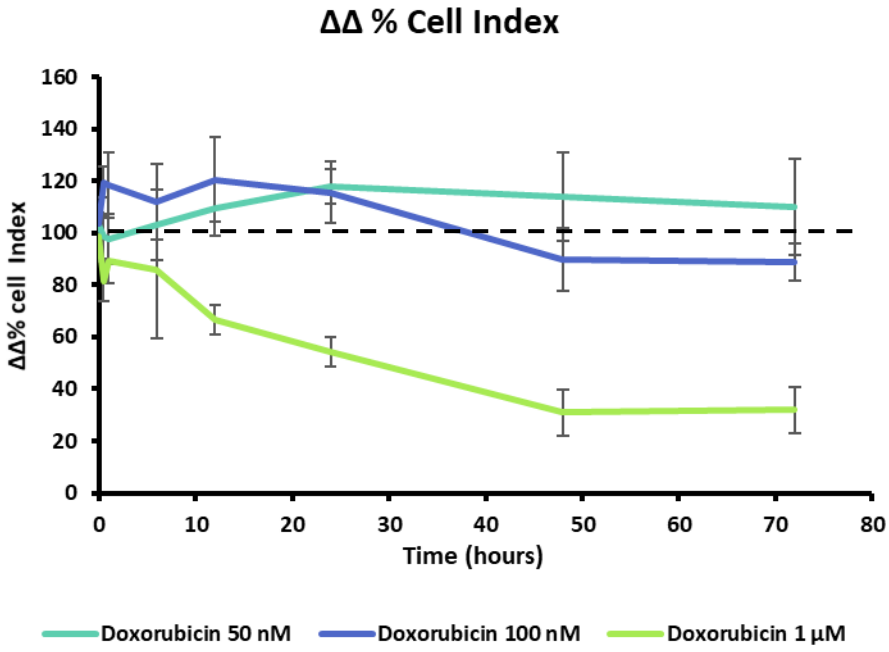

B

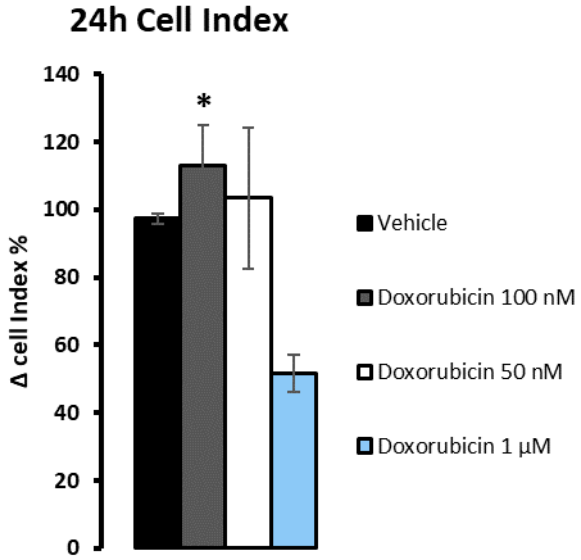

Figure 5.4 Doxorubicin induces characteristic hypertrophic changes in AC10 cells. AC10 cells were exposed to doxorubicin at a range of concentrations for 72 h. **A.** Doxorubicin induced a transient increase in cell index at concentrations between 50 nM and 100 nM, and a decrease in cell index at 1 µM. **B.** Cell index changes 24 h post compound addition, * = $p<0.05$. Impedance data are normalised to time-matched vehicle control and baseline values (ΔΔ%) and are the average ±SEM of at least 3 different experiments. Tested by ANOVA with Bonferroni post hoc modifications.

5.2.3 AC10 cell line characterisation for structural studies in three-dimensional cultures

Following the characterisation of growth and kinetics of the AC10 cell line model, and the confirmation of its suitability for the detection of structural liabilities using standard two-dimensional cultures, it was hypothesised that AC10 cells could be utilised in three-dimensional cultures. Within these studies, AC10 cells were used for the first time to establish single-lineage spheroid monocultures, as well as multi-lineage spheroid tricultures comprising human primary cardiac fibroblast and human primary cardiac endothelial cells (methodology described in section 2.4). Firstly, AC10 cells were assessed to characterise their ability to successfully aggregate into viable 3D structures. Next, the newly formed spheroids were monitored to assess overall growth and size over time (figure 5.5A). Both monoculture and triculture spheroids appeared spherical in shape, maintaining this feature over time. Monoculture and triculture spheroids reached their maximum size within approximately 20 days post plating, with a maximum diameter of 540 ± 90 µm for monoculture spheroids, and a maximum diameter of 700 ±88 µm for triculture spheroids. Following this timepoint, spheroids displayed structural instability likely due to continuous cellular proliferation, subsequently leading to the formation of an unviable hypoxic core. Interestingly, despite an equal initial cellular number used, AC10 monoculture spheroids remained smaller in size compared to triculture spheroids.

Immunofluorescent staining was used to investigate structural features in both monoculture and triculture spheroids (figure 5.6 A and B). For these studies, spheroids cultured for 14 days were fixed, stained and mounted onto microscope slides according to the methodology described in section 2.10. Both monoculture and triculture spheroids were shown to retain the expression of cardiac troponin I (cTnI), albeit cTnI staining did not evidence the formation of a syncytium-like cellular organisation. In tricultures, staining with phalloidin evidenced a network of f-actin filaments, allowing to assess the internal cytoskeletal organisation throughout the spheroids. Staining for the platelet endothelial cell adhesion molecule CD31 was used to locate cardiac endothelial cells within the spheroids, highlighting clustering of endothelial cells in one physical location within the spheroid in a potential effort to form minor primitive vessel-like formations, although further validation would be required to evaluate the

function of these structures. Hoechst stain was used to identify cell nuclei throughout the spheroids.

Overall, these studies demonstrate that AC10 cells can be used to successfully construct 3D spheroids, both using a monoculture and a triculture approach. These studies also allowed to identify the optimal experimental timeframe for AC10 spheroid studies: to avoid loss of structural stability and other non-drug dependent disturbances, AC10 spheroids were used 14 days post initial seeding in all subsequent studies.

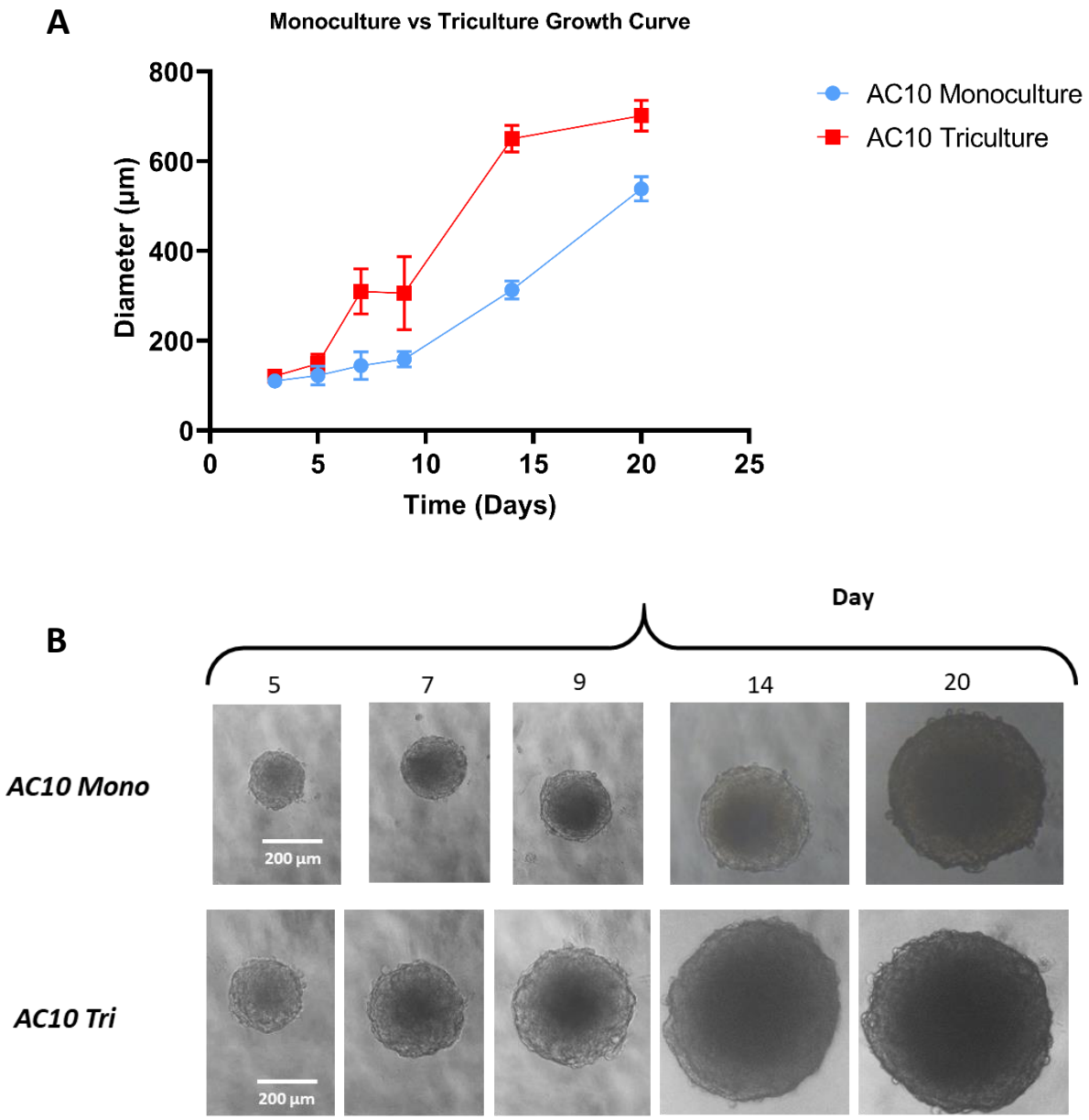

Figure 5.5. AC10 cells form viable monoculture and triculture spheroids. A. Growth curves of AC10 monoculture and triculture spheroids cultured in ultra low adhesion plates. Data is the average size in µm ±SD of at least three separate spheroids, imaged using brightfield microscopy. **B.** Representative brightfield images illustrating spheroid size, growth and morphology over time, from day 5 to day 20 post initial seeding.

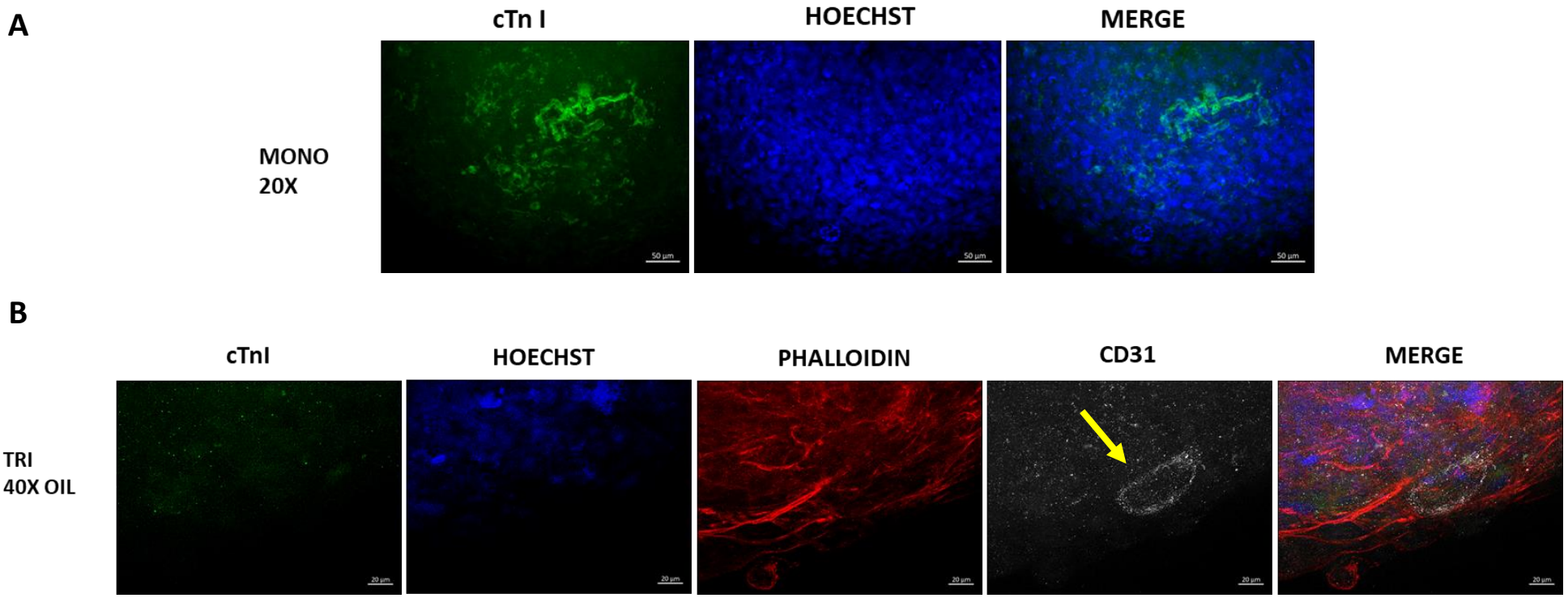

Figure 5.6. Internal structure of AC10 monoculture and triculture spheroids. Spheroids were cultured on ULA plates for 14 days, fixed and stained with anti-cardiac troponin I (green), Hoechst to stain the cell nuclei (blue), phalloidin to stain cytoskeletal structures (red) and anti CD31 antibody to stain endothelial cells (white; yellow arrow shows primitive vessel-like endothelial cell aggregation). Images are maximum intensity projections representative of a mid-section of each spheroid, typical of at least 3 different spheroids. **A. Monoculture AC10:** 20x magnification, scale bar is 50 µm **B. Triculture AC10:** 40x magnification with oil immersion, scale bar is 20 µm.

5.3 HDACi induce structural cardiotoxic changes in AC10 cells

5.3.1 Pan-HDACi induce structural changes in 2D AC10 cell line monolayer

Previous studies described in chapters 3 and 4 confirmed that pan-HDACi induced functional alterations in hiPSC and HL-1 two-dimensional cell models, in addition to significant structural and metabolic cardiomyocyte changes in the HL-1 model. Consequently, the effects of the pan-HDACi SAHA and TSA were evaluated in AC10 cells, particularly focusing on the detection of structural and morphological cellular alterations. For these studies, AC10 cells were initially assessed for cell index changes in response to pan-HDACi exposure using the xCELLigence DP system.

In line with previous studies using the HL-1 model, the pan-HDACI SAHA and TSA induced a significant ($p<0.05$) drop in cell index within 24 hours post compound addition at concentrations between 5µM and 200 nM for SAHA , and between 3 µM and 200 nM for TSA.

The decrease in cell index at higher compound concentrations (5 - 1.2 µM SAHA and 3 – 1 µM TSA) was attributed to pan-HDACi-induced cytotoxicity as demonstrated by relevant MTT assays, identifying IC_{50} values in AC10 cells at 1.82 ± 0.4 µM for SAHA (Figure 5.7 B) and 1.67 ± 0.5 µM for TSA (Figure 5.8B). Remarkably, the significant decrease in cell index was observable at concentrations below the cytotoxic threshold. To investigate whether these effects were dependent on structural changes, and not on cellular death or effects on cellular metabolic activity, manual cell counts were performed. Data indicated that cell numbers in AC10 cells treated with sub-cytotoxic concentrations of pan-HDACI SAHA and TSA remained unaltered, suggesting that the observed effects on cell index were dependent on cellular morphological alterations (Figures 5.7 C and 5.8C).

Further studies using brightfield microscopy on non-confluent pan-HDACi-treated AC10 cells evidenced a drastic and irreversible change in cellular appearance and morphology following pan-HDACi exposure (Figure 5.9A and 5.9B). In these studies, non-confluent AC10 cells were exposed to a single 200 nM sub-cytotoxic concentration of TSA for 24 hours, before supplementation with drug-free media. Imaging shows a clear morphological transition from

a fibroblast-like cellular structure typical of AC10 cells to a more elongated and stretched appearance (Figure 5.9). From these results it is plausible to assume that any reduction in impedance cell index, recorded after exposure to sub-cytotoxic pan-HDACi concentrations, is a direct consequence of hypotrophic morphological changes, which would result in a reduced E-plate electrode surface-to-cell contact ratio. Additionally, cells did not resume their original morphology upon compound removal, demonstrating the occurrence of a permanent morphological change.

Taken together, these results confirm that morphological changes in AC10 cells are associated with sub-cytotoxic pan-HDACi exposure, and are also in line with the impedance cell index findings reported in the HL-1 cardiomyocyte model described in section 4.8.

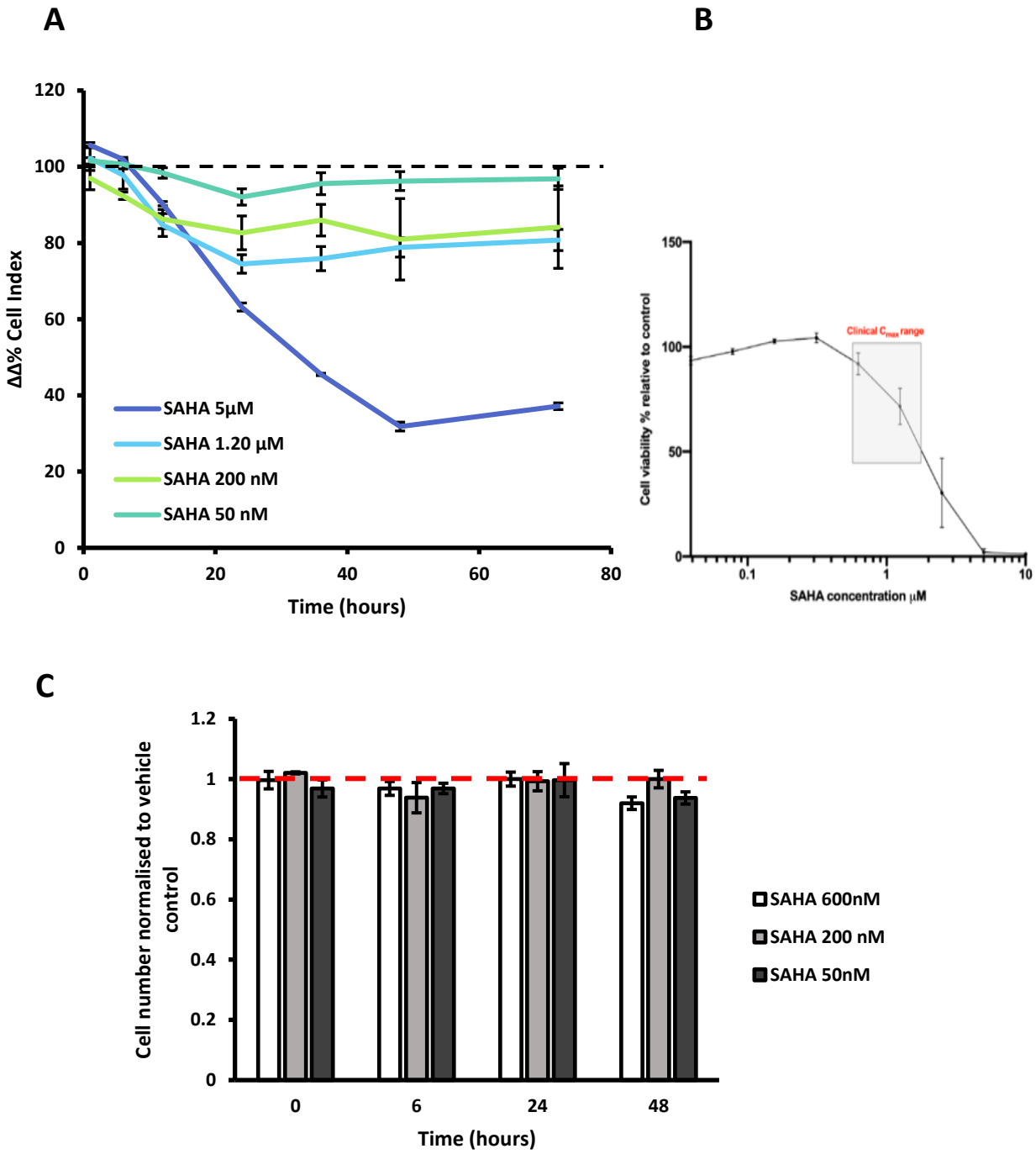

Figure 5.7 Pan-HDACIs induce changes in cell index and viability at toxic and sub-toxic concentrations in AC10 cells. AC10 cells were exposed to SAHA at a range of concentrations for 72 h. A. SAHA induced a significant decrease in CI at concentrations between 5 µM and 200 nM starting 12 h post compound addition. B. MTT assays did not evidence any reduction in cell viability following SAHA addition at concentrations between 200 and 500 nM. C. sub-clinical concentrations of SAHA did not affect average cell numbers. Impedance data are normalised to time-matched vehicle control and baseline values (ΔΔ%) and are the average ±SE of at least 3 different experiments. Cell counts and MTTs are normalised to vehicle control and are typical of at least 3 separate experiments. Tested by ANOVA with Bonferroni post-hoc modifications.

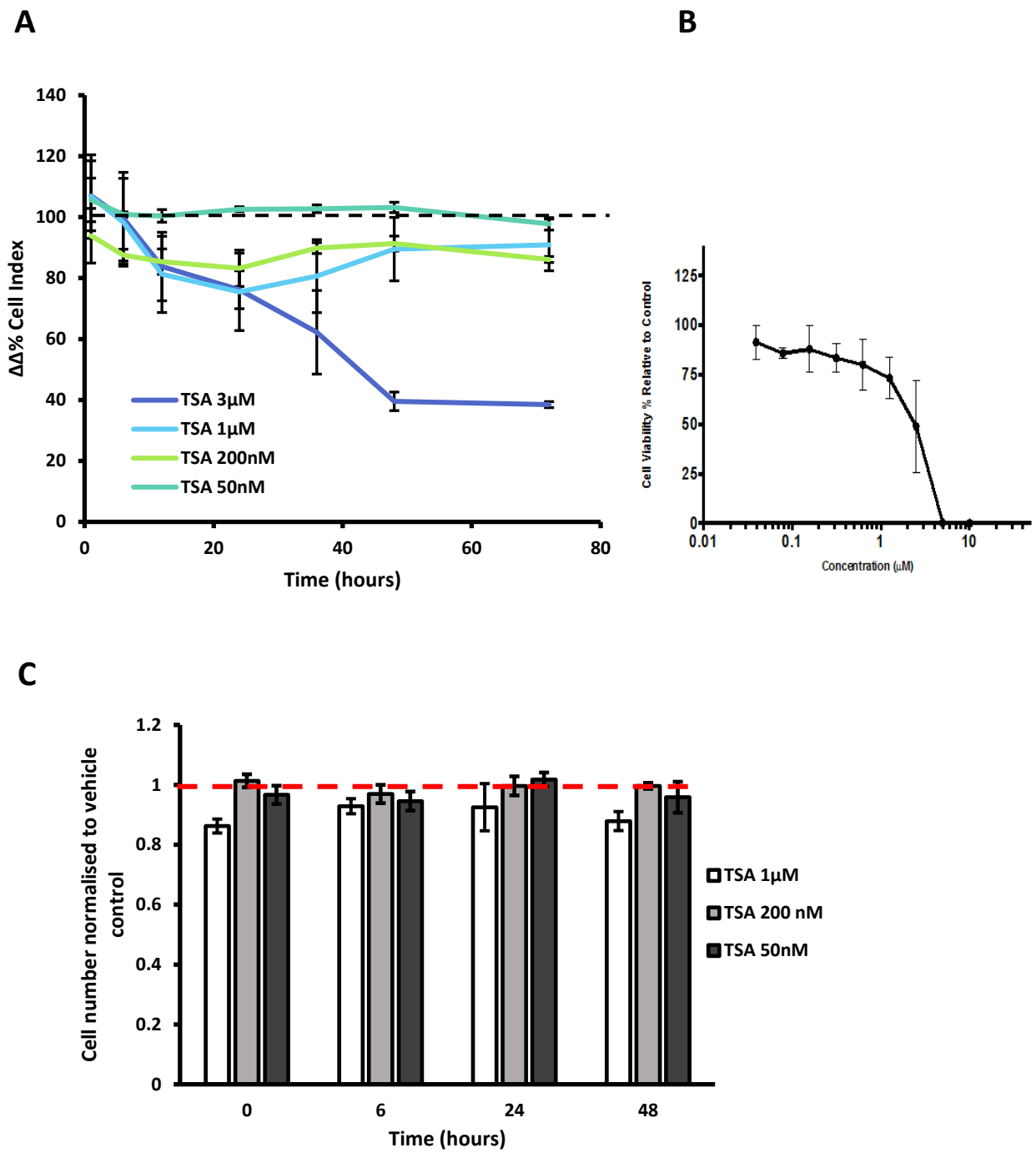

Figure 5.8 Pan-HDACIs induce changes in cell index and viability at clinical and subclinical concentrations in AC10 cells. AC10 cells were exposed to TSA at a range of concentrations for 72 h. TSA induced a significant decrease in CI at concentrations between 3 µM and 200 nM starting 12 h post compound addition. B. MTT assays did not evidence any significant reduction in cell viability following TSA addition at concentrations between 200 and 500 nM. C. Sub-cytotoxic concentrations of TSA did not affect average cell numbers Impedance data are normalised to time-matched vehicle control and baseline values (ΔΔ%) and are the average ±SE of at least 3 different experiments. Cell counts and MTTs are normalised to vehicle control and are typical of at least 3 separate experiments. Tested by ANOVA with Bonferroni post-hoc modifications.

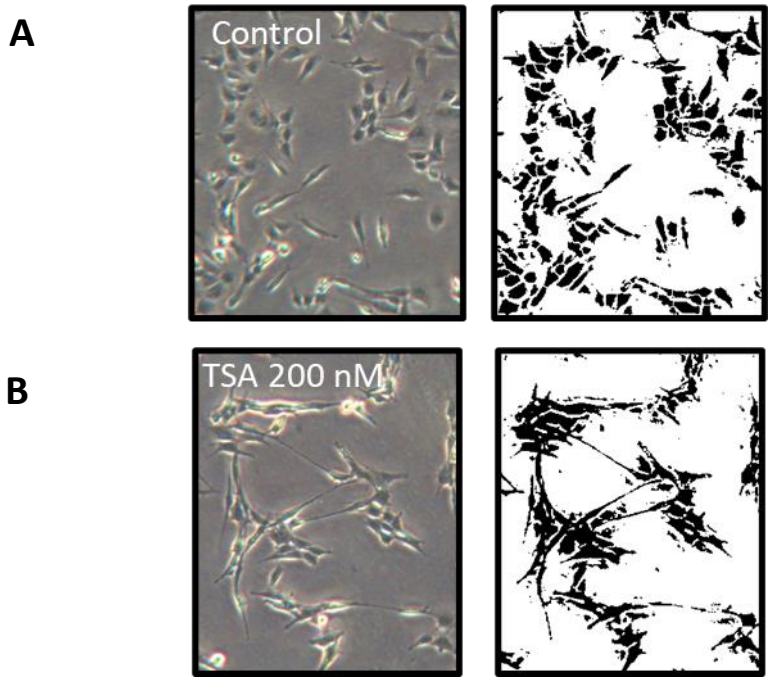

Figure 5.9 Pan-HDACi induce cellular structural remodelling at sub-cytotoxic concentrations in AC10 cells. AC10 cells were exposed to 200 nM TSA for 24 h and imaged under phase contrast microscopy (magnification 20X).**A.** Typical AC10 cell morphology after exposure to vehicle DMSO. **B**. TSA induced elongation and structural remodelling of AC10 cells without affecting cellular integrity and viability Images are representative of at least 4 different separate experiments. Enhanced contrast (right) was used to highlight cell surface and morphological features.

5.3.2 Determination of HDACI pharmacological targets in AC10 cells

After confirming that pan-HDACi induced morphological alterations in AC10 cells at sub-clinical and sub-cytotoxic concentrations, studies were carried out to gain mechanistic insight into the pharmacological activity of SAHA and TSA in the AC10 model. As in the analogous studies reported in section 4.9, two primary HDACi targets were assessed in AC10 whole protein lysates following exposure to various pan-HDACi concentrations (methodology described in section 2.8). Acetylation of histone H4 and α-tubulin were therefore assessed in response to TSA and SAHA (figure 5.10 and 5.11).

Treatment with the cytotoxic 1.2 µM concentration of SAHA resulted in an increase in both histone H4 and α-tubulin acetylation levels. However, exposure to sub-cytotoxic concentrations of SAHA ≤ 200 nM did not change protein acetylation levels (figure 5.10).

A similar effect was observed following exposure to TSA: the cytotoxic 1 µM concentration elicited marked acetylation of both α-tubulin and histone H4 in a time-dependent manner. Conversely, no change in acetylation was observed following exposure to the non-cytotoxic 200 nM concentration of TSA.

Together, these observations suggest that any structural effects induced following sub-cytotoxic exposure to pan-HDACi are likely to be attributed to secondary pharmacology effects rather than main HDACi pharmacological targets. These results therefore further corroborate analogous findings observed in the HL-1 cardiomyocyte model (Chapter 4).

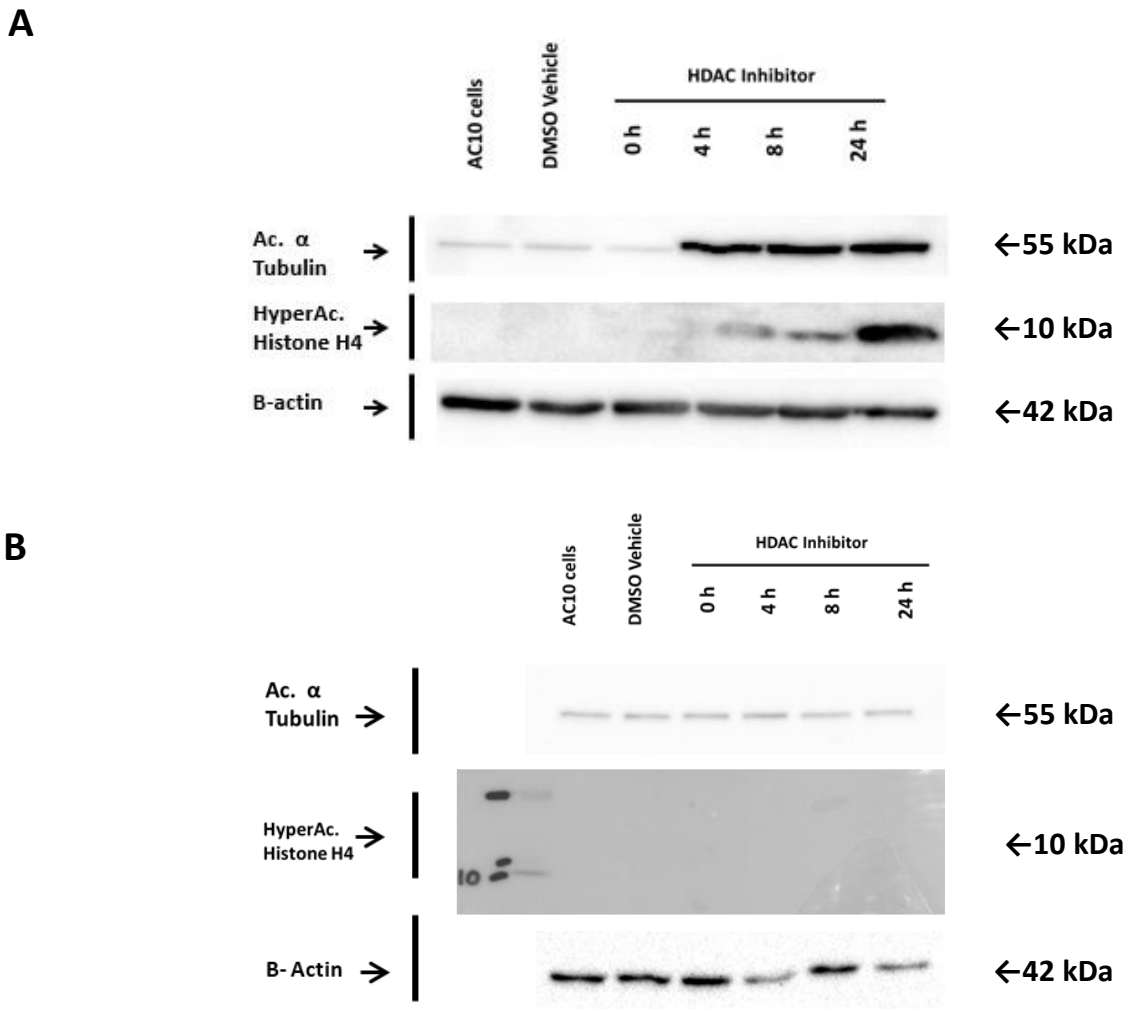

Figure 5.10 Determination of pan-HDACi pharmacological targets in AC10 cells. Western Blot analysis of AC10 whole protein extracts assessing levels of acetylated α tubulin (55 kDa) and acetylated histone H4 (10 kDa) following treatment with **A.** 1µM and **B.** 200 nM concentrations of Pan-HDACi TSA. Each lane contained 20µg protein/lane. Results are representative of one typical experiment of at least 3 separate experiments.

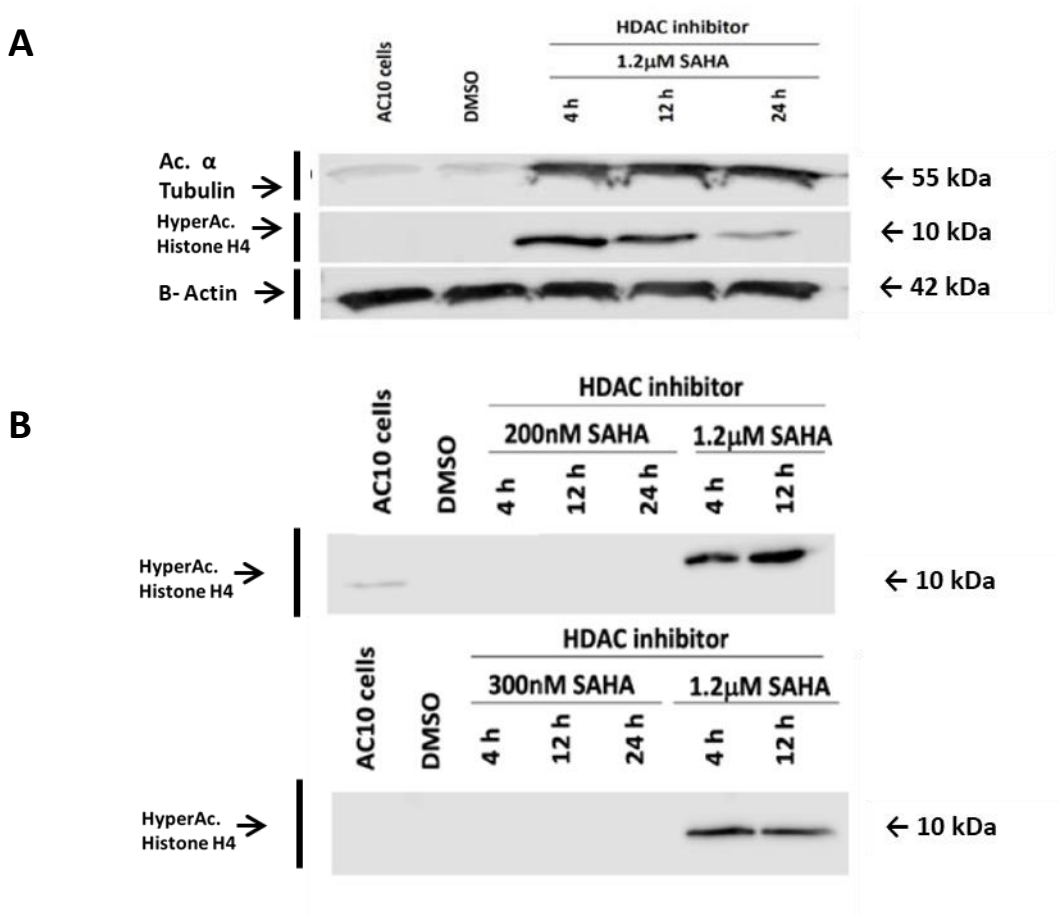

Figure 5.11 Determination of pan-HDACi pharmacological targets in AC10 cells. Western Blot analysis of AC10 whole protein extracts assessing levels of acetylated α tubulin (55 kDa) and acetylated histone H4 (10 kDa) following treatment with **A.** 1µM and **B.** 200 and 300 nM concentrations of Pan-HDACi SAHA. Each lane contained 20µg protein/lane. Results are representative of one typical experiment of at least 3 separate experiments

5.3.3 Sub-selective class I HDAC inhibition, but not class IIb, is associated with structural alterations in AC10 cell monolayers

To confirm whether HDACi-induced structural changes could be attributed to selective HDAC inhibition in AC10 cells, an investigation into the effects of class I and IIb HDAC selective inhibitors was carried out. For these studies, AC10 cells were grown to confluency in a xCELLigence DP E-plate, and subsequently exposed to class I HDACi MS-275 and class IIb HDACi tubacin.

Results indicate that class I selective inhibitor, but not class IIb, induced a decrease in cell index (figure 5.12A and 5.12B). Specifically, MS-275 induced a significant ($p<0.05$) decrease in cell index by 31% 24 hours post compound addition at the cytotoxic concentration of 1 µM. No decrease in cell index was however recorded following exposure to 200 nM MS-275.

Class IIb selective inhibitor tubacin did not induce detectable changes in cell index even at the highest tested concentrations (figure 5.12B).

Overall, these results confirm that class I, but not class IIb, is partly implicated in HDACi-induced cardiotoxicity. Lastly, these results are consistent with the structural effects observed upon sub-selective HDAC inhibition in the HL-1 cell line model (chapter 4).

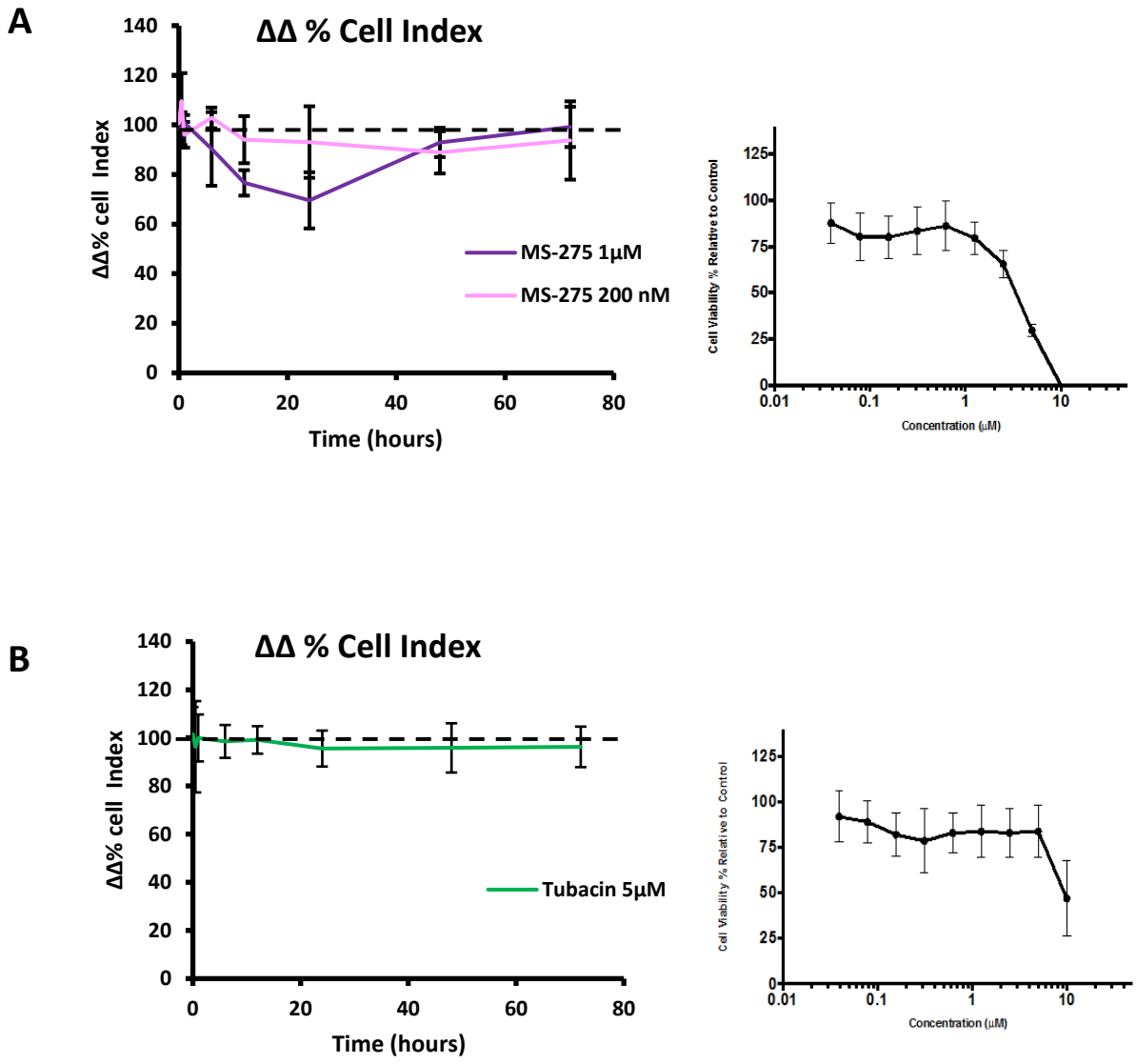

Figure 5.12 Class I selective inhibitor, but not class IIb, induced a transient decrease in cell index in AC10 cells. AC10 cells were exposed to MS-275 and tubacin for 72 h. **A.** MS-275 induced a transient decrease in cell index following exposure to 1 µM but not 200 nM. A concentration of ≤ 1 µM did not induce cytotoxicity. **B.** Tubacin at 5 µM did not induce detectable changes in cell index and did not induce cytotoxicity. Impedance data are normalised to time-matched vehicle control and baseline values (ΔΔ%) and are the average ±SE of at least 3 different experiments. MTTs are normalised to vehicle control and are typical of at least 3 separate experiments. Tested by ANOVA with Bonferroni post-hoc modifications.

5.3.4 Pan-HDACi induce structural changes in AC10 spheroids

Studies on AC10 cell monolayers confirmed that pan-HDACi induce structural and morphological changes. AC10 monoculture and triculture spheroids were therefore used to assess pan-HDACi structural effects in a three-dimensional microenvironment. The first phase of these studies was designed to assess chemosensitivity and viability of 3D AC10 structures against HDACi compounds using ATP viability assays. Next, studies were focused on the identification of structural perturbations using a combination of bioimaging techniques, assessing whole-spheroid morphological features as well as internal structural alterations.

5.3.4.1 AC10 spheroids demonstrate enhanced sensitivity to pan-HDACi

Chemosensitivity of monoculture and triculture spheroids against pan-HDACi TSA and SAHA was evaluated using Cell Titer-Glo ATP assays (methodology described in section 2.5.2). Dose-response curves are illustrated in figure 5.13. Both monoculture and triculture AC10 spheroids demonstrated higher sensitivity to pan-HDACi exposure compared to 2D AC10 monolayers. IC_{50} values were obtained following 24-hour exposure to a single dose of pan-HDACi. The IC_{50} values for TSA were 0.7 ± 0.2 and 0.8 ± 0.2 μM for monocultures and tricultures, respectively. The IC_{50} values for SAHA were 1.7 ± 0.3 μM and 1.3 ± 0.6 μM for monocultures and tricultures respectively (Figure 5.13).

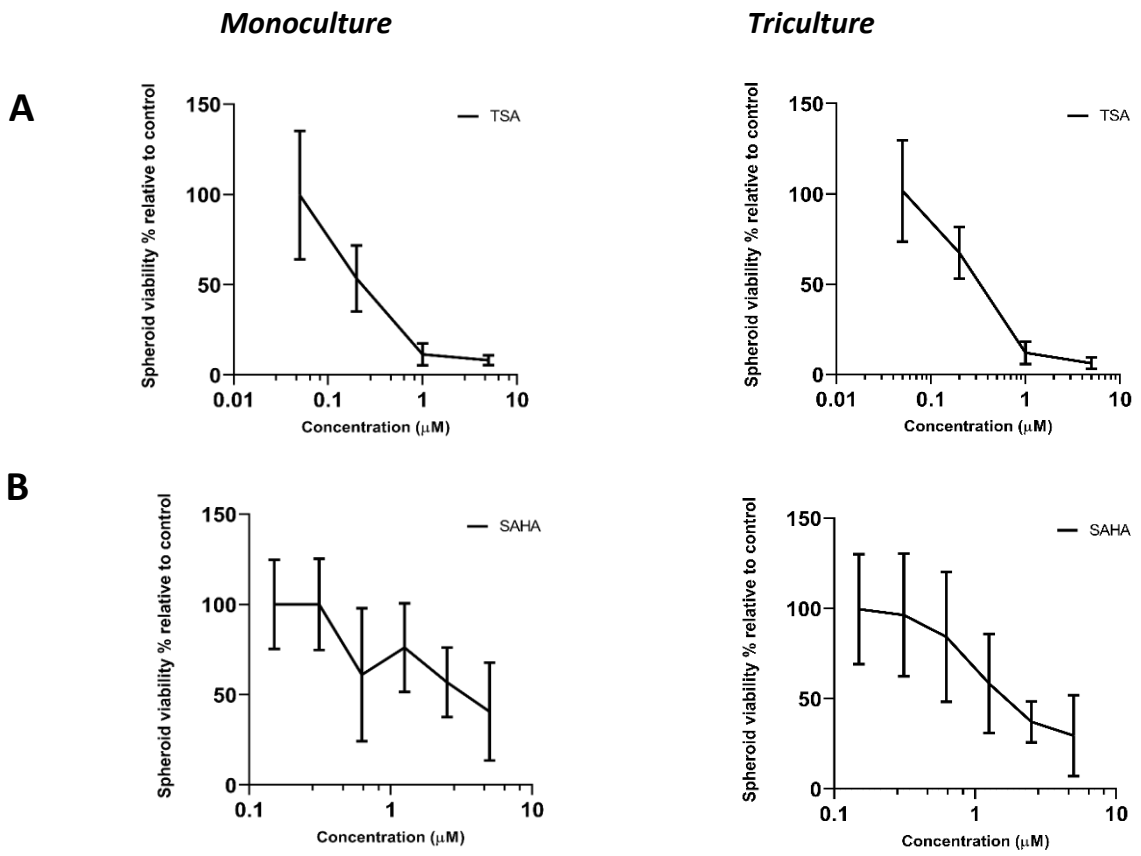

Compound	*2D monolayer*	*Spheroid monoculture*	*Spheroid triculture*
	IC_{50} (μM)		
TSA	1.3 ± 0.43	0.69 ± 0.2	0.8 ± 0.15
SAHA	2.56 ± 0.76	1.7 ± 0.31	1.30 ± 0.61

Figure 5.13. AC10 spheroids display enhanced sensitivity to pan-HDACi. AC10 monoculture and triculture spheroid dose-response curves derived from 24-hour exposure to pan-HDACi TSA (**A**) and SAHA (**B**). Data are the mean ±SD of at least 3 separate experiments. Extrapolated IC_{50} value for 2D and 3D models shown in table.

5.3.4.2 Pan-HDACi induce changes in whole-spheroid morphology

Untreated AC10 spheroids were shown to maintain a uniform spherical shape over time. A study was designed to investigate whether structural changes in whole-spheroid morphology occurred following exposure to pan-HDACi compounds. For these studies, AC10 monoculture spheroids were grown for 14 days before being exposed to various concentrations of TSA for 20 hours. Morphological features including whole-spheroid size, shape and diameter were monitored using brightfield imaging. Imaging indicates that TSA at 5 µM and 1 µM concentrations induced a disruption in spheroid morphology and appearance: this is demonstrated by the occurrence of uneven spheroid borders, displaying through peripheral protrusions and blebbing (figure 5.14A). Following exposure to TSA concentrations between 0.5 µM and 0.2 µM, spheroid borders did not display blebbing or other disruptions, and appeared integral. However, whole-spheroid morphology appeared elliptical rather than spherical. To establish whether the transition from a spherical shaped spheroid into an elliptical shaped spheroid was a direct consequence of pan-HDACi exposure, AC10 spheroids were assessed using brightfield bioimaging before and after treatment with TSA. Spheroid size and morphology was recorded on the same sample prior to and post-treatment with TSA for 20 hours. Imaging indicates an observable transition from spherical to elliptical shape in most treated spheroids (figure 5.14B) (sample size ≥ 20 spheroids per treatment, per experiment). Further analysis confirmed that the ratio of perpendicular spheroid diameters was significantly different ($p<0.01$) compared to vehicle exposure, confirming the occurrence of whole-spheroid morphological changes (figure 5.14C).

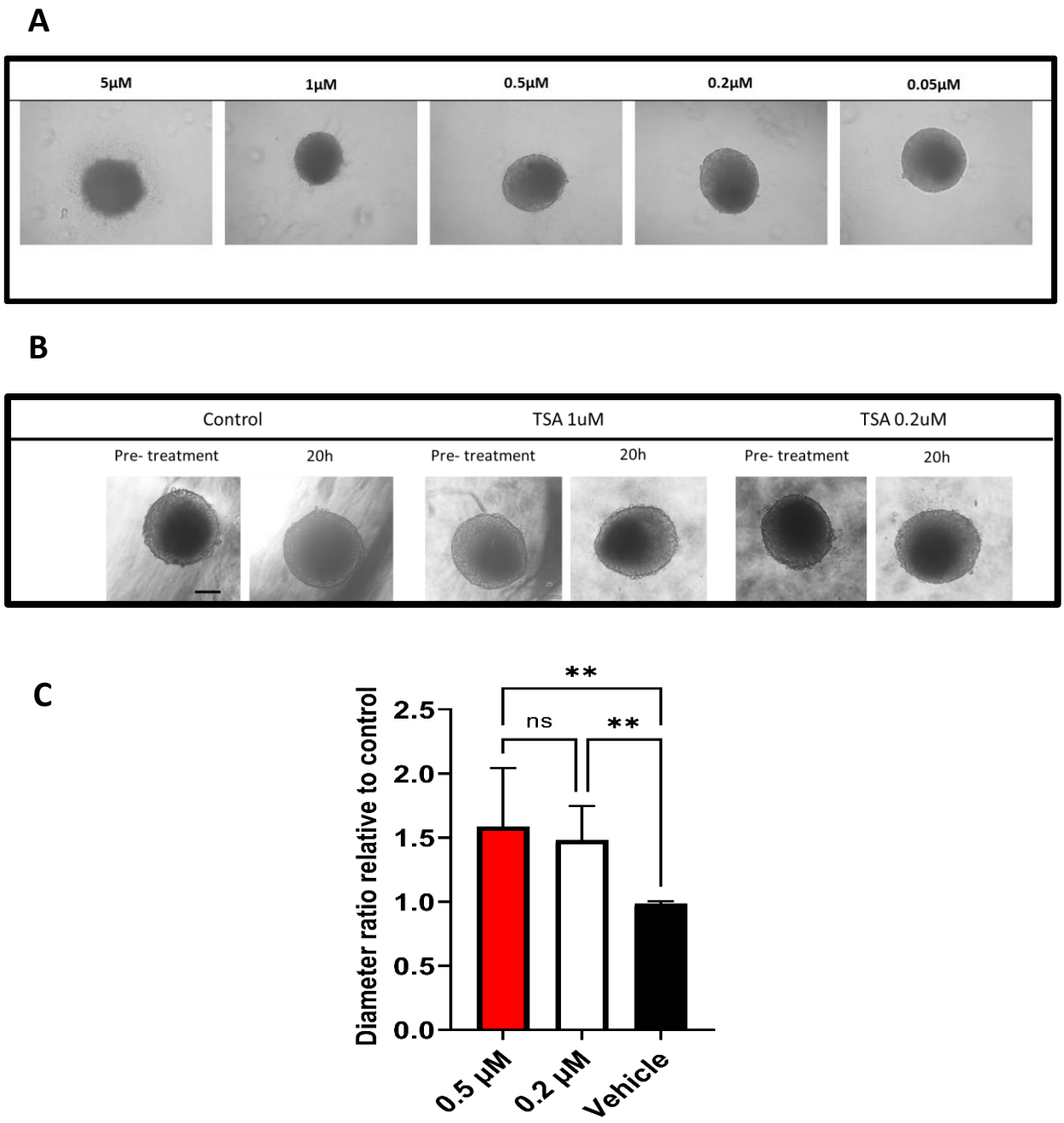

Figure 5.14 TSA causes whole-spheroid morphology changes in monoculture AC10 spheroids. AC10 monoculture spheroids were cultured for 14 days and subsequently treated with various concentrations of TSA for 20 h. **A.** TSA induced edge blebbing and protrusions at concentrations between 5-1µM, and induced whole-spheroid morphological changes at concentrations between 1-0.2µM. **B.** Whole-spheroid morphology was compared before and after exposure to TSA, showing transition from spherical to elliptical shapes at concentrations between 1-0.2µM. Images are 10x magnification, scale bar 200µm **C.** Diameter ratio of whole-spheroids was compared, indicating ratios of non-spherical shaped spheroids were significantly ($p<0.01$) different compared to control. Data are the mean and SEM from at least 3 separate experiments (≥20 spheroids per treatment). Tested by ANOVA and Tukey's post hoc modifications. **= $p<0.01$

5.3.4.3 Pan-HDACi induce disruption of internal spheroid structures

Whole-spheroid morphological assessment confirmed the occurrence of pan-HDACi-induced spheroid restructuring in AC10 monoculture spheroids. To investigate the effects of pan-HDACi compounds on the internal framework of the spheroid, experiments were designed to visualise spheroid section stacks using immunofluorescence analysis for relevant structural markers. Specifically, AC10 spheroids were cultured for 14 days, then fixed and stained for cardiac troponin I (cTnI), phalloidin to highlight F-actin, and Hoechst-33342 dye to stain nuclei (methodology described in section 2.10).

Ultrastructural analysis of spheroid mid-sections demonstrated that pan-HDACi TSA induced a marked increase in cTnI signal at both cytotoxic and sub-cytotoxic concentrations. CTnI staining however did not highlight specific intracellular structures, but rather resulted in accumulation within the spheroid, confirming cTnI release likely occurred due to disruption typical of cardiac structural damage. Additionally, phalloidin staining for f-actin evidenced a marked disruption following both TSA tested concentrations. Following exposure to the cytotoxic concentration of 1 µM, TSA induced a significant ($p<0.01$) increase in phalloidin signal intensity, suggesting the occurrence of a perturbation within the f-actin cytoskeletal filament network (Figures 5.15, 5.16 and 5.17)

Interestingly, following exposure to the sub-cytotoxic concentration of 200 nM, TSA did not induce an increase in phalloidin signal intensity, albeit the F-actin network appeared remarkably fragmented, suggesting the occurrence of a disruptive effect on cytoskeletal organisation. Analogous findings were observed following exposure to sub-cytotoxic concentrations of SAHA, where at 200 nM no significant increases were observed in cTnI signal intensity. However, a significant decrease ($p<0.05$) in phalloidin signal intensity evidenced a disruption to F-actin filaments, and f-actin fragmentation was also observed (figure 5.18 and 5.19).

Overall, these results indicate that pan-HDACi elicited marked alterations of the internal spheroid structure. TSA induced particularly strong effects, with evident disruptions to cTnI indicative of cardiomyocyte damage. While the effects of cytotoxic TSA concentrations also resulted in an evident disruption of the cytoskeleton compatible with the occurrence of cell

death, sub-cytotoxic concentrations of TSA and SAHA demonstrated a clear F-actin disarrangement consistent with the cellular cytoskeletal remodelling observed in 2D AC10 monolayers.

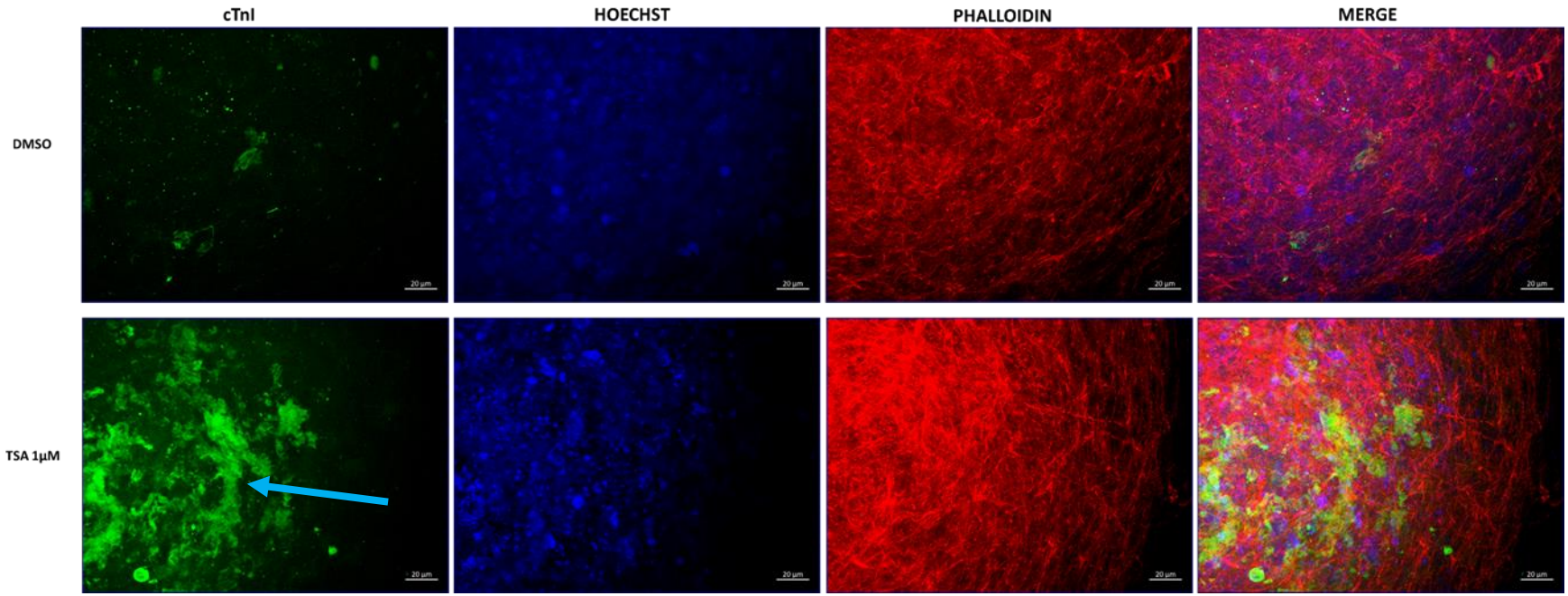

Figure 5.15 TSA induces internal structural perturbations in AC10 monoculture spheroids at cytotoxic concentrations. AC10 monoculture spheroids were cultured in ULA plates for 14 days, exposed to TSA for 20 hours fixed and stained with anti-cardiac troponin I (green), Hoechst to stain the cell nuclei (blue) and phalloidin to stain cytoskeletal structures (red). TSA induced cTnI disruption with visible intra-spheroid accumulation (blue arrow). TSA induced a marked disruption in f-actin organisation. Images are maximum intensity projections representative of a mid-section of each spheroid, typical of at least 3 different spheroids. Images were taken at equal exposure times, magnification is 20X, scale bar = 20 µm.

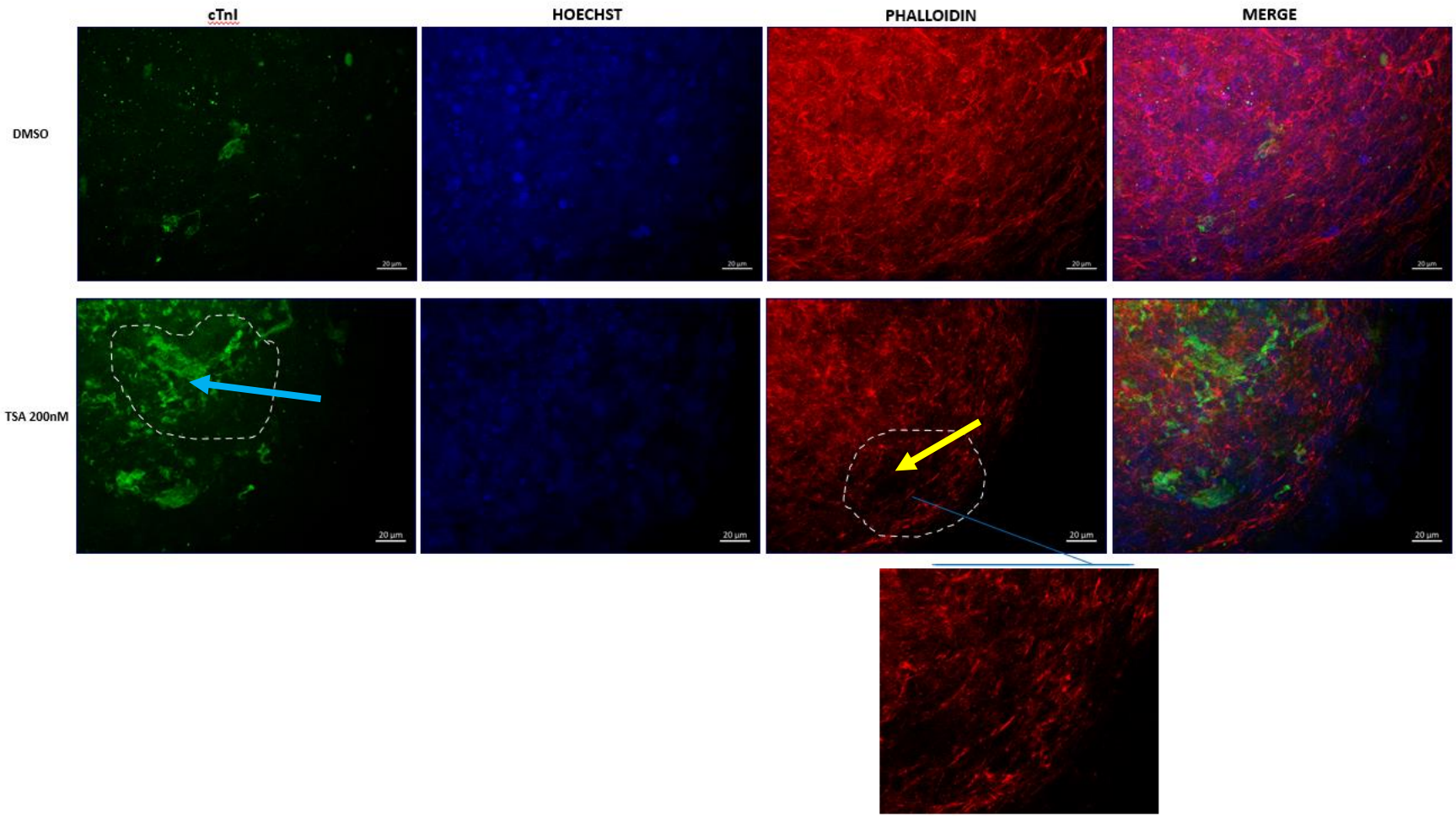

Figure 5.16 TSA induces internal structural perturbations in AC10 monoculture spheroids at sub-cytotoxic concentrations.
[Caption continued on the next page]

Figure 5.16 [continued] TSA induces internal structural perturbations in AC10 monoculture spheroids at sub-cytotoxic concentrations. AC10 monoculture spheroids were cultured in ULA plates for 14 days, exposed to TSA and vehicle DMSO control for 20 hours, fixed and stained with anti-cardiac troponin I (green), Hoechst to stain the cell nuclei (blue) and phalloidin to stain cytoskeletal structures (red).TSA induced cTnI disruption with visible intra-spheroid accumulation (blue arrow). TSA induced fragmentation of f-actin network (yellow arrow; zoomed image). Images are maximum intensity projections representative of a mid-section of each spheroid, typical of at least 3 different spheroids. Images were taken at equal exposure times, magnification is 20X, scale bar = 20 µm.

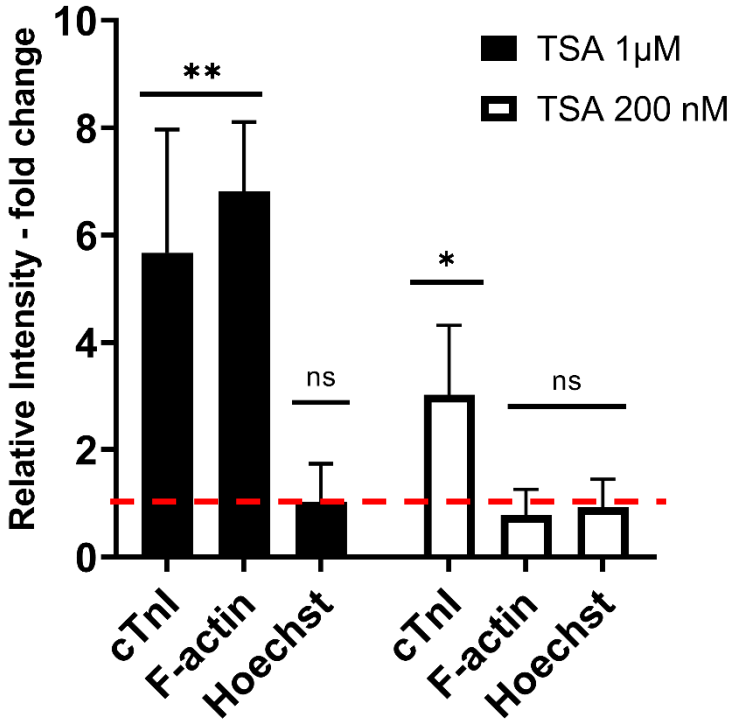

Figure 5.17 TSA induces internal structural perturbations in AC10 monoculture spheroids - Fluorescence signal intensity analysis AC10 monoculture spheroids were cultured in ULA plates for 14 days, exposed to TSA for 20 hours, fixed and stained with anti-cardiac troponin I, Hoechst to stain the cell nuclei and phalloidin to stain cytoskeletal structures. Signal intensity was evaluated on mid-spheroid section images taken at identical exposure settings. CTnI and f-actin signals were significantly increased following 1 µM TSA exposure. CTnI signal was increased following 200 nM TSA exposure. Hoechst stained nuclei signal was not affected and showed equal intensity. Data are the mean and SD of at least three independent determinations and are expressed as fold change relative to control. *= $p<0.05$; **= $p<0.01$

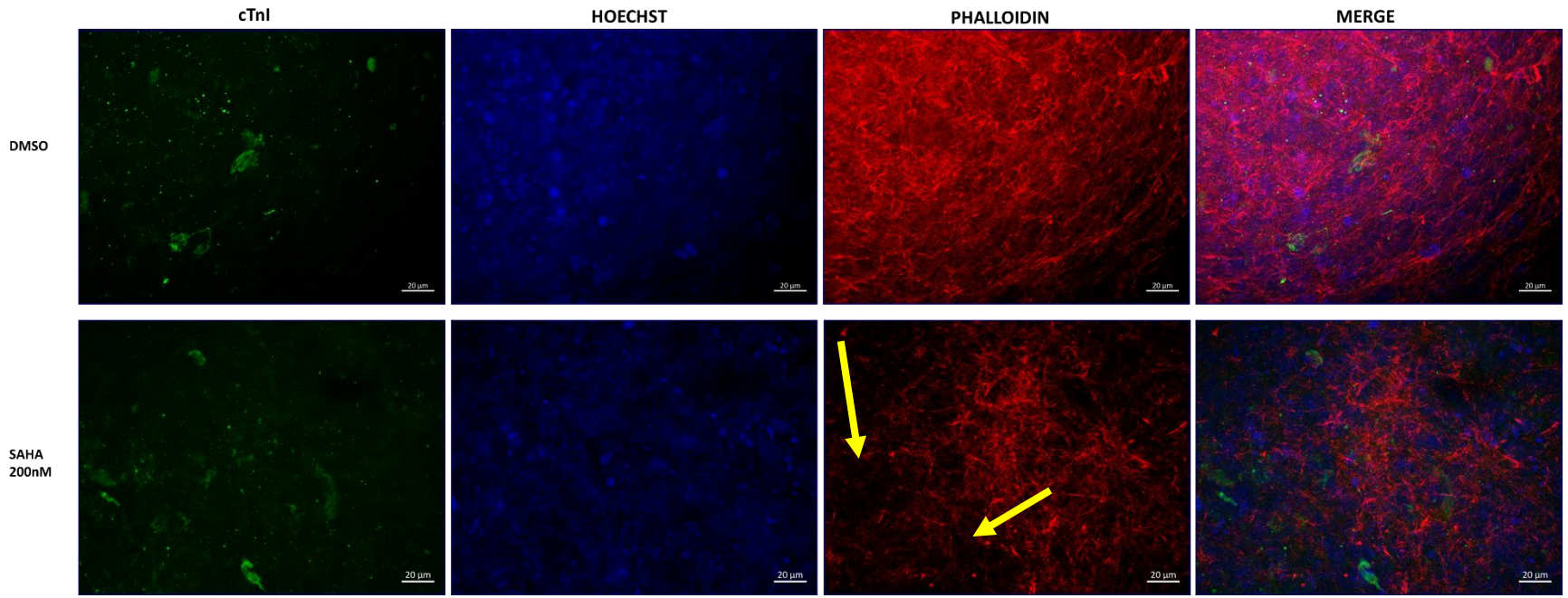

Figure 5.18 SAHA **induces internal structural perturbations in AC10 monoculture spheroids at sub-cytotoxic concentrations**. AC10 monoculture spheroids were cultured in ULA plates for 14 days, exposed to vehicle DMSO control and SAHA for 20 hours, fixed and stained with anti-cardiac troponin I (green), Hoechst to stain the cell nuclei (blue) and phalloidin to stain cytoskeletal structures (red).SAHA did not induce cTnI disruption. TSA induced fragmentation of f-actin network (yellow arrow). Images are maximum intensity projections representative of a mid-section of each spheroid, typical of at least 3 different spheroids. Images were taken at equal exposure times, magnification is 20X, scale bar = 20 µm.

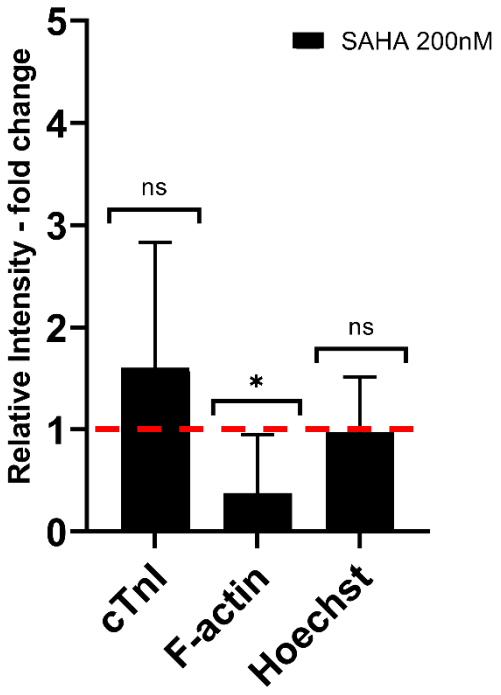

Figure 5.19 SAHA induces internal structural perturbations in AC10 monoculture spheroids -Fluorescence signal intensity analysis. analysis AC10 monoculture spheroids were cultured in ULA plates for 14 days, exposed to SAHA for 20 hours, fixed and stained with anti-cardiac troponin I, Hoechst to stain the cell nuclei and phalloidin to stain cytoskeletal structures. Signal intensity was evaluated on mid-spheroid section images taken at identical exposure settings. F-actin but not cTnI intensity was affected following 200nM SAHA exposure. Hoechst nuclei signal was unaffected. Data are the mean and SD of at least three independent determinations and are expressed as fold change relative to control. *= $p<0.05$

5.4 Discussion

The availability of simple and cost-effective models for early screening of cardiotoxicity is currently limited. While the study of acute functional cardiotoxicity has shown considerable advances in recent years due the advent of contractile and phenotypically relevant hiPSC-CM models, detection of drug-induced structural changes with these cell models remains limited (Földes et al. 2014). Similarly, early signs and markers of structural cardiotoxicity screening are still mostly not easily detectable or insufficient in models utilising hiPSC-CMs (Satsuka and Kanda 2019; Da Rocha et al. 2017; Johansson et al. 2020). Additionally, preclinical cardiotoxicity safety assays are often designed to provide high-throughput data collection, wherein the use of costly cardiac cell models such as hiPSC-CMs is carefully optimised to provide a sustainable cost-to-benefit ratio. As such, the use of hiPSC-CMs on a large scale is therefore limited, and generally relegated to the detection of drug-induced functional cardiotoxicity. The AC10 human ventricular cardiomyocyte cell line represents a source of readily expandable and cost-effective cardiac-like cells (Davidson et al. 2005), which remains unexplored for its potential application and utility in early structural cardiotoxicity screening. The aim of this chapter was to assess the suitability of AC10 cells as a model for the detection of drug-induced structural perturbations, both in combination with high-throughput impedance-based technologies, as well as through the use of advanced three-dimensional culture systems.

The first phase of this study focused on the optimisation of a protocol for the use of two-dimensional AC10 cell monolayers in combination with impedance-based technologies. AC10 cells are typically described as cardiomyocyte-like cells that remain in a pre-contractile state (Davidson et al. 2005), and as such they do not form a functional contractile syncytium. Unlike terminally differentiated cardiomyocytes, AC10 cells also retain a proliferative capacity due to their immortalised nature. Therefore, to better represent and mimic the cardiac environment, studies were designed to understand the growth kinetics of AC10 cells, and subsequently identify optimal seeding densities for their use on the xCELLigence DP platform. This study indicated that AC10 cells could achieve an impedance cell index plateau due to cellular confluency within 36 hours post initial seeding at 1-2 x 10^5 cells/mL, forming a cellular

monolayer and maintaining stable impedance values for over 48 hours, therefore making them suitable for both acute and delayed-onset toxicity studies (section 5.2.1). Using the optimised cell seeding protocol, the structural cardiotoxicant doxorubicin was used to evaluate effects upon cell index impedance: this resulted in the induction of detectable cell index perturbations. In particular, a sub-therapeutically relevant doxorubicin concentration induced a cell index increase imputable to cellular hypertrophic changes, a finding also previously reported in the AC10 model (Rockley 2018). At higher concentrations, doxorubicin induced a cytotoxic response in AC10 cells, as reflected by the decrease in cell index parameters (section 5.2.2). In a recent study, doxorubicin has been successfully used as a proof-of-concept compound to investigate the mechanistic pathways of mitochondrial toxicity in the AC16 model, thus corroborating the relevance of this model for structural preliminary cardiac toxicity assessments (Yuan et al. 2016).

The effects of HDACi on cardiac cell structure were evaluated in AC10 two-dimensional monolayers analysed using impedance-based systems (section 5.3.1). In agreement with the previously reported HL-1 cell model, the pan-HDACi TSA and SAHA elicited a marked transient decrease in impedance cell index values at both cytotoxic and sub-cytotoxic drug concentrations. This transient effect on cell index parameters was likely attributed to the compensatory expansion of adjacent AC10 cells, rather than a temporary/reversible change of individual cellular structures. To reinforce this hypothesis, imaging of individual AC10 cells demonstrated that pan-HDACi-induced structural alterations were irreversible, and occurred within 24 hours post compound addition (section 5.3.1). Further observations established that pan-HDACi caused cellular morphological elongation and hypotrophy, ultimately justifying the observed reduction in impedance cell index parameters. Although class I HDACs are fundamentally related to epigenetic regulation through histone acetylation, there are also many non-histone post-translational roles of HDACs established, including regulation of intracellular protein activities and localisation, activity of transcription factors, modification of cellular cytoskeletal interactions, and intracellular protein transport. These effects and roles have subsequently resulted in their re-classification of KDACs rather than just HDACs (Becker et al. 2018). The implications of HDAC/KDAC modulation on peculiar aspects of cellular morphology within individual organ systems have thus not been fully elucidated to date. In this context, modulation of the class IIb HDAC6 has been reported to play a key role in the

regulation of cytoskeletal preservation and functioning, particularly through tubulin deacetylation mechanisms that underpin cellular morphology (Valenzuela-Fernández et al. 2009). In this study, pan-HDACi TSA and SAHA confirmed the occurrence of structural remodelling in AC10 cells, however the HDAC6 class IIb-selective inhibitor tubacin did not elicit any detectable morphological or cytotoxic changes, therefore suggesting either that HDACi-induced structural perturbations are not solely dependent upon HDAC6 or that the cytoskeletal structure is less affected by tubulin in this model. The proposition that HDACi-induced structural changes may depend on off-target secondary pharmacological activity was further supported by the assessment of acetylation levels of relevant HDACi targets in AC10 cells: these results confirmed that cellular morphological changes occurred even at sub-pharmacologically active pan-HDACi concentrations . A study proposed by Lee et al. identified the onset of mitochondrial elongation following treatment with SAHA in non-cardiac *in-vitro* primary cell models, with elongation being irrespective of apoptotic induction (Lee et al. 2012). Furthermore, the study also reported that mitochondrial elongation was not correlated with microtubule-dependent mechanisms, but rather on the downregulation of two proteins involved in mitochondrial morphology modulation (Lee et al. 2012). Since cardiomyocytes possess the highest amount of mitochondria of any tissue due to the high energetic and metabolic requirements necessary for cardiac contractility, with mitochondria located in abundance throughout the cell (Sabbah 2020), it is possible that structural remodelling and morphological changes resulting in AC10 elongation could be a consequence of mitochondrial-related structural toxicity. While pan-HDACis were shown to induce changes in mitochondrial respiration in the HL-1 model (chapter 4), further studies are required to investigate structural mitochondrial and metabolic toxicity in this model. Overall, the studies on 2D monolayers support the use of the AC10 model for preliminary drug-induced structural toxicity.

While ease-of-use and accessibility of AC10 monolayers could provide a convenient platform to complement preclinical *in-vitro* assessments, several limitations associated with the cardiac representative nature this model still remain, primarily in relation to the rapid AC10 turnover rate and pre-differentiated state, single cell lineage, and monolayer structure limiting cellular interactions and communications. Advanced three-dimensional culture techniques were therefore hypothesised to enhance AC10 cardiac properties and subsequently improve the applicability of this model. Previous studies have demonstrated the importance of 3D

microenvironments in terms of providing superior performance and functionality of various models over respective 2D monolayer cultures (Gaskell et al. 2016). For example, several liver spheroid models have been characterised, and have demonstrated increased expression of tissue-specific markers, enhanced metabolic functionality and an improved sensitivity to toxic insults (Gaskell et al. 2016). These improvements have been strictly associated with the presence of a 3D microenvironment and a physiologically relevant extracellular matrix, which allows to enhance cell-cell interactions and ultimately mimics *in-vivo* systems. Several expandable cell line spheroid models are now routinely used in preclinical screening, as in the case of the immortalised hepatic line HepG2, which has demonstrated reduced proliferative rates when cultured in 3D spheroids (Wrzesinski et al. 2014). On this basis, an objective of this study was to evaluate and characterise for the first time the utility of AC10 cells for preclinical cardiotoxicity studies in three-dimensional spheroid cultures. This study confirmed that AC10 cells can be used to successfully construct single-lineage monoculture spheroids as well as multi-lineage triculture spheroids (section 5.2.3). Both monoculture and triculture cardiac spheroids have been previously characterised using hiPSC-CMs in combination with non-myocyte cells, demonstrating enhanced phenotypical maturity and contractility (Ravenscroft et al. 2016; Tomlinson et al. 2019). In this study, AC10 spheroids cultured with a standardised starting cell number of 500 cells/well (Ravenscroft et al. 2016), were cultured for a maximum of 20 days before displaying signs of cell death and spheroid disruption (section 5.2.3). The observed disruption of spheroids can be attributed to the inability of media nutrient and oxygen to efficiently diffuse through the spheroid tissue as the spheroid grows in size, leading to the formation of a necrotic core and ultimately leading to cell death (Barisam et al. 2018). Previous studies have shown that successful oxygenation can be achieved in spheroids ≤ 400 µm, therefore AC10 spheroids were grown between 7 and 14 days, reaching a size sufficient to minimise the impact of a necrotic core formation (Mittler et al. 2017; Gaskell et al. 2016). Nonetheless, despite the culturing time span limitations that depend on the formation of a necrotic region, AC10 spheroids demonstrated successful viability for a longer period than 2D monolayer cultures, with spheroids fully viable for at least 14 days, and non-passaged monolayers viable for ≤ 80 hours post initial seeding. Investigations on the internal AC10 spheroid structure revealed the formation of an organised extracellular matrix, as evidenced by immunofluorescent staining of the F-actin network (section 5.2.3). Both AC10 monoculture and triculture spheroids however did not achieve syncytial or sarcomeric formation, as

indicated by the uneven presence of cardiac troponin I, in line with the pre-differentiated phenotypical features of the AC10 model (Davidson et al. 2005). It remains yet to be determined whether an improved syncytial formation could be achieved with dedicated work involving the promotion of terminal differentiation of AC10 cells into functional myocytes. Lastly, in AC10 tricultures, non-myocyte cell organisation within the spheroid evidenced the formation of a complex extracellular matrix network due to the presence of cardiac fibroblasts, as well as cardiac endothelial cell clustering reminiscent of rudimental vessel formation (section 5.2.3).

Following the successful establishment of AC10 spheroids, the last phase of this study focused on the evaluation of the effects of HDACi compounds against AC10 spheroids. In this context, initial investigations revealed a remarkably enhanced sensitivity of AC10 spheroids to pan-HDACi compounds compared to 2D monolayers (section 5.3.4.1). Similarly, enhanced spheroid chemosensitivity to toxic insults has been reported with the use of hepatic spheroids, where these have demonstrated higher sensitivity to relevant hepatotoxins, and consequently provided an improved toxicological predictivity profile (Gaskell et al, 2016).

The pan-HDACIs were demonstrated to cause a whole-spheroid morphological shape change following exposure to sub-cytotoxic concentrations, causing structural remodelling from a spherical to an elliptical shape. Ultrastructural investigations demonstrated release of cardiac troponin I as a consequence of TSA exposure, particularly evident at cytotoxic concentrations, where a marked disruption to the cytoskeletal F-actin filaments was also detected. Concomitant intra-spheroid accumulation of troponin I (cTnI) and cytoskeletal f-actin alterations were also identified at sub-cytotoxic concentrations of TSA, but not SAHA, plausibly due to the higher pharmacological potency of TSA (Smith et al. 2010). Remarkably, fragmentation of the F-actin network occurred at all tested pan-HDACi concentrations. Studies have recently reported a HDACi-mediated effect on molecular pathways linked with cardiac remodelling, including the regulation of several proteins associated with cytoskeletal organization, cell-cell and cell-matrix interaction, metabolism, inflammation, and dysfunction of mitochondria in a cardiac *in-vivo* murine model (Scholz et al. 2019). The findings presented in this chapter clearly demonstrate the occurrence of pan-HDACi-induced structural modifications occurring at the cytoskeletal level in in both 2D and 3D AC10 cultures, and

therefore support the relevance of this model in the detection of drug-mediated structural cardiotoxicity.

When evaluated under a comparative perspective, AC10 spheroids demonstrated a superior applicability over 2D monolayers for the preliminary screening of structural effects, because of greater cellular stability, multicellular capability, and a more relevant structural physiological representation. Given the prolonged culturing time span which allows the use of repeated/long term compound additions, AC10 spheroids provide a scalable and human-derived model that can be used in both high-throughput applications, or in advanced multi-system bioreactor and organ-on-chip technologies. Although further protocol optimisation is required to enhance the cardiac phenotype of AC10 cells, this study supports the use of both 2D and 3D AC10 models in conjunction with currently existing methodologies, and provides the basis for further applications within the early-drug discovery pipeline.

6 General Discussion

6.1 Project outcomes

Cardiotoxicity is a major cause of drug attrition (Laverty et al. 2011; Weaver and Valentin 2019). Recent advances in drug discovery have determined the need for the development of improved *in-vitro* models that could accurately detect drug candidates with cardiac liabilities sufficiently early in the drug discovery pipeline (Gintant, Sager, and Stockbridge 2016b; Laverty et al. 2011). This would avoid their progression into late-stage project phases, ultimately maximising the advancement of safer novel drug candidates, and consequently reducing the cost of drug development. Current assessments of *in-vitro* preclinical drug-induced cardiotoxicity predominantly rely on an integrated screening system of methodologies, evaluating acute proarrhythmic effects that could alter the electrical function of the heart. However, the current screening paradigm has several limitations for robust assessment of drug-induced cardiotoxicities, particularly in terms of longer-term assessments, instability and reduced longevity of cellular models and high experimental cost. Furthermore, drug-induced cardiotoxicity is known to be a multifaceted process involving both functional and structural cellular changes, with current models focusing almost exclusively on drug-induced functional changes and drug-induced proarrhythmias, with limited scope for evaluation of morphological and structural cardiac cellular change. As such, there is an evident shortfall of models suitable for predictivity of structural cardiotoxicities

On this basis, the overall aim of this project was the development and characterisation of *in-vitro* cardiac cell models, along with the development of novel protocols, designed to be integrated with current methodologies for an enhanced detection of drug-induced cardiotoxicity. In this context, a particular focus was dedicated to the qualification of *in-vitro* models for the early screening of structural cardiotoxicity. The main outcomes of this thesis can be summarised as follows:

1 This study demonstrated the successful development of a novel protocol for the use of the HL-1 murine atrial cell model in combination with impedance-based technologies (xCELLigence Cardio system), and qualified the HL-1 model for functional and structural drug-induced cardiotoxicity studies.

2 This study characterised the use of the AC10 human ventricular cell line for the detection of structural drug-induced liabilities in two-dimensional monolayers through the use of impedance-based technologies (xCELLigence DP system), and established for the first time the use of AC10 three-dimensional spheroids for the detection of drug-induced structural cardiotoxicity.

3 Lastly, through the integrated application of established hiPSC-CM *in-vitro* assays alongside the newly developed protocols, this study elucidated previously unexplored structural cardiotoxicity mechanisms induced by the histone deacetylase inhibitor class of molecular-targeted therapeutics.

6.2 Integrative use of in-vitro models for preclinical detection of cardiotoxicity is beneficial to maximise predictivity

At present, preclinical screening of drug-induced cardiotoxicity involves predominantly a multi-step approach of *in-vitro* and *in-vivo* methodologies, with a marked focus on the detection of proarrhythmias that could lead to Torsade de Pointes (TdP) (E14/S7B 2020; Gintant, Sager, and Stockbridge 2016a). Under a regulatory perspective, *in-vivo* tests are still fundamentally required, particularly for the assessment of multiparameter physiological and pathological cardiac disturbances, integration of ADME principles into the context of drug fate and subsequent toxicity, and ultimately integrated assessment, as outlined in the ICH E14 and S7B guidelines (E14/S7B 2020). However, despite their imperative utility, the clinic translation of animal models are hindered by inter-species and metabolic differences. This in combination with restrictive scope of current *in-vitro* methodologies, namely the hERG assay, has led to either underdetection of cardiac liabilities, or false-positive findings and thus unwarranted drug attrition (Fermini et al. 2016). Furthermore, there is now an appreciation that this screening approach has overestimated the potential for drug-induced clinical proarrhythmia and the retardation of development of several viable drug candidates (Fermini et al. 2016).

The advent of commercial human-derived induced pluripotent stem (hiPSC) cells has undoubtedly revolutionised the standardisation of preclinical investigations *in-vitro*, allowing the design of more comprehensive high-throughput screening, particularly when combined with multiparametric assays. The use of hiPSC derived cardiomyocytes (hiPSC-CM) is

increasingly becoming implemented in standardised preclinical investigations, both using two-dimensional and three-dimensional technologies to detect acute functional liabilities (Ribeiro et al. 2019), where hiPSC-CMs have demonstrated good predictivity for highly torsadogenic compounds (Blinova et al. 2018). Subsequently, this has resulted in development of a new screening paradigm to potentially integrate the hERG-focused approach (the CiPA initiative), incorporating *in silico* toxicity prediction and evaluation of drug candidates on hiPSC-CM, followed by evaluations *in vivo* ("Https://Cipaproject.Org/" n.d.; Cavero and Holzgrefe 2015). However, despite this significant advancement in preclinical drug-induced cardiotoxicity predictions, incorporating a focus on human cells, the use of hiPSC-CMs is partially hindered by a number of unresolved limitations, particularly in relation to the short culturing time span, persisting electrophysiological phenotype incongruities, lack of consistency between different manufacturers which leads to different predictions (Holbrook 2019) and, not least, high maintenance costs. Some of these limitations were evidenced in this study (chapter 3), where hiPSC-CMs were used in combination with high-throughput impedance and multi-electrode electrophysiology assessments (xCELLigence Cardio ECR system), demonstrating inaccuracies in response to proarrhythmic compounds, including calcium channel blockers and autonomic drugs. While electrophysiological fallacies may be partially revised through protocol optimisation and the advancement of multi-parametric technologies, challenges remain as to the full utility of these cell models.

Despite hiPSC-CMs significantly improving the identification of drug-induced proarrhythmias, the relevance of this model for identification of drug-induced perturbations non-functional cardiotoxicity is very limited. This was exemplified in this thesis with the assessment of HDACi compounds, which have elicited the occurrence of morphological alterations imputable to structural cardiotoxic effects in the HL-1 and AC10 models, but not in hiPSC-CMs. One reason can be that current hiPSC-CM assays are mostly designed to detect acute effects that develop within a 24-48-hour timeframe, thus neglecting sub-acute and long-term effects. This is a key issue, considering many known structural cardiotoxic drugs (i.e., Anthracyclines) manifest some of their irreversible effects with a delayed onset, leading to heart failure (Curigliano et al. 2010; Findlay et al. 2019). Additionally, there is the possibility that hiPSC-CM models may elude the detection of acute structural cardiotoxicity endpoints, either because of insufficient assay sensitivity, or due to a lack of specific mechanistic toxicity understanding derived from

the increasing diversity of novel drug candidates. The use of complex modelling involving multifluidics and/or organ-on-chip systems paired with the use of hiPSC-CMs may improve the ability of this cell model to identify a level of structural liabilities. However, the need for specialised training, dedicated equipment and robust validation, alongside the high costs associated with the implementation of such systems have led to a low uptake of these technologies within the pharmaceutical sector to date (Gintant, Sager, and Stockbridge 2016b; Weaver and Valentin 2019). In this regard, the utilisation of a low-cost model with an enhanced sensitivity against structural cardiotoxicants finds its scope, particularly within a model informed drug design and discovery (MID3) perspective (Figure 6.1). The AC10 human ventricular cell line demonstrated a significant sensitivity to HDACi-induced toxicity, both in two-dimensional and three-dimensional models, and enabled the early identification of sub-acute morphological changes occurring even at sub-pharmacologically active concentrations (chapter 5). Similarly, the HL-1 murine atrial cell line exhibited structural and contractile alterations in response to HDACi compounds, showcasing sub-acute irreversible changes in contractility and mitochondrial toxicity (chapter 4). The integrated use of these models, in 2D and 3D, was therefore essential in the early identification of several potential mechanisms underpinning HDACi-induced off-target cardiotoxicity. These newly identified effects, including cytoskeletal remodelling, cardiac troponin release, delayed-onset (≥ 80 hours) of contractile aberrations and metabolic changes, were *de facto* undetected in hiPSC-CM models exposed to similar drug concentrations. While HDACi-induced cardiac effects have previously been reported *in-vitro* (Kopljar et al. 2016) and *in-vivo* (Wallner et al. 2020; Kuai et al. 2016; Freundt et al. 2019), these were exclusively determined at pharmacologically active, supra-pharmacological, or elevated cytotoxic concentrations. The proposed HDACi off-target mechanisms defined with the use of HL-1 and AC10 models are indeed supportive of several recent *in-vivo* findings, where HDACis have been linked to reduction of left-ventricular hypertrophy (and thus cardiac restructuring) in a HFpEF model (Wallner et al. 2020). In this context, the studies presented herein have demonstrated the occurrence of structural and morphological cardiomyocyte remodelling: while the reduction of cardiac hypertrophy may be considered as a cardioprotective effect under a pathological perspective, the occurrence of structural remodelling in healthy subjects may in fact underpin cardiotoxicity (M. H. Shah et al. 2006). In this regard, these studies prove that a full elucidation of HDACi-induced cardiac remodelling in non-pathological *in-vivo* models is needed.

This work additionally supports the use of HL-1 and AC10 models for the assessment of cardiotoxicity of highly promiscuous drugs, such is the case of HDACi, where an exhaustive record of molecular targets has not been fully defined. Despite the initial *in-vitro* pharmacological profiling that is routinely performed against a panel of undesirable targets (Jenkinson et al. 2020), It has been reported that highly promiscuous drugs are more likely to be discontinued during late-stage clinical development as a result of latent secondary pharmacology (off-target) effects (Bowes et al. 2012; Valentin et al. 2018). The scalable use of a battery of 2D and 3D models paired with high-content assessments can therefore not only aid the early identification of hazards, but also assist in the identification of on-and-off target effects that can inform and direct subsequent *in-vivo* toxicity studies.

As demonstrated throughout the studies presented in this thesis, the synergistic use of two-dimensional and three-dimensional cell line-based models provides an effective and scalable strategy for the enhancement of early hazard identification, which can guide and, and consequently maximise, the design of complementary studies in existing models.

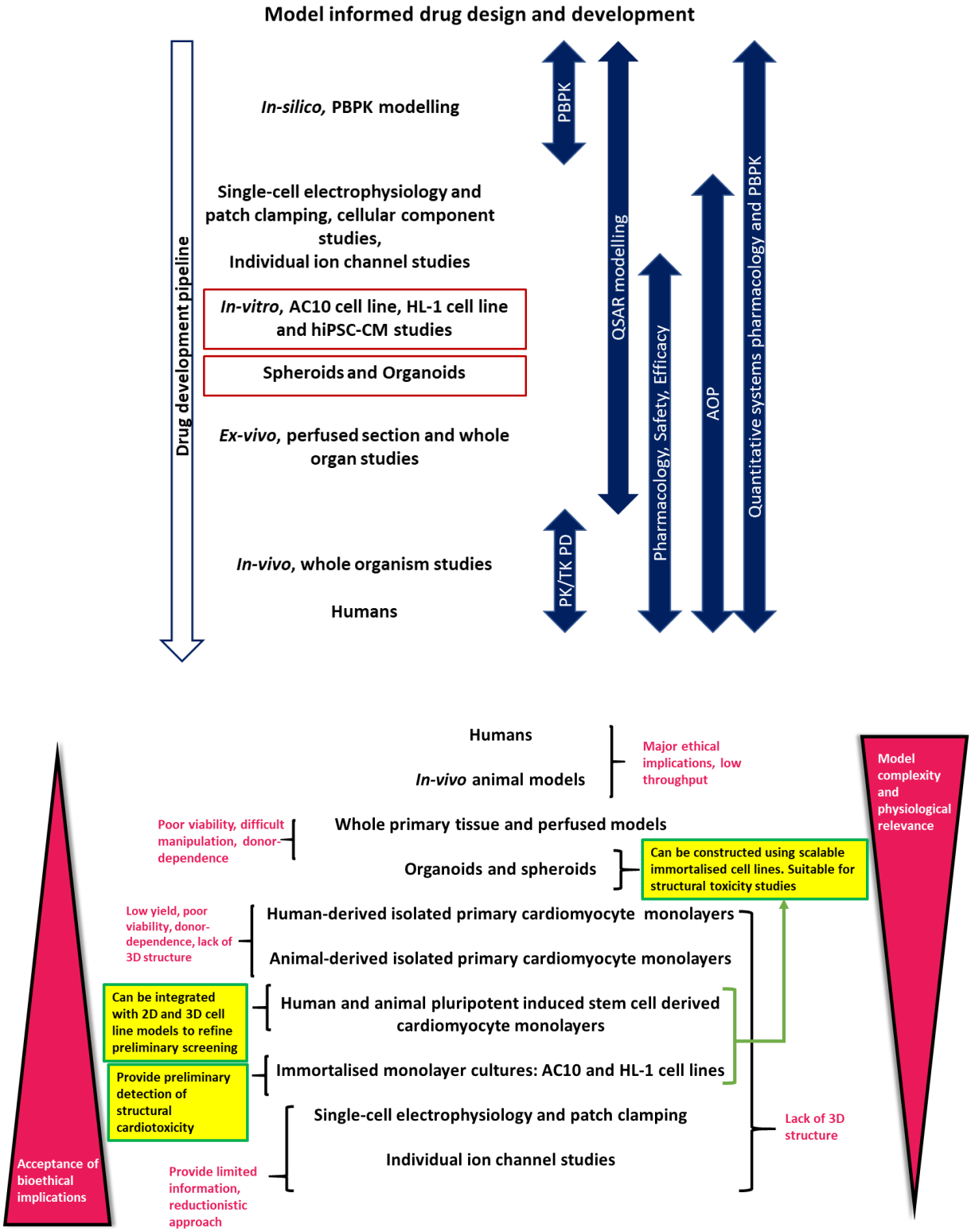

Figure 6.1 Integrated use of cardiac models for cardiotoxicity screening. 2D and 3D cell line-based models characterised in this thesis can be integrated to enhance preclinical cardiotoxicity screening and early hazard identification in the drug discovery process. The complexity of these models can be upscaled for high-throughput applications (2D systems), or downscaled for use in bioreactor/organ-on-chip technologies (3D systems).

Model	*Suitability for functional cardiotoxicity studies*	*Suitability for structural cardiotoxicity studies*	*Use in 3D cultures*	*Suitability for long-term studies*	*Accessibility*
hiPSC-CM	**Model is widely used for acute functional studies**	**Very limited for acute studies, not established for long-term studies**	**Established** (Ravenscroft et al. 2016)	• **2D: validated for up to 48 hours experimental window** • **3D: up to 28 days**	**High maintenance cost. Not expandable**
HL-1 murine atrial cell line	**Characterised for use with patch clamping** (Kammonen et al. 2017) **Characterised with impedance systems**	**Yes, can be used for mechanistic studies. Demonstrated structural cardiotoxicity to HDACi**	**Forms spheroids with CF and EC*. Characterisation is required**	• **2D: up to 150 hours between passages** • **3D: up to 14 days***	**Low cost. Expandable**
AC10 human ventricular cell line	**Model lacks syncytia and sarcomere structures, therefore is not suitable for contractility assays**	**Can be used for mechanistic studies. Demonstrated structural cardiotoxicity to anthracyclines and HDACi**	**Forms spheroid as mono and triculture with CF and EC. Demonstrated structural cardiotoxicity to HDACi**	• **2D: up to 72 hours between passages** • **3D: up to 20 days**	**Low cost. Expandable**

Table 6-1. Summary of appraised *in-vitro* cardiac models, evaluated for their suitability for the detection of functional, structural cardiotoxicity studies, use in 3D cultures and suitability for long-term and sub-acute studies. Suitability for each category is classified as *Good*, *Not fully established*, *Poor*. *HL-1 spheroid preliminary data is presented in Appendix 1

6.3 Limitations and future perspectives

The integration of multiple models and technologies is crucial for the effective investigation of drug-induced cardiotoxicity. While the proposed novel protocols presented in this thesis could offer additional resources to be integrated within the constantly evolving screening paradigms, a few limitations need to be considered. Most efforts *in-vitro* have thus far been centred on the detection of cardiotoxic effects on cardiac myocytes. Even though cardiomyocytes are indeed the cell type primarily involved in cardiac contractility, *in-vivo* these cells rely on the synergistic interaction with other cell lineages, including cardiac fibroblasts and endothelial cells. Given the multifactorial nature of xenobiotic toxicity, more heterogeneous and physiologically representative models are needed to fully evaluate cardiotoxicity. The lack of cell lineage diversity is a well-established limitation of current *in-vitro* models, and studies aimed at the construction of three-dimensional multi-lineage co-cultures have partly attempted to resolve the issue (Wrzesinski et al. 2014; Ravenscroft et al. 2016; Tomlinson et al. 2019) . Work in this thesis has demonstrated the successful construction of 3D multi-lineage spheroids, however, despite the tangible advantages of 3D microtissues and spheroids over 2D platforms, tissue perfusion and functional vascularisation of such cultures remains an unresolved aspect. The development of protocols aimed at achieving successful vascularisation would plausibly determine a significant improvement in model complexity and, consequently, positively impact their predictive power. Additionally, the integration of cardiac models into multi-compartmental/multi-organ bioreactors could further enhance predictivity, however standardisation and accessibility of such methodologies should be revised. In this context, the development of novel 3D bioprinting technologies is demonstrating a promising potential.

In-vitro-in-vivo extrapolation (IVIVE) and data translatability is another key limitation associated with the use of *in-vitro* models that requires improvements (Weaver and Valentin 2019). The continuous optimisation of more representative and complex models that support multiparametric and long-term studies can advance the mechanistic understanding of drug-induced toxicity, and therefore assist in the process of data extrapolation and translation to the clinic. The mechanistic understanding of specific toxicities is however partly hindered by

the limited genotype that hiPSC-CMs and cell lines offer, as these are limited to a single genotype (derived from individual donor/progenitor cell) that does not necessarily reflect the wider population, particularly when it comes to the detection of cardiotoxicity in patient populations with co-morbidities (Poluzzi et al. 2017). The availability of more complex standardised models can certainly enhance in-vitro-in-vivo translatability, nonetheless future efforts should also be directed towards the implementation of more genotypically inclusive models.

The use of multiple models and assays inevitably leads to the generation of an extensive amount of data. In this context, significant advances in the use of machine learning and artificial intelligence could further maximise preclinical data extrapolation. These innovative approaches have the potential of revolutionising the vast amount of data analysis that derives from the integration of increasingly complex high throughput assays and models (Basile, Yahi, and Tatonetti 2019). It is hoped that, in the near future, efforts will be made to incorporate these innovative approaches to improve drug safety science.

References

Abassi, Yama A., Biao Xi, Nan Li, Wei Ouyang, Alexander Seiler, Manfred Watzele, Ralf Kettenhofen, et al. 2012. “Dynamic Monitoring of Beating Periodicity of Stem Cell-Derived Cardiomyocytes as a Predictive Tool for Preclinical Safety Assessment.” *British Journal of Pharmacology* 165 (5): 1424–41. https://doi.org/10.1111/j.1476-5381.2011.01623.x.

Adamcova, Michaela, Veronika Skarkova, Jitka Seifertova, and Emil Rudolf. 2019. “Cardiac Troponins Are Among Targets of Doxorubicin-Induced Cardiotoxicity in HiPCS-CMs.” *International Journal of Molecular Sciences Article*. https://doi.org/10.3390/ijms20112638.

Alameddine, Raafat S., Ahmad Sharif Yakan, Hadi Skouri, Deborah Mukherji, Sally Temraz, and Ali Shamseddine. 2014. “Cardiac and Vascular Toxicities of Angiogenesis Inhibitors: The Other Side of the Coin.” *Critical Reviews in Oncology/Hematology*. Elsevier Ireland Ltd. https://doi.org/10.1016/j.critrevonc.2015.05.004.

Álamo, Juan C. del, Derek Lemons, Ricardo Serrano, Alex Savchenko, Fabio Cerignoli, Rolf Bodmer, and Mark Mercola. 2016. “High Throughput Physiological Screening of IPSC-Derived Cardiomyocytes for Drug Development.” *Biochimica et Biophysica Acta - Molecular Cell Research*. https://doi.org/10.1016/j.bbamcr.2016.03.003.

Ando, Hiroyuki, Takashi Yoshinaga, Wataru Yamamoto, Keiichi Asakura, Takaaki Uda, Tomohiko Taniguchi, Atsuko Ojima, et al. 2017. “A New Paradigm for Drug-Induced Torsadogenic Risk Assessment Using Human IPS Cell-Derived Cardiomyocytes.” *Journal of Pharmacological and Toxicological Methods*. https://doi.org/10.1016/j.vascn.2016.12.003.

Babuin, Luciano, and Allan S. Jaffe. 2005. “Troponin: The Biomarker of Choice for the Detection of Cardiac Injury.” *CMAJ : Canadian Medical Association Journal* 173 (10): 1191. https://doi.org/10.1503/CMAJ.050141.

Backs, Johannes, Kunhua Song, Svetlana Bezprozvannaya, Shurong Chang, and Eric N. Olson. 2006. “CaM Kinase II Selectively Signals to Histone Deacetylase 4 during Cardiomyocyte Hypertrophy.” *Journal of Clinical Investigation* 116 (7): 1853–64. https://doi.org/10.1172/JCI27438.

Bagnes, Claudia, Patricia Panchuk, and Gonzalo Recondo. 2009. “Antineoplastic Chemotherapy Induced QTc Prolongation.” *Current Drug Safety* 5 (1): 93–96. https://doi.org/10.2174/157488610789869111.

Banerjee, Amitava, Robin Chung, and Arjun Kumar Ghosh. 2018. “Open Access Cardiotoxicity: Precision Medicine with Imprecise Definitions.” *Open Heart* 5: 774.

https://doi.org/10.1136/openhrt-2018-000774.

Barisam, Maryam, Mohammad Said Saidi, Navid Kashaninejad, and Nam Trung Nguyen. 2018. “Prediction of Necrotic Core and Hypoxic Zone of Multicellular Spheroids in a Microbioreactor with a U-Shaped Barrier.” *Micromachines* 9 (3). https://doi.org/10.3390/mi9030094.

Bartos, Daniel C., Eleonora Grandi, and Crystal M. Ripplinger. 2015. “Ion Channels in the Heart.” In *Comprehensive Physiology*, 5:1423–64. Hoboken, NJ, USA: John Wiley & Sons, Inc. https://doi.org/10.1002/cphy.c140069.

Basile, Anna O., Alexandre Yahi, and Nicholas P. Tatonetti. 2019. “Artificial Intelligence for Drug Toxicity and Safety.” *Trends in Pharmacological Sciences*. Elsevier Ltd. https://doi.org/10.1016/j.tips.2019.07.005.

Becker, Lore, Melanie Schmitt Nogueira, Caroline Klima, Martin Hrabe De Angelis, and Shahaf Peleg. 2018. “Rapid and Transient Oxygen Consumption Increase Following Acute HDAC/KDAC Inhibition in Drosophila Tissue.” *Scientific Reports* 8 (1): 1–7. https://doi.org/10.1038/s41598-018-22674-2.

Bellinger, Andrew M., Carlos L. Arteaga, Thomas Force, Benjamin D. Humphreys, George D. Demetri, Brian J. Druker, and Javid J. Moslehi. 2015. “Cardio-Oncology: How New Targeted Cancer Therapies and Precision Medicine Can Inform Cardiovascular Discovery.” *Circulation*. Lippincott Williams and Wilkins. https://doi.org/10.1161/CIRCULATIONAHA.115.010484.

Bendels, Stefanie, Caterina Bissantz, Bernhard Fasching, Grégori Gerebtzoff, Wolfgang Guba, Manfred Kansy, Jacques Migeon, et al. 2018. “Safety Screening in Early Drug Discovery: An Optimized Assay Panel.” *Journal of Pharmacological and Toxicological Methods* 99 (September). https://doi.org/10.1016/j.vascn.2019.106609.

Bergmann, Olaf, Sofia Zdunek, Anastasia Felker, Mehran Salehpour, Kanar Alkass, Samuel Bernard, Staffan L. Sjostrom, et al. 2015. “Dynamics of Cell Generation and Turnover in the Human Heart.” *Cell* 161 (7): 1566–75. https://doi.org/10.1016/j.cell.2015.05.026.

Bers, Donald. 2002. “Cardiac Excitation–Contraction Coupling.” *Nature* 415: 198–205. https://doi.org/10.1038/415198a.

Blinova, Ksenia, Qianyu Dang, Daniel Millard, Godfrey Smith, Jennifer Pierson, Liang Guo, Mathew Brock, et al. 2018. “International Multisite Study of Human-Induced Pluripotent Stem Cell-Derived Cardiomyocytes for Drug Proarrhythmic Potential Assessment.” *Cell Reports*. https://doi.org/10.1016/j.celrep.2018.08.079.

Bowes, Joanne, Andrew J. Brown, Jacques Hamon, Wolfgang Jarolimek, Arun Sridhar, Gareth Waldron, and Steven Whitebread. 2012. “Reducing Safety-Related Drug Attrition: The Use of in Vitro Pharmacological Profiling.” *Nature Reviews Drug Discovery*. Nature Publishing Group. https://doi.org/10.1038/nrd3845.

Bü, Roland W, Christopher A Luckhurst, Omar Aziz, Kim L Matthews, Dawn Yates, Kathy A Lyons, Maria Beconi, et al. 2013. “Design, Synthesis, and Biological Evaluation of Potent and Selective Class IIa Histone Deacetylase (HDAC) Inhibitors as a Potential Therapy for Huntington’s Disease.” https://doi.org/10.1021/jm4011884.

Callaghan, Neal I., Shin Haw Lee, Sina Hadipour-Lakmehsari, Xavier A. Lee, M. Ahsan Siraj, Amine Driouchi, Christopher M. Yip, Mansoor Husain, Craig A. Simmons, and Anthony O. Gramolini. 2020. "Functional Culture and in Vitro Genetic and Small-Molecule Manipulation of Adult Mouse Cardiomyocytes." *Communications Biology* 3 (1): 1–10. https://doi.org/10.1038/s42003-020-0946-9.

Cardinale, Daniela Maria, Martina Zaninotto, Carlo Maria Cipolla, Claudio Passino, Mario Plebani, and Aldo Clerico. 2020. "Cardiotoxic Effects and Myocardial Injury: The Search for a More Precise Definition of Drug Cardiotoxicity." *Clinical Chemistry and Laboratory Medicine* 1 (ahead-of-print). https://doi.org/10.1515/cclm-2020-0566.

Cavero, Icilio, Jean Michel Guillon, Veronique Ballet, Mike Clements, Jean Frédéric Gerbeau, and Henry Holzgrefe. 2016. "Comprehensive in Vitro Proarrhythmia Assay (CiPA): Pending Issues for Successful Validation and Implementation." *Journal of Pharmacological and Toxicological Methods*. https://doi.org/10.1016/j.vascn.2016.05.012.

Cavero, Icilio, and Henry Holzgrefe. 2015. "CiPA: Ongoing Testing, Future Qualification Procedures, and Pending Issues." *Journal of Pharmacological and Toxicological Methods* 76 (November): 27–37. https://doi.org/10.1016/j.vascn.2015.06.004.

Chen, William C.W., James E. Baily, Mirko Corselli, Mary E. Díaz, Bin Sun, Guosheng Xiang, Gillian A. Gray, Johnny Huard, and Bruno Péault. 2015. "Human Myocardial Pericytes: Multipotent Mesodermal Precursors Exhibiting Cardiac Specificity." *Stem Cells* 33 (2): 557–73. https://doi.org/10.1002/stem.1868.

Claycomb, William C, Nicholas A Lanson, Beverly S Stallworth, Daniel B Egeland, Joseph B Delcarpio, Anthony Bahinski, and Nicholas J Izzo. 1998. "HL-1 Cells: A Cardiac Muscle Cell Line That Contracts and Retains Phenotypic Characteristics of the Adult Cardiomyocyte (Simian Virus 40 T Oncogenepotassium Channelsdofetilide)." *Cell Biology*. Vol. 95. www.pnas.org.

Clements, Mike, Val Millar, Angela S. Williams, and Sian Kalinka. 2015. "Bridging Functional and Structural Cardiotoxicity Assays Using Human Embryonic Stem Cell-Derived Cardiomyocytes for a More Comprehensive Risk Assessment." *Toxicological Sciences*. https://doi.org/10.1093/toxsci/kfv180.

Correia, Cláudia, Alexey Koshkin, Patrícia Duarte, Dongjian Hu, Ana Teixeira, Ibrahim Domian, Margarida Serra, and Paula M. Alves. 2017. "Distinct Carbon Sources Affect Structural and Functional Maturation of Cardiomyocytes Derived from Human Pluripotent Stem Cells." *Scientific Reports* 7 (1): 1–17. https://doi.org/10.1038/s41598-017-08713-4.

Curigliano, Giuseppe, Erica L. Mayer, Harold J. Burstein, Eric P. Winer, and Aron Goldhirsch. 2010. "Cardiac Toxicity from Systemic Cancer Therapy: A Comprehensive Review." *Progress in Cardiovascular Diseases*. W.B. Saunders. https://doi.org/10.1016/j.pcad.2010.05.006.

Daimi, Houria, Estefania Lozano-Velasco, Amel Haj Khelil, Jemni B.E. Chibani, Adriana Barana, Irene Amorós, Marta González De La Fuente, Ricardo Caballero, Amelia Aranega, and Diego Franco. 2015. "Regulation of SCN5A by MicroRNAs: MiR-219 Modulates SCN5A Transcript Expression and the Effects of Flecainide Intoxication in Mice." *Heart Rhythm*

12 (6): 1333–42. https://doi.org/10.1016/j.hrthm.2015.02.018.

Darpo, Borje, Christine Garnett, Charles T. Benson, James Keirns, Derek Leishman, Marek Malik, Nitin Mehrotra, et al. 2014. “Cardiac Safety Research Consortium: Can the Thorough QT/QTc Study Be Replaced by Early QT Assessment in Routine Clinical Pharmacology Studies? Scientific Update and a Research Proposal for a Path Forward.” *American Heart Journal*. https://doi.org/10.1016/j.ahj.2014.06.003.

Darpo, Borje, Thierry Nebout, and Philip T. Sager. 2006. “Clinical Evaluation of QT/QTc Prolongation and Proarrhythmic Potential for Nonantiarrhythmic Drugs: The International Conference on Harmonization of Technical Requirements for Registration of Pharmaceuticals for Human Use E14 Guideline.” *Journal of Clinical Pharmacology*. Vol. 46. https://doi.org/10.1177/0091270006286436.

Davidson, Mercy M., Claudia Nesti, Lluis Palenzuela, Winsome F. Walker, Evelyn Hernandez, Lev Protas, Michio Hirano, and Nithila D. Isaac. 2005. “Novel Cell Lines Derived from Adult Human Ventricular Cardiomyocytes.” *Journal of Molecular and Cellular Cardiology* 39 (1): 133–47. https://doi.org/10.1016/j.yjmcc.2005.03.003.

Delcuve, Geneviève P., Dilshad H. Khan, and James R. Davie. 2012. “Roles of Histone Deacetylases in Epigenetic Regulation: Emerging Paradigms from Studies with Inhibitors.” *Clinical Epigenetics*. BioMed Central. https://doi.org/10.1186/1868-7083-4-5.

Dias, Priyanthi, Thomas Desplantez, Majd A. El-Harasis, Rasheda A. Chowdhury, Nina D. Ullrich, Alberto Cabestrero De Diego, Nicholas S. Peters, Nicholas J. Severs, Kenneth T. MacLeod, and Emmanuel Dupont. 2014. “Characterisation of Connexin Expression and Electrophysiological Properties in Stable Clones of the Hl-1 Myocyte Cell Line.” *PLoS ONE*. https://doi.org/10.1371/journal.pone.0090266.

Doherty, Kimberly R., Dominique R. Talbert, Patricia B. Trusk, Diarmuid M. Moran, Scott A. Shell, and Sarah Bacus. 2015. “Structural and Functional Screening in Human Induced-Pluripotent Stem Cell-Derived Cardiomyocytes Accurately Identifies Cardiotoxicity of Multiple Drug Types.” *Toxicology and Applied Pharmacology*. https://doi.org/10.1016/j.taap.2015.03.008.

Dong, Jerry, and Hong Chen. 2018. “Cardiotoxicity of Anticancer Therapeutics.” *Frontiers in Cardiovascular Medicine*. Frontiers Media S.A. https://doi.org/10.3389/fcvm.2018.00009.

Dong, Zengxiang, Chaolan Lin, Yujiao Liu, Hongbo Jin, Hong Wu, Zhenjun Li, Liping Sun, et al. 2017. “Upregulation of Sestrins Protect Atriums against Oxidative Damage and Fibrosis in Human and Experimental Atrial Fibrillation.” *Scientific Reports* 7 (April). https://doi.org/10.1038/srep46307.

Dy, Grace K., and Alex A. Adjei. 2013. “Understanding, Recognizing, and Managing Toxicities of Targeted Anticancer Therapies.” *CA: A Cancer Journal for Clinicians* 63 (4): 249–79. https://doi.org/10.3322/caac.21184.

E14/S7B. 2005. “ICH Topic S 7 B The Nonclinical Evaluation of the Potential for Delayed Ventricular Repolarization (QT Interval Prolongation) by Human Pharmaceuticals Step 5 NOTE FOR GUIDANCE ON THE NONCLINICAL EVALUATION OF THE POTENTIAL FOR

DELAYED VENTRICULAR REPOLARI.” http://www.emea.eu.int.

E14/S7B, ICH guideline. 2020. “International Council for Harmonisation of Technical Requirements for Pharmaceuticals for Human Use ICH E14/S7B Implementation Working Group: Clinical and Nonclinical Evaluation of QT/QTc Interval Prolongation and Proarrhythmic Potential Questions and Ans.” http://www.ich.org.

Ebert, Antje, Amit U. Joshi, Sandra Andorf, Yuanyuan Dai, Shrivatsan Sampathkumar, Haodong Chen, Yingxin Li, et al. 2019. “Proteasome-Dependent Regulation of Distinct Metabolic States during Long-Term Culture of Human IPSC-Derived Cardiomyocytes.” *Circulation Research* 125 (1): 90–103. https://doi.org/10.1161/CIRCRESAHA.118.313973.

Eimre, Margus, Kalju Paju, Sophie Pelloux, Nathalie Beraud, Mart Roosimaa, Lumme Kadaja, Marju Gruno, et al. 2008. “Distinct Organization of Energy Metabolism in HL-1 Cardiac Cell Line and Cardiomyocytes.” *Biochimica et Biophysica Acta - Bioenergetics* 1777 (6): 514–24. https://doi.org/10.1016/j.bbabio.2008.03.019.

Eschenhagen, Thomas, Thomas Force, Michael S. Ewer, Gilles W. De Keulenaer, Thomas M. Suter, Stefan D. Anker, Metin Avkiran, et al. 2011. “Cardiovascular Side Effects of Cancer Therapies: A Position Statement from the Heart Failure Association of the European Society of Cardiology.” *European Journal of Heart Failure* 13 (1): 1–10. https://doi.org/10.1093/eurjhf/hfq213.

Falkenberg, Katrina J., and Ricky W. Johnstone. 2014. “Histone Deacetylases and Their Inhibitors in Cancer, Neurological Diseases and Immune Disorders.” *Nature Reviews Drug Discovery*. https://doi.org/10.1038/nrd4360.

Fatima, Naheed, James F. Schooley, Willliam C. Claycomb, and Thomas P. Flagg. 2012. “Promoter DNA Methylation Regulates Murine SUR1 (Abcc8) and SUR2 (Abcc9) Expression in HL-1 Cardiomyocytes.” *PLoS ONE*. https://doi.org/10.1371/journal.pone.0041533.

Ferdinandy, Péter, István Baczkó, Péter Bencsik, Zoltán Giricz, Anikó Görbe, Pál Pacher, Zoltán V. Varga, András Varró, and Rainer Schulz. 2019. “Definition of Hidden Drug Cardiotoxicity: Paradigm Change in Cardiac Safety Testing and Its Clinical Implications.” *European Heart Journal*. Oxford University Press. https://doi.org/10.1093/eurheartj/ehy365.

Fermini, Bernard, Jules C. Hancox, Najah Abi-Gerges, Matthew Bridgland-Taylor, Khuram W. Chaudhary, Thomas Colatsky, Krystle Correll, et al. 2016. “A New Perspective in the Field of Cardiac Safety Testing through the Comprehensive in Vitro Proarrhythmia Assay Paradigm.” *Journal of Biomolecular Screening*. https://doi.org/10.1177/1087057115594589.

Feyen, Dries A.M., Wesley L. McKeithan, Arne A.N. Bruyneel, Sean Spiering, Larissa Hörmann, Bärbel Ulmer, Hui Zhang, et al. 2020. “Metabolic Maturation Media Improve Physiological Function of Human IPSC-Derived Cardiomyocytes.” *Cell Reports* 32 (3): 107925. https://doi.org/10.1016/j.celrep.2020.107925.

Fiegle, Dominik J., Tilmann Volk, and Thomas Seidel. 2020. “Isolation of Human Ventricular Cardiomyocytes from Vibratome-Cut Myocardial Slices.” *Journal of Visualized*

Experiments 2020 (159). https://doi.org/10.3791/61167.

Findlay, Simon G., Jason H. Gill, Ruth Plummer, Carol DeSantis, and Chris Plummer. 2019. "Chronic Cardiovascular Toxicity in the Older Oncology Patient Population." *Journal of Geriatric Oncology*, February. https://doi.org/10.1016/J.JGO.2019.01.018.

Földes, Gabor, Elena Matsa, János Kriston-Vizi, Thomas Leja, Stefan Amisten, Ljudmila Kolker, Thusharika Kodagoda, et al. 2014. "Aberrant α-Adrenergic Hypertrophic Response in Cardiomyocytes from Human Induced Pluripotent Cells." *Stem Cell Reports* 3 (5): 905–14. https://doi.org/10.1016/j.stemcr.2014.09.002.

Freundt, Johanna K., Gerrit Frommeyer, Tilmann Spieker, Fabian Wötzel, Jochen Schulze Grotthoff, Jörg Stypmann, Georg Hempel, et al. 2019. "Histone Deacetylase Inhibition by Entinostat for the Prevention of Electrical and Structural Remodeling in Heart Failure 11 Medical and Health Sciences 1102 Cardiorespiratory Medicine and Haematology." *BMC Pharmacology and Toxicology* 20 (1). https://doi.org/10.1186/s40360-019-0294-x.

Garg, Priyanka, Vivek Garg, Rajani Shrestha, Michael C Sanguinetti, Timothy J Kamp, and Joseph C Wu. 2018. "Human Induced Pluripotent Stem Cell-Derived Cardiomyocytes as Models for Cardiac Channelopathies: A Primer for Non-Electrophysiologists HHS Public Access." *Circ Res* 123 (2): 224–43. https://doi.org/10.1161/CIRCRESAHA.118.311209.

Gaskell, Harriet, Parveen Sharma, Helen E. Colley, Craig Murdoch, Dominic P. Williams, and Steven D. Webb. 2016. "Characterization of a Functional C3A Liver Spheroid Model." *Toxicology Research* 5 (4): 1053–65. https://doi.org/10.1039/c6tx00101g.

Gassanov, Natig, Fikret Er, Naufal Zagidullin, Marek Jankowski, Jolanta Gutkowska, and Uta C. Hoppe. 2008. "Retinoid Acid-Induced Effects on Atrial and Pacemaker Cell Differentiation and Expression of Cardiac Ion Channels." *Differentiation* 76 (9): 971–80. https://doi.org/10.1111/j.1432-0436.2008.00283.x.

Gill, Jason H., Kimberly L. Rockley, Carol De Santis, and Asma K. Mohamed. 2019. "Vascular Disrupting Agents in Cancer Treatment: Cardiovascular Toxicity and Implications for Co-Administration with Other Cancer Chemotherapeutics." *Pharmacology & Therapeutics*. https://doi.org/10.1016/j.pharmthera.2019.06.001.

Gintant, Gary, Philip T. Sager, and Norman Stockbridge. 2016a. "Evolution of Strategies to Improve Preclinical Cardiac Safety Testing." *Nature Reviews Drug Discovery*. https://doi.org/10.1038/nrd.2015.34.

Gintant, Gary, Philip T. Sager, and Norman Stockbridge. 2016b. "Evolution of Strategies to Improve Preclinical Cardiac Safety Testing." *Nature Reviews Drug Discovery*. Nature Publishing Group. https://doi.org/10.1038/nrd.2015.34.

Gordan, Richard, Judith K Gwathmey, and Lai-Hua Xie. 2015. "Autonomic and Endocrine Control of Cardiovascular Function." *World Journal of Cardiology* 7 (4): 204. https://doi.org/10.4330/wjc.v7.i4.204.

Grant, Augustus O. 2009. "Cardiac Ion Channels." *Circulation. Arrhythmia and Electrophysiology* 2 (2): 185–94. https://doi.org/10.1161/CIRCEP.108.789081.

Gray, G. A., I. S. Toor, R. F.P. Castellan, M. Crisan, and M. Meloni. 2018. "Resident Cells of the Myocardium: More than Spectators in Cardiac Injury, Repair and Regeneration."

Current Opinion in Physiology. https://doi.org/10.1016/j.cophys.2017.08.001.

Grilo, Liliana Sintra, Pierre-Alain Carrupt, and Hugues Abriel. 2010. "Stereoselective Inhibition of the HERG1 Potassium Channel." *Frontiers in Pharmacology* 1 (1): 137. https://doi.org/10.3389/fphar.2010.00137.

Gryder, Berkley E., Quaovi H. Sodji, and Adegboyega K. Oyelere. 2012a. "Targeted Cancer Therapy: Giving Histone Deacetylase Inhibitors All They Need to Succeed." *Future Medicinal Chemistry*. https://doi.org/10.4155/fmc.12.3.

Gryder, Berkley E., Quaovi H. Sodji, and Adegboyega K. Oyelere. 2012b. "Targeted Cancer Therapy: Giving Histone Deacetylase Inhibitors All They Need to Succeed." *Future Medicinal Chemistry*. NIH Public Access. https://doi.org/10.4155/fmc.12.3.

Hanahan, Douglas, and Robert A. Weinberg. 2011. "Hallmarks of Cancer: The next Generation." *Cell*. Elsevier. https://doi.org/10.1016/j.cell.2011.02.013.

Haque, Mohammed Z., Victoria J. McIntosh, Abdul B.Abou Samra, Ramzi M. Mohammad, and Robert D. Lasley. 2016. "Cholesterol Depletion Alters Cardiomyocyte Subcellular Signaling and Increases Contractility." *PLoS ONE* 11 (7). https://doi.org/10.1371/journal.pone.0154151.

Herr, Daniel J., Mauhamad Baarine, Sverre E. Aune, Xiaoyang Li, Lauren E. Ball, John J. Lemasters, Craig C. Beeson, James C. Chou, and Donald R. Menick. 2018. "HDAC1 Localizes to the Mitochondria of Cardiac Myocytes and Contributes to Early Cardiac Reperfusion Injury." *Journal of Molecular and Cellular Cardiology* 114 (January): 309–19. https://doi.org/10.1016/j.yjmcc.2017.12.004.

Higgins, Angela Y., Thomas D. O'Halloran, and James D. Chang. 2015. "Chemotherapy-Induced Cardiomyopathy." *Heart Failure Reviews*. https://doi.org/10.1007/s10741-015-9502-y.

Hirai, Kenta, Daiki Ousaka, Yosuke Fukushima, Maiko Kondo, Takahiro Eitoku, Yusuke Shigemitsu, Mayuko Hara, et al. 2020. "Cardiosphere-Derived Exosomal MicroRNAs for Myocardial Repair in Pediatric Dilated Cardiomyopathy." *Science Translational Medicine* 12 (573): 3336. https://doi.org/10.1126/scitranslmed.abb3336.

Holbrook, Mark. 2019. "How Do We Drive the Evolution and Implementation of Novel in Vitro Techniques in Partnership with in Vivo, Ex Vivo and in Silico Siblings?"

Holmes, Anthony, Frank Bonner, and David Jones. 2015. "Assessing Drug Safety in Human Tissues — What Are the Barriers?" *Nature Reviews Drug Discovery*. https://doi.org/10.1038/nrd4662.

Hondeghem, Luc M., and Bertram G. Katzung. 1977. "Time- and Voltage-Dependent Interactions of Antiarrhythmic Drugs with Cardiac Sodium Channels." *BBA - Reviews on Biomembranes*. Elsevier. https://doi.org/10.1016/0304-4157(77)90003-X.

Hornberg, Jorrit J., Morten Laursen, Nina Brenden, Mikael Persson, Annemette V. Thougaard, Dorthe B. Toft, and Tomas Mow. 2014. "Exploratory Toxicology as an Integrated Part of Drug Discovery. Part II: Screening Strategies." *Drug Discovery Today*. Elsevier Ltd. https://doi.org/10.1016/j.drudis.2013.12.009.

Hsu, Kai Cheng, Chang Yi Liu, Tony Eight Lin, Jui Hua Hsieh, Tzu Ying Sung, Hui Ju Tseng, Jinn Moon Yang, and Wei Jan Huang. 2017. "Novel Class IIa-Selective Histone Deacetylase Inhibitors Discovered Using an in Silico Virtual Screening Approach." *Scientific Reports* 7 (1): 1–13. https://doi.org/10.1038/s41598-017-03417-1.

"Https://Cipaproject.Org/." n.d. Accessed December 12, 2020. https://cipaproject.org/.

Https://nc3rs.org.uk/the-3rs. 2020. "The 3Rs | NC3Rs." 2020. https://nc3rs.org.uk/the-3rs.

Https://www.ich.org/. 2020. "ICH Official Web Site : ICH." 2020. https://www.ich.org/.

Humeres, Claudio, and Nikolaos G. Frangogiannis. 2019. "Fibroblasts in the Infarcted, Remodeling, and Failing Heart." *JACC: Basic to Translational Science*. Elsevier Inc. https://doi.org/10.1016/j.jacbts.2019.02.006.

Izumi-Nakaseko, Hiroko, Yasunari Kanda, Yuji Nakamura, Mihoko Hagiwara-Nagasawa, Takeshi Wada, Kentaro Ando, Atsuhiko T. Naito, Yuko Sekino, and Atsushi Sugiyama. 2017. "Development of Correction Formula for Field Potential Duration of Human Induced Pluripotent Stem Cell-Derived Cardiomyocytes Sheets." *Journal of Pharmacological Sciences* 135 (1): 44–50. https://doi.org/10.1016/j.jphs.2017.08.008.

Jenkinson, Stephen, Friedemann Schmidt, Lyn Rosenbrier Ribeiro, Annie Delaunois, and Jean Pierre Valentin. 2020. "A Practical Guide to Secondary Pharmacology in Drug Discovery." *Journal of Pharmacological and Toxicological Methods*. https://doi.org/10.1016/j.vascn.2020.106869.

Johansson, Markus, Benjamin Ulfenborg, Christian X. Andersson, Sepideh Heydarkhan-Hagvall, Anders Jeppsson, Peter Sartipy, and Jane Synnergren. 2020. "Cardiac Hypertrophy in a Dish: A Human Stem Cell Based Model." *Biology Open* 9 (9). https://doi.org/10.1242/bio.052381.

Kaese, Sven, and Sander Verheule. 2012. "Cardiac Electrophysiology in Mice: A Matter of Size." *Frontiers in Physiology*. Frontiers. https://doi.org/10.3389/fphys.2012.00345.

Kammonen, Juha, Said El Haou, Sarah Williams, Louise Webdale, Kathy Sutton, Marc Rogers, Metrion Biosciences, Riverside Suite, Granta Park, and Cambridge Cb. 2017. "HL-1 Atrial Cardiomyocytes for Cardiac Drug Discovery : Voltage & Current Clamp Biophysics & Pharmacology on Manual & Automated Patch Clamp Platforms," 21.

Karakikes, Ioannis, Mohamed Ameen, Vittavat Termglinchan, and Joseph C. Wu. 2015. "Human Induced Pluripotent Stem Cell-Derived Cardiomyocytes: Insights into Molecular, Cellular, and Functional Phenotypes." *Circulation Research*. Lippincott Williams and Wilkins. https://doi.org/10.1161/CIRCRESAHA.117.305365.

Knollmann, Björn C. 2013. "Induced Pluripotent Stem Cell-Derived Cardiomyocytes: Boutique Science or Valuable Arrhythmia Model?" *Circulation Research*. https://doi.org/10.1161/CIRCRESAHA.112.300567.

Koivumäki, Jussi T., Nikolay Naumenko, Tomi Tuomainen, Jouni Takalo, Minna Oksanen, Katja A. Puttonen, Šárka Lehtonen, et al. 2018. "Structural Immaturity of Human IPSC-Derived Cardiomyocytes: In Silico Investigation of Effects on Function and Disease Modeling." *Frontiers in Physiology* 9 (FEB): 80. https://doi.org/10.3389/fphys.2018.00080.

Kopljar, Ivan, David J. Gallacher, An De Bondt, Laure Cougnaud, Eddy Vlaminckx, Ilse Van den Wyngaert, and Hua Rong Lu. 2016. “Functional and Transcriptional Characterization of Histone Deacetylase Inhibitor-Mediated Cardiac Adverse Effects in Human Induced Pluripotent Stem Cell-Derived Cardiomyocytes.” *STEM CELLS Translational Medicine* 5 (5): 602–12. https://doi.org/10.5966/sctm.2015-0279.

Kuai, Qiyuan, Chunyan Wang, Yanbing Wang, Weijing Li, Gongqing Zhang, Zhixin Qiao, Min He, et al. 2016. “Energy Metabolism Regulated by HDAC Inhibitor Attenuates Cardiac Injury in Hemorrhagic Rat Model OPEN.” https://doi.org/10.1038/srep38219.

Kulka, Linda Anna Michelle, Pia Victoria Fangmann, Diana Panfilova, and Heidi Olzscha. 2020. “Impact of HDAC Inhibitors on Protein Quality Control Systems: Consequences for Precision Medicine in Malignant Disease.” *Frontiers in Cell and Developmental Biology*. Frontiers Media S.A. https://doi.org/10.3389/fcell.2020.00425.

Kutil, Zsofia, Zora Novakova, Marat Meleshin, Jana Mikesova, Mike Schutkowski, and Cyril Barinka. 2018. “Histone Deacetylase 11 Is a Fatty-Acid Deacylase.” *ACS Chemical Biology* 13 (3): 685–93. https://doi.org/10.1021/acschembio.7b00942.

Kyffin, Jonathan A., Parveen Sharma, Joseph Leedale, Helen E. Colley, Craig Murdoch, Amy L. Harding, Pratibha Mistry, and Steven D. Webb. 2019. “Characterisation of a Functional Rat Hepatocyte Spheroid Model.” *Toxicology in Vitro* 55 (March): 160–72. https://doi.org/10.1016/j.tiv.2018.12.014.

Lakatta, Edward G., and Dario DiFrancesco. 2009. “What Keeps Us Ticking: A Funny Current, a Calcium Clock, or Both?” *Journal of Molecular and Cellular Cardiology*. https://doi.org/10.1016/j.yjmcc.2009.03.022.

Lane, Andrew A., and Bruce A. Chabner. 2009. “Histone Deacetylase Inhibitors in Cancer Therapy.” *Journal of Clinical Oncology* 27 (32): 5459–68. https://doi.org/10.1200/JCO.2009.22.1291.

Laverty, HG, C Benson, EJ Cartwright, MJ Cross, C Garland, T Hammond, C Holloway, et al. 2011. “How Can We Improve Our Understanding of Cardiovascular Safety Liabilities to Develop Safer Medicines?” *British Journal of Pharmacology* 163 (4): 675–93. https://doi.org/10.1111/j.1476-5381.2011.01255.x.

Lee, Jee Suk, Young Geol Yoon, Seung Hee Yoo, Na Young Jeong, Seung Hun Jeong, Sang Yeob Lee, Dai-il Jung, Seon-Yong Jeong, and Young Hyun Yoo. 2012. “Histone Deacetylase Inhibitors Induce Mitochondrial Elongation.” *Journal of Cellular Physiology* 227 (7): 2856–69. https://doi.org/10.1002/jcp.23027.

Lehmann, Martin, Filomain Nguemo, Vilas Wagh, Kurt Pfannkuche, Jürgen Hescheler, and Michael Reppel. 2013. “Evidence for a Critical Role of Catecholamines for Cardiomyocyte Lineage Commitment in Murine Embryonic Stem Cells.” *PLoS ONE* 8 (8): 70913. https://doi.org/10.1371/journal.pone.0070913.

Litviňuková, Monika, Carlos Talavera-López, Henrike Maatz, Daniel Reichart, Catherine L. Worth, Eric L. Lindberg, Masatoshi Kanda, et al. 2020. “Cells of the Adult Human Heart.” *Nature*, no. September. https://doi.org/10.1038/s41586-020-2797-4.

Lkhagva, Baigalmaa, Yu Hsun Kao, Ting I. Lee, Ting Wei Lee, Wan Li Cheng, and Yi Jen Chen.

2018. “Activation of Class I Histone Deacetylases Contributes to Mitochondrial Dysfunction in Cardiomyocytes with Altered Complex Activities.” *Epigenetics* 13 (4): 376–85. https://doi.org/10.1080/15592294.2018.1460032.

Lopez, G., Y. Song, R. Lam, D. Ruder, C. J. Creighton, H. K. Bid, K. L. Bill, et al. 2016. “HDAC Inhibition for the Treatment of Epithelioid Sarcoma: Novel Cross Talk Between Epigenetic Components.” *Molecular Cancer Research*. https://doi.org/10.1158/1541-7786.MCR-15-0295.

Lother, Achim, Stella Bergemann, Lisa Deng, Martin Moser, Christoph Bode, and Lutz Hein. 2018. “Cardiac Endothelial Cell Transcriptome.” *Arteriosclerosis, Thrombosis, and Vascular Biology* 38 (3): 566–74. https://doi.org/10.1161/ATVBAHA.117.310549.

Ma, Junyi, Liang Guo, Steve J Fiene, Blake D Anson, James A Thomson, Timothy J Kamp, Kyle L Kolaja, Bradley J Swanson, and Craig T January. 2011. “High Purity Human-Induced Pluripotent Stem Cell-Derived Cardiomyocytes: Electrophysiological Properties of Action Potentials and Ionic Currents.” *Am J Physiol Heart Circ Physiol* 301: 2006–17. https://doi.org/10.1152/ajpheart.00694.2011.-Human-induced.

Maekawa, Satoshi, Shingo Takada, Hideo Nambu, Takaaki Furihata, Naoya Kakutani, Daiki Setoyama, Yasushi Ueyanagi, Dongchon Kang, Hisataka Sabe, and Shintaro Kinugawa. 2019. “Linoleic Acid Improves Assembly of the CII Subunit and CIII2/CIV Complex of the Mitochondrial Oxidative Phosphorylation System in Heart Failure.” *Cell Communication and Signaling* 17 (1): 1–11. https://doi.org/10.1186/s12964-019-0445-0.

Magdy, Tarek, Adam J T Schuldt, Joseph C Wu, Daniel Bernstein, and Paul W Burridge. 2018. “Human Induced Pluripotent Stem Cell (HiPSC)-Derived Cells to Assess Drug Cardiotoxicity: Opportunities and Problems.” *Annual Review of Pharmacology and Toxicology. Rev. Pharmacol. Toxicol* 58: 83–103. https://doi.org/10.1146/annurev-pharmtox.

Mann, Douglas L., and Ronald J. Krone. 2010. “Cardiac Disease in Cancer Patients: An Overview.” *Progress in Cardiovascular Diseases*. W.B. Saunders. https://doi.org/10.1016/j.pcad.2010.05.004.

McKinsey, Timothy A. 2012. “Therapeutic Potential for HDAC Inhibitors in the Heart.” *Annual Review of Pharmacology and Toxicology*. https://doi.org/10.1146/annurev-pharmtox-010611-134712.

Melendez, Giselle, Daniela Cardinale, Fabiani Iacopo, and Carlo Maria Cipolla. 2020. “Cardiotoxicity of Anthracyclines.” *Frontiers in Cardiovascular Medicine | Www.Frontiersin.Org* 7: 26. https://doi.org/10.3389/fcvm.2020.00026.

Michel, Lars, and Tienush Rassaf. 2019. “Cardio-Oncology: Need for Novel Structures 11 Medical and Health Sciences 1112 Oncology and Carcinogenesis.” *European Journal of Medical Research*. BioMed Central Ltd. https://doi.org/10.1186/s40001-018-0359-0.

Mittler, Frédérique, Patricia Obeïd, Anastasia V. Rulina, Vincent Haguet, Xavier Gidrol, and Maxim Y. Balakirev. 2017. “High-Content Monitoring of Drug Effects in a 3D Spheroid Model.” *Frontiers in Oncology* 7 (DEC): 293. https://doi.org/10.3389/fonc.2017.00293.

Morales, Cyndi R., Dan L. Li, Zully Pedrozo, Herman I. May, Nan Jiang, Viktoriia Kyrychenko,

Geoffrey W. Cho, et al. 2016. “Inhibition of Class I Histone Deacetylases Blunts Cardiac Hypertrophy through TSC2-Dependent MTOR Repression.” *Science Signaling*. https://doi.org/10.1126/scisignal.aad5736.

Nahrendorf, M. 2019. “Myeloid Cells in Cardiovascular Organs.” *Journal of Internal Medicine* 285 (5): 491–502. https://doi.org/10.1111/joim.12844.

Netter, Frank H. 2014. *Atlas of Human Anatomy*. 6th ed. Saunders.

Niehoff, Julius, Matthias Matzkies, Filomain Nguemo, Jürgen Hescheler, and Michael Reppel. 2016. “Beat Rate Variability in Murine Embryonic Stem Cell-Derived Cardiomyocytes: Effect of Antiarrhythmic Drugs.” *Cellular Physiology and Biochemistry* 38 (2): 646–58. https://doi.org/10.1159/000438657.

Noonan, Anne M., Robin A. Eisch, David J. Liewehr, Tristan M. Sissung, David J. Venzon, Thomas P. Flagg, Mark C. Haigney, et al. 2013. “Electrocardiographic Studies of Romidepsin Demonstrate Its Safety and Identify a Potential Role for KATP Channel.” *Clinical Cancer Research*. https://doi.org/10.1158/1078-0432.CCR-13-0109.

Obergrussberger, Alison, Krisztina Juhasz, Ulrich Thomas, Sonja Stölzle-Feix, Nadine Becker, Leo Dörr, Matthias Beckler, Corina Bot, Michael George, and Niels Fertig. 2016. “Safety Pharmacology Studies Using EFP and Impedance.” *Journal of Pharmacological and Toxicological Methods* 81 (September): 223–32. https://doi.org/10.1016/j.vascn.2016.04.006.

Ontoria-Oviedo, Imelda, Akaitz Dorronsoro, Rafael Sánchez, Maria Ciria, Marta Gómez-Ferrer, Marc Buigues, Elena Grueso, et al. 2018. “Extracellular Vesicles Secreted by Hypoxic AC10 Cardiomyocytes Modulate Fibroblast Cell Motility.” *Frontiers in Cardiovascular Medicine* 5 (October): 152. https://doi.org/10.3389/fcvm.2018.00152.

Parra, Maribel. 2015. “Class IIa HDACs - New Insights into Their Functions in Physiology and Pathology.” *FEBS Journal* 282 (9): 1736–44. https://doi.org/10.1111/febs.13061.

Pellman, Jason, Jing Zhang, and Farah Sheikh. 2016. “Myocyte-Fibroblast Communication in Cardiac Fibrosis and Arrhythmias: Mechanisms and Model Systems.” *Journal of Molecular and Cellular Cardiology*. Academic Press. https://doi.org/10.1016/j.yjmcc.2016.03.005.

Peters, Matthew F., Sarah D. Lamore, Liang Guo, Clay W. Scott, and Kyle L. Kolaja. 2015. “Human Stem Cell-Derived Cardiomyocytes in Cellular Impedance Assays: Bringing Cardiotoxicity Screening to the Front Line.” *Cardiovascular Toxicology*. https://doi.org/10.1007/s12012-014-9268-9.

Pinto, Alexander R., Alexei Ilinykh, Malina J. Ivey, Jill T. Kuwabara, Michelle L. D’antoni, Ryan Debuque, Anjana Chandran, et al. 2016. “Revisiting Cardiac Cellular Composition.” *Circulation Research* 118 (3): 400–409. https://doi.org/10.1161/CIRCRESAHA.115.307778.

Pointon, Amy, Najah Abi-gerges, Michael J. Cross, and James E. Sidaway. 2013. “Phenotypic Profiling of Structural Cardiotoxins in Vitro Reveals Dependency on Multiple Mechanisms of Toxicity.” *Toxicological Sciences*. https://doi.org/10.1093/toxsci/kft005.

Pollard, C. E., N. Abi Gerges, M. H. Bridgland-Taylor, A. Easter, T. G. Hammond, and J. P.

Valentin. 2010. “An Introduction to QT Interval Prolongation and Non-Clinical Approaches to Assessing and Reducing Risk.” *British Journal of Pharmacology*. Br J Pharmacol. https://doi.org/10.1111/j.1476-5381.2009.00207.x.

Poluzzi, Elisabetta, Emanuel Raschi, Igor Diemberger, and Fabrizio De Ponti. 2017. “Drug-Induced Arrhythmia: Bridging the Gap Between Pathophysiological Knowledge and Clinical Practice.” *Drug Safety*. Springer International Publishing. https://doi.org/10.1007/s40264-017-0529-y.

Protze, Stephanie I., Jie Liu, Udi Nussinovitch, Lily Ohana, Peter H. Backx, Lior Gepstein, and Gordon M. Keller. 2017. “Sinoatrial Node Cardiomyocytes Derived from Human Pluripotent Cells Function as a Biological Pacemaker.” *Nature Biotechnology* 35 (1): 56–68. https://doi.org/10.1038/nbt.3745.

Raschi, Emanuel, Valentina Vasina, Maria Grazia Ursino, Giuseppe Boriani, Andrea Martoni, and Fabrizio de Ponti. 2010. “Anticancer Drugs and Cardiotoxicity: Insights and Perspectives in the Era of Targeted Therapy.” *Pharmacology and Therapeutics*. Pharmacol Ther. https://doi.org/10.1016/j.pharmthera.2009.10.002.

Ravenscroft, Stephanie M., Amy Pointon, Awel W. Williams, Michael J. Cross, and James E. Sidaway. 2016. “Cardiac Non-Myocyte Cells Show Enhanced Pharmacological Function Suggestive of Contractile Maturity in Stem Cell Derived Cardiomyocyte Microtissues.” *Toxicological Sciences* 152 (1): 99–112. https://doi.org/10.1093/toxsci/kfw069.

Redfern, W. S., L. Carlsson, A. S. Davis, W. G. Lynch, I. MacKenzie, S. Palethorpe, P. K.S. Siegl, et al. 2003. “Relationships between Preclinical Cardiac Electrophysiology, Clinical QT Interval Prolongation and Torsade de Pointes for a Broad Range of Drugs: Evidence for a Provisional Safety Margin in Drug Development.” *Cardiovascular Research*. Elsevier. https://doi.org/10.1016/S0008-6363(02)00846-5.

Ribeiro, Alexandre J. S., Brian D. Guth, Michael Engwall, Sandy Eldridge, C. Michael Foley, Liang Guo, Gary Gintant, et al. 2019. “Considerations for an In Vitro, Cell-Based Testing Platform for Detection of Drug-Induced Inotropic Effects in Early Drug Development. Part 2: Designing and Fabricating Microsystems for Assaying Cardiac Contractility With Physiological Relevance Using Human IPSC-Cardiomyocytes.” *Frontiers in Pharmacology* 10 (August): 934. https://doi.org/10.3389/FPHAR.2019.00934.

Riedel, Michael, Chuanchau J Jou, Shuping Lai, Robert L Lux, Alonso P Moreno, Kenneth W Spitzer, Elizabeth Christians, Martin Tristani-Firouzi, and Ivor J Benjamin. 2014. “Stem Cell Reports Ar Ticle Functional and Pharmacological Analysis of Cardiomyocytes Differentiated from Human Peripheral Blood Mononuclear-Derived Pluripotent Stem Cells.” https://doi.org/10.1016/j.stemcr.2014.04.017.

Rocha, André Monteiro Da, Katherine Campbell, Sergey Mironov, Jiang Jiang, Lakshmi Mundada, Guadalupe Guerrero-Serna, José Jalife, and Todd J. Herron. 2017. “HiPSC-CM Monolayer Maturation State Determines Drug Responsiveness in High Throughput Pro-Arrhythmia Screen.” *Scientific Reports* 7 (1). https://doi.org/10.1038/s41598-017-13590-y.

Roche, Brian, John Ross, Carlos A. Obejero-Paz, and James Kramer. 2019. “Is the Current Non-Clinical Drug Development Safety Paradigm Effective for Assessing Cardiovascular

Liabilities?" *Journal of Pharmacological and Toxicological Methods* 99: 106595. https://doi.org/10.1016/j.vascn.2019.05.125.

Rockley, Kimberly. 2018. "Durham E-Theses In Vitro Evaluation of Anthracycline-Induced Cardiotoxicity and Mitigation by Perturbation of Angiotensin Signalling."

Rodrigues, Daniel A., Pedro de S. M. Pinheiro, Fernanda S. Sagrillo, Maria L. Bolognesi, and Carlos A. M. Fraga. 2020. "Histone Deacetylases as Targets for the Treatment of Neurodegenerative Disorders: Challenges and Future Opportunities." *Medicinal Research Reviews* 40 (6): 2177–2211. https://doi.org/10.1002/med.21701.

Rowinsky, E. K., S. Pacey, A. Patnaik, A. O'Donnell, M. M. Mita, P. Atadja, B. Peng, M. Dugan, J. W. Scott, and J. S. De Bono. 2004. "A Phase I, Pharmacokinetic (PK) and Pharmacodynamic (PD) Study of a Novel Histone Deacetylase (HDAC) Inhibitor LAQ824 in Patients with Advanced Solid Tumors." *Journal of Clinical Oncology* 22 (14_suppl): 3022–3022. https://doi.org/10.1200/jco.2004.22.90140.3022.

Ruijter, Annemieke J.M. De, Albert H. Van Gennip, Huib N. Caron, Stephan Kemp, and André B.P. Van Kuilenburg. 2003. "Histone Deacetylases (HDACs): Characterization of the Classical HDAC Family." *Biochemical Journal*. Biochem J. https://doi.org/10.1042/BJ20021321.

Sabbah, Hani N. 2020. "Targeting the Mitochondria in Heart Failure: A Translational Perspective." *JACC: Basic to Translational Science*. Elsevier Inc. https://doi.org/10.1016/j.jacbts.2019.07.009.

Sager, Philip T., Gary Gintant, J. Rick Turner, Syril Pettit, and Norman Stockbridge. 2014. "Rechanneling the Cardiac Proarrhythmia Safety Paradigm: A Meeting Report from the Cardiac Safety Research Consortium." *American Heart Journal*. https://doi.org/10.1016/j.ahj.2013.11.004.

Sala, Luca, Milena Bellin, and Christine L. Mummery. 2017. "Integrating Cardiomyocytes from Human Pluripotent Stem Cells in Safety Pharmacology: Has the Time Come?" *British Journal of Pharmacology* 174 (21): 3749–65. https://doi.org/10.1111/bph.13577.

Sartiani, Laura, Pascal Bochet, Elisabetta Cerbai, Alessandro Mugelli, and Rodolphe Fischmeister. 2002. "Functional Expression of the Hyperpolarization-activated, Non-selective Cation Current I_f in Immortalized HL-1 Cardiomyocytes." *The Journal of Physiology* 545 (1): 81–92. https://doi.org/10.1113/jphysiol.2002.021535.

Satsuka, Ayano, and Yasunari Kanda. 2019. "Cardiotoxicity Assessment of Drugs Using Human IPS Cell-Derived Cardiomyocytes: Toward Proarrhythmic Risk and Cardio-Oncology." *Current Pharmaceutical Biotechnology* 21 (9): 765–72. https://doi.org/10.2174/1389201020666190628143345.

Saxena, P., E. M. Zangerl-Plessl, T. Linder, A. Windisch, A. Hohaus, E. Timin, S. Hering, and A. Stary-Weinzinger. 2016. "New Potential Binding Determinant for HERG Channel Inhibitors." *Scientific Reports* 6 (April). https://doi.org/10.1038/srep24182.

Schiattarella, Gabriele Giacomo, Anna Sannino, Evelina Toscano, Fabio Cattaneo, Bruno Trimarco, Giovanni Esposito, and Cinzia Perrino. 2016. "Cardiovascular Effects of Histone Deacetylase Inhibitors Epigenetic Therapies: Systematic Review of 62 Studies

and New Hypotheses for Future Research." *International Journal of Cardiology* 219 (September): 396–403. https://doi.org/10.1016/j.ijcard.2016.06.012.

Scholz, Beatrix, Jan Sebastian Schulte, Sabine Hamer, Kirsten Himmler, Florentina Pluteanu, Matthias Dodo Seidl, Juliane Stein, et al. 2019. "HDAC (Histone Deacetylase) Inhibitor Valproic Acid Attenuates Atrial Remodeling and Delays the Onset of Atrial Fibrillation in Mice." *Circulation: Arrhythmia and Electrophysiology* 12 (3). https://doi.org/10.1161/CIRCEP.118.007071.

Schwach, Verena, Rolf H. Slaats, and Robert Passier. 2020. "Human Pluripotent Stem Cell-Derived Cardiomyocytes for Assessment of Anticancer Drug-Induced Cardiotoxicity." *Frontiers in Cardiovascular Medicine* 7 (April). https://doi.org/10.3389/fcvm.2020.00050.

Seymour, Elisabeth M., Shu Yung James Wu, Melissa A. Kovach, Matthew A. Romano, Jonathan R. Traynor, William C. Claycomb, and Steven F. Bolling. 2003. "HL-1 Myocytes Exhibit PKC and KATP Channel-Dependent Delta Opioid Preconditioning." In *Journal of Surgical Research*, 114:187–94. Academic Press Inc. https://doi.org/10.1016/S0022-4804(03)00248-8.

Shah, Manisha H, Philip Binkley, Kenneth Chan, Jim Xiao, Daria Arbogast, Minden Collamore, Yasser Farra, and Michael Grever. 2006. "Cardiotoxicity of Histone Deacetylase Inhibitor Depsipeptide in Patients with Metastatic Neuroendocrine Tumors." *Clinical Cancer Research*. https://doi.org/10.1158/1078-0432.CCR-05-2689.

Shah, Rashmi R. 2005. "Drugs, QT Interval Prolongation and ICH E14: The Need to Get It Right." *Drug Safety*. https://doi.org/10.2165/00002018-200528020-00003.

Shah, Rashmi R. 2019. "Safety and Tolerability of Histone Deacetylase (HDAC) Inhibitors in Oncology." *Drug Safety*. Springer International Publishing. https://doi.org/10.1007/s40264-018-0773-9.

Shultz, Michael D., Xueying Cao, Christine H. Chen, Young Shin Cho, Nicole R. Davis, Joe Eckman, Jianmei Fan, et al. 2011. "Optimization of the in Vitro Cardiac Safety of Hydroxamate-Based Histone Deacetylase Inhibitors." *Journal of Medicinal Chemistry* 54 (13): 4752–72. https://doi.org/10.1021/jm200388e.

Silverthorn, Dee Unglaub. 2016. *Human Physiology: An Integrated Approach*. 7th ed. Pearson.

Smith, Karen T., Skylar A. Martin-Brown, Laurence Florens, Michael P. Washburn, and Jerry L. Workman. 2010. "Deacetylase Inhibitors Dissociate the Histone-Targeting ING2 Subunit from the Sin3 Complex." *Chemistry and Biology* 17 (1): 65–74. https://doi.org/10.1016/j.chembiol.2009.12.010.

Stefanovic, Sonia, and Stéphane Zaffran. 2017. "Mechanisms of Retinoic Acid Signaling during Cardiogenesis." *Mechanisms of Development*. Elsevier Ireland Ltd. https://doi.org/10.1016/j.mod.2016.12.002.

Subramanian, Srividya, Susan E. Bates, John J. Wright, Igor Espinoza-Delgado, and Richard L. Piekarz. 2010. "Clinical Toxicities of Histone Deacetylase Inhibitors." *Pharmaceuticals*. MDPI AG. https://doi.org/10.3390/ph3092751.

Suraweera, Amila, Kenneth J. O'Byrne, and Derek J. Richard. 2018. "Combination Therapy with Histone Deacetylase Inhibitors (HDACi) for the Treatment of Cancer: Achieving the Full Therapeutic Potential of HDACi." *Frontiers in Oncology*. Frontiers Media S.A. https://doi.org/10.3389/fonc.2018.00092.

Swain, Sandra M., Fredrick S. Whaley, and Michael S. Ewer. 2003. "Congestive Heart Failure in Patients Treated with Doxorubicin: A Retrospective Analysis of Three Trials." *Cancer* 97 (11): 2869–79. https://doi.org/10.1002/cncr.11407.

Tocchetti, Carlo Gabriele, Pietro Ameri, Rudolf A. de Boer, Yuri D'Alessandra, Michele Russo, Daniela Sorriento, Michele Ciccarelli, et al. 2020. "Cardiac Dysfunction in Cancer Patients: Beyond Direct Cardiomyocyte Damage of Anticancer Drugs: Novel Cardio-Oncology Insights from the Joint 2019 Meeting of the ESC Working Groups of Myocardial Function and Cellular Biology of the Heart." *Cardiovascular Research*. Oxford University Press. https://doi.org/10.1093/cvr/cvaa222.

Tomlinson, Lauren, Zhen Qi Lu, Robert A. Bentley, Helen E. Colley, Craig Murdoch, Steven D. Webb, Michael J. Cross, Ian M. Copple, and Parveen Sharma. 2019. "Attenuation of Doxorubicin-Induced Cardiotoxicity in a Human in Vitro Cardiac Model by the Induction of the NRF-2 Pathway." *Biomedicine and Pharmacotherapy* 112 (April). https://doi.org/10.1016/j.biopha.2019.108637.

Tomsits, Philipp, Dominik Schüttler, Stefan Kääb, Sebastian Clauss, and Niels Voigt. 2020. "Isolation of High Quality Murine Atrial and Ventricular Myocytes for Simultaneous Measurements of Ca2+ Transients and L-Type Calcium Current." *Journal of Visualized Experiments* 2020 (165): 1–17. https://doi.org/10.3791/61964.

Toro, Tasha B., and Terry J. Watt. 2020. "Critical Review of Non-Histone Human Substrates of Metal-Dependent Lysine Deacetylases." *FASEB Journal* 34 (10): 13140–55. https://doi.org/10.1096/fj.202001301RR.

Toyoda, Futoshi, Wei Guang Ding, Dimitar P. Zankov, Mariko Omatsu-Kanbe, Takahiro Isono, Minoru Horie, and Hiroshi Matsuura. 2010. "Characterization of the Rapidly Activating Delayed Rectifier Potassium Current, i Kr, in HL-1 Mouse Atrial Myocytes." *Journal of Membrane Biology* 235 (2): 73–87. https://doi.org/10.1007/s00232-010-9257-2.

Valentin, Jean-Pierre, Jean-Michel Guillon, Stephen Jenkinson, Vivek Kadambi, Peri Ravikumar, Sonia Roberts, Lyn Rosenbrier-Ribeiro, Friedemann Schmidt, and Duncan Armstrong. 2018. "In Vitro Secondary Pharmacological Profiling: An IQ-DruSafe Industry Survey on Current Practices." https://doi.org/10.1016/j.vascn.2018.07.001.

Valentin, Jean-Pierre, and W. S. Redfern. 2017. "The Toxicologist 56 Th Annual Meeting and ToxExpo ™ Www.Toxicology.Org The Official Journal of the Society of Toxicology Www.Toxsci.Oxfordjournals.Org," 150–70. www.toxicology.org.

Valenzuela-Fernández, Agustín, J Romá N Cabrero, Juan M Serrador, and Francisco Sá Nchez-Madrid. 2009. "HDAC6: A Key Regulator of Cytoskeleton, Cell Migration and Cell-Cell Interactions." https://doi.org/10.1016/j.tcb.2008.04.003.

Varricchi, Gilda, Giancarlo Marone, Valentina Mercurio, Maria Rosaria Galdiero, Domenico Bonaduce, and Carlo G. Tocchetti. 2017. "Immune Checkpoint Inhibitors and Cardiac Toxicity: An Emerging Issue." *Current Medicinal Chemistry* 25 (11).

https://doi.org/10.2174/0929867324666170407125017.

Vaughan Williams, E.M. 1989. *Classification of Antiarrhythmic Actions. Handbook of Experimental Pharmacology*. Springer, Berlin, Heidelberg. https://doi.org/https://doi.org/10.1007/978-3-642-73666-7_2.

Vicente, Jose, Norman Stockbridge, and David G. Strauss. 2016. “Evolving Regulatory Paradigm for Proarrhythmic Risk Assessment for New Drugs.” *Journal of Electrocardiology* 49 (6): 837–42. https://doi.org/10.1016/j.jelectrocard.2016.07.017.

Wallner, Markus, Deborah M. Eaton, Remus M. Berretta, Laura Liesinger, Matthias Schittmayer, Juergen Gindlhuber, Jichuan Wu, et al. 2020. “HDAC Inhibition Improves Cardiopulmonary Function in a Feline Model of Diastolic Dysfunction.” *Science Translational Medicine* 12 (525): 7205. https://doi.org/10.1126/scitranslmed.aay7205.

Weaver, Richard J, and Jean-Pierre Valentin. 2019. “Today’s Challenges to De-Risk and Predict Drug Safety in Human ‘Mind-the-Gap.’” *Toxicological Sciences*, no. 167(2): 307–21. https://doi.org/10.1093/toxsci/kfy270.

Weeks, Kate L. 2019. “Commentary HDAC Inhibitors and Cardioprotection: Homing in on a Mechanism of Action.” https://doi.org/10.1016/j.ebiom.2018.12.003.

Wei, Feng, Marc Pourrier, David G Strauss, Norman Stockbridge, and Li Pang. 2020. “Effects of Electrical Stimulation on HiPSC-CM Responses to Classic Ion Channel Blockers” 174 (2): 254–65. https://doi.org/10.1093/toxsci/kfaa010.

Wen, Junru, Junwei Shen, Yajie Zhou, Xianhui Zhao, Zhensheng Dai, and Yueling Jin. 2020. “Pyrroloquinoline Quinone Attenuates Isoproterenol Hydrochloride-Induced Cardiac Hypertrophy in AC16 Cells by Inhibiting the NF-KB Signaling Pathway.” *International Journal of Molecular Medicine* 45 (3): 873–85. https://doi.org/10.3892/ijmm.2020.4463.

West, Alison C., and Ricky W. Johnstone. 2014. “New and Emerging HDAC Inhibitors for Cancer Treatment.” *Journal of Clinical Investigation*. American Society for Clinical Investigation. https://doi.org/10.1172/JCI69738.

White, Steven M., Phillip E. Constantin, and William C. Claycomb. 2004. “Cardiac Physiology at the Cellular Level: Use of Cultured HL-1 Cardiomyocytes for Studies of Cardiac Muscle Cell Structure and Function.” *American Journal of Physiology - Heart and Circulatory Physiology*. American Physiological Society. https://doi.org/10.1152/ajpheart.00986.2003.

Wiersma, Marit, Denise M.S. van Marion, Rob C.I. Wüst, Riekelt H. Houtkooper, Deli Zhang, Natasja M.S.de Groot, Robert H. Henning, and Bianca J.J.M. Brundel. 2019. “Mitochondrial Dysfunction Underlies Cardiomyocyte Remodeling in Experimental and Clinical Atrial Fibrillation.” *Cells* 8 (10): 1–21. https://doi.org/10.3390/cells8101202.

Wrzesinski, Krzysztof, Adelina Rogowska-Wrzesinska, Rattiyaporn Kanlaya, Kamil Borkowski, Veit Schwämmle, Jie Dai, Kira Eyd Joensen, Katarzyna Wojdyla, Vasco Botelho Carvalho, and Stephen J. Fey. 2014. “The Cultural Divide: Exponential Growth in Classical 2D and Metabolic Equilibrium in 3D Environments.” *PLoS ONE* 9 (9). https://doi.org/10.1371/journal.pone.0106973.

Xia, M., J. J. Salata, D. J. Figueroa, A. M. Lawlor, H. A. Liang, Y. Liu, and T. M. Connolly. 2004. "Functional Expression of L- and T-Type Ca2+ Channels in Murine HL-1 Cells." *Journal of Molecular and Cellular Cardiology* 36 (1): 111–19. https://doi.org/10.1016/j.yjmcc.2003.10.007.

Xu, Qin, Dakshesh Patel, Xian Zhang, and Richard D. Veenstra. 2016. "Changes in Cardiac Na $_v$ 1.5 Expression, Function, and Acetylation by Pan-Histone Deacetylase Inhibitors." *American Journal of Physiology - Heart and Circulatory Physiology*. https://doi.org/10.1152/ajpheart.00156.2016.

Yardley, DA, RR Ismail-Khan, and PM Klein. 2011. "PD01-04: Entinostat, a Novel Histone Deacetylase Inhibitor, Added to Exemestane Improves PFS in Advanced Breast Cancer in a Randomized, Phase II, Double-Blind Study." In *Cancer Research*, 71:PD01-04-PD01-04. American Association for Cancer Research (AACR). https://doi.org/10.1158/0008-5472.sabcs11-pd01-04.

Yuan, Haitao, Qiang Zhang, Jiabin Guo, Tingfen Zhang, Jun Zhao, Jin Li, Andrew White, Paul L. Carmichael, Carl Westmoreland, and Shuangqing Peng. 2016. "A PGC-1α-Mediated Transcriptional Network Maintains Mitochondrial Redox and Bioenergetic Homeostasis against Doxorubicin-Induced Toxicity in Human Cardiomyocytes: Implementation of TT21C." *Toxicological Sciences* 150 (2): 400–417. https://doi.org/10.1093/toxsci/kfw006.

"Z Stack | Center for Advanced Microscopy." n.d. Accessed December 16, 2020. https://cam.facilities.northwestern.edu/588-2/z-stack/.

Zamorano, Jose Luis, Patrizio Lancellotti, Daniel Rodriguez Muñoz, Victor Aboyans, Riccardo Asteggiano, Maurizio Galderisi, Gilbert Habib, et al. 2016. "2016 ESC Position Paper on Cancer Treatments and Cardiovascular Toxicity Developed under the Auspices of the ESC Committee for Practice Guidelines." *European Heart Journal*. Oxford University Press. https://doi.org/10.1093/eurheartj/ehw211.

Zeng, Haoyu, Bharathi Balasubramanian, Armando Lagrutta, and Frederick Sannajust. 2018. "Response of Human Induced Pluripotent Stem Cell-Derived Cardiomyocytes to Several Pharmacological Agents When Intrinsic Syncytial Pacing Is Overcome by Acute External Stimulation." *Journal of Pharmacological and Toxicological Methods*. https://doi.org/10.1016/j.vascn.2017.12.004.

Zeng, Haoyu, Jixin Wang, Holly Clouse, Armando Lagrutta, and Frederick Sannajust. 2019. "Resolving the Reversed Rate Effect of Calcium Channel Blockers on Human-Induced Pluripotent Stem Cell-Derived Cardiomyocytes and the Impact on In Vitro Cardiac Safety Evaluation." *Toxicological Sciences* 167 (2): 573–80. https://doi.org/10.1093/toxsci/kfy264.

Zhang, Xian, Dakshesh Patel, Qin Xu, and Richard Veenstra. 2018. "Differences in Functional Expression of Connexin43 and NaV 1.5 by Pan-and Class-Selective Histone Deacetylase Inhibition in Heart." *International Journal of Molecular Sciences* 19 (8). https://doi.org/10.3390/ijms19082288.

Zhang, Xiao hua, and Martin Morad. 2020. "Ca2+ Signaling of Human Pluripotent Stem Cells-Derived Cardiomyocytes as Compared to Adult Mammalian Cardiomyocytes." *Cell*

Calcium. Elsevier Ltd. https://doi.org/10.1016/j.ceca.2020.102244.

Zhang, Xiaoyu, and Yama A. Abassi. 2018. “Functional Maturation of Human IPSC-Derived Cardiomyocytes and Assessment of Inotropic Compounds.” *Journal of Pharmacological and Toxicological Methods* 93 (September): 170–71. https://doi.org/10.1016/J.VASCN.2018.01.551.

Zhou, Pingzhu, and William T. Pu. 2016. “Recounting Cardiac Cellular Composition.” *Circulation Research*. Lippincott Williams and Wilkins. https://doi.org/10.1161/CIRCRESAHA.116.308139.

Appendix 1:

Formation and preliminary characterisation of HL-1 triculture spheroids.

Culture Time (days)	4	7	14
AC10 triculture			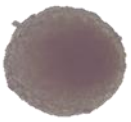
HL1 triculture			

Comparison of AC10 and HL-1 triculture spheroids 4, 7 and 14 days post seeding.

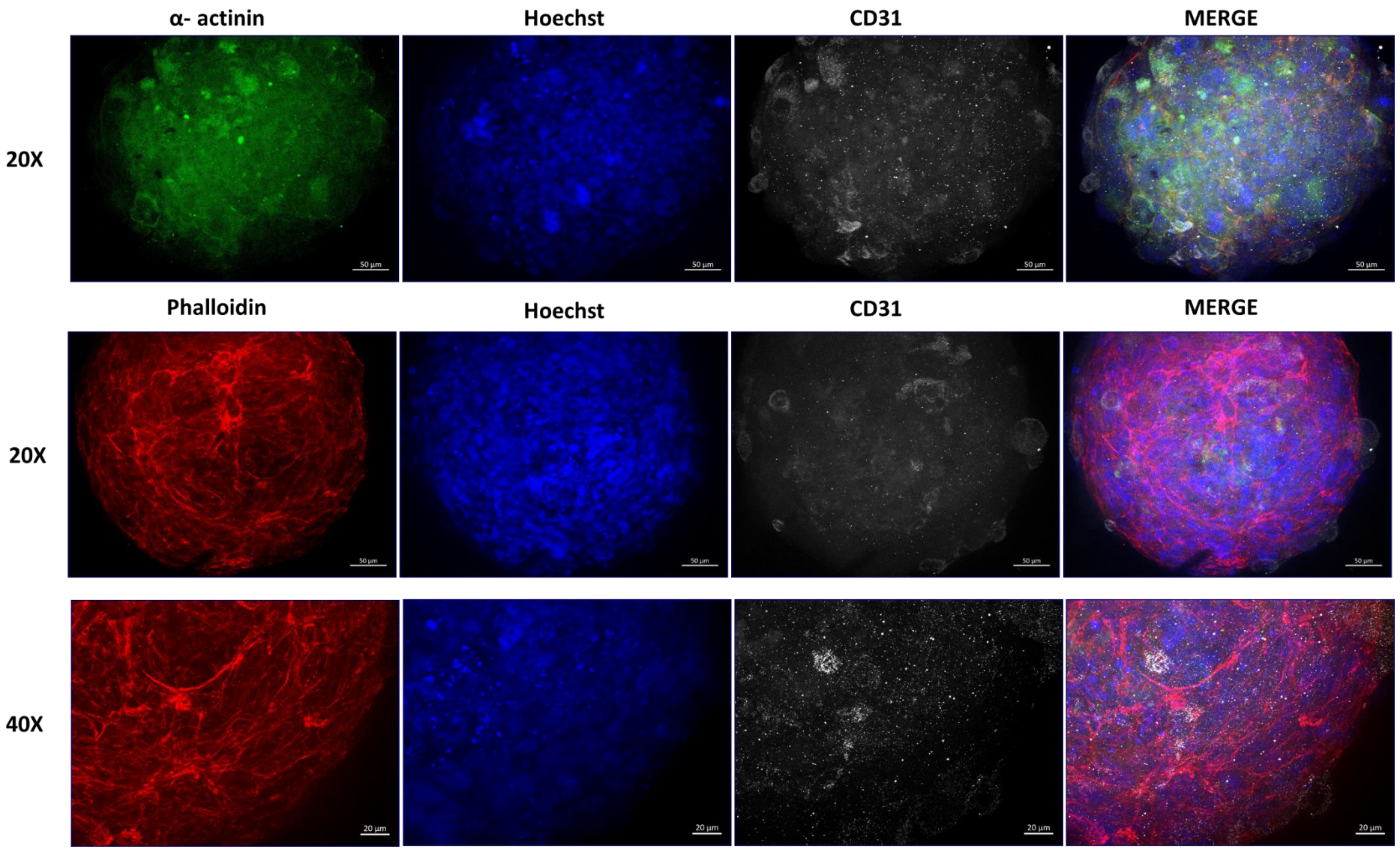
α- actinin
Hoechst
CD31
MERGE
20X
50 µm
Phalloidin
Hoechst
CD31
MERGE
20X
50 µm
40X
20 µm

[continued from previous page] **Internal structure of HL-1 triculture spheroids**. Spheroids were cultured on ULA plates for 14 days, fixed and stained with anti-alpha actinin (green), Hoechst to stain the cell nuclei (blue), phalloidin to stain cytoskeletal structures (red) and anti CD31 antibody to stain endothelial cells (white). Images are maximum intensity projections representative of a mid-section of each spheroid, typical of at least 3 different spheroids. At 20x magnification, scale bar is 50 µm. At 40x magnification with oil immersion, scale bar is 20 µm.

Appendix 2:

Selected publications and presented abstracts.

Evaluation of *in-vitro* cellular models for use in functional and structural studies of drug-induced cardiotoxicity

C. De Santis; JH Gill

Keywords: Cardiotoxicity; Histone deacetylase inhibitors; Human-induced stem cell-derived cardiomyocytes; Cellular impedance.

Detrimental effects upon the cardiac system are a major cause of drug attrition. Current *in vitro* methodologies for assessment of drug-induced cardiotoxicity involve sub-optimal screens of non-cardiac cell lines engineered to express cardiac ion channels, or primary tissue with limited utility for clinical translation. The advent of human induced pluripotent stem cell-derived cardiomyocytes (hiPSC-CM), with the ability to synchronously beat (contract) *in vitro*; opened up opportunities for improved identification of cardiotoxicity. However, these cells are costly, time-limited, and require complex maintenance techniques, posing constraints in terms of widespread use. One resolution is the use of immortalised cardiac cell lines, with capability for continuous growth and clinical translation. However, the limitations of these models for detecting both structural and functional cardiotoxicity is unknown. In this study we assess the predictive value of an immortalised non-contractile human cardiac cell line (AC10) and functionally-responsive hiPSC-CM to determine toxicity of the histone deacetylase inhibitor (HDACi) class of drug, thus highlighting the advantages of each type of cell model in relation to structural and functional cardiotoxicity. This not only supports the value of comprehensive cellular screening models, but offers a predictive tool to assess cardiotoxicity that would allow development of efficacious and safer drugs in this class.

Invited keynote speaker and poster presentation at the In-vitro toxicology society IVTS annual meeting 2017, London, UK

Awarded Early Career Scientist Prize 2017

Evaluation of *in-vitro* Cellular Models for Functional and Structural Studies of Drug-Induced Cardiotoxicity

De Santis C; Gill JH.
Northern Institute for Cancer Research, Newcastle University, UK

Cardiotoxicity is a major complication of many anticancer therapies, which frequently impacts the quality of life and overall survival of patients. Recent advances have identified modulation of epigenetics as a viable therapeutic strategy for cancer treatment, with small molecule histone deacetylase inhibitors (HDACi) demonstrating significant clinical potential. However, despite indicating clinical efficacy these drugs have been associated with development of adverse effects upon the cardiac system, toxicities which were not identified in preclinical drug development studies. Consequently, preclinical models with improved ability to predict structural and functional cardiac liabilities are required to identify toxicological mechanisms, reduce clinical cardiotoxicity potential and identify therapeutic strategies to mitigate these life-threatening effects.

STUDY AIMS:

- To compare the ability of an immortalised human cardiac cell line (AC10) and human-induced pluripotent stem-cell derived cardiomyocytes (hiPSC-CM) to detect toxicity of the HDACi drug class.
- Using impedance based real-time cell analysis (xCELLigence RTCA), evaluate the ability of these cardiac cell models to detect structural (Figure 2) and functional (Figure 3) drug-induced cardiotoxicity

Methodology

Fig 1. Cardiac phenotype of AC10 cells

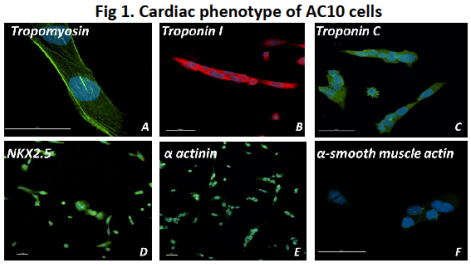

AC10 cells are positive for A. Tropomyosin, B. Troponin I, C. Troponin C, D. NKX2.5 and E. alpha-actin. Negative for F. alpha smooth muscle actin

Fig 2. xCELLigence Real-Time Cell analysis:

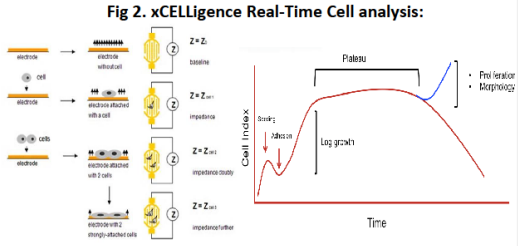

Principle of xCELLigence impedance based cell monitoring

Fig 3. xCELLigence: Cardiac Contractility:

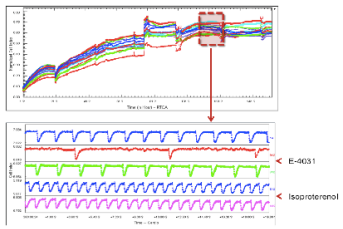

Changes in hiPSC-CM cardiomyocyte contractility induced by hERG channel block (E4031) and adrenoceptor agonism (Iso), determined by xCELLigence RTCA

Results

Fig 4. Cytotoxicity of HDACi against AC10 cardiomyocytes

HDACi (Selectivity)	In vitro toxicity (IC_{50})	Maximum non-toxic dose
TSA (Pan-HDAC)	2.2 µM ± 5.81	0.15 µM ± 4.66
MS-275 (Class I HDAC selective)	3.4 µM ± 7.23	0.6 µM ± 3.68
CHDI (Class IIa selective)	5 µM ± 7.1	1.25 µM ± 4.2
Tubacin (Class IIb selective)	9.6 µM ± 12.6	5.0 µM ± 10.07

AC10 cells at confluency were exposed to class-selective HDACi for 96-hours and cytotoxicity determined using the MTT assay. Data is presented as 50% growth inhibitory concentration (IC_{50}) and maximum non-toxic dose

Fig 5. TSA-mediated HDACi induces Time-dependent Histone and Tubulin acetylation in AC10 cardiomyocytes

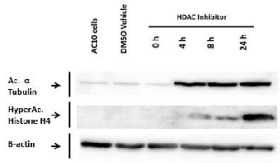

AC10 cardiomyocytes at confluency were exposed to the pan-HDACi TSA (10 µM). Expression of acetylated histone H4 and α-tubulin protein was determined by western blot analysis

Fig 6. Inhibition of HDAC sub-class induces proliferative and structural changes in cardiomyocytes.

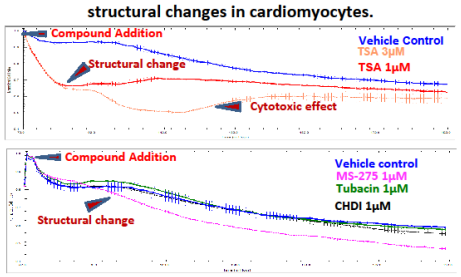

Fig 7. TSA-mediated HDACi induces functional contractility changes in hiPS cardiomyocytes at clinically relevant concentrations

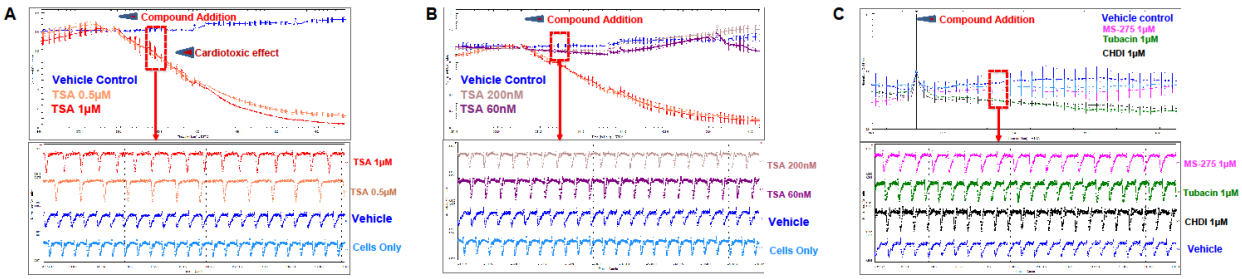

TSA is associated with major proarrhythmic and acute cardiotoxic events detected using impedance assays in Cor.4U cells (A and B).
HDACis Tubacin and CHDI induce a moderate decrease in cell index but no beating irregularities in Cor.4U cells (C); changes in contractility frequency are observable upon treatment with MS-275 (C).

CONCLUSIONS:

- **Human-derived, immortalised cardiomyocytes (AC10) provide a suitable *in-vitro* model for the assessment of structural cardiotoxicity, but are non-contractile**
- **hiPS-cardiomyocytes can be utilised to detect drug-induced functional changes in cellular contractility *in-vitro***
- **HDACi induce both structural and functional changes to cardiomyocytes *in-vitro* at clinically relevant concentrations**
- **HDACi-associated cardiotoxicity is dependent on selective inhibition of HDAC sub-classes**

Qualification of cardiac cell models for preclinical predictive studies of drug-induced cardiotoxicity

Carol De Santis[1]; Simon Findlay[1]; Jason H. Gill[1,2]
[1]Northern Institute for Cancer Research, Newcastle University, UK; [2]School of Pharmacy, Newcastle University, UK.

Cardiotoxicity is a major cause of drug attrition and life-threatening complication of many anticancer therapies. Current *in-vitro* methodologies for identification of drug-induced structural and/or functional cardiotoxicity and their underlying mechanism are sub-optimal, involving either non-cardiac cell lines expressing specific ion channels, or ex-vivo cardiac tissues with limited utility for longer-term analyses and clinical translation.

The emergence of innovative technologies combined with the use of human induced pluripotent stem cell-derived cardiomyocytes (hiPSC-CM), with the ability to synchronously contract *in-vitro*, revolutionised identification of drug-induced cardiotoxicity. However, major limitations to this approach are their complexity, specialised culture conditions, high cost and subsequent limitations for assessment of drug-induced cardiotoxicity. One resolution is incorporation of cardiac cell lines into the initial screening paradigm. The study objective was to evaluate the responsiveness of current cardiac cell-lines to both structural and functional cardiotoxicants, specifically the human ventricular cardiomyocyte cell-line, AC10, and the murine atrial cell-line, HL-1, relative to both primary neonatal rodent cardiomyocytes and hiPSC-CM. Real-time assessment of pathophysiological changes were determined by impedance-based *in vitro* methodologies (xCELLigence RTCA), with known cardiac therapeutics and the histone deacetylase inhibitor (HDACi) class of drugs being evaluated in this context.

The AC10 cell-line, although non-contractile, was able to detect drug-induced structural changes. The HL-1 cell-line was also able to detect structural cardiotoxicants, and exhibited a contractile phenotype *in vitro,* albeit non-uniformly and time-limited. This study indicates there is scope for inclusion of cardiac cell-lines alongside primary cells and hiPSC-CM in preclinical evaluation of drug-induced cardiotoxicity.

Oral presentation at the British Toxicology Society annual Congress 2019, Cambridge, UK

Qualification of *in* vitro cardiomyocyte cell models for prediction of drug-induced toxicity studies

Carol De Santis[1]; Jason H. Gill[1,2]
[1]Northern Institute for Cancer Research, Newcastle University, UK; [2]School of Pharmacy, Newcastle University, UK.

Detrimental effects upon the cardiac system are a major cause of attrition during drug development, withdrawal of marketed medicines, and development of heart failure in survivors of chronic therapies. Drug-induced cardiotoxicity is a consequence of effects upon a range of molecular pathways involved with either structural or functional attributes of the heart. Current in vitro methodologies for assessment of drug-induced cardiotoxicity involve either sub-optimal screens involving non-cardiac cell lines engineered to express individual cardiac ion channels, or primary animal cardiomyocytes and cardiac tissue with their limited utility for in vitro culture and clinical translation. The emergence of innovative technologies combined with the use of human induced pluripotent stem cell-derived cardiomyocytes (hiPSC-CM), with the ability to synchronously beat (contract) in vitro, opened up opportunities for improved identification of cardiotoxicity. However, the costly and complex maintenance techniques pose limitations in terms of widespread use. A possible solution to these limitations is the utilisation of a panel of cardiac cell lines, with defined attributes for clinical translation, scope for molecular manipulation, and the beneficial capability for continuous and expandable in vitro growth. However, the advantages and limitations for these cell models for prediction and detection of the various perturbations of structural and functional cardiotoxicity are as yet unclear. The objective of this study was to characterise and profile the capabilities for toxicity prediction of different cardiac cell lines, specifically the immortalized human ventricular cardiomyocyte cell line - AC10, the immortalized murine atrial cell line - HL1, and the rat embryonic cardiomyoblast cell line - H9c2, relative to primary cardiomyocytes and ultimately hiPSC-CM. This study evaluated these cell systems using impedance based real-time analyses (xCELLigence RTCA) to address the ability of these cardiac cell models to detect both structural and functional drug-induced cardiotoxicity. Data is presented of the evaluation of these cell models against a panel of drugs with known cardiotoxic effects, identifying their advantages and limitations for screening of drug-induced cardiotoxicity.

Poster presentation at the International Union of Toxicology IUTOX Meeting 2019, Honolulu, Hawaii, USA

Qualification of in-vitro cardiomyocyte cell models for prediction of drug-induced toxicity studies

De Santis C; Sharma P; Gill JH;
Northern Institute for Cancer Research, Newcastle University, UK ; MRC Centre for Drug Safety Science, University of Liverpool, UK

Newcastle University
UK | Malaysia | Singapore

INTRODUCTION

Cardiotoxicity is a major complication of many anticancer therapies that impacts the quality of life and overall survival of patients.

Preclinical models with improved ability to predict structural and functional cardiac liabilities are required to identify toxicological mechanisms, reduce clinical cardiotoxicity potential and identify therapeutic strategies to mitigate these life-threatening effects.

STUDY AIMS:

- Using impedance based real-time cell analysis (xCELLigence RTCA), evaluate the ability of different cardiac cell models to detect structural and functional drug-induced cardiotoxicity

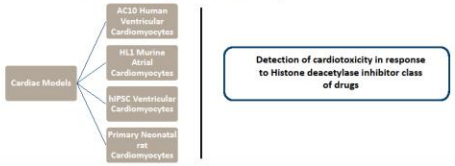

METHODOLOGY

xCELLigence Cardio System

Fig 1. xCELLigence Real-Time Cell analysis and Contractility:

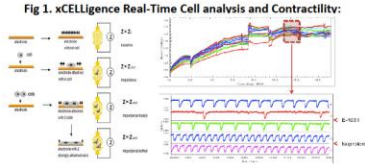

Changes in hiPSC-CM cardiomyocyte contractility induced by hERG channel block (E4031) and adrenoceptor agonism (Iso), determined by xCELLigence RTCA

RESULTS

HDAC inhibitor at clinically relevant concentrations induces structural changes in AC10 cardiomyocytes

AC10 ventricular human cell line

Fig 2. Cardiac phenotype of AC10 cells

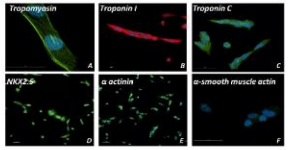

AC10 cells are positive for A. Tropomyosin, B. Troponin I, C. Troponin C, D. NKX2.5 and E. alpha-actin. Negative for F. alpha smooth muscle actin

Fig 3. TSA-mediated HDACi induces Time-dependent Histone and Tubulin acetylation in human AC10 cardiomyocyte cell line

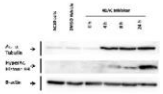

AC10 cells at confluency were exposed to the pan-HDACi TSA (1 μM). Expression of acetylated histone H4 and acetylated α-tubulin protein was determined by western blot analysis

Fig 4. Inhibition of HDACs at sub-toxic concentrations induces structural change in AC10 cells

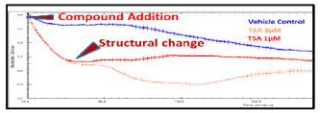

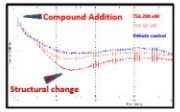

Sub-toxic concentration of TSA induced a decrease in cell index but not a decrease in cell number, suggesting cytotoxicity may depend on cell hypotrophy secondary to HDACi downstream effects

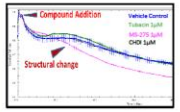

Selective inhibition of class I HDACs induces structural changes in AC10 cell line. Selective inhibition of class II HDACs does not induce significant cell index alterations.

HDAC inhibitor at clinically relevant concentrations induces structural and partial functional changes in HL1 cardiomyocytes

HL1 atrial murine cell line

Fig 5. Electrophysiology of HL1 cells

Compound	Mechanism	Detectable effect in HL-1 cell line using xCELLigence Cardio
Quinidine	Sodium channel blocker class Ia	☑
Disopyramide	Sodium channel blocker class Ia	X
Lidocaine	Sodium channel blocker class Ib	☑
Propafenone	Sodium channel blocker class Ic	X
Metoprolol	Selective B-adrenergic blocker (short acting)	X
Carvedilol	Non-selective α/B-adrenergic blocker (long acting)	X
Amiodarone	Potassium channel blocker	X
Verapamil	Calcium channel blocker	☑
E-4031	Experimental hERG blocker	☑
Isoprenaline	B-adrenoceptor agonist	☑

Fig 6. TSA-mediated HDACi induces Time-dependent Histone and Tubulin acetylation in HL-1 cell line

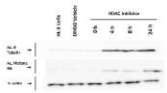

HL-1 cells at confluency were exposed to the pan-HDACi TSA (1 μM). Expression of acetylated histone H4 and acetylated α-tubulin protein was determined by western blot analysis

Fig 7. TSA-mediated HDACi induces functional changes in HL1 contractility

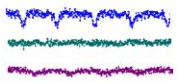

HL1 show functional changes in response to HDACi treatment (XCELLIGENCE TRACE)

Fig 8. Inhibition of HDACs at sub-toxic concentrations induces structural change in HL1 cells

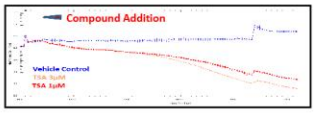

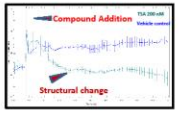

Consistently with AC 10 findings, sub-toxic concentration of TSA induced a decrease in cell index but not a decrease in cell number in HL1 cells, suggesting cytotoxicity may depend on cell hypotrophy secondary to HDACi downstream effects

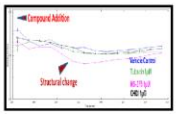

Selective inhibition of class I HDACs induces structural changes in HL1 cell line. Selective inhibition of class II HDACs does not induce significant cell index alterations.

hIPSC- CMs detect functional changes but not structural changes in response to HDAC inhibitor

Human iPS-derived cardiomyocytes

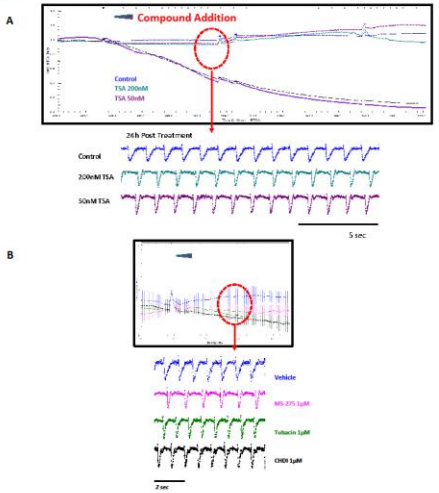

Trichostatin-A (TSA; pan-HDAC inhibitor) is associated with proarrhythmic and acute cytotoxic events detected using impedance assays in Cor.4U cells (A).
Selective Class II HDACis (Class IIa-Tubacin and Class IIb-CHDI) induce moderate decreases in cell index but no beating irregularities (A and B); changes in contractility frequency are observable upon treatment with class I HDACi (MS-275) (B).

HDAC inhibitor at clinically relevant concentrations induces functional and structural changes in primary rat cardiomyocytes

Primary rat-derived cardiomyocytes

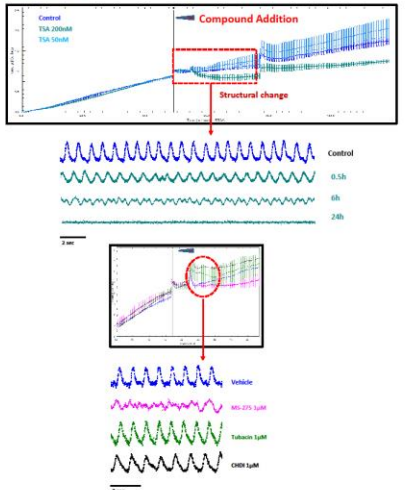

Trichostatin-A (TSA; pan-HDAC inhibitor) displayed a decrease in cell index at sub-therapeutic dose of 200nM in primary rat cells. Complete loss of contractility was achieved within 24hours from initial exposure (A).
Selective Class II HDACis (Class IIa-Tubacin and Class IIb-CHDI) did not induce changes in contractility, changes in contractility pattern are observable upon treatment with class I HDACi (MS-275) (B).

CONCLUSIONS

The combination of non-contractile primary cardiomyocytes and contractile cardiomyocytes offers a comprehensive model system for the detection of drug-induced structural and functional changes

Cardiac Model	Structural Screening	Functional screening
AC10 Human Ventricular Cell Line	YES	NO
HL-1 Murine Atrial Cell Line	YES	LIMITED
Human hiPS-CMs	LIMITED	YES
Primary Neonatal Rat CMs	YES	YES

The integration of different in-vitro models allowed to gain insights into HDACi-mediated cardiotoxocity

HDACi- Induced Cardiotoxicity
HDAC inhibition causes both structural and functional aberrations to cardiac cells at sub-clinical drug concentrations
Class I HDACi induced detectable toxicity in the form of structural and functional perturbations
Class IIa and IIb HDACi did not cause detectable toxicity

MRC Medical Research Council
bts driving excellence in toxicology

Qualification of in vitro cardiac cell models for preclinical assessment of oncology drug-induced cardiotoxicity

Carol De Santis[1]; Simon Findlay[1]; Jason H. Gill[1,2]

[1]Northern Institute for Cancer Research, Newcastle University, UK; [2]School of Pharmacy, Newcastle University, UK

Cardiotoxicity is a major cause of drug attrition and life-threatening complication of many anticancer therapies. Current preclinical methodologies for identification of drug-induced structural and/or functional cardiotoxicity and their underlying mechanism are sub-optimal, involving either non cardiac cell lines expressing specific ion channels, or ex-vivo cardiac tissues with limited utility for longer-term analyses and clinical translation. The emergence of innovative technologies combined with the use of human induced pluripotent stem cell-derived cardiomyocytes (hiPSC-CM), with the ability to synchronously contract in-vitro, revolutionised identification of drug-induced cardiotoxicity. However, major limitations to this approach are their complexity, specialised culture conditions, high cost and subsequent limitations for assessment of drug-induced cardiotoxicity. One resolution is incorporation of cardiac cell lines into the initial screening paradigm. The study objective was to evaluate the responsiveness of current cardiac cell-lines to both structural and functional cardiotoxicants, specifically the human ventricular cardiomyocyte cell-line, AC10, and the murine atrial cell-line, HL-1, relative to both primary neonatal rodent cardiomyocytes and hiPSC-CM. Real-time assessment of pathophysiological changes were determined by impedance-based in vitro methodologies (xCELLigence RTCA), with known cardiac therapeutics and the histone deacetylase inhibitor (HDACi) class of drugs being evaluated in this context. The AC10 cell-line, although non-contractile, was able to detect drug-induced structural changes. The HL-1 cell-line was also able to detect structural cardiotoxicants, and exhibited a contractile phenotype in vitro, albeit non-uniformly and time-limited. This study indicates there is scope for inclusion of cardiac cell-lines alongside primary cells and hiPSC-CM in preclinical evaluation of drug-induced cardiotoxicity.

Poster presentation at the European Cardio-Oncology Symposium 2019, Barcelona, Spain

Poster available at: https://eurocardio-onc.cme-cpd.org

Qualification of *in-vitro* Cardiac Cell Models for Preclinical Assessment of Oncology Drug-induced Cardiotoxicity

De Santis C; Findlay S; Gill JH.
Northern Institute for Cancer Research, Newcastle University, UK

INTRODUCTION

Cardiotoxicity is a major complication of many anticancer therapies that impacts the quality of life and overall survival of patients. Preclinical models with improved ability to predict structural and functional cardiac liabilities are required to identify toxicological mechanisms, reduce clinical cardiotoxicity potential and identify therapeutic strategies to mitigate these life-threatening effects.

STUDY AIMS:

- Using impedance based real-time cell analysis (xCELLigence RTCA), evaluate the ability of different cardiac cell models to detect structural and functional drug-induced cardiotoxicity

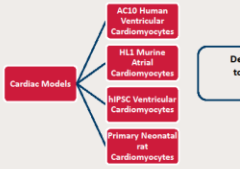

- Several HDAC inhibitors have been introduced to the clinic or are currently in trial
- HDAC inhibitors demonstrate clinical cardiotoxicity
- **What is the involvement of HDAC sub-classes in HDACi-induced cardiotoxicity?**

METHODOLOGY

Fig 1. xCELLigence Real-Time Cell analysis and Contractility:

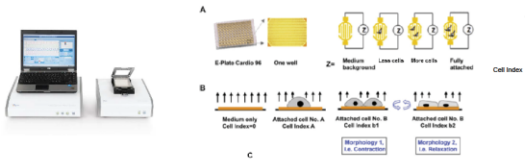

Fig.1 ***Impedance-based Real Time Cell Analysis – How does it work?*** Cells are seeded on an electrode coated plate. When a mild current is applied the attachment of the cells will impede the current flow. ***What does it measure?*** Changes in impedance due to cellular growth and morphology are recorded in real time. These can change in response to drugs or toxic insults.

Fig 2. Qualification of xCELLigence system to detect functional changes in cardiomyocyte contractility

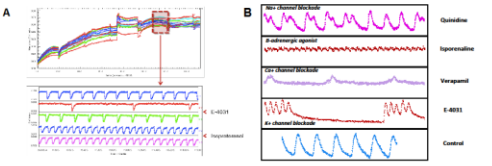

Fig. 2. Changes in contractility in hiPSC-CM (A) and primary neonatal CMs (B) induced by cardioactive agents

RESULTS

HDAC inhibitor at clinically relevant concentrations induces structural changes in AC10 ventricular cardiomyocytes

AC10 ventricular human cell line

Fig 3. Cardiac phenotype of AC10 cells

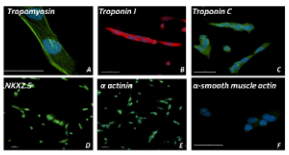

AC10 cells are positive for A. Tropomyosin, B. Troponin I, C. Troponin C, D. NKX2.5 and E. alpha-actin. Negative for F. alpha smooth muscle actin

Fig 4. TSA-mediated HDACi induces Time-dependent Histone and Tubulin acetylation in human AC10 cardiomyocyte cell line

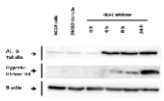

AC10 cells at confluency were exposed to the pan-HDACi TSA (1 μM). Expression of acetylated histone H4 and acetylated α-tubulin protein was determined by western blot analysis

Fig 5. Inhibition of HDACs at sub-toxic concentrations induces structural change in AC10 cells

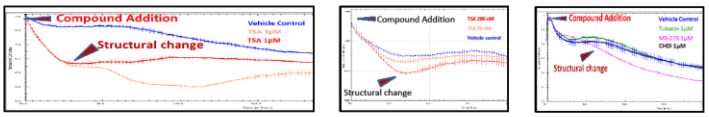

Sub-toxic concentration of TSA induced a decrease in cell index but not a decrease in cell number, suggesting cytotoxicity may depend on cell hypotrophy secondary to HDACi downstream effects

Selective inhibition of class I HDACs induces structural changes in AC10 cell line. Selective inhibition of class II HDACs does not induce significant cell index alterations.

HDAC inhibitor at clinically relevant concentrations induces structural and partial functional changes in HL1 atrial cardiomyocytes

HL1 atrial murine cell line

Fig 6. Electrophysiology of HL1 cells

Compound	Mechanism	Detectable effect in HL-1 cell line using xCELLigence Cardio
Quinidine	Sodium channel blocker class Ia	☑
Disopyramide	Sodium channel blocker class Ia	X
Lidocaine	Sodium channel blocker class Ib	☑
Propafenone	Sodium channel blocker class Ic	X
Metoprolol	Selective B-adrenergic blocker (short acting)	X
Carvedilol	Non-selective α/B-adrenergic blocker (long acting)	X
Amiodarone	Potassium channel blocker	X
Verapamil	Calcium channel blocker	☑
E-4031	Experimental hERG blocker	☑
Isoprenaline	B-adrenoceptor agonist	☑

Fig 7. TSA-mediated HDACi induces Time-dependent Histone and Tubulin acetylation in HL-1 cell line

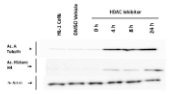

HL-1 cells at confluency were exposed to the pan-HDACi TSA (1 μM). Expression of acetylated histone H4 and acetylated α-tubulin protein was determined by western blot analysis

Fig 8. TSA-mediated HDACi induces functional changes in HL1 contractility

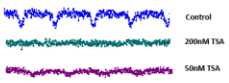

HL1 show functional changes in response to HDACi treatment. Loss of contractility is observed within 24h post drug exposure at 200nM.

Fig 9. Inhibition of HDACs at sub-toxic concentrations induces structural change in HL1 cells

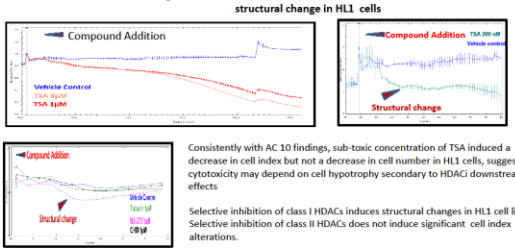

Consistently with AC 10 findings, sub-toxic concentration of TSA induced a decrease in cell index but not a decrease in cell number in HL1 cells, suggesting cytotoxicity may depend on cell hypotrophy secondary to HDACi downstream effects

Selective inhibition of class I HDACs induces structural changes in HL1 cell line. Selective inhibition of class II HDACs does not induce significant cell index alterations.

hIPSC- CMs detect functional changes but not structural changes in response to HDAC inhibitor

Human iPS-derived cardiomyocytes

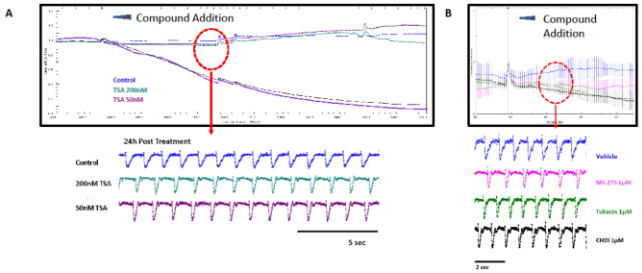

Fig 10. Trichostatin-A (TSA; pan-HDAC inhibitor) is associated with proarrhythmic and acute cytotoxic events detected using impedance assays in Cor.4U cells (A). Selective Class II HDACis (Class IIa-Tubacin and Class IIb-CHDI) induce moderate decreases in cell index but no beating irregularities (A and B) ; changes in contractility frequency are observable upon treatment with class I HDACi (MS-275) (B).

HDAC inhibitor at clinically relevant concentrations induces functional and structural changes in primary rat cardiomyocytes

Primary rat-derived cardiomyocytes

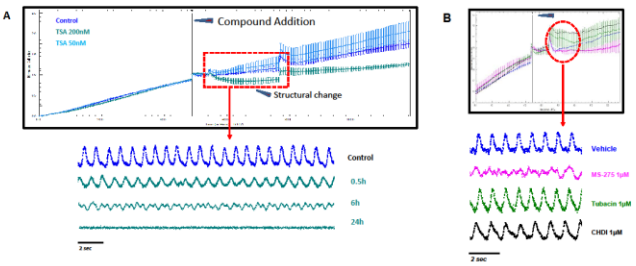

Fig 11. Trichostatin-A (TSA; pan-HDAC inhibitor) displayed a decrease in cell index at sub-therapeutic dose of 200nM in primary rat cells. Complete loss of contractility was achieved within 24hours from initial exposure (A). Selective Class II HDACis (Class IIa-Tubacin and Class IIb-CHDI) did not induce changes in contractility, changes in contractility pattern are observable upon treatment with class I HDACi (MS-275) (B).

CONCLUSIONS

The combination of non-contractile primary cardiomyocytes and contractile cardiomyocytes offers a comprehensive model system for the detection of drug-induced structural and functional cardiotoxicity

Cardiac Model	Structural Screening	Functional screening
AC10 Human Ventricular Cell Line	YES	NO
HL-1 Murine Atrial Cell Line	YES	LIMITED
Human hiPS-CMs	LIMITED	YES
Primary Neonatal Rat CMs	YES	YES

The integration of different in-vitro models allowed to gain insights into HDACi-mediated cardiotoxocity

HDACI- Induced Cardiotoxicity
HDAC inhibition causes both structural and functional aberrations to cardiac cells at sub-clinical drug concentrations
Class I HDACi induced detectable toxicity in the form of structural and functional perturbations
Class IIa and IIb HDACi did not cause detectable toxicity

Contact Details:

Ms Carol De Santis

c.de-santis1@Newcastle.ac.uk

Journal of Geriatric Oncology 10 (2019) 685–689

Contents lists available at ScienceDirect

Journal of Geriatric Oncology

Chronic cardiovascular toxicity in the older oncology patient population

Simon G. Findlay [a], Jason H. Gill [a,b], Ruth Plummer [a,c], Carol DeSantis [a], Chris Plummer [a,d,*]

[a] Northern Institute for Cancer Research (NICR), Paul O'Gorman Building, Faculty of Medical Sciences, Newcastle University, Newcastle upon Tyne NE2 4HH, UK
[b] School of Pharmacy, King George VI Building, Faculty of Medical Sciences, Newcastle University, Newcastle upon Tyne NE1 7RU, UK
[c] Northern Centre for Cancer Care, Freeman Hospital, Newcastle upon Tyne Hospitals NHS Foundation Trust, Newcastle upon Tyne NE7 7DN, UK
[d] Department of Cardiology, Freeman Hospital, Newcastle upon Tyne Hospitals NHS Foundation Trust, Newcastle upon Tyne NE7 7DN, UK

ARTICLE INFO

Article history:
Received 2 November 2018
Received in revised form 21 January 2019
Accepted 24 January 2019
Available online 5 February 2019

Keywords:
Cardio-oncology
Older cancer patients
Cardiovascular risk

ABSTRACT

Survivorship statistics demonstrate that the incidence of cancer continues to rise worldwide, with a further 60% increase in diagnoses predicted by 2030 attributed to lifestyle risk factors, screening programmes resulting in earlier diagnosis but also the changing demographics of the population. More than a third of new cancer diagnoses and almost half of cancer survivors are now aged 70 years or older. Despite this increasing incidence, worldwide five-year cancer survival rates have improved significantly over the past two decades. After cancer, cardiovascular disease is the second most common cause of death in developed countries. With continued improvements in overall prognosis, patients with cancer have an increased exposure to cardiovascular risk factors resulting in higher cardiovascular morbidity and mortality, particularly in older patients. This relationship between cancer and cardiovascular disease is not surprising as they share the common risk factors of aging, smoking, obesity, and poor diet. In this review, we discuss the toxicity of cancer treatments on the cardiovascular system, particularly in older patients. We focus primarily on radiotherapy and anthracycline chemotherapy because of their chronic adverse effects and appraise approaches toward the detection and treatment of this toxicity to maximise survival and quality of life of older patients with cancer.

Contents

DOI: 10.1016/j.jgo.2019.01.018

Pharmacology & Therapeutics 202 (2019) 18–31

Contents lists available at ScienceDirect

Pharmacology & Therapeutics

journal homepage: www.elsevier.com/locate/pharmthera

Vascular Disrupting Agents in cancer treatment: Cardiovascular toxicity and implications for co-administration with other cancer chemotherapeutics

Jason H. Gill [a,b,*], Kimberly L. Rockley [a], Carol De Santis [a], Asma K. Mohamed [a]

[a] Northern Institute for Cancer Research (NICR), Faculty of Medical Sciences, Newcastle University, UK
[b] School of Pharmacy, Faculty of Medical Sciences, Newcastle University, UK

ARTICLE INFO

Available online 5 June 2019

Keywords:
Cancer therapy
Cardiovascular toxicity
Cardioncology
Vascular disrupting agents

ABSTRACT

Destruction of the established tumour vasculature by a class of compound termed Vascular Disrupting Agents (VDAs) is showing considerable promise as a viable approach for the management of solid tumours. VDAs induce a rapid shutdown and collapse of tumour blood vessels, leading to ischaemia and consequent necrosis of the tumour mass. Their efficacy is hindered by the persistence of a viable rim of tumour cells, supported by the peripheral normal vasculature, necessitating their co-administration with additional chemotherapeutics for maximal therapeutic benefit. However, a major limitation for the use of many cancer therapeutics is the development of life-threatening cardiovascular toxicities, with significant consequences for treatment response and the patient's quality of life. The aim of this review is to outline VDAs as a cancer therapeutic approach and define the mechanistic basis of cardiovascular toxicities of current chemotherapeutics, with the overall objective of discussing whether VDA combinations with specific chemotherapeutic classes would be good or bad in terms of cardiovascular toxicity.

Contents

DOI: 10.1016/j.pharmthera.2019.06.001

Differentiation 102 (2018) 10–18

Contents lists available at ScienceDirect

Differentiation

journal homepage: www.elsevier.com/locate/diff

Glucocorticoid-induced pancreatic-hepatic trans-differentiation in a human cell line in vitro

Emma A. Fairhall[1], Alistair C. Leitch, Anne F. Lakey, Philip M.E. Probert[2], Gabriella Richardson, Carol De Santis, Matthew C. Wright*

Institute of Cellular Medicine, Newcastle University, Level 4 William Leech Building, Medical School, Framlington Place, Newcastle Upon Tyne NE2 4HH, UK

ARTICLE INFO

Keywords:
Liver
Pancreas
HPAC
B-13
AR42J
AR42J-B13
NR3C1

ABSTRACT

The rodent pancreatic AR42J-B13 (B-13) cell line differentiates into non-replicative hepatocyte-like cells in response to glucocorticoid mediated via the glucocorticoid receptor (GR). The aims of this study were to identify a human cell line that responds similarly and investigate the mechanisms underpinning any alteration in differentiation. Exposing the human pancreatic adenocarcinoma (HPAC) cell line to 1–10 μM concentrations of dexamethasone (DEX) resulted an inhibition of proliferation, suppressed carcinoembryonic antigen expression, limited expression of pancreatic acinar and hepatic gene expression and significant induction of the constitutively-expressed hepatic CYP3A5 mRNA transcript. These changes were associated with a pulse of genomic DNA methylation and suppressed notch signalling activity. HPAC cells expressed high levels of GR transcript in contrast to other nuclear receptors – such as the glucocorticoid-activated pregnane X receptor (PXR) – and GR transcriptional function was activated by DEX in HPAC cells. Expression of selected hepatocyte transcripts in response to DEX was blocked by co-treatment with the GR antagonist RU486. These data indicate that the HPAC response to glucocorticoid exposure includes an inhibition in proliferation, alterations in notch signalling and a limited change in the expression of genes associated with an acinar and hepatic phenotype. This is the first demonstration of a human cell responding to similarly to the rodent B-13 cell regarding formation of hepatocyte-like cells in response to glucocorticoid. Identifying and modulating the ablating factor(s) may enhance the hepatocyte-like forming capacity of HPAC cells after exposure to glucocorticoid and generate an unlimited in vitro supply of human hepatocytes for toxicology studies and a variety of clinical applications.

DOI: 10.1016/j.diff.2018.05.003